

A STUDY OF MORPHOLOGICAL EFFECT OF  
OXYGEN REDUCTION CATALYST ON  
MICROBIAL FUEL CELL PERFORMANCE

RAVINDER KUMAR

UIMP  
Doctor of Philosophy

UNIVERSITI MALAYSIA PAHANG

## UNIVERSITI MALAYSIA PAHANG

### DECLARATION OF THESIS AND COPYRIGHT

Author's Full Name: Ravinder Kumar

Date of Birth : 14-07-1989

Title : A study of morphological effect of oxygen reduction catalyst on microbial fuel cell performance.

Academic Session: 2016/2017

I declare that this thesis is classified as:

- CONFIDENTIAL** (Contain confidential information under the official secret Act 1997)\*
- RESTRICTED** (Contains restricted information as specified by the organization where research was done)\*
- OPEN ACCESS** I agree that my thesis to be published as online open access (Full Text)

I acknowledge that Universiti Malaysia Pahang reserve the right as follows:

1. The Thesis is the Property of Universiti Malaysia Pahang
2. The Library of Universiti Malaysia Pahang has the right to make copies for the purpose of research only.
3. The library has the right to make copies of the Thesis for academic exchange.

Certified By:

(Student's Signature)

(Supervisor's Signature)

Ravinder Kumar  
K0689803  
Date: 22/05/2017

Dr. Lakhveer Singh  
Date: 22/05/2017

### SUPERVISOR'S DECLARATION

We hereby declare that we have checked this thesis and in our opinion, this thesis is adequate in terms of scope and quality for the award of the degree of PhD in Energy and Environmental Engineering.

---

(Supervisor's Signature)

Full Name : DR. LAKHVEER SINGH

Position : SENIOR LECTURER

Date : 22 MAY, 2017

---

(Co-supervisor's Signature)

Full Name : PROF. DATO' DR. ZULARISAM AB WAHID

Position : PROFESSOR

Date : 22 MAY, 2017

### STUDENT'S DECLARATION

I hereby declare that the work in this thesis is based on my original work except for quotations and citation which have been duly acknowledged. I also declare that it has not been previously or concurrently submitted for any other degree at Universiti Malaysia Pahang or any other institutions.

---

(Author's Signature)

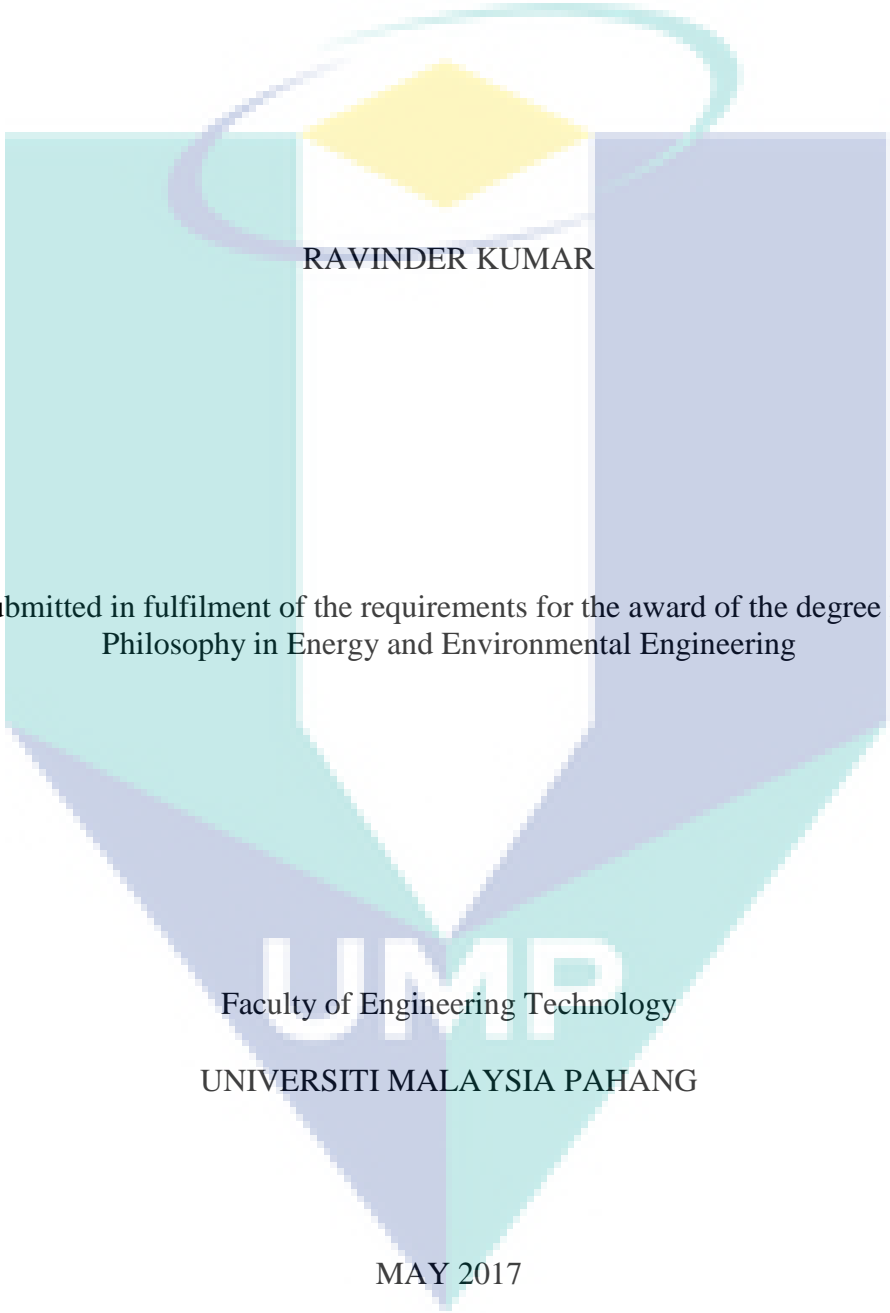
Full Name : RAVINDER KUMAR

ID Number : PPT 14007

Date : 22 MAY, 2017

UMP

A STUDY OF MORPHOLOGICAL EFFECT OF OXYGEN REDUCTION CATALYST  
ON MICROBIAL FUEL CELL PERFORMANCE

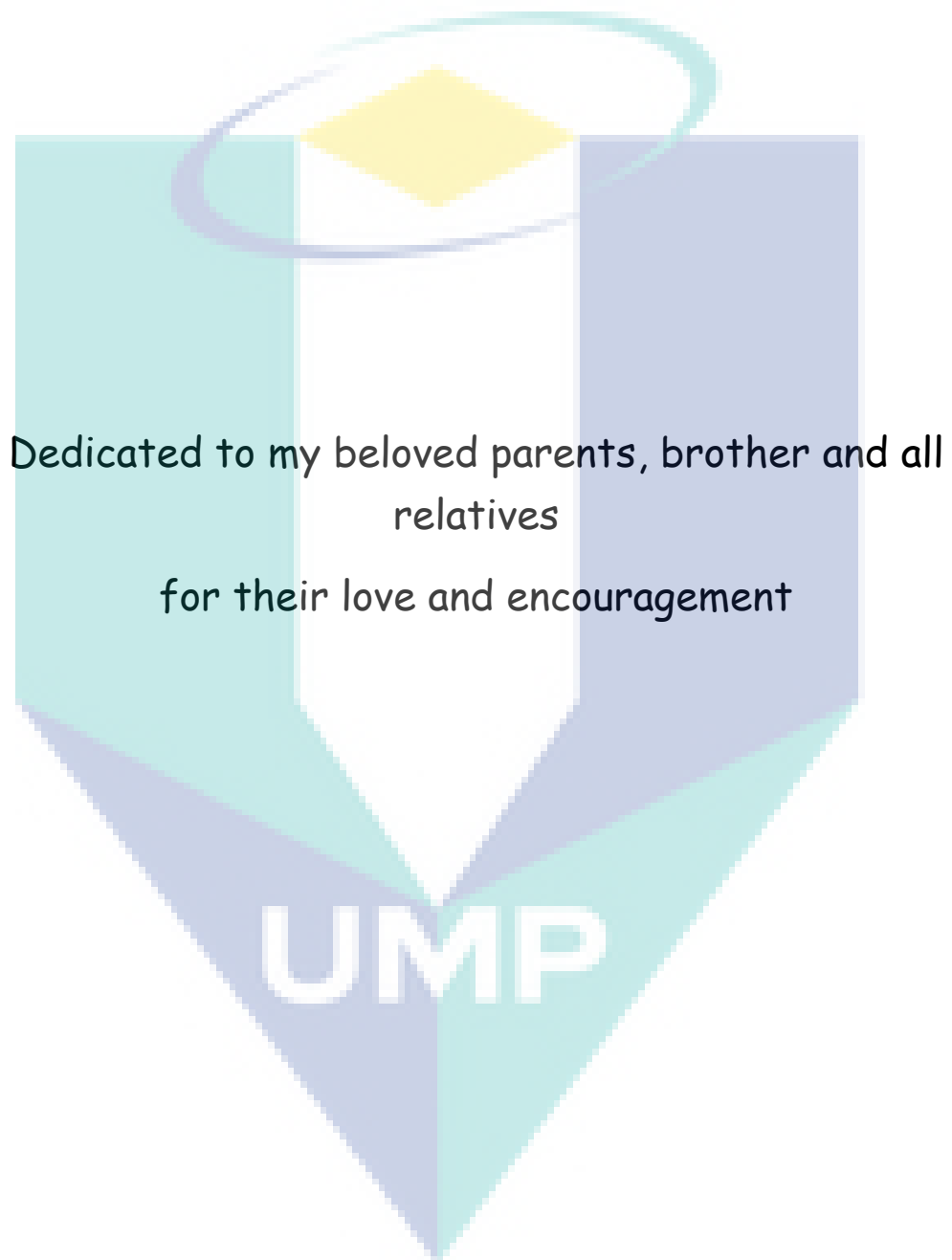


RAVINDER KUMAR

Thesis submitted in fulfilment of the requirements for the award of the degree Doctor of  
Philosophy in Energy and Environmental Engineering

UIMP  
Faculty of Engineering Technology  
UNIVERSITI MALAYSIA PAHANG

MAY 2017



## ACKNOWLEDGEMENTS

My humble thanks to the almighty to pursue the study period with good health, concentration, and dedication resulting in the research completion and thesis writing.

Words as are not enough to express my gratitude and regards to my supervisor, Dr. Lakhveer Singh, whose advice, knowledge, patience and most importantly constructive criticism towards this research work, motivated me as a researcher throughout this research. I express my deep gratitude towards my co-supervisor, Professor Dato' Dr. Zularisam Ab Wahid whose advice and knowledge helped me to complete my research work. I also thank Dr. Sunil Anil Patil, Research Associate, Institute of Environmental and Sustainable Chemistry, Germany, and Dr. Fang Zhang, Assistant Professor, Tsinghua University, China for helping me in my research activities.

I thank technical staffs of the lab, Mr. Mohd Firdaus Mohd Lazim, Mimi Nabila Mohd Noordin, Mr. Ikram and Mr. Hafizi for providing needful access to use essential instruments in toxicology laboratory. I also thank the technical staff of the central lab for FESEM analysis. Special thanks to Mr. Vijay Kumar from Himachal Pradesh University, Shimla, India for providing some necessary chemicals that facilitated to accomplish my research work.

I would like to express my deepest gratitude towards the members of Nanostructured Renewable Energy Material Laboratory for their knowledge sharing, encouragement, and support. I thank Prof. Jose Rajan, Dr. Baiju Vidyadharan, Dr. Syam G. Krishnan, Dr. Bhupender Pal, Mr. Midhun Harilal, and Miss. Bincy L. Vijyan for their knowledge, sharing and help in research activities. My special thanks to Mrs. Anju V. Nair from Faculty of Industrial Sciences and Technology for helping me in Tafel plot study.

I thank Mr. Sharanjit Singh, Mr. Pradeep Poddar, Mr. Vignesh Waran, Mr. Sumit Yadav, Mrs. Swati Sharma, my colleagues, Mr. Santhana Krishnan, Mr. Puranjan Mishra, Mrs. Rini Jarial for useful discussion and encouragement throughout my studies.

Moreover, I thank UMP Doctoral Scheme Scholarship (DSS) and UMP Post Graduate Research Grants Scheme (GRS 1403138) for the financial support.

I also thank my parents for their sacrifices and continuous support throughout the study. Last but not the least, I also thank my brother, all relatives, and friends for their constant support and motivation throughout the research work.

## ABSTRAK

Sel bahan api mikrob (MFC) adalah teknologi yang menjanjikan penghasilan tenaga elektrik daripada pelbagai substrat organik. Walau bagaimanapun, teknologi ini sedang menghadapi pelbagai cabaran untuk dikomersialkan. Salah satu daripada cabaran-cabaran ini adalah untuk menggantikan pemangkin platinum yang mahal dengan pemangkin katod yang murah dan cekap untuk tindak balas penurunan oksigen (ORR) dalam MFC katod udara.  $\text{Co}_3\text{O}_4$  (kobalt oksida) menunjukkan kecenderungan yang lebih tinggi ke arah molekul oksigen yang menjadikannya lebih baik untuk penyerapan kimia molekul oksigen ke permukaan pemangkin. Morfologi pemangkin memainkan peranan penting dalam aktiviti ORR yang memberi kesan kepada prestasi MFC itu. Oleh itu, dalam kerja penyelidikan ini, tiga morfologi  $\text{Co}_3\text{O}_4$  yang berbeza iaitu nanorod  $\text{Co}_3\text{O}_4$ , emping nano  $\text{Co}_3\text{O}_4$  dan  $\text{Co}_3\text{O}_4$  berbentuk bunga telah disediakan melalui kaedah hidroterma dan potensi untuk aktiviti ORR dan penjanaan elektrik telah disiasat di dalam MFC dua ruang. Hasil kajian menunjukkan nanorod  $\text{Co}_3\text{O}_4$  menunjukkan aktiviti ORR lebih tinggi dan menjana ketumpatan kuasa tertinggi di dalam MFC berbanding emping nano  $\text{Co}_3\text{O}_4$  dan  $\text{Co}_3\text{O}_4$  berbentuk bunga. Nanorod  $\text{Co}_3\text{O}_4$  menunjukkan luas permukaan BET yang  $15.55 \text{ m}^2/\text{g}$ , lebih tinggi daripada emping nano ( $11.05 \text{ m}^2/\text{g}$ ) dan 209% lebih tinggi daripada  $\text{Co}_3\text{O}_4$  berbentuk bunga ( $5.03 \text{ m}^2/\text{g}$ ). Selain itu, impedans spektroskopi elektrokimia (EIS) mencadangkan bahawa nanorod mengurangkan rintangan sistem yang ketara lalu meningkatkan pemindahan elektron pada antara muka katod dan meningkatkan ORR sekaligus ketumpatan kuasanya. Kinetik ORR katod telah dikaji dengan plot Tafel, yang menunjukkan bahawa nanorod  $\text{Co}_3\text{O}_4$  mencapai ketumpatan arus pertukaran tertinggi iaitu  $5.67 \text{ A}/\text{m}^2$ . Aktiviti ORR nanorod  $\text{Co}_3\text{O}_4$  yang lebih tinggi telah mempengaruhi prestasi MFC dan menjana ketumpatan kuasa yang  $454 \text{ mW}/\text{m}^2$ , iaitu 49% lebih tinggi daripada emping nano  $\text{Co}_3\text{O}_4$  dan 165% lebih tinggi daripada  $\text{Co}_3\text{O}_4$  berbentuk bunga. Keputusan ini mencadangkan bahawa  $\text{Co}_3\text{O}_4$  nanorods menunjukkan aktiviti ORR lebih tinggi berbanding dengan flakes  $\text{Co}_3\text{O}_4$  dan  $\text{Co}_3\text{O}_4$  flower, oleh itu, aktiviti ORR di nanorods  $\text{Co}_3\text{O}_4$  telah dipertingkatkan lagi dengan penambahan mangan (Mn) dan disediakan nanorods  $\text{MnCo}_2\text{O}_4$  dengan kaedah hidroterma dan potensinya untuk ORR aktiviti dan penjanaan elektrik telah disiasat di MFC yang sama. Keputusan CV, LSV, dan Tafel mendedahkan aktiviti ORR daripada nanorod yang telah dipertingkatkan selepas penambahan Mn, yang akhirnya meningkatkan kuasa output MFC dan menjana ketumpatan kuasa maksimum sebanyak  $587 \text{ mW}/\text{m}^2$  iaitu 29% lebih tinggi daripada nanorod  $\text{Co}_3\text{O}_4$  dan ~500% lebih tinggi daripada katod terdedah. Pengeluaran kuasa yang lebih baik boleh disifatkan kepada kecermelangan aktiviti ORR  $\text{Co}^{2+}/\text{Co}^{3+}$  dan  $\text{Mn}^{3+}/\text{Mn}^{4+}$  di atas luas permukaan katod. Oleh itu, kerja-kerja penyelidikan ini menunjukkan bahawa prestasi MFC boleh terkesan daripada morfologi pemangkin katod.

## ABSTRACT

Microbial fuel cell (MFC) is a promising technology that produces electricity from various organic substrates using microorganisms as biocatalysts. However, the technology is facing numerous challenges for its commercialization. One of these challenges is to replace the expensive platinum catalyst by an efficient and cost-effective cathode catalyst for oxygen reduction reaction (ORR) in air-cathode MFCs.  $\text{Co}_3\text{O}_4$  (cobalt oxide) shows higher affinity towards oxygen molecules that makes it more favorable for chemisorptions of oxygen molecules onto the catalyst surface. The morphology of the catalyst plays an indispensable role in ORR activity that further affects the MFC performance. Therefore, in this research work, three different morphologies of  $\text{Co}_3\text{O}_4$  that is  $\text{Co}_3\text{O}_4$  nanorods,  $\text{Co}_3\text{O}_4$  flakes, and  $\text{Co}_3\text{O}_4$  flower were prepared by hydrothermal methods and their potential for ORR activity and electricity generation was investigated in a double-chamber MFC. The results revealed that  $\text{Co}_3\text{O}_4$  nanorods showed higher ORR activity and generated the highest power density in MFC as compared to  $\text{Co}_3\text{O}_4$  flakes, and  $\text{Co}_3\text{O}_4$  flower, which can be attributed to higher BET surface area of the nanorods that comparatively provided more reduction sites for oxygen. Evidently,  $\text{Co}_3\text{O}_4$  nanorods exhibited a BET surface area of  $15.55 \text{ m}^2/\text{g}$ , which was 40% higher than the flakes ( $11.05 \text{ m}^2/\text{g}$ ) and 209% higher than flower-like  $\text{Co}_3\text{O}_4$  ( $5.03 \text{ m}^2/\text{g}$ ). Moreover, electrochemical impedance spectroscopy (EIS) suggested that the nanorods reduced the resistance of the system significantly that enhanced the electron transfer on the cathode interfaces and increased the ORR activity and consequently, the power density. The ORR kinetics of the cathodes were studied by Tafel plots, which indicated that  $\text{Co}_3\text{O}_4$  nanorods achieved the highest exchange current density that is  $5.67 \text{ A}/\text{m}^2$ . This higher ORR activity of  $\text{Co}_3\text{O}_4$  nanorods influenced the MFC performance and generated the highest power density of  $454 \text{ mW}/\text{m}^2$ , which was 49% higher than  $\text{Co}_3\text{O}_4$  flakes and 165% higher than flower-like  $\text{Co}_3\text{O}_4$ . These results suggested that  $\text{Co}_3\text{O}_4$  nanorods showed higher ORR activity as compared to  $\text{Co}_3\text{O}_4$  flakes and  $\text{Co}_3\text{O}_4$  flower, therefore, the ORR activity of  $\text{Co}_3\text{O}_4$  nanorods was further improved with the addition of manganese (Mn) and  $\text{MnCo}_2\text{O}_4$  nanorods were prepared by a hydrothermal method and its potential for ORR activity and electricity generation was investigated in the similar MFC. The CV, LSV, and Tafel results revealed that the ORR activity of the nanorods was enhanced after the introduction of Mn, which ultimately increased the power output in the MFC and generated a maximum power density of  $587 \text{ mW}/\text{m}^2$  that was 29% higher than  $\text{Co}_3\text{O}_4$  nanorods and ~500% higher than the bare cathode. The improved power output can be ascribed to the excellent ORR activity of  $\text{Co}^{2+}/\text{Co}^{3+}$  and  $\text{Mn}^{3+}/\text{Mn}^{4+}$  on the cathode surface. Therefore, this research work showed that the MFC performance can be greatly affected by the morphology of the cathode catalyst.

## TABLE OF CONTENTS

<b>DECLARATION</b>	
<b>TITLE PAGE</b>	
<b>ACKNOWLEDGEMENTS</b>	<b>iii</b>
<b>ABSTRAK</b>	<b>iv</b>
<b>ABSTRACT</b>	<b>v</b>
<b>TABLE OF CONTENT</b>	<b>vi</b>
<b>LIST OF TABLES</b>	<b>xi</b>
<b>LIST OF FIGURES</b>	<b>xii</b>
<b>LIST OF SYMBOLS</b>	<b>xv</b>
<b>LIST OF ABBREVIATIONS</b>	<b>xvii</b>
<b>CHAPTER 1 INTRODUCTION</b>	<b>1</b>
1.1 Introduction	1
1.2 Energy crisis and the challenge of global climate change	1
1.3 Microbial fuel cells for bioenergy production	2
1.4 Oxygen reduction reaction and cathode catalysts	2
1.5 Problem statement	3
1.6 Objectives	5
1.7 Scope of research	6
1.8 Novelty of study	6
1.9 Thesis outline	7

<b>CHAPTER 2 LITERATURE REVIEW</b>	<b>8</b>
2.1 Introduction	8
2.2 Types of MFC	8
2.2.1 Double chamber MFC	8
2.2.2 Single chamber MFC (SC-MFC)	9
2.2.3 Up-flow MFC	9
2.2.4 Stacked MFC	10
2.2.5 Other designs	12
2.3 Electrode materials	12
2.3.1 Anode materials	13
2.3.1.1 Conventional carbon materials	13
2.3.1.2 Nanomaterials	15
2.3.1.3 Metal materials	15
2.3.2 Cathode materials	16
2.3.2.1 Cathode supporting material	16
2.3.2.2 Catalyst	18
<i>Platinum (Pt)</i>	18
<i>Carbon-based catalysts</i>	18
<i>Metal-based catalysts</i>	21
2.3.3 Binder	25
2.4 Membranes	27
2.5 Microorganisms or biocatalysts	28
2.5.1 Biocatalysts in anode	29
2.5.2 Bioelectrogenesis	32
2.5.2 Biocatalysts in cathode	34
2.6 Substrate	35
2.7 Electrolyte	38
2.8 Hydrothermal method for nanomaterial synthesis	39
2.9 Summary	40

<b>CHAPTER 3 METHODOLOGY</b>	<b>42</b>
3.1 Introduction	42
3.2 Research methodology	42
3.3 Synthesis of materials	43
3.3.1 Synthesis of $\text{Co}_3\text{O}_4$ nanorods	43
3.3.2 Synthesis of $\text{Co}_3\text{O}_4$ nanoflakes	44
3.3.3 Synthesis of flower-like $\text{Co}_3\text{O}_4$ flower	44
3.3.4 Synthesis of $\text{MnCo}_2\text{O}_4$ nanorods	44
3.4 Materials characterization	45
3.4.1 Powder X-ray Diffraction (XRD) Technique	45
3.4.2 Field Emission Scanning Electron Microscopy (FESEM)	46
3.4.3 Transmission electron microscopy (TEM)	46
3.4.4 Brunauer-Emmett-Teller (BET) measurement	46
3.4.5 X-ray Photoelectron Spectroscopy (XPS)	47
3.5 Preparation of catalyst ink and its coating on cathodes	48
3.6 Electrochemical characterization of the prepared cathodes	49
3.6.1 Cyclic voltammetry (CV)	49
3.6.2 Linear sweep voltammetry (LSV)	50
3.6.3 Electrochemical impedance spectroscopy	51
3.7 Oxygen reduction reaction kinetics study by Tafel plots	51
3.8 Microbial fuel cell construction and operation	52
3.9 Inoculum	54
3.10 Polarization curves	54

<b>CHAPTER 4 RESULTS AND DISCUSSION</b>	<b>55</b>
4.1 Introduction	55
4.2 To synthesize three morphologies of $\text{Co}_3\text{O}_4$ (nanorods, flakes, and flower) by a particular hydrothermal method and their characterization by physico-chemical and microscopy techniques	55
4.2.1 XRD analysis of $\text{Co}_3\text{O}_4$ nanorods, flakes, and flower	56
4.2.2 FESEM and TEM results	57
4.2.3 BET results	60
4.3 To fabricate cathodes with prepared catalysts and examine their oxygen reduction activity by electrochemical techniques and investigate their potential for bioelectricity generation in MFCs	65
4.3.1 Cyclic voltammetry of all the cathodes	66
4.3.2 Linear sweep voltammetry of all the cathodes	69
4.3.3 Nyquist plots to estimate the resistance	72
4.3.4 Analysis of ORR kinetics by Tafel plot study	75
4.3.5 Performance of the cathodes for bioelectricity generation in MFCs	79
4.4 To enhance the performance of $\text{Co}_3\text{O}_4$ nanorods towards oxygen reduction by making a compound with Mn that $\text{MnCo}_2\text{O}_4$ nanorods and investigate its ORR activity and electricity generation potential in MFCs	86
4.4.1 XRD and electron microscopy results	86
4.4.2 BET analysis of $\text{MnCo}_2\text{O}_4$ nanorods	89
4.4.3 X-ray Photoelectron Spectroscopy (XPS) results of $\text{MnCo}_2\text{O}_4$ nanorods	92
4.4.4 Electrochemical characterization of cathodes	93
4.4.5 ORR kinetics by Tafel plots	98

4.4.6	Performance of the cathodes for bioelectricity generation in MFCs	102
-------	---	-----

<b>CHAPTER 5 CONCLUSION</b>	<b>104</b>
-----------------------------	------------

5.1	Conclusions	104
-----	-------------	-----

5.2	Recommendations for Future Work	106
-----	---------------------------------	-----

<b>REFERENCES</b>	<b>107</b>
-------------------	------------

<b>APPENDIX A</b>	<b>125</b>
-------------------	------------

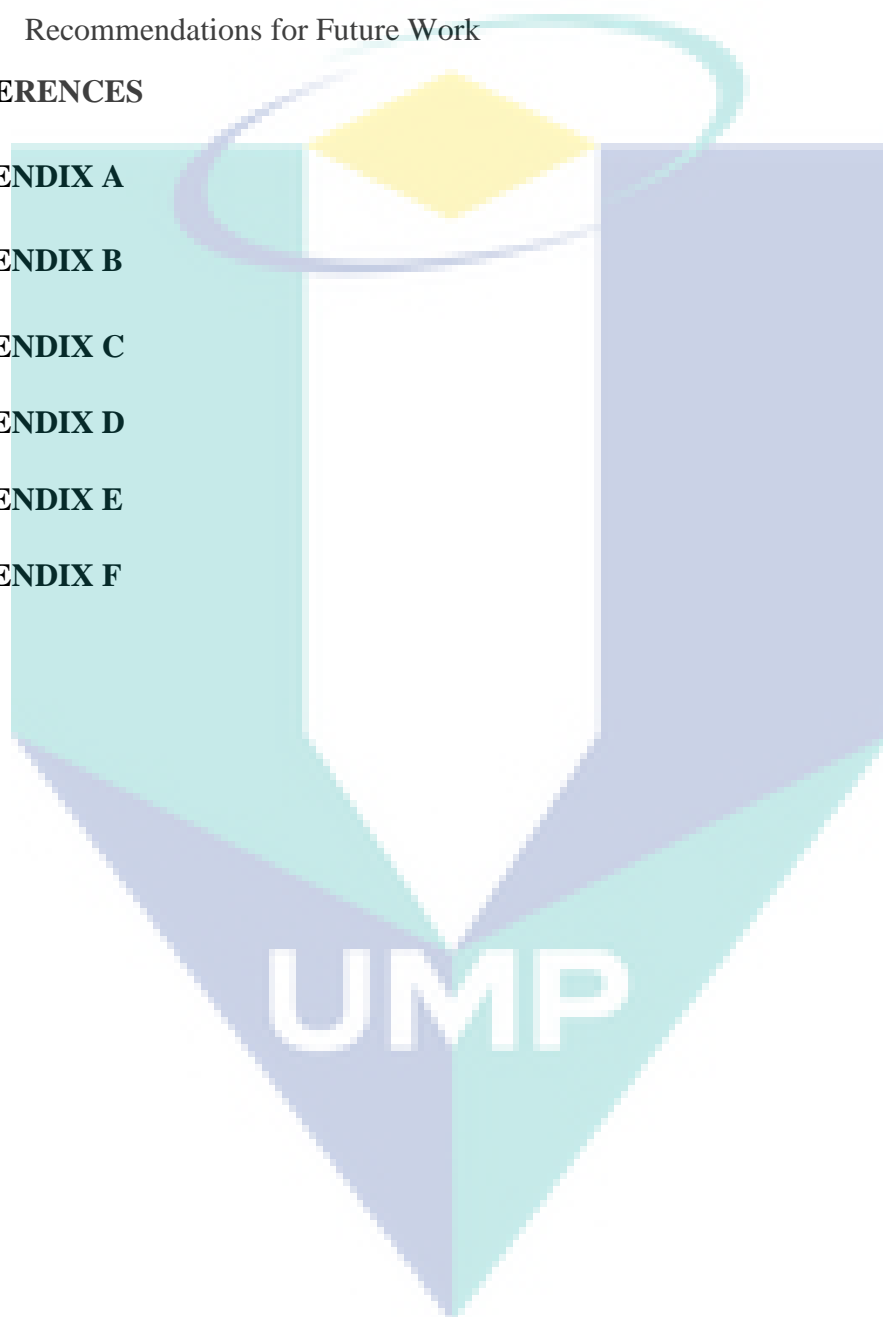
<b>APPENDIX B</b>	<b>127</b>
-------------------	------------

<b>APPENDIX C</b>	<b>128</b>
-------------------	------------

<b>APPENDIX D</b>	<b>129</b>
-------------------	------------

<b>APPENDIX E</b>	<b>130</b>
-------------------	------------

<b>APPENDIX F</b>	<b>131</b>
-------------------	------------



## LIST OF TABLES

<b>Table</b>	<b>Title</b>	<b>Page</b>
Table 2.1	Performance of cobalt and manganese based cathode catalysts in air-cathode microbial fuel cells.	25
Table 2.2	Performance of microbial fuel cells for bioelectricity generation using pure cultures	31
Table 2.3	Performance of microbial fuel cells for bioelectricity generation using mixed cultures	32
Table 2.4	An overview of performance of MFCs with simple substrates.	36
Table 2.5	An overview of performance of MFCs with undefined wastewater substrates.	37
Table 3.1	Precursors and parameters used to synthesize cathode catalysts.	45
Table 3.2	Catalyst concentrations used in the study.	49
Table 4.1	BET results for different morphologies of $\text{Co}_3\text{O}_4$ .	60
Table 4.2	Cathodes prepared with specific concentration.	65
Table 4.3	Resistance values for all the cathodes calculated from the Nyquist plots.	74
Table 4.4	Exchange current density of all the cathodes.	75
Table 4.5	Maximum power density achieved by the cathodes in a double-chamber air-cathode MFC.	80
Table 4.6	Performance of different oxygen reduction catalysts in MFCs.	85
Table 4.7	BET results of $\text{MnCo}_2\text{O}_4$ nanorods and $\text{Co}_3\text{O}_4$ nanorods.	89
Table 4.8	Resistance values for the cathodes calculated from the fitting results of Nyquist plots.	96
Table 4.9	Exchange current densities for the cathodes.	98
Table 5.1	Performance of all catalysts used in this study and comparison with previous studies.	105

## LIST OF FIGURES

Figure	Title	Page
Figure 2.1	Different MFC designs (a) double chamber MFC, (b) single chamber MFC, (c) tubular up-flow MFC, and (d) stacked MFC.	10
Figure 2.2	Pictures of anode materials (a) graphite rod, (b) graphite felt, (c) graphite sheet, (d) graphite brush, (e) carbon paper, (f) carbon felt, (g) carbon cloth, and (h) reticulated vitreous carbon.	14
Figure 2.3	Figure 2.3 Comparison of power generation by cathode catalysts with mesoporous architecture with conventional cathode catalysts.	23
Figure 2.4	Schematic image of the proposed EET of two metal respiring bacteria and their interactions with an electrode in a bioelectrochemical system (Kracke et al., 2015).	29
Figure 2.5	Reduction of $\text{NAD}^+$ and $\text{FAD}$ to their electron carrier forms ( $\text{NADH}$ and $\text{FADH}_2$ ) through the Citric Acid Cycle (also known as tricarboxylic acid cycle or TCA cycle). (Schaeztle et al., 2008).	33
Figure 3.1	Flow chart of research methodology.	43
Figure 3.2	Preparation of cathodes for 1 mg catalyst.	48
Figure 3.3	(a) Photograph of potentiostat used in this research (b) principle of three electrode measurement.	50
Figure 3.4	(a) Picture of double chamber MFC used in this work (b) MFC during operation.	52
Figure 3.5	Diagram of the connection for polarization curves.	53
Figure 4.1	XRD pattern of $\text{Co}_3\text{O}_4$ nanorods, $\text{Co}_3\text{O}_4$ flakes and $\text{Co}_3\text{O}_4$ flower.	57
Figure 4.2	FESEM images of porous $\text{Co}_3\text{O}_4$ nanorods at different magnifications.	58
Figure 4.3	TEM images of $\text{Co}_3\text{O}_4$ nanorods.	58
Figure 4.4	FESEM images of $\text{Co}_3\text{O}_4$ flakes at different magnifications.	59
Figure 4.5	FESEM images of $\text{Co}_3\text{O}_4$ flower at different magnifications.	59
Figure 4.6	(a) Nitrogen adsorption-desorption isotherms of $\text{Co}_3\text{O}_4$ nanorods, (b) variations in pore diameter of $\text{Co}_3\text{O}_4$ nanorods.	61

Figure 4.7	(a) Nitrogen adsorption-desorption isotherms of $\text{Co}_3\text{O}_4$ flakes, (b) variations in pore diameter of $\text{Co}_3\text{O}_4$ flakes.	62
Figure 4.8	(a) Nitrogen adsorption-desorption isotherms of $\text{Co}_3\text{O}_4$ flower, (b) variations in pore diameter of $\text{Co}_3\text{O}_4$ flower.	63
Figure 4.9	Cyclic voltammograms of all the cathodes with $\text{Co}_3\text{O}_4$ nanorods.	66
Figure 4.10	(a) Cyclic voltammogram of the cathode with $\text{Co}_3\text{O}_4$ flakes and (b) the cathode with $\text{Co}_3\text{O}_4$ flower.	67
Figure 4.11	LSVs of cathodes with different concentrations of $\text{Co}_3\text{O}_4$ nanorods at a scan rate of 10 mV/s.	69
Figure 4.12	LSVs of cathodes with $\text{Co}_3\text{O}_4$ nanorods, $\text{Co}_3\text{O}_4$ flakes and $\text{Co}_3\text{O}_4$ flower at a scan rate of 10 mV/s.	70
Figure 4.13	A possible oxygen reduction mechanism by Co ions on the surface of the cathodes.	71
Figure 4.14	Equivalent circuit for Nyquist plots.	72
Figure 4.15	Nyquist plots of cathodes coated with $\text{Co}_3\text{O}_4$ nanorods.	72
Figure 4.16	Nyquist plots of cathodes coated with $\text{Co}_3\text{O}_4$ nanorods, $\text{Co}_3\text{O}_4$ flakes and $\text{Co}_3\text{O}_4$ flower.	74
Figure 4.17	(a) Tafel plots of different cathodes with varying concentration of $\text{Co}_3\text{O}_4$ nanorods by sweeping the overpotential from 20 mV to 100 mV at $1 \text{ mVs}^{-1}$ and (b) linear fit for the Tafel plots of overpotential from 60 to 80 mV.	74
Figure 4.18	(a) Tafel plots of different cathodes with $\text{Co}_3\text{O}_4$ nanorods, flakes and the flower by sweeping the overpotential from 20 mV to 100 mV at $1 \text{ mVs}^{-1}$ and (b) linear fit for the Tafel plots of overpotential from 60 to 80 mV.	76
Figure 4.19	(a) Polarization and power density curves of MFCs and (b) electrode potentials using different concentration of $\text{Co}_3\text{O}_4$ nanorods.	78
Figure 4.20	Proteins involved in electron transfer mechanisms.	81
Figure 4.21	(a) Polarization and power density curves of MFCs and (b) electrode potentials using cathodes with $\text{Co}_3\text{O}_4$ nanorods, $\text{Co}_3\text{O}_4$ flakes, and $\text{Co}_3\text{O}_4$ flower.	82
Figure 4.22	XRD pattern of $\text{MnCo}_2\text{O}_4$ nanorods.	87

Figure 4.23	FESEM images of MnCo <sub>2</sub> O <sub>4</sub> nanorods at different magnifications.	88
Figure 4.24	FESEM images of Co <sub>3</sub> O <sub>4</sub> nanorods at different magnifications.	88
Figure 4.25	TEM images of MnCo <sub>2</sub> O <sub>4</sub> nanorods at different scales.	89
Figure 4.26	(a) Nitrogen adsorption-desorption isotherms of MnCo <sub>2</sub> O <sub>4</sub> nanorods, (b) variations in pore diameter of MnCo <sub>2</sub> O <sub>4</sub> nanorods.	90
Figure 4.27	XPS Survey spectra of (a) MnCo <sub>2</sub> O <sub>4</sub> nanorods, Individual XPS spectrum of (b) Co 2p, (c) Mn 2p and (d) O 1s.	91
Figure 4.28	CV of MnCo <sub>2</sub> O <sub>4</sub> nanorods.	93
Figure 4.29	Possible mechanism of oxygen reduction by MnCo <sub>2</sub> O <sub>4</sub> nanorods.	95
Figure 4.30	LSVs of MnCo <sub>2</sub> O <sub>4</sub> nanorods at a scan rate of 10 mV/s.	95
Figure 4.31	Nyquist plot of the cathodes measured over a frequency range of 1 Hz-100000 Hz at the initial open circuit potential with a sinusoidal perturbation of 10 mV amplitude.	97
Figure 4.32	(a) Tafel plots of the cathodes by sweeping the overpotential from 20 mV to 100 mV at 1 mVs <sup>-1</sup> and (b) the linear fit for the Tafel plots of overpotential from 60 to 80 mV.	99
Figure 4.33	(a) Polarization and power density curves of MFCs and (b) electrode potentials of bare cathode, MnCo <sub>2</sub> O <sub>4</sub> nanorods, and Co <sub>3</sub> O <sub>4</sub> nanorods.	101

UMP

## LIST OF SYMBOLS

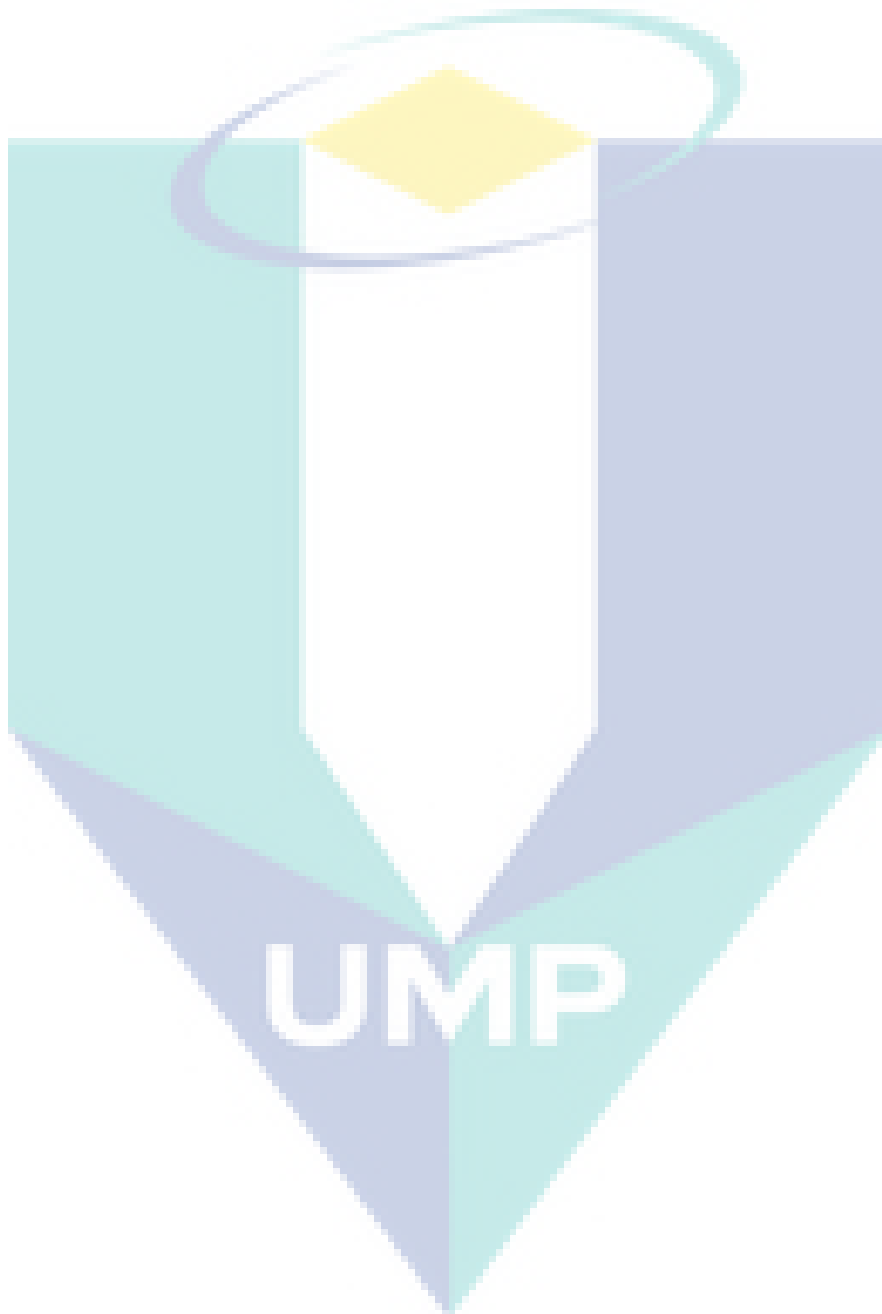
~	approximately
%	percentage
$\lambda$	wavelength
$\mu$	micron ( $10^{-6}$ )
$\theta$	angle
$\text{\AA}$	angstrom ( $10^{-10}$ )
A	ampere
A/cm <sup>2</sup>	ampere per centimetre square
°C	degree celcius
<i>ca.</i>	circa (approximately)
cm <sup>2</sup>	centimeter square
<i>d</i>	distance
<i>e.g.</i>	<i>exempli gratia</i> (example)
<i>et al.</i>	<i>et alii</i> (and others)
<i>E</i>	potential
<i>g</i>	grams
<i>h</i>	hours
<i>i</i> <sub>0</sub>	exchange current density
i.e.	<i>id est</i> (that is)
L	litre
m <sup>2</sup> g <sup>-1</sup>	meter square per gram
M	molar (mol/litre)
mM	milli molar
min	minute
mL	milli litre
mW	milli watt
mA/cm <sup>2</sup>	milli ampere per centimetre square
mW/m <sup>2</sup>	milli watt per meter square
mW/m <sup>3</sup>	milli watt per meter cube
mV s <sup>-1</sup>	millivolt per second

nm

nanometre

V

voltage



## LIST OF ABBREVIATIONS

AC	activated carbon
AEI	anion exchange ionomer
AEM	anion exchange membranes
BET	Brunauer-Emmett-Teller
BOD	biochemical oxygen demand
C	carbon
CB	carbon black
CE	coulombic efficiency
CEM	cation exchange membranes
COD	chemical oxygen demand
COFK	cobalt oxide flakes (1 mg/cm <sup>2</sup> )
COFL	cobalt oxide flower (1 mg/cm <sup>2</sup> )
CON-1	cobalt oxide nanorods (0.5 mg/cm <sup>2</sup> )
CON-2	cobalt oxide nanorods (1 mg/cm <sup>2</sup> )
CON-3	cobalt oxide nanorods (2 mg/cm <sup>2</sup> )
CO <sub>2</sub>	carbon dioxide
Co	cobalt
Co <sub>3</sub> O <sub>4</sub>	cobalt oxide
Co <sub>3</sub> O <sub>4</sub> -NGO	cobalt oxide-nitrogen-doped graphene oxide
Co <sub>3</sub> O <sub>4</sub> -NCNT	cobalt oxide-nitrogen-doped carbon nanotubes
Co/Co <sub>9</sub> S <sub>8</sub> /NPGC	nitrogen-doped Co/Co <sub>9</sub> S <sub>8</sub> /partly-graphitized carbon
CoTMPP	cobalt tetramethyl phenyl porphyrin
CNFs	carbon nanofibers

CNT	carbon nanotubes
CV	cyclic voltammetry
DABCO	1,4-diazabicyclo-[2.2.2]-octane
DEA	diethylamine-functionalized polymer
FL	flavin molecules
FPMFC	flat plate microbial fuel cell
FO	forward osmosis
EIS	electrochemical impedance spectroscopy
ETC	electron transport chain
FESEM	field emission scanning electron microscopy
GO	graphene oxide
IEC	ion exchange capacities
IPCC	Intergovernmental Panel on Climate Change
LSV	linear sweep voltammetry
MEC	microbial electrolysis cell
MFC	microbial fuel cell
MPD	maximum power density
MWCNTs	multiwall carbon nanotubes
Mn	manganese
MnO <sub>2</sub>	manganese dioxide
MnCo <sub>2</sub> O <sub>4</sub>	manganese cobaltite
MQ	menaquinones
N-G@CoNi/BCNT	nitrogen-doped graphene/CoNi alloy encased within bamboo-like carbon nanotube hybrids
NiCo <sub>2</sub> O <sub>4</sub>	nickel cobaltite

OCV	open circuit voltage
ORR	oxygen reduction reaction
OMCs	outer membrane cytochromes
PANI	polyaniline
PBS	phosphate buffer saline
PC	phthalocyanine
PDMS	poly (dimethylsiloxane)
PEM	proton exchange membrane
PPy	polypyrrole
Pt	platinum
PTFE	polytetrafluoroethylene
PVDF	polyvinylidene fluoride
Q	quinones
Q-FPAE	quaternary ammonium functionalized fluorinated poly (arylene ether)
QDPSU	quaternary 1,4-diazabicyclo-[2.2.2]-octane (DABCO) polysulfone
RVC	reticulated vitreous carbon
S	sulphur
SC-MFC	single chamber- microbial fuel cell
SS	stainless steel
TEM	transmission electron microscopy
UF	ultrafiltration
XRD	X-ray diffraction

## CHAPTER 1

### INTRODUCTION

#### 1.1 Introduction

This chapter introduces the microbial fuel cell (MFC) technology and oxygen reduction reaction (ORR) and catalysts for ORR. A detailed statement of the problem, broad and specific objectives of this research have been outlined in this chapter. The scopes of this research have been elaborated and the novelty of the research work is also stated. Finally, the outline of the thesis is detailed.

#### 1.2 Energy crisis and the challenge of global climate change

The energy crisis and global climate change are among the most important challenges and the greatest threats facing the world. Fossil fuels such as oil, coal and natural gas are the primary energy sources for the world, accounting for more than 85% of the world energy consumption (BP Statistical Review of World Energy, 2011). However, fossil fuels are non-renewable resources which take millions of years to form from the plant and animal biomass, and the reserves are being depleted much faster than the formation rate. The global annual energy consumption growth rate has been  $>2\%$  for years, and in the year 2010, consumption growth reached 5.6%, which is the highest rate since 1973 (BP Energy Outlook 2030, 2012). Energy consumption has grown even more rapidly than the economy, indicating the low efficiency of energy utilization. Although energy efficiencies are improving globally and primary energy consumption growth is expected to decrease in the future (BP Energy Outlook 2030, 2012), fossil fuels cannot indefinitely sustain a global economy, especially with a growing population. Renewable energy sources with much higher energy utilization efficiencies are needed for the sustainable development.

### **1.3 Microbial fuel cells for bioenergy production**

Microbial fuel cell technology is one of the most attractive technologies at present for renewable energy production and simultaneous wastewater treatment. MFCs are the bioelectrochemical devices that utilize microorganisms as the biocatalysts to convert the chemical energy present in organic or inorganic compounds into electrical current. (Aelterman et al., 2006; Logan et al., 2006). A double chamber MFC is made up of two chambers i.e. the anode and the cathode. Usually a proton exchange membrane (PEM) is placed between these two chambers that allows the protons produced at the anode to pass through itself to the cathode (Logan et al., 2006). The cathode and the anode are connected by an electrical circuit (e.g., with titanium wires or copper wires) to make it a complete system. The organic substrates are oxidized by the microorganisms at the anode chamber and produce electrons, protons and carbon dioxide. The electrons generated from the microbial metabolic activity are firstly transferred to the anode surface by redox-active proteins or cytochromes and then passed to the cathode through electrical circuit (Nevin et al., 2008; Borole et al., 2012). At the cathode chamber, the reduction of electrons takes place. Generally, an electron acceptor is provided at the cathode e.g., oxygen or ferricyanide. Subsequently, electrons combine with protons and oxygen at the cathode and form water. This reaction can be further facilitated by a catalyst such as, platinum.

MFCs can have other applications besides electricity generation with wastewater as the fuel (Baranitharan et al., 2015), including desalination (Chen et al., 2012), recovery of nutrients in wastewater (Borole et al., 2012), recovery of low-grade thermal energy (Chookaew et al., 2014), and production of valuable products such as hydrogen gas and other biofuels (Cui et al., 2014), and chemicals (Logan 2006; Patil et al., 2011). These added values make MFCs more attractive for simultaneous electric power generation, wastewater treatment, and co-product recovery but it is critical that the costs of MFCs be reduced so that these systems can be economical and implemented in large-scale wastewater treatment plants.

### **1.4 Oxygen reduction reaction and cathode catalysts**

In an MFC device, oxygen has been used as the most sustainable electron acceptor in the cathode, because of its unlimited availability in the environment and capacity to produce a high-power output. Moreover, oxygen is widely applied as an electron acceptor for its high standard potential. The kinetic rate of the oxygen reduction reaction (ORR) is

low because of the high activation energy required to break the O=O bond (498 kJmol<sup>-1</sup>) (Shao et al., 2008).

The poor kinetics of ORR at neutral pH and low temperature hinder improvement in the performance of MFCs. To improve the slow ORR rate, platinum and platinum-based catalysts have been commonly used as MFCs cathode catalyst, because of their effectiveness in lowering the activation energy of cathodic reactions (Pant et al., 2010; Nørskov et al., 2004). Unfortunately, their high cost, limited supply, and weak durability severely restrict their applicability to broad commercialization. Hence, researchers are faced with the challenge of developing efficient, durable, and inexpensive non-platinum ORR catalysts for MFCs. To date, ORR catalysts based on metals, carbon, conductive polymers, and microbes have been tested in MFCs (Ortiz-Martínez et al., 2016; Minteer et al., 2012; Mink et al., 2012). Moreover, the catalyst with porous architecture are more active for ORR as compared to the conventional catalysts because the catalysts with unique mesoporous morphology or structure exhibit additional active sites that maximizes the availability of the catalytic sites for oxygen molecules and facilitates the diffusion of electrons and reactants, which might be responsible for higher ORR activity (Ge et al., 2015; Ge et al., 2016). For example, recently, mesoporous nano urchin-like NiCo<sub>2</sub>O<sub>4</sub> was successfully synthesized by hydrothermal method. The mesoporous NiCo<sub>2</sub>O<sub>4</sub> provided more active sites for oxygen, improving the electrocatalytic activity significantly. The cathode showed a maximum exchange current density of 25.49 ( $\times 10^{-4}$  A/m<sup>2</sup>) and a maximum power density of ca. 1730 mW/m<sup>2</sup>, which was 2.28 times higher than the control (Ge et al., 2016). Hence, it is quite evident that catalysts with porous structure show higher ORR activity and could be a substantial alternative for costly platinum in MFCs.

### **1.5 Problem statement**

MFC technology has drawn a significant consideration for a decade, since it demonstrates the incredible potential to produce electrical energy from organic materials. However, some constraints such as high cost of materials required in manufacturing the MFCs are discouraging the use of MFC technology for commercial-scale applications. Moreover, the total electric output also remains low and highly expensive when the investment is taken into consideration for an MFC system. The cost for the preparation of the cathode (including the catalyst) accounts for ca. 60% of the overall expense of an

MFC (Gong et al., 2014). An air-cathode has been broadly acknowledged as the cathode of MFC because of the accessibility of abundant oxygen in air utilized as a free electron acceptor (Hou et al., 2016; Huang et al., 2015b). An electrochemically active catalyst is generally required for ORR at the cathode (Huggins et., 2015; Yazdi et al., 2016; Winfield et al., 2016). Generally, platinum is used as a cathode catalyst in MFCs. Platinum is a highly expensive, which costs approximately USD140 for per gram (Logan et al., 2007) and a rare element on the earth, so its use makes the MFC technology uneconomical and will not be feasible to upscale the technology. Besides, it is quite evident that the higher ORR rate is also one of the vital factors for enhanced power generation (Ghasemi et al., 2013; Huang et al., 2015a; Yang et al., 2015). Therefore, development of an efficient and cost-effective cathode catalyst could be an asset for improved MFC applications.

Nevertheless, many different types cathode catalysts have been synthesized by various methods and utilized in MFCs for a suitable alternative of platinum. For example, graphite oxide (Wen et al., 2012) and porous nitrogen-doped carbon nanosheets on graphene were synthesized from natural graphite by a modified Hummers method (Wen et al., 2014). In an alternative study, nitrogen-doped Co/Co<sub>9</sub>S<sub>8</sub>/partly-graphitized carbon was synthesized by a chemical method (Huang & Kaner, 2004). However, these methods are complex which further increase the preparation cost of the cathode and generally, requires more efforts. Therefore, the synthesis process to form a cathode catalyst should be a simple and cost-effective. Hydrothermal synthesis offers many advantages over conventional and non-conventional synthesis methods. Unlike many advanced methods that can prepare a large variety of forms, the respective costs for instrumentation, energy and precursors are far less for hydrothermal methods (Byrappa and Yoshimura, 2001). Moreover, a desired morphology of the nanomaterials can be developed easily using a hydrothermal method. The unique pressure-temperature interaction of the hydrothermal solution allows the preparation of different phases of materials that are difficult to prepare with other synthetic methods (Rabenau, 1985).

Different cathode catalysts with a variety of mesoporous architecture have been synthesized to improve the performance of the cathode in MFCs. Specifically, cobalt oxide (Co<sub>3</sub>O<sub>4</sub>) and manganese oxide (MnO<sub>2</sub>) showed excellent oxygen reduction activity in MFCs (Lima et al., 2010; Liu et al., 2006; Ge et al., 2015; Ge et al., 2016). This is probably because Co<sub>3</sub>O<sub>4</sub> and MnO<sub>2</sub> contain cations such as Co<sup>3+</sup>, Co<sup>2+</sup>/Mn<sup>4+</sup>, Mn<sup>3+</sup> that show high affinity towards oxygen molecules (Lima et al., 2006). Besides, the Co and Mn

containing cathode catalysts have shown high stability and less toxicity as compared to platinum. MnO<sub>2</sub>-carbon nanotubes were used as a cathode catalyst in an MFC that produced a maximum power density of 210 mW/m<sup>2</sup>, which was competitive to that produced by platinum (229 mW/m<sup>2</sup>) (Liew et al., 2015). In an alternative approach, Liu et al. studied the ORR kinetics of manganese-polypyrrole-carbon nanotube coated air-cathode in a single chamber MFC (Liu et al., 2010). Ge et al. (2015) investigated the application of ortho-hexagon nano spinel Co<sub>3</sub>O<sub>4</sub>, which improved the performance of activated carbon air cathode microbial fuel cell. In the successive study, Ge et al. (2016) prepared nano urchin-like NiCo<sub>2</sub>O<sub>4</sub> (nickel cobaltite) and studied its potential as a cathode catalyst in MFCs. Some mesoporous morphologies such as carnation-like MnO<sub>2</sub> (Zhang et al., 2014), mesoporous NiCo<sub>2</sub>O<sub>4</sub> nanoneedles (Liu et al., 2015) have been also experimented in MFCs. However, no findings are reported on the morphological effect of cathode catalyst on ORR in MFCs, which can be studied by selecting a material and forming its different morphologies. Cobalt or cobalt oxide has been successfully used as the cathode catalyst for ORR kinetics in MFCs and it also shows high affinity towards oxygen. Hence, the ORR activity of cobalt oxide can be further improved by fabricating its mesoporous morphologies and can be used as the cathode catalyst and further its effect on bioelectricity generation can be studied.

## 1.6 Objectives

Co<sub>3</sub>O<sub>4</sub> was selected for this research work and its different mesoporous morphologies were synthesized by the hydrothermal methods, which were further investigated for ORR in MFCs. The following sub-objectives were aimed to achieve the main objective of this research work:

1. To synthesize three morphologies of Co<sub>3</sub>O<sub>4</sub> (nanorods, flakes and flower) for cathode catalysts by hydrothermal methods and their characterization by physiochemical and microscopy techniques.
2. To fabricate cathodes with the prepared catalysts and examine their oxygen reduction activity by electrochemical techniques and investigate their potential for bioelectricity generation in MFCs.
3. To enhance the performance of Co<sub>3</sub>O<sub>4</sub> nanorods towards oxygen reduction by making a compound with Mn that is MnCo<sub>2</sub>O<sub>4</sub> nanorods and investigate its ORR activity and electricity generation potential in MFCs.

## 1.7 Scope of research

The following methodology was adopted to accomplish the above objectives.

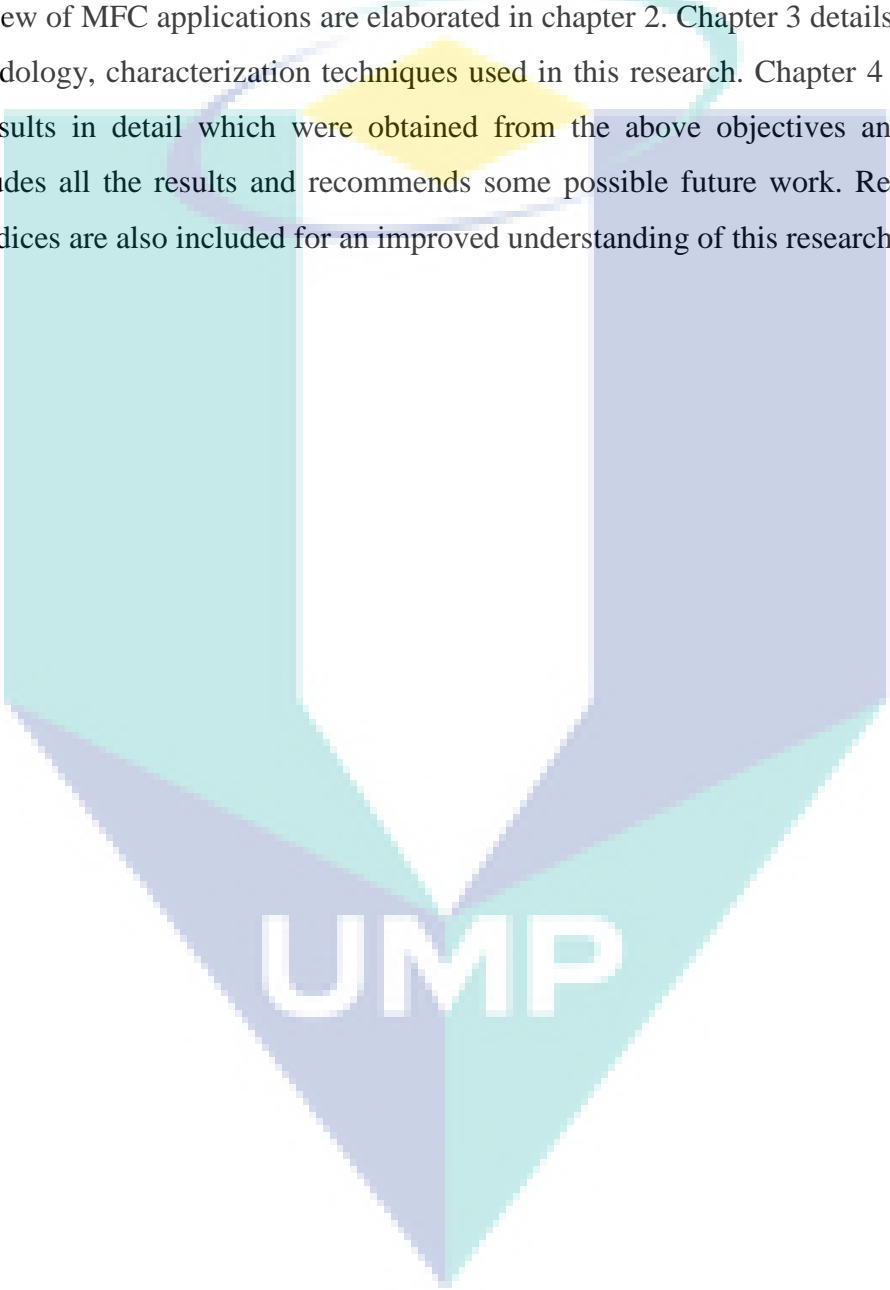
1. All the four catalysts were synthesized by a hydrothermal method.
2. The nanostructured materials prepared in each objective were identified by X-ray diffraction (XRD) technique.  $\text{Co}_3\text{O}_4$  nanorods and  $\text{MnCo}_2\text{O}_4$  nanorods were characterized by FESEM and TEM while  $\text{Co}_3\text{O}_4$  flakes and flower-like  $\text{Co}_3\text{O}_4$  were identified by FESEM.  $\text{MnCo}_2\text{O}_4$  nanorods were also identified by X-ray photoelectron spectroscopy (XPS) technique. The specific surface areas and porous properties of all the nanomaterials were studied by Brunauer-Emmett-Teller (BET) technique.
3. The nanomaterials were coated on the graphite sheets to prepare the cathodes.
4. The cathodes were further characterized by electrochemical techniques such as cyclic voltammetry (CV), linear sweep voltammetry (LSV), and electrochemical impedance spectroscopy (EIS) in 100 mM phosphate buffer saline (PBS) in a three-electrode system by using a potentiostat.
5. Oxygen reduction reaction kinetics of all the cathodes was studied by Tafel plots analysis.
6. After the electrochemical characterization of all the cathodes, they were employed in a double-chamber aqueous air-cathode MFC to investigate their performance for electricity generation. Polarization curves were performed to calculate the maximum power density generated in the MFC.

## 1.8 Novelty of study

This thesis reports the morphological effect of  $\text{Co}_3\text{O}_4$  as the cathode catalyst for ORR in MFCs for the first time. Moreover,  $\text{Co}_3\text{O}_4$  nanorods,  $\text{Co}_3\text{O}_4$  flakes, flower-like  $\text{Co}_3\text{O}_4$ , and  $\text{MnCo}_2\text{O}_4$  nanorods synthesized in this research work were used as the cathode catalyst for the first time in MFCs.

## 1.9 Thesis outline

This thesis is divided into five chapters. Chapter 1 comprises of the research problem, its objective as well as its research scope and novelty of the work. The literature review regarding the materials used in these systems including anode materials, cathode materials, cathode catalysts, proton exchange membranes, exoelectrogens, and an overview of MFC applications are elaborated in chapter 2. Chapter 3 details the research methodology, characterization techniques used in this research. Chapter 4 discusses all the results in detail which were obtained from the above objectives and Chapter 5 concludes all the results and recommends some possible future work. References and appendices are also included for an improved understanding of this research work.

The logo for UIMP (Universiti Malaysia Perlis) is a large, downward-pointing arrow shape. It is composed of four triangular sections meeting at a central point. The top-left and bottom-right sections are light blue, while the top-right and bottom-left sections are a slightly darker shade of blue. The letters 'UIMP' are printed in white, bold, sans-serif font across the center of the arrow.

UIMP

## CHAPTER 2

### LITERATURE REVIEW

#### 2.1 Introduction

In an MFC, bacteria grow on the anode and oxidize organic matter or inorganic matter, releasing electrons to the anode and protons into the solution. One of the most promising applications of MFCs is wastewater treatment, as organic matter can be removed while at the same time producing power. Oxygen is the most sustainable and cost-effective electron acceptor at the cathode, because oxygen in the air is readily available and free of charge, and air cathode MFCs avoid the need for water aeration. The high cost for materials used in MFCs remains one of the greatest challenges that need to be addressed to make the large-scale systems economically viable. A lot of progress has been made on the development of cost-effective materials for MFCs, some of which have achieved improved power production and better operational stability. This chapter is a review of MFCs with an emphasis on the materials used in these systems, including anode materials, cathode materials, cathode catalysts, proton exchange membranes, exoelectrogens, and an overview of MFC applications.

#### 2.2 Types of MFC

##### 2.2.1 Double chamber MFC

Double-chamber MFC (*Figure 2.1a*) is the simplest design among all MFCs (Niessen et al., 2004; Phung et al., 2004). In this design, one bottle (can be of different designs) is used as anode while the other one used cathode, separated by a PEM. Usually in two chambers MFC, defined medium (or substrate) in the anode and defined catholyte solution is used to generate energy. In other words, the double-chamber MFC is often operated in batch mode. The double chamber MFC may be in the shape of bottles or cube. The choice of catholyte in the MFC can define the nomenclature of the design. For

example, if the air is used in the cathode to provide the electron acceptor i.e. oxygen then the MFC can be called as two chamber air-cathode MFC (Ringeisen et al., 2004; Shantaram et al., 2005). Such MFCs may prove valuable to generate electricity in remote sensing regions.

In a double-chamber MFC, the anode and the cathode chamber are separated, therefore, it is comparatively easy to study the reaction mechanism individually in the anode and the cathode. This was the reason that a double-chamber MFC was chosen in this study.

### **2.2.2 Single chamber MFC (SC-MFC)**

This type of MFC is made up of one chamber only that contains both the anode and the cathode (*Figure 2.1b*), was introduced by Doo Hyun Park and J. Gregory Zeikus (Park and Zeikus 2003). The anode is either positioned far or near to the cathode separated by PEM. It has been stated that by decreasing inter electrode spacing internal ohmic resistance can also be diminished. This can be achieved by evading the use of catholyte as a result of joining two chambers and thus raises the power density. Such MFC is simple, economical and also produces much power in rival to double chamber MFC (Chaudhuri et al., 2003; Ringeisen et al., 2004). However, in SCMFC the major problems such as microbial adulteration and reverse passage of oxygen from cathode to anode occur normally. SCMFCs propose simpler and economic designs. Such MFCs generally have simply an anodic chamber with no requisite of air in a cathodic chamber (Rabaey et al., 2004; Rabaey et al., 2005).

### **2.2.3 Up-flow MFC**

The new designed came into existence with increase in the interest in MFC research. The Up-flow MFC is cylinder shaped MFC (*Figure 2.1c*) (He et al., 2006). The MFC is made up of the cathode chamber at the top and the anode at the bottom. Both the chambers are apportioned by glass wool and glass beads layers. The substrate is provided from the bottom of the anode that moves upward to the cathode and leaves at the top. A gradient is formed between the electrodes which also help in the favourable action of the fuel cell (Cheng et al., 2006a). In his design, there are no distinct anolyte and catholyte. Moreover, it does not have any physical parting. Therefore, proton transmission related difficulties are very less (Zhou et al., 2013; Venkata et al., 2014).

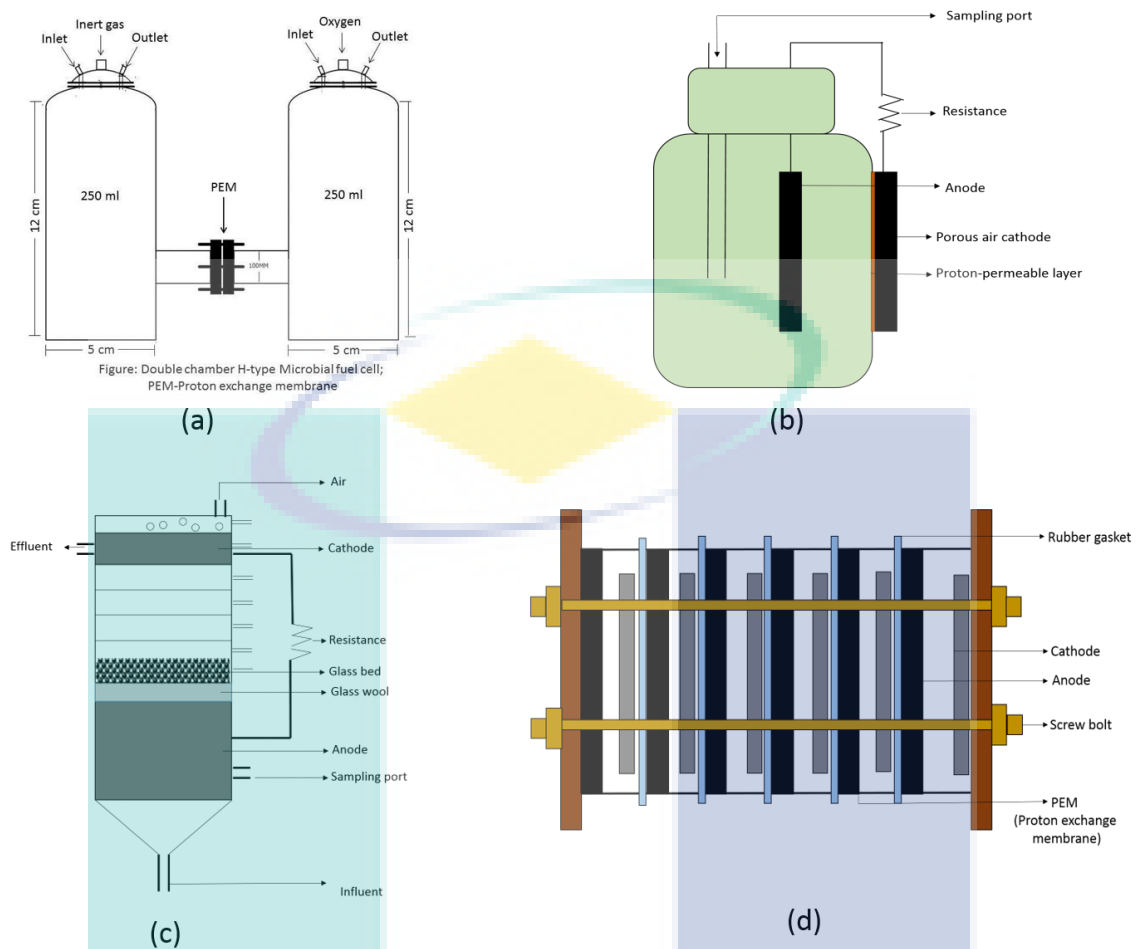


Figure 2.1 Different MFC designs (a) double chamber MFC, (b) single chamber MFC, (c) tubular up-flow MFC, and (d) stacked MFC.

Up-flow mode MFCs are fascinating for wastewater treatment since they can be easily scaled-up as compared to other designs of MFCs. However, the major drawback of the fuel cell is the energy costs to pump the substrate that are highly greater than their power outcome (Zhou et al., 2013). So we can conclude that the prime purpose of up-flow MFC is wastewater treatment instead of power generation (Brutinel et al., 2012). These kinds of MFCs are commonly employed in basic research and the studies propose that the power densities are low due to high internal resistance, electrode based losses and complex design.

#### 2.2.4 Stacked MFC

A stacked MFC is generally a combination of some MFCs that are either coupled in series or in parallel to enhance the power output (Logan and Regan 2006; Aelterman et al., 2006; Sun et al., 2012). A diagram of stacked MFC is depicted in *Figure 2.1d*. The

output of MFC is increased by connecting some MFCs by multiplying individual power output or current output. Generally, a single unit of MFC (with oxygen as an electron acceptor) can generate a maximum an open circuit voltage (OCV) of 0.8 V (Logan et al., 2006). Therefore, a number of MFC unit cells can be stacked in a series or parallel connection and their individual power output can be multiplied to get the resultant power output. However, some other operational factors also play an important role in current generation in a stacked MFC, which can either decrease or increase the overall performance of the MFC (Zhou et al., 2013; Venkata et al., 2014). Moreover, after connecting the individual MFC in a stacked MFC, the final voltage may not be exactly the total of the individual cell voltages because there will be a loss of voltage when every cell is connected either in series or parallel. The parallel-connected stack MFCs have proven to produce more current as in rival when the MFCs are stacked in a series connection. Therefore, we can say that in parallel-connected stack MFCs higher bioelectrochemical reaction rate is achieved than in series-connected stack MFCs (Gil et al., 2006). Moreover, a parallel connection is favoured to maximize Chemical Oxygen Demand (COD) removal for enhanced wastewater treatment efficiency, if the MFC units are not autonomously functioned. In a successful study, six MFCs were connected in series or in parallel with copper wires. The MFC was fed with acetate as substrate in the anode and ferricyanide as the catholyte and graphite rods were used as the anode and the cathode. The results of the study demonstrated that the stacked MFC in a series connection produced a volumetric power density of  $59 \text{ W/m}^3$  and when connected in parallel generated  $51 \text{ W/m}^3$  of power density (Aelterman et al., 2006).

The coulombic efficiency (CE) in MFCs can give the estimation of the electrons transferred (from the total electrons generated theoretically from substrate oxidation) from the anode that help to generate the current. In stacked MFCs, the different rates of CE can be achieved while linking the cells in different connections. The former study exhibited that the stacked MFC achieved higher rate of CE when operated in parallel i.e. 78 % than in series that produced the CE of only 12 %. The major obstacle in stack MFC to achieve higher voltage outputs is the voltage reversal. The voltage reversal may be due to the depletion of the substrate in the cell, pointing to the diminished ability of the bacteria to produce higher voltage (Logan and Regan 2006; Aelterman et al., 2006).

### 2.2.5 Other designs

The basic designs of MFCs are overwhelmingly used for the studies, and less attention is paid to develop new designs to overcome the drawbacks of the existing designs. In order to diminish one obstacle, a Flat Plate MFC (FPMFC) in 2005 was designed by Min and Logan to reduce the ohmic resistance that is caused due to more inter electrode spacing (Min et al., 2005a). This kind of design is generally used in chemical fuel cells; also generate more power than the former designs. In FPMFC, the anode and the cathode were made up of flat plates (each plate with a projected surface area of 225 cm<sup>2</sup>). A Nafion membrane was placed between the two plates. This reactor generated the power density of 56 mW/m<sup>2</sup> with domestic wastewater as a substrate and 58 % COD was achieved in the study (Min et al., 2005a). The reactor was also used to produce power with other substrates like acetate, glucose, starch etc. but produced less power output than the other designs i.e. cube reactor. It may be due the too closely joined electrodes and oxygen may pass through the membrane to the bacteria in the anode chamber, therefore, affecting the growth of the microbial community (Phung et al., 2004; Patil et al., 2011).

### 2.3 Electrode materials

In the MFCs, the anode and the cathode are made up of the electrode material that should be conductive in nature, non-corrosive, non-fouling to the bacteria (in case of anode), cost effective. The electrode material with high surface area also increases the performance of the MFC (Zhang et al., 2012; Alatraktchi et al., 2014). The development of the electrodes for the MFC has reached to the higher level. Moreover, many electrodes with modification of nanoparticles have produced electricity manifold than the plain electrodes. In the anode, the electrode modification with the nanomaterial or catalyst that can support the biofilm formation and increase the electron transfer rates is highly beneficial for increased power output. For example, magnetite nanoparticles increased the current production in the MFC using *G. sulfurreducens* as an inoculum. (Alatraktchi et al., 2014) The study found that the nanoparticles increased the electrical conductivity of biofilm-electrode interface, thus boosted the electron transfer mechanism. In the cathode, Pt or Pt-coated cathodes produced higher electric current as compared to plain cathodes containing no catalyst. Pt has been regarded the best catalyst for oxygen (when used as

electron acceptor) reduction in MFCs (Bond and Lovely 2003), but its higher cost is also one of the obstacles for the technology to get launched at large scale applications.

### **2.3.1 Anode Materials**

Electrode materials play an important role in the performance (e.g., power output) and cost of MFCs, which use bacteria as the catalysts to oxidize organic (inorganic) matter and convert chemical energy into electricity. A good anode material should have the following properties: (a) good electrical conductivity and low resistance; (b) strong biocompatibility; (c) chemical stability and anti-corrosion; (d) large surface area; and (e) appropriate mechanical strength and toughness.

#### **2.3.1.1 Conventional carbon materials**

Carbon materials are the most commonly used anode materials as they are electrochemically and biologically stable, they can provide high specific surface area for biofilm growth, and they have good electrical conductivity. Various carbon materials have been examined and compared in MFCs. It has been found that increasing the accessible surface area to bacteria increase the current density, but the performance of different anode materials also depends on various other factors, such as reactor configuration, electrode spacing, substrate type and solution conductivity. The conventional anode materials (*Figure 2.2*) used in MFCs are graphite rod, graphite fiber brush, carbon cloth, carbon paper, carbon felt, and reticulated vitreous carbon (RVC).

Graphite rod has become one of the most commonly used electrodes in MFCs due to its excellent electrical conductivity and chemical stability. The most representative work was done by Liu et al. (2004), in which a single-chamber MFC included eight graphite rod anodes and an air cathode was developed. A maximum power of 26 mW/m<sup>2</sup> and 80% COD removal were fulfilled, using sewage from the primary sedimentation tank of a treatment plant as fuel. However, the application of the graphite rod was limited because of its low porosity and surface area for microorganism adsorption. Chaudhuri and his co-workers found that the power output was much larger when the graphite rod was replaced instead by graphite felt, indicating that increasing the surface area was beneficial to the performance of the MFC (Chaudhuri et al., 2003).

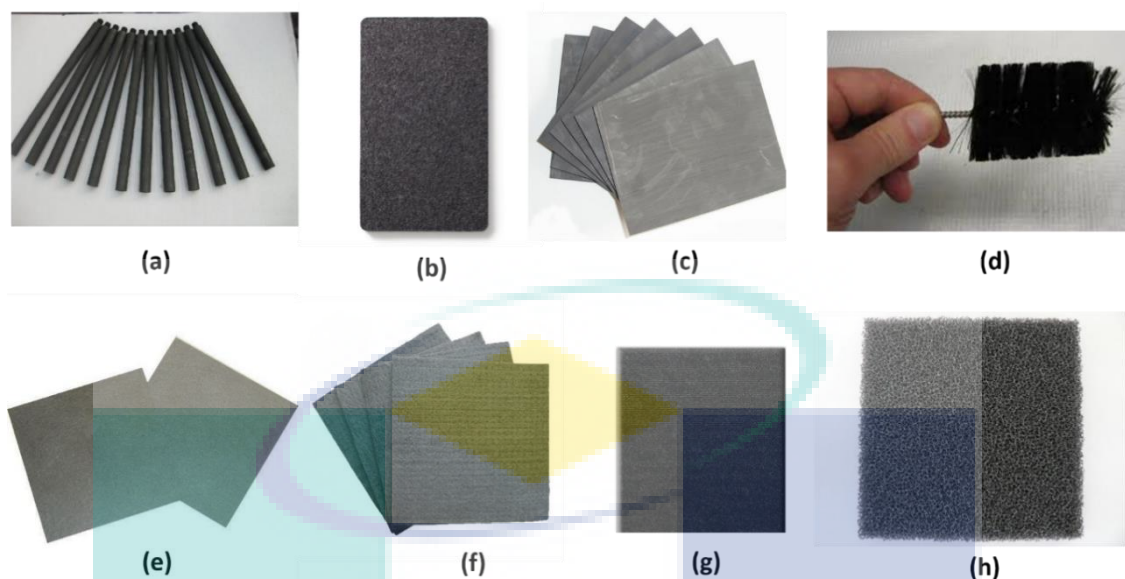


Figure 2.2 Pictures of anode materials (a) graphite rod, (b) graphite felt, (c) graphite sheet, (d) graphite brush, (e) carbon paper, (f) carbon felt, (g) carbon cloth, and (h) reticulated vitreous carbon.

Carbon paper and carbon cloth, which are often applied in the hydrogen fuel cells, are now used in MFCs as flat-plate electrodes. These kinds of electrodes benefit from a reduction in the distance between the two electrodes to improve the performance of the MFCs. Kim et al. (2007) constructed a dual-chamber MFC with carbon paper, and the power density was up to  $40 \text{ mW/m}^2$ . Wang et al. (2008) built a single-chamber MFC that used carbon cloth as the electrode and actual brewery wastewater as the anode substrate, and the maximum power density was  $483 \text{ mW/m}^2$ .

RVC is less frequently used in MFCs as compared with the carbon materials due to its large resistance. He et al. (2005) obtained a power density of  $170 \text{ mW/m}^2$  in an upflow MFC using RVC as the anode material. Moreover, RVC, with a surface area of  $51 \text{ m}^2/\text{m}^3$ , was tested in a two chamber packed-bed upflow MFC as both anode and cathode, and it produced  $170 \text{ mW/m}^2$  (based on anode surface area;  $8.7 \text{ W/m}^3$  based on anode chamber volume) (He et al., 2005).

In addition, graphite granules, with diameters of 1.5-5 mm, specific surface areas of  $817\text{-}2720 \text{ m}^2/\text{m}^3$ , were used as the anode material in a tubular packed-bed reactor (total anode compartment volume of 0.39 L), producing  $48 \text{ W m}^{-3}$  with acetate and  $38 \text{ W/m}^3$  with glucose (Rabaey et al., 2005). When this material was used for both the anode and

cathode, six individual continuous MFC units in a stacked configuration produced a maximum power of 258 W/m<sup>3</sup> (hourly average) with acetate as the fuel, and a hexacyanoferrate catholyte (Aelterman et al., 2006). For the packed-bed reactors, the anode granules need to make good electrical connections to make the complete bed conductive, which is difficult to achieve due to the shape of granules and the bed porosity. These carbon granules are also heavy and could clog due to relatively low porosities.

### **2.3.1.2 Nanomaterials**

Nanomaterials, such as carbon nanotubes (CNTs) and graphene, have drawn intensive attention in MFC anode studies due to the large surface area provided by these materials, and the improved electron transfer between bacteria and the electrode surface (Minteer et al., 2012). Nanomaterials have been applied as decoration materials for modifying existing anode materials. It has been shown that a glassy carbon electrode modified with CNT promoted direct electron transfer with *Shewanella oneidensis* (Peng et al., 2010). CNTs and nanostructured titanium dioxide have been added to polyaniline coated nickel foam anodes to enhance electrical conductivity, and these showed improved performance compared to anodes with only polyaniline (Qiao et al., 2007). However, *Escherichia coli*, a non-exoelectrogen was used as anode inoculum in their studies, and the nickel foam can corrode under these conditions. Although one study showed that strain evolution eventually resulted in current generation by *E. coli* using a carbon/PTFE composite anode (Zhang et al., 2006), this bacterium failed to generate current in most studies, and it has been used as a negative control for current production (Qu et al., 2012). Multi-wall CNT modified carbon cloth or carbon paper anodes have shown improved power production compared to a plain anode in single chamber air cathode MFCs (Sun et al., 2010; Tsai et al., 2009). Simultaneously adding CNT powders with a *Geobacter sulfurreducens* inoculum into the anode chamber showed improved stability, in terms of voltage production and internal resistance over 40 days, compared to MFCs without CNT addition (Liang et al., 2011). Therefore, anode modifications with nanomaterials are a feasible method to improve MFC performance.

### **2.3.1.3 Metal materials**

Metal materials are much more conductive than carbon materials, and they have been used as current collectors in several studies (Xie et al., 2012; Liang et al., 2011). In large scale applications, the metal current collectors are likely to be necessary to ensure

good conductivity of the large electrodes. The metal materials need to be non-corrosive, and titanium and certain type of stainless steel meet this requirement. It has been shown that stainless steel with 6% of molybdenum can be used as an anode even in seawater (Dumas et al., 2007). Thus, this type of stainless steel can be used as an alternative to expensive titanium when anode current collectors are needed (Logan et al., 2007).

### **2.3.2 Cathode materials**

In this section, the focus was given primarily on air-cathode materials because: (1) oxygen in the air is the most sustainable and economical electron acceptor for MFC applications; (2) this configuration has produced high power densities; and (3) aeration should be avoided in large scale systems as it is an energy intensive process. Cathode performance is usually the limiting factor for power production in most air cathode MFC studies (Natarajan et al., 2003; He et al., 2006; Zhao et al., 2006), due to the poor kinetics of oxygen reduction at neutral pH and ambient temperature, and mass transfer limitations (Adler et al., 1998). It has been recognized that cathode geometry is not as important as surface area, as power densities are essentially the same with either tubular cathodes or flat cathodes, as long as the same materials and same surface areas are used (Zuo et al., 2011). Cathode surface area and the performance are therefore the most important factors for scaling up MFCs.

Air cathodes usually consist of a supporting material, a diffusion layer (facing air) to prevent water leakage and sometimes to control oxygen transfer, and a catalyst layer (facing solution) for catalysing oxygen reaction. However, in this research work, the catalyst was coated on both side of the cathode and applied them in double-chamber MFCs instead of a single chamber MFC and the cathode with a diffusion layer.

#### **2.3.2.1 Cathode supporting material**

Carbon cloth or carbon paper have been commonly used as MFC cathode supporting materials, but fuel cell grade carbon cloth is very expensive (\$1000 per m<sup>2</sup>). Various materials have been tested as low-cost alternatives, including non-conductive materials coated with a conductive paint (Zhuang et al., 2009; Zuo et al., 2007), and different types of metal mesh (Chen et al., 2012). Membranes including cation and anion exchange membranes (AEM, CEM) and ultrafiltration (UF) membranes were examined as cathode supporting materials for air cathodes (Zuo et al., 2007). A graphite conductive layer was coated outside the membrane to make the surface conductive, but power

production was still limited by the poor conductivity of the supporting materials. The highest maximum power of  $449 \text{ mW/m}^2$  was produced by the AEM cathode, due to the lower internal resistance of AEM compared to CEM or UF membranes. Pressing a piece of stainless steel mesh against the AEM membrane increased the power by 28%, with a 38% reduction of internal resistance due to the improved conductivity (Zhuang et al., 2009). Canvas cloth was also tested with either nickel or graphite based conductive paint using a non-precious catalyst of  $\text{MnO}_2$  in a tubular reactor (170 mL empty volume) (Zuo et al., 2011). More power ( $86 \text{ mW/m}^2$ ,  $10 \text{ W/m}^3$ ) was obtained with nickel paint due to its higher electrical conductivity than the graphite paint. Although this cathode assembly costs only 5% of that of membrane cathodes, its power production was still primarily limited by the conductivity of canvas materials.

Another alternative is to replace the carbon cloth with a current collector that is very conductive, such as stainless steel (SS) or nickel mesh, and to build a catalyst layer (Pt with carbon black, or activated carbon) around the metal mesh. Current collectors are necessary to ensure electrical conductivity for large electrodes. In a study, metal mesh was used as the cathode supporting material to replace carbon cloth (Chen et al., 2012). This approach inherently integrated the current collector into the cathode structure. SS mesh cathodes produced similar power densities to carbon cloth cathodes, with a poly(dimethylsiloxane) (PDMS)/carbon black diffusion layer (Chen et al., 2012). SS mesh was also tested with polymethylphenyl siloxane as the diffusion layer (Mink et al., 2012). Inexpensive carbon mesh, which has been used as a low-cost anode, was also tested as a cathode material. Carbon mesh with a PDMS/carbon black diffusion layer produced the highest power among the carbon mesh cathodes with different diffusion layers, and the power density was close to that of a carbon cloth cathode with a polytetrafluoroethylene (PTFE) diffusion layer (Cheng et al., 2007). Although carbon mesh cathodes need current collectors in large scale applications, less metal is needed with a carbon mesh than an electrode made primarily using only SS mesh, and therefore the reduced cost may justify the use of the carbon mesh.

### 2.3.2.2 Cathode Catalyst

#### *Platinum*

Platinum (Pt) is a very effective catalyst for oxygen reduction, and it has been widely used in fuel cell studies, but it is expensive (\$140/g) and prone to fouling. Studies have shown that decreasing the Pt amount to as low as  $0.1 \text{ mg cm}^{-2}$  will not appreciably affect power densities in air cathode MFCs (Cheng et al., 2006). Development of biofilm on the cathode could inhibit proton transfer, causing decreased power production. Removal of biofilm developed on a Pt/C cathode completely restored cathode performance after 42 days of operation (Zhang et al., 2009). However, a longer-term test of one year with Pt/C cathodes showed that there was significant degradation in performance over time. Power was increased up to 26% when the cathode biofilms were removed, and by 118% when new cathodes were used (Kiely et al., 2011). Thus, development of cathode biofilm alone was not the primary reason for the long-term degradation in cathode performance.

Vulcan XC-72 carbon black is the most commonly used support for Pt. Better catalyst supports such as CNTs (Wang et al., 2011; Shao et al., 2008), or better methods for applying the catalyst, such as electrochemical deposition (Xie et al., 2011) and plasma sputtering (Lefebvre et al., 2012a), have shown improved performance compared to cathodes made using the more typical painting method. In another study, polyamidoamine dendrimer-encapsulated platinum nanoparticles showed better performance with a lower loading amount than electrodeposited Pt (Yang et al., 2011). However, the use of Pt catalyst is still not cost-effective due to its extremely high cost. Low-cost alternatives with better long-term stability are needed for practical applications.

#### *Carbon-based catalysts*

Carbon black (CB) is a product from incomplete combustion or thermal decomposition of hydrocarbons (Donnet, 1993). Due to its high stability and large specific surface area, CB is widely used as the support material for metal catalysts (Donnet, 1993). However, simple chemical modification and/or the introduction of functional groups can create active sites that make CB itself a metal-free ORR catalyst. For example, in a study treating CB with nitric acid, the maximum power density (MPD) of the MFC equipped with the modified CB was 3.3 times that with pristine CB and was 78% of that with Pt/C (Duteanu et al., 2010) Similar enhancement in MPD (71% of that with Pt/C) was reported

in another study by using nitric acid and ammonia gas as treatment reagents, which was likely attributed to the successful introduction of oxygen and nitrogen atoms on the CB surface (Yang et al., 2014).

Activated carbon (AC) refers to porous carbon materials (surface area  $> 1000 \text{ m}^2\text{g}^{-1}$ ) that are produced by the thermal or chemical activation of a wide range of carbonaceous precursors (Marsh & Reinoso, 2006). A number of modifications of AC have been carried out to improve the performance of AC in MFCs. For example, chemical treatment with alkaline or acid has also been reported to enhance ORR performance via the formation of possible chemical bonding. The AC pre-treated with potassium hydroxide reduced the internal resistance and yielded a MPD 16% higher than the untreated AC did, possibly because of the increased electrolyte-catalyst affinity caused by the adsorbed OH (Wang et al., 2013). Meanwhile, the pre-treatment of AC with phosphoric acid at 80 and 400 °C showed 35% and 55% increase in the MPD, respectively (Chen et al., 2014). The introduction of non-acidic oxygen content and P in the form of C-O-P bonding might account for the improved catalysis (Chen et al., 2015). On the other hand, the acidic functional groups resulting from  $\text{H}_3\text{PO}_4$  treatment were speculated to be detrimental to ORR catalysis (Chen et al., 2015). Treatment using nitrogen-containing chemicals is one of the most effective methods for improving the ORR catalysis of AC as it can achieve multiple benefits. Treating AC in ammonia gas at 700 °C not only removed oxygen functional groups, but also introduced nitrogen atoms, leading to a MPD ( $2,450 \text{ mW/m}^2$ ) 28% higher than untreated AC and 16% higher than Pt/C, respectively (Watson et al., 2013). Nitrogen doping has been demonstrated to be an effective strategy to enhance catalytic activity (Dai et al., 2015). Three different types of doped nitrogen may play important roles in ORR catalysis: graphitic-N may favour the reduction of  $\text{O}_2$  to  $\text{H}_2\text{O}_2$  via the  $2\text{-e}^-$  pathway, whereas pyridinic- and pyrrolic-N are likely to contribute to the  $4\text{-e}^-$  pathway (Lai et al., 2012; Wang et al., 2012). A recent study reported a N-doped AC catalyst with a remarkably high nitrogen content (8.65% total N and 5.56% pyridinic-N) by acid/alkaline pre-treatment and using cyanamide as the nitrogen precursor (Zhang et al., 2014). The modified AC achieved an electron transfer number of 3.99 and a MPD ( $650 \text{ mW/m}^2$ ) 44% higher than Pt/C. In addition to nitrogen-doping, nitrogen containing chemicals such as ammonium bicarbonate could serve as a pore former to increase porosity and alter pore size distribution, which could reduce charge transfer resistance and consequently, enhance the MFC performance (Li et al., 2014).

Carbon nanofibers (CNFs) are composed of stacked corn-shape graphene sheets and show high electrical conductivity and high BET specific surface area (Huang et al., 2010). The performance of CNFs can be improved by the similar methods utilised for the improvement of AC. For example, immersing CNFs into 8 M KOH solution increased its surface area from  $275 \text{ m}^2 \text{ g}^{-1}$  to  $2100 \text{ m}^2 \text{ g}^{-1}$ , and consequently, enhanced the MPD by 79% with respect to the untreated CNF (Ghasemi et al., 2011). However,  $\text{HNO}_3$  treatment of CNFs did not significantly change the BET surface area, but shifted the pore size distribution, which might favour ORR catalysis (Santoro et al., 2013). In addition, nitrogen-doped CNFs via the pyrolysis of pyridine showed high catalytic activity and obtained a MPD comparable to that with Pt/C (Chen et al., 2012). The combination of nitrogen doping and chemical activation with KOH yielded a CNF material with large BET surface area ( $1,984 \text{ m}^2 \text{ g}^{-1}$ ) and high catalytic activity (electron transfer number 3.6), and the MFC equipped with the modified CNFs generated a MPD ( $1,377 \text{ mW/m}^2$ ) similar to that of the Pt/C-based MFC (Yang et al., 2014). Recently, heteroatom-doped porous CNFs were obtained via the pyrolysis of natural spider silk (Zhou et al., 2016). Owing to the abundant electronegative N and S atoms within the carbon lattice and the high BET surface area ( $721.6 \text{ m}^2 \text{ g}^{-1}$ ), the CNFs achieved a MPD of  $1,800 \text{ mW/m}^2$ , 1.6 time higher than Pt/C.

Carbon nanotubes (CNTs) are one or multiple layers of graphene sheets wrapped in a concentric manner, whose catalytic activity can be tuned by heteroatom doping (Van Dommele et al., 2008). It has been reported that vertically aligned nitrogen-doped CNTs catalyse ORR mainly via the  $4\text{-e}^-$  pathway (Feng et al., 2011). The N-doped CNTs showed lower internal resistance and more positive onset potential in cyclic voltammetry (CV) tests compared to Pt/C (He et al., 2016). In addition to pre-treatment and nitrogen doping, mixing CNTs with a conductive polymer, such as polyaniline (PANI) or polypyrrole (PPy), presents a simple method to enhance the cathode performance (Jiang et al., 2014, Ghasemi et al., 2016). Although the ORR catalysis of those CNT/polymer composites was slightly inferior to that of N-doped CNTs and Pt/C, the simple and large-scale production makes them competitive alternative catalysts for practical applications.

Graphite is multiple layers of carbon sheet bonded through weak van-der-Waals interaction. Due to its high electrical conductivity and high stability, graphite is commonly used as a fuel cell electrode (Chung et al., 2002). Exfoliation of graphite can form single layer carbon nanosheets known as graphene (Novoselov et al., 2004). With

high electrical conductivity and high BET surface area, graphene-based cathode catalysts have been demonstrated to effectively catalyse ORR in MFCs.

Graphite is usually not considered catalytic toward ORR because of the lack of active sites. However, the MFC filled with granular graphite generated a stable MPD of  $50 \text{ W/m}^3$ , comparable to many common catalysts (Freguia et al., 2007). Furthermore, the COD removal ( $1.46 \text{ kgm}^{-3}\text{d}^{-1}$ ) by the graphite-based MFC was higher than that of conventional aerobic processes, which was of practical significance regarding wastewater treatment. Activation of graphite with  $\text{HNO}_3$  and  $\text{H}_3\text{PO}_4$  could enhance the MPD by 2 and 2.4 times, respectively (Erable et al., 2009; Zhang et al., 2016). In another study, the graphite treated with  $\text{HNO}_3$  achieved a MPD similar to that with Pt/C, which could be attributed to the high BET surface area of the modified graphite and the introduction of nitrogen and oxygen functional groups (Shi et al., 2012).

The modification of graphene has mainly focused on the doping of heteroatoms. Detonation of cyanuric chloride and trinitrophenol could effectively incorporate three different nitrogen species (i.e., pyridinic-N, pyrrolic-N, and graphitic-N) in graphene, leading to a high electron transfer number of 3.7 (Wen et al., 2014). Implantation of mesoporous graphitic carbon nitride in N-doped graphene further enhanced the catalytic activity (complete  $4\text{-e}^-$  ORR pathway), and yielded a MPD of  $1,618 \text{ mW/m}^2$ , 14% higher than Pt/C (Feng et al., 2011). The co-doping of nitrogen and sulfur in carbon could provide dual active sites for ORR catalysis (Liang et al., 2012). The N/S co-doped carbon nanosheets produced lower MPD but comparable current density to Pt/C, suggesting that this catalyst could be used in bioelectrochemical systems that required high current output (Wang et al., 2016). Graphene and N-doped graphene generally have relatively low surface area, which can be increased by using KOH activation (Wen et al., 2014). A more direct way to increase the BET surface area is to prepare crumpled graphene particles by capillary compression in rapidly evaporating aerosol droplets (Luo et al., 2011; Xiao et al., 2012).

#### *Metal-based catalysts*

Many pure metals exhibit strong ORR catalytic activity. For example, noble metal Pt is considered to be the most active catalyst for ORR in MFCs. Many efforts have been devoted to reduce the amount of Pt loading on the MFC cathode without compromising the catalytic performance. The deposition of Pt on carbon paper with electron beam

evaporation reduced the thickness of the Pt layer and minimized Pt loading, but significantly increased the current output of the MFC. A more practical way of reducing the loading is to alloy Pt with inexpensive transition metals, such as Fe, Co and Ni (Zhang et al., 2011; Chang et al., 2014), which has been studied to further reduce the oxygen binding energies and enhance the catalytic activity (Nørskov et al., 2004). With proper Pt: metal ratios, Pt-based alloys could generate higher MPDs than commercial Pt/C (Yan et al., 2014).

Cobalt or cobalt oxide has been successfully used as the cathode catalyst for improved ORR kinetics in MFCs (Hou et al., 2016; Li et al., 2016; Liu et al., 2014; Song et al., 2015; Xu et al., 2012; Yang et al., 2016). In a study,  $\text{Co}_3\text{O}_4$  micro-particles were directly grown on stainless steel mesh by using an ammonia-evaporation-induced method. The cathode used in a double chamber MFC produced a maximum power of  $17.8 \text{ W/m}^3$ , which was manifolds higher than the bare stainless steel mesh (Gong et al., 2014). Moreover, in an alternative demonstration,  $\text{Co}_3\text{O}_4$  nanosheets decorated on activated carbon was used as the air cathode that generated the maximum power density of ca.  $1420 \text{ mW/m}^2$  and exhibited an exchange current density 2.6 times higher than the control (Liu et al., 2016). Cobalt has also been used in many composite catalysts for ORR with a variety of morphologies. For example, nitrogen-doped graphene/CoNi alloy encased within bamboo-like carbon nanotube hybrids (N-G@CoNi/BCNT) was developed as cathode catalyst, which exhibited a high ORR activity and analogous exchange current density as compared to commercial available Pt/C (Hou et al., 2016). The performance of various cobalt based cathode catalyst in MFCs is given in Table 2.1. A MFC employed with a cathode that is carbon cloth coated with  $\text{Co}_3\text{O}_4$ /carbon nanotubes produced a maximum power density of  $469 \pm 17 \text{ mW/m}^2$ , which was competitive with the cathode containing carbon cloth/platinum ( $603 \pm 23 \text{ mW/m}^2$ ) (Song et al., 2015). Moreover, in an alternative study, nano cobalt oxide anchored on nitrogen-doped graphene was used as cathode catalyst in a single-chambered MFC that generated a maximum power output of  $713.6 \text{ mW/m}^2$ , which was  $\sim 25\%$  more than platinum (Hou et al., 2016). The other approach that is widely used to improve the ORR activity of the catalysts is synthesizing the porous structure of metals/metal oxides. The porous nanomaterial provides numerous extra active sites for oxygen reduction that play a key role in enhancing the ORR kinetics of the catalyst (Haoran et al., 2014). Evidently, such porous catalysts have shown faster ORR rate as compared to other conventional cathode

catalysts. For example, recently, porous ortho-hexagon nano spinel  $\text{Co}_3\text{O}_4$  showed a maximum exchange current density of  $18.86 (10^{-4} \times \text{A m}^{-2})$ , which was  $\sim 2.2$  times higher than the non-porous commercial  $\text{Co}_3\text{O}_4$  (Ge et al., 2015). The Figure 2.3 shows that the cathode catalysts with mesoporous morphology produce significantly higher power density as compared to conventional cathode catalysts.

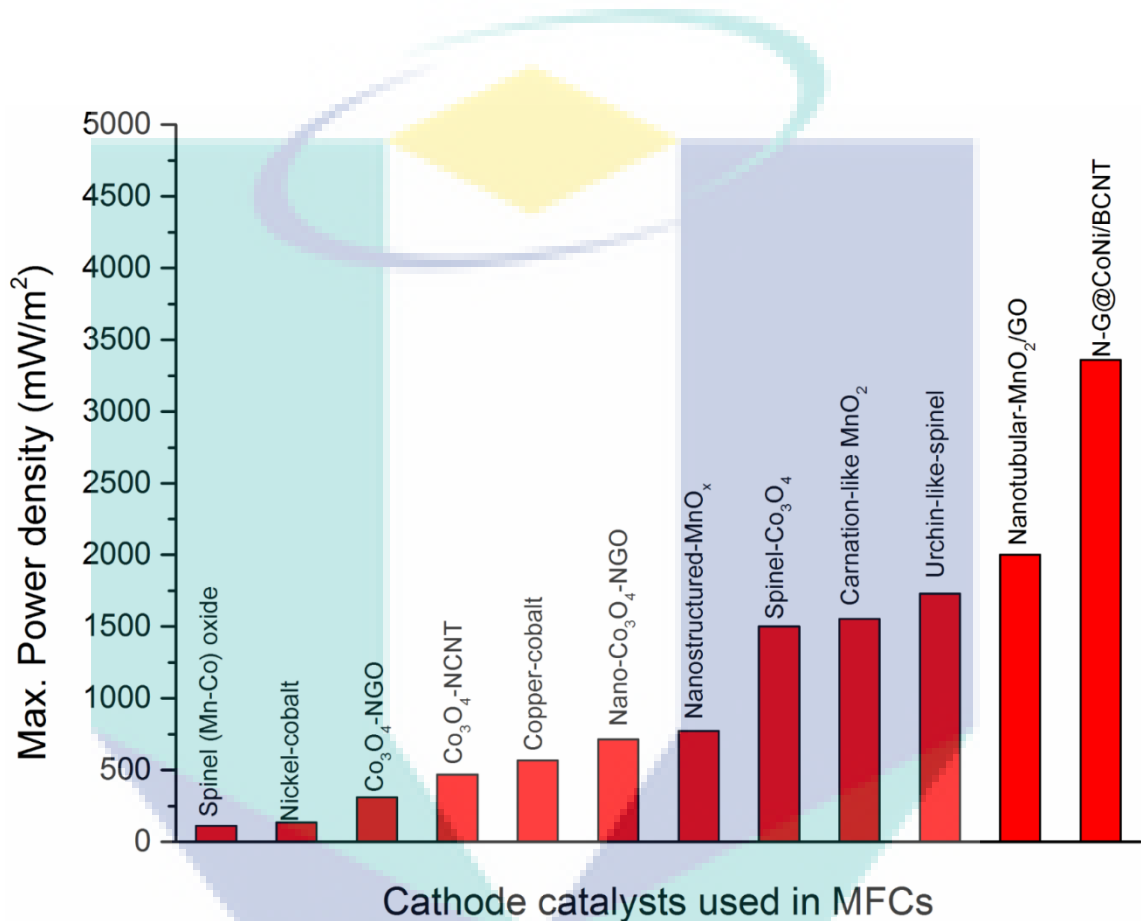
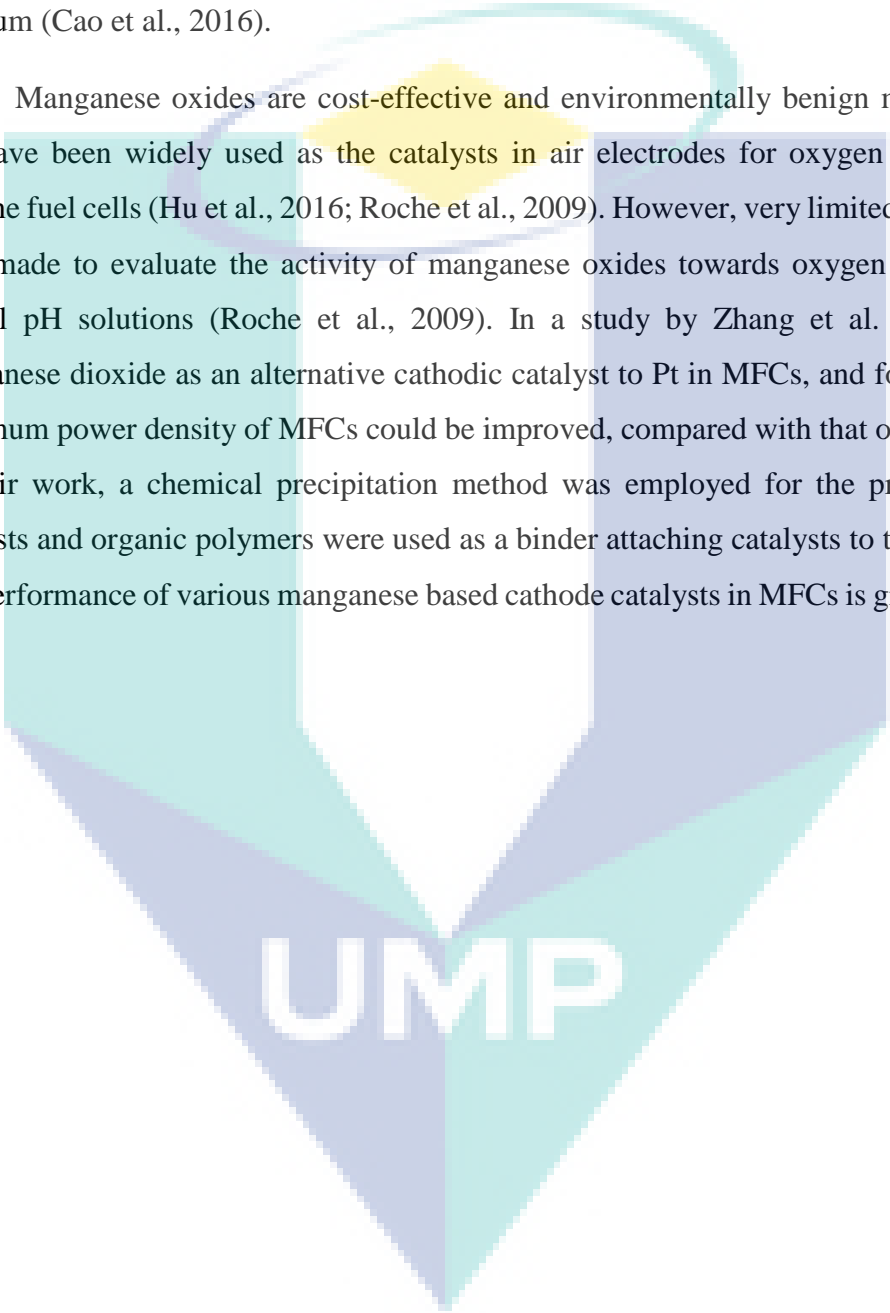


Figure 2.3 Comparison of power generation by cathode catalysts with mesoporous architecture with conventional cathode catalysts.

The catalysts with unique morphology or structure may also exhibit additional active sites for oxygen, which might be responsible for higher ORR activity. For example, recently, mesoporous nano urchin-like  $\text{NiCo}_2\text{O}_4$  was successfully synthesized by hydrothermal method. The mesoporous  $\text{NiCo}_2\text{O}_4$  provided more active sites for oxygen, improving the electrocatalytic activity significantly. The cathode showed a maximum exchange current density of  $25.49 (\times 10^{-4} \text{ A m}^{-2})$  and a maximum power density of ca.  $1730 \text{ mW m}^{-2}$ , which was 2.28 times higher than the control (Ge et al., 2016). Moreover, , an MFC employed with a cathode that is carbon cloth coated with

$\text{Co}_3\text{O}_4$ /carbon nanotubes produced a maximum power density of  $469 \pm 17 \text{ mW/m}^2$ , which was competitive with the cathode containing carbon cloth/platinum ( $603 \pm 23 \text{ mW/m}^2$ )(Song et al., 2015). In an alternative study, nano cobalt oxide anchored on nitrogen-doped graphene was used as cathode catalyst in a single-chambered MFC that generated a maximum power output of  $713.6 \text{ mW/m}^2$ , which was ~25% more than platinum (Cao et al., 2016).

Manganese oxides are cost-effective and environmentally benign metal oxides, and have been widely used as the catalysts in air electrodes for oxygen reduction in alkaline fuel cells (Hu et al., 2016; Roche et al., 2009). However, very limited efforts have been made to evaluate the activity of manganese oxides towards oxygen reduction at neutral pH solutions (Roche et al., 2009). In a study by Zhang et al. (2009) used manganese dioxide as an alternative cathodic catalyst to Pt in MFCs, and found that the maximum power density of MFCs could be improved, compared with that of no catalyst. In their work, a chemical precipitation method was employed for the preparation of catalysts and organic polymers were used as a binder attaching catalysts to the electrode. The performance of various manganese based cathode catalysts in MFCs is given in Table 2.1.

The logo of UMPA (Universitas Mitra Widyacarya) is a large, stylized letter 'V' shape. The top part of the 'V' is a light blue oval. The two sides of the 'V' are composed of overlapping geometric shapes in shades of light blue and teal. At the bottom of the 'V', the letters 'UMPA' are written in a bold, white, sans-serif font.

UMPA

Table 2.1 Performance of cobalt and manganese based cathode catalysts in air-cathode microbial fuel cells.

Catalyst	Cathode	MPD (mW/m <sup>2</sup> )	Reference
Co-naphthalocyanine	Carbon paper	64	(Kim et al., 2011)
Copper-cobalt	Carbon cloth	567	(Ortiz et al., 2016)
Nickel-cobalt	Carbon cloth	136	(Ortiz et al., 2016)
Co <sub>3</sub> O <sub>4</sub> -iron-PC	Carbon cloth	654	(Ahmed et al., 2012)
Co <sub>3</sub> O <sub>4</sub> -NGO	Carbon cloth	312	(Song et al., 2015)
Co <sub>3</sub> O <sub>4</sub> -NCNT	Carbon cloth	469	(Song et al., 2015)
Co/Fe/N/CNT	Carbon cloth	751	(Deng et al., 2010)
Co <sub>3</sub> O <sub>4</sub> nanoparticles	Carbon cloth	780	(Ahmed et al., 2014)
Co-nitrogen-carbon	SS mesh	1665	(You et al., 2014)
Nano-Co <sub>3</sub> O <sub>4</sub> -NGO	Carbon cloth	713	(Cao et al., 2016)
Binuclear-Co-PC	Carbon cloth	368	(Li et al., 2014)
Co/Co <sub>9</sub> S <sub>8</sub> /NPGC	SS mesh	1117	(Li et al., 2016)
N-G@CoNi/BCNT	Carbon cloth	2000	(Hou et al., 2016)
Spinel (Mn-Co) oxide	Carbon paper	113	(Mahmoud et al., 2011)
Pyrolyzed-Co-PC	Carbon cloth	604	(Li et al., 2015)
Spinel- Co <sub>3</sub> O <sub>4</sub>	SS mesh	1500	(Ge et al., 2015)
Co(OH) <sub>2</sub> -AC	SS mesh	1234	(Liu et al., 2016)
Co <sub>3</sub> O <sub>4</sub> - AC	SS mesh	1420	(Liu et al., 2016)
Urchin-like spinel	SS mesh	1730	(Ge et al., 2016)
NiCo <sub>2</sub> O <sub>4</sub>			
Manganese oxide	Carbon cloth	161	(Roche et al., 2009)
Nanoparticle MnCo <sub>2</sub> O <sub>4</sub>	Carbon cloth	545	(Hu et al., 2016)
Carnation-like MnO <sub>2</sub> -AC	Carbon cloth	1554	(Zhang et al., 2014)
MnO <sub>2</sub>	Carbon cloth	897	(Li et al., 2011)
MnO <sub>2</sub> -CNT	Carbon paper	520	(Liew et al., 2015)
Nanostructured-MnO <sub>2</sub>	Carbon cloth	119	(Haoran et al., 2014)
MnO <sub>2</sub> -CNT	Carbon cloth	511	(Touach et al., 2016)
Iron phthalocyanine-MnO <sub>x</sub>	Carbon paper	143	(Burkitt et al., 2016)
MnO <sub>2</sub> -CNT	Carbon paper	210	(Zhang et al., 2011)
Mn-polypyrrole-CNT	Carbon cloth	169	(Lu et al., 2013)
Nanostructured- MnO <sub>x</sub>	Carbon cloth	773	(Liu et al., 2010)
Nanotubular-MnO <sub>2</sub> /GO	Carbon cloth	3359	(Gnana et al., 2014)

Note: AC=activated carbon, CNT=carbon nanotubes, N=nitrogen, GO=graphene oxide, PC=phthalocyanine, SS=stainless steel

### 2.3.3 Binder

A binder is usually needed when the catalyst is applied to a supporting material. The binder is usually a polymer, and it plays an important role in maintaining a good three-phase interface for oxygen reduction: air (oxygen), water (protons), and solid (electricity) (Minteer et al., 2012). Nafion is the most widely used binder as it has high proton conductivity and strong chemical stability. However, Nafion is quite expensive, as

it costs more than \$600 per m<sup>2</sup> when used as a binder in an MFC. Inexpensive alternatives to Nafion are therefore needed for the practical applications. Low-cost hydrophobic polytetrafluoroethylene (PTFE) has been tested as the binder in several studies with Pt/C catalyst (Cheng et al., 2006). Adding PTFE with Nafion as a binder adversely affected power production, with power decreasing almost linearly from 1060 mW m<sup>-2</sup> with only Nafion to 549 mW m<sup>-2</sup> with only PTFE (Wang et al., 2010). In another study comparing a PTFE binder with Nafion, although less power production was obtained with PTFE binder, it showed less performance degradation over time than the Nafion binder (Cheng et al., 2006). PTFE binder has been successfully used as the binder in the construction of activated carbon air cathodes (Zuo et al., 2007).

Other low-cost polymers were also synthesized and tested as binders in MFCs, with different ion exchange capacities (IEC) or with different functionalization, allowing the understanding of the effects of different functional groups or other factors affecting the cathode performance. Cathodes with poly(phenylsulfone) (Radel) sulfonated to various extents to vary the binder IECs were tested as alternatives to Nafion in air cathode MFCs. Hydrophobic non-sulfonated Radel showed better electrochemical performance and the lower charge transfer resistance than the sulfonated Radel. Cathodes made with the non-sulfonated Radel had the most stable performance compared to the sulfonated Radel binder cathodes over more than 20 cycles, and after this time it had comparable performance to cathodes made with the Nafion binder. This suggested that the ionic binder resulted in ionic gradients that impeded proton transfer (Saito et al., 2010). Non-ionic hydrophilic polymers poly(styrene)-*b*-poly(ethylene oxide) diblock copolymers (PS-*b*-PEO) with different PEO lengths were tested to investigate the effect of the hydrophilicity on cathode performance. It was demonstrated that increasing the hydrophilicity of the neutral catalyst binders enhanced electrochemical and MFC performance, likely due to the increased accessible surface area for oxygen reduction (Saito et al., 2011). Although cathodes with these alternative binders all initially had a lower power production than those with Nafion, performance of the best materials became nearly equivalent to Nafion in longer term tests (Saito et al., 2010; Saito et al., 2011).

Cationic fluorinated polymer binders, which are quaternary ammonium functionalized fluorinated poly(arylene ether) (Q-FPAE), have also been tested in MFCs, showing similar performance to those made with a Nafion binder (Chen et al., 2012). Cathodes made with the Q-FPAE binder also showed more stable performance and higher

power production than those with anionic (sulfonated) or cationic (quaternary ammonium-functionalized) Radel. More quaternary ammonium groups promoted the absorption of water, which was thought to improve proton transfer. The presence of fluorine in these hydrophilic polymer binders increased the ionic transport and improved resistance to biofouling, resulting in a more stable long-term cathode performance (Chen et al., 2012). A hydrophilic anion exchange ionomer (AEI), quaternary 1,4-diazabicyclo-[2.2.2]-octane (DABCO) polysulfone (QDPSU) was also proposed as air cathode catalyst binders (Yu et al., 2012). Using the FePc catalyst, this binder showed higher cathode potentials in the polarization tests than the Nafion binder, but the reactors were not acclimated well before the polarization test. Both anodes failed to sustain high current densities, and the anode in the reactor with the Nafion binder cathode had higher anode potentials than the one with the QDPSU binder, so there were differences in the reactors other than those due to the cathodes. Despite these differences, it was suggested that the improved oxygen reduction activity from QDPSU was due to the interaction between the ionomer and oxygen, and the improved  $\text{OH}^-$  transfer (Yu et al., 2012).

Other polymers have been used as binders for air cathodes. Polyvinylidene fluoride (PVDF) was used as a binder for CNT supported  $\text{MnO}_2$  catalysts for oxygen reduction with domestic wastewater, and MFCs with these cathodes produced  $98 \text{ mW/m}^2$  (Lu et al., 2011). Positively charged diethylamine-functionalized polymer (DEA) was used as a Pt catalyst binder on the cathode to improve the establishment of a nitrifying biofilm and enhance ammonia removal. MFCs with the DEA binder had a higher ammonia removal efficiency of up to 97% than Nafion (91%), but a slightly lower power density of  $900 \text{ mW/m}^2$ , compared to  $945 \text{ mW/m}^2$  with a Nafion binder (Yan et al., 2012).

## 2.4 Membranes

It has been shown that proton exchange membranes (PEMs) are not necessary for power generation in single chamber air cathode MFCs. When a PEM (Nafion) was hot-pressed to a carbon cloth air cathode, the CE increased from 9–12% to 40–50%, but power was reduced from  $12.5$  to  $6.6 \text{ W/m}^3$  (Liu et al., 2004). Various types of membranes have been used to separate the anode and the cathode chambers in MFCs, including AEM, CEM, forward osmosis (FO) and bipolar, for reasons other than just power production. Pairs of AEMs and CEMs have been inserted between the anode and the cathode chambers for simultaneous desalination, electricity generation and wastewater treatment

(Mehanna et al., 2010; Kim et al., 2011). Thinner, laboratory-synthesized membranes produced better salt removal efficiencies than commercial AEMs and CEMs (Membrane International Inc.) (Mehanna et al., 2010). Adding a bipolar membrane between anode chamber and AEM allowed for simultaneous production of HCl and NaOH in the cell, in addition to achieving desalination, when additional voltage was added to the cell (Chen et al., 2012). The combination of a reverse electrodialysis stack (RED), which consists of several AEM and CEM pairs, with an MFC greatly enhanced the MFC performance, resulting in a high power of  $4.3 \text{ W/m}^2$  when acetate was used as the fuel (Kim et al., 2011). Capture of low-grade thermal energy as electricity can be achieved by using ammonia bicarbonate as a draw solution, while at the same time producing  $2.9 \text{ W/m}^2$  using domestic wastewater (Cusick et al., 2012). Using FO membrane as a separator between the anode and cathode chamber accomplished wastewater treatment, water extraction (from the wastewater), and electricity generation (Zhang et al., 2011).

## **2.5 Microorganisms or biocatalysts**

The microorganisms are used as catalysts to oxidize the substrate in the anode chamber, have been denoted as the power house of MFCs, which are the key for all the MFC applications. The unique characteristic of the microorganisms used in MFCs is their ability to transfer the electrons (resulted from their metabolism) from their outer cell surface to the electrode surface (in anode) and to accept the electrons from the electrode surface (in cathode) to catalyse the reduction of electron acceptors e.g. oxygen reduction (Potter, 1911; Strik et al., 2008). The proteins or genes involved in the electron transfer are shown in *Figure 2.4*. The microorganisms that exhibit the potential to transfer the electrons exogenously to an electron acceptor or to accept electrons are usually called as exoelectrogens.

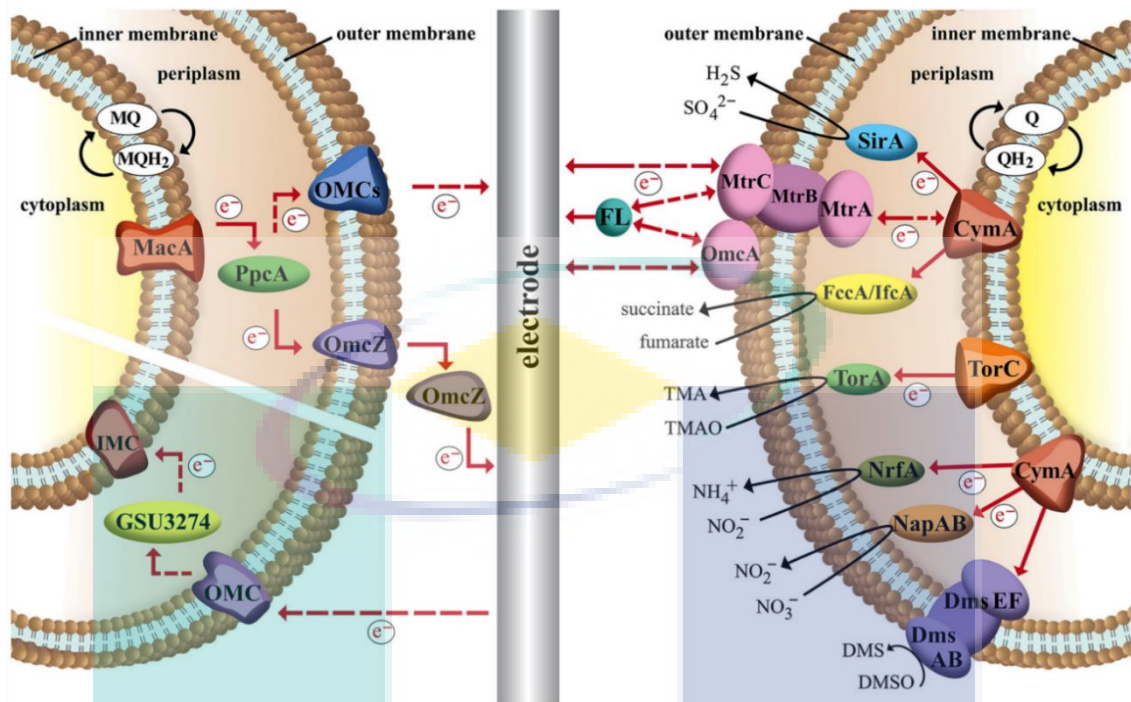


Figure 2.4 Schematic image of the proposed EET of two metal respiring bacteria and their interactions with an electrode in a bioelectrochemical system

Source: Kracke et al., (2015).

The previous studies suggest that a mixed culture usually produce higher power output than the pure culture in MFCs. For example, in a single-chamber, air cathode MFC, an enriched consortium of exoelectrogens produced 22% more power ( $576 \text{ mW/m}^2$ ) as compared to pure culture of *Geobacter sulfurreducens* that produced power density of  $461 \text{ mW/m}^2$  in a similar MFC (Reguera et al., 2006). Keeping this point in mind, a mixed community of microorganisms from anaerobic sludge was used in this work. Further, in this thesis, some microorganisms are reviewed that had been used in MFCs for bioelectricity generation.

### 2.5.1 Biocatalysts in anode

In the earliest study by Potter, *Bacillus coli communis* (*E. coli*) was able to produce maximum EMF of only 0.3-0.5V (Potter, 1911). But, in present due to wide and deep research in microbiology in MFCs, the sophisticated technology is able to produce much efficient electrical energy than the former. The most studied and efficient exoelectrogens in MFC technology belong to *Geobacteraceae* family of bacteria. *G. sulfurreducens*,  $\delta$ -proteobacteria can reduce acetate with ca.100% electron recovery to generate electricity.

The organism has successfully produced the current density of 3.1 A/m<sup>2</sup> in a MFC with gold electrodes, acetate as the electron donor and fumarate as the electron acceptor (Min et al., 2005b). However, *G. metallireducens* (pure culture) could produce only 40 mW/m<sup>2</sup> power output in MFC using wastewater as inoculum (Ringeisen et al., 2006). *Shewanella spp.*,  $\gamma$ - proteobacteria can reduce iron and manganese and can use them as electron acceptors. *Shewanella oneidensis* DSP10 in a miniature microbial fuel cell using lactate as the anolyte and buffered ferricyanide solutions as catholyte, produced power density of 3000 mW/m<sup>2</sup> which is quite appreciable (Pandit et al., 2014). *Shewanella putrefaciens* was the first organism to produce electricity in the absence of electron mediator. Recently, *S. putrefaciens* in a single chamber-MFC (SC-MFC) produced maximum power density of 4.92 W/m<sup>3</sup> using CaCl<sub>2</sub> as anolyte (Xing et al., 2008). *Rhodospseudomonas palustris*,  $\alpha$ - proteobacteria, a photosynthetic purple non sulphur bacterium can utilize volatile acids, yeast extract, and thiosulfate; produced power density of 2720 mW/m<sup>2</sup> higher than mixed cultures in indistinguishable MFCs (Kang et al., 2014). A thermophilic, Gram-positive, metal-reducing bacterium, *Thermincola ferriacetica* is adept to generate current from acetate, exhibited maximum current density 12 A/m<sup>2</sup> (Wrighton et al., 2011). *Pseudomonas aeruginosa*,  $\gamma$ - proteobacteria in MFC produced power density of 4310 mW/m<sup>2</sup> using glucose as electron donor and graphite electrodes as the electron acceptor (Jiang et al., 2014). A sulfate-reducing bacterium, *Desulfovibrio desulfuricans* in MFC with surface-treated graphite felt electrodes generated maximum current density of 0.22 A/m<sup>2</sup> which was ca. 50% higher than with untreated electrodes (Qiao et al., 2008). *E.coli*, Gram-negative bacteria in MFC successfully achieved power density of 1300 mW/m<sup>2</sup> at 3.3 A/m<sup>2</sup> current density (Raghavulu et al., 2011).

*Saccharomyces cerevisiae* in SC-MFC (open-air cathode) fed with synthetic wastewater using noncatalyzed graphite as electrodes without the use of artificial mediators, generated maximum current density 0.28 A/m<sup>2</sup> (Prasad et al., 2007). Other yeast *Hansenula anomala* using Pt electrode and ferricyanide as catholyte produced power density of 2.9 W/m<sup>3</sup> (El-Naggar et al., 2010). Moreover, *Candida melibiosica* in an MFC of modified carbon felt electrode with surface nickel nanostructures produced significant power output of 720 mW/m<sup>2</sup> (Hubenova et al., 2010). Some exoelectrogens not used commonly in MFC and a few novel exoelectrogens discovered recently have also shown the ability to produce electricity. The performance of pure culture and mixed cultures for electricity generation is given in Table 2.2 and Table 2.3, respectively.

Table 2.2 Performance of microbial fuel cells for bioelectricity generation using pure cultures.

Microorganism	Type of MFC	Substrate	MPD (mW/m <sup>2</sup> )	Reference
<i>Candida melibiosica</i>	Double	Acetate	720	(Hubenova et al., 2010)
<i>Geobacter sulfurreducens</i>	Double	Acetate	1.9	(Nevin et al., 2008)
<i>Geobacter metallireducens</i>	Double	Wastewater	40	(Min et al., 2005a)
<i>Rhodospseudomonas palustris</i>	Single	Wastewater	2720	(Xing et al., 2011)
<i>Chlorella vulgaris</i>	Double	Wastewater	2485	(Zhou et al., 2012)
<i>Cyanobacteria</i>	Single	Wastewater	114	(Yuan et al., 2011b)
<i>Shewanella oneidensis</i>	Mini-MFC	Lactate	3000	(Ringeisen et al., 2006)
<i>Scenedesmus</i>	Double	Acetate	1926	(Cui et al., 2014)
<i>Lysinibacillus</i>	Double	Glucose	58	(Nandy et al., 2013)

*Klebsiella pneumonia*, Gram-negative, non-motile, lactose-fermenting bacteria in a cubic air-chamber MFC generated 0.19 A/m<sup>2</sup> current density and maximum voltage output of 426.2 mV (Torres et al., 2010). A Gram-positive bacterium *Lysinibacillus sphaericus* in MFC using graphite felt as electrode generated a maximum current density of ca. 0.27 A/m<sup>2</sup> and power density of 85 mW/m<sup>2</sup> (Nandy et al., 2013). Further, *Citrobacter sp.* SX-1 can utilize diverse simple substrates like acetate, glucose, sucrose, glycerol and lactose in MFCs but produced the highest current density of 205 mA/m<sup>2</sup> from citrate (Xu et al., 2011). However, the mechanisms of electron transfer or the redox components involved in electron transport in *Lysinibacillus sphaericus* and *Citrobacter sp.* are not known. Recently, many strains including *Raoultella electrica sp.* (Kimura et al., 2014) and *Fontibacter ferrireducens sp.* (Zhang et al., 2013) have been isolated from glucose fed microbial fuel cells, but, their ability for electricity generation is yet to be studied. *Geobacter sp.* SD-1 produced a maximum current density of 290 A/ m<sup>3</sup> in a high-concentration phosphate buffer solution (PBS-H, 200 mM) in rival to the mixed culture 189 A/ m<sup>3</sup> (Sun et al., 2014a). Analysis of 16S rRNA gene sequences has unveiled a new exoelectrogen, *Geobacter anodireducens* showed 98% similarity to *Geobacter sulfurreducens* but cannot reduce fumarate as the electron acceptor (Sun et al., 2014b). Another novel strain, *Ochrobactrum sp.*575 is isolated recently from the anodic chamber of a xylose MFC, produced maximum power density of 2625 mW/m<sup>3</sup>. Further, the results suggested that xylose digestion in *Ochrobactrum sp.*575 was different to other

electroactive bacterial strains, which depends on the succinate oxidation respiratory chain instead of traditional NADH oxidation respiratory chain (Li et al., 2014).

Table 2.3 Performance of microbial fuel cells for bioelectricity generation using mixed cultures.

Source of inoculum	Type of MFC	Substrate	MPD (mW/m <sup>2</sup> )	Reference
Dairy manure wastewater	Single	Dairy manure wastewater	190	(Kiely et al., 2011a)
Potato wastewater	Single	Potato wastewater	270	(Kiely et al., 2011a)
Activated sludge	Single	Acetate, glucose	1084	(Yuan et al., 2011a)
Activated sludge	Single	Glucose	68	(Han et al., 2010)
Activated sludge	Single	Acetate	670	(Tang et al., 2015)
Primary wastewater	Single	Acetic acid	835	(Kiely et al., 2011b)
Primary wastewater	Single	Ethanol	820	(Kiely et al., 2011b)
Primary wastewater	Single	Lactic acid	739	(Kiely et al., 2011b)
Primary wastewater	Single	Succinic acid	444	(Kiely et al., 2011b)
Anaerobic sludge	Double	Slaughterhouse wastewater	578	(Katuri et al., 2012)
Anaerobic reactor effluent	Double	Acetate	188	(Hassan et al., 2012)

Besides bacteria and yeast, microalgae have been also used in MFC technology either as bioanode or a substrate assisting the anode for the prevalent application. *Scenedesmus*, green algae in powder form as substrate was used in anode and *Chlorella vulgaris* as a biocathode in MFC produced maximum power density of 1926 mW/m<sup>2</sup> (Cui et al., 2014). In another study, *Arthrospira maxima* was used as a substrate as well as a carbon source for the metabolism and growth of *R. palustris* in a micro MFC, exhibited volumetric power density of 10.4 mW/m<sup>3</sup>, the highest in rival to other substrates used in the study (Inglesby et al., 2012). Furthermore, blue-green algae (cyanobacteria) in a sMFC produced maximum power density of 114 mW/m<sup>2</sup> (Yuan et al., 2011). In microalgae assisted MFCs, algae degradation produces intermediate compounds like acetate and lactate which can be further used by exoelectrogens such as *G. sulfurreducens* for bioelectricity production.

### 2.5.2 Bioelectrogenesis

In MFC, organic substrates containing carbohydrates, lipids and proteins serve as electron donors for redox reactions at the anode to produce energy. These complex organic molecules further undergo through glycolysis and other respective processes to

yield acetyl Co-A, which then participate in citric acid cycle (also known as TCA cycle or Krebs's cycle), as shown in *Figure 2.5*. One complete turn of the cycle converts three equivalents of nicotinamide adenine dinucleotide ( $\text{NAD}^+$ ) into three equivalents of reduced NADH; one flavin adenosine dinucleotide (FAD) reduces to  $\text{FADH}_2$  and  $\text{CO}_2$  is released as by-product. These metabolic pathways (glycolysis and Krebs's cycle) occur in cytoplasm in both prokaryotes (bacteria) and eukaryotes (yeast). NADH and  $\text{FADH}_2$  acts as electron carriers, which then transfer their electrons to electron transport chain (ETC) to produce energy carrier molecule adenosine triphosphate (ATP). In bacteria, respiratory reaction occurs in the cell membrane (constituting outer cell membrane, inner cell membrane and periplasm), the machinery containing all the proteins or enzymes required for the electron transfers (the basis of MFC). While in yeast, ETC resides on the inner mitochondrial membrane. The ETC contains four intermediary proteins; NADH dehydrogenase, ubiquinone, coenzyme Q and cytochromes (however, these intermediary proteins may vary with species). The electrons are passed through these proteins to the final electron acceptor and the protons (reduced) are pumped out of the cell in the anode which is then transferred to the cathode through PEM. Prior to the prominence that bacteria can facilitate electron transfer chemical mediators were utilized to catalyse electron transfer from inside the bacterial cell to the anode surface. These mediators usually react with ETC components and get reduced, release out of the cell and transfer their electrons to the anode.

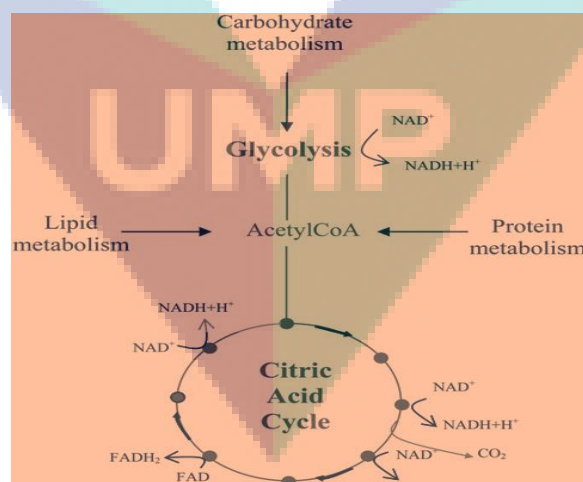


Figure 2.5 Reduction of  $\text{NAD}^+$  and FAD to their electron carrier forms (NADH and  $\text{FADH}_2$ ) through the Citric Acid Cycle (also known as tricarboxylic acid cycle or TCA cycle).

Source: Schaetzle et al., (2008).

### 2.5.3 Biocatalysts in cathode

The MFC technology can be made more economic by using biocathodes instead of highly expensive catalysts such as platinum to reduce oxygen at the cathode and for the bioremediation application like treatment of azo dye. Moreover, the cost for an external oxygen supply can be omitted with the application of phototropic biocathodes (e.g. *Chlorella vulgaris*) at the cathode in MFC. Gram-positive as well as Gram-negative bacteria, microalgae and fungi have shown the ability to act as biocathodes. *Geobacter spp.* highly efficient as bioanodes in MFC also evidenced to be prelusive biocathodes to accept the electrons from cathodic electrodes (Xafenias et al., 2013). The study revealed that *G. metallireducens* reduced nitrate to nitrite and *G. sulfurreducens* reduced fumarate to succinate with the electrode as the sole electron donor (Xafenias et al., 2013). Furthermore, *G. sulfurreducens* reduced fumarate in a reactor with stainless steel electrodes producing the current density of 20.5 A/m<sup>2</sup> (Schaefer et al., 2008). *Shewanella oneidensis* MR-1 was used as a biocatalyst in the cathode under aerated conditions in the presence of lactate showed increase in Cr (VI) reduction rate with maximum current density of 0.33 A/m<sup>2</sup> (Freguia et al., 2010). The study demonstrated the expression of riboflavin in the electron transport. In an alternative investigation, *Shewanella putrefaciens* and *Acinetobacter calcoaceticus* showed the ability to enhance the rate of cathodic oxygen reduction to water by utilising outer membrane-bound cytochromes and self-excreted pyrroloquinoline quinone (PQQ) respectively (Carbajosa et al., 2010). An acidophile microorganism, *Acidithiobacillus ferrooxidans* fed as a biocathode in MFC, up to 5 A/m<sup>2</sup> of current densities were obtained for O<sub>2</sub> reduction at low pH (Inglesby et al., 2012). In a study, *Enterobacter* and *Pseudomonas spp.* demonstrated for the catalysis of acetate oxidation actually resulted to catalyse the electrochemical reduction of oxygen producing maximum current density of 0.14 A/m<sup>2</sup> (Parot et al., 2009). CV results unveiled that *Micrococcus luteus* and other Gram-positive (*Staphylococcus spp.*, *Lactobacillus farciminis*) and Gram-negative bacteria (*Pseudomonas fluorescens*, *Escherichia coli*, *Acinetobacter sp.*) are able to catalyze the electrochemical reduction of oxygen on the carbon electrode (Thrash et al., 2007). Seawater formed aerobic biofilms coated on stainless steel electrodes have shown significant ability to catalyze oxygen reduction, achieved current densities up to 0.46 A/m<sup>2</sup> at different set potentials (Bergel et al., 2005).

An acetate-fed MFC utilizing *Chlorella vulgaris* as a biocathode produced maximum power density of 1926 mW/m<sup>2</sup>. CO<sub>2</sub> produced at the anode was used by *C.*

*vulgaris* as a carbon source for its growth. Further, the study demonstrated that *C. vulgaris* could not grow in acetate-fed MFC without anodic CO<sub>2</sub> supply (Cui et al., 2014). Alternatively, *C. vulgaris* at the cathode, with light radiation, utilizes CO<sub>2</sub> as the carbon source for photosynthesis and produces oxygen, which acts as an electron acceptor, sustained the power density, 13.5 mW/m<sup>2</sup> (del Campo et al., 2013). The immobilization of *C. vulgaris* into the cathode chamber turned the MFC highly efficient, consequently, produced the power density 2485 mW/m<sup>3</sup> at a current density of 7.9 A/m<sup>3</sup>, while, the MFC with suspended *C. vulgaris* achieved 1324 mW/m<sup>3</sup> power density (Zhou et al., 2014). A strain of white-rot fungus, *Coriolus versicolor* (secretes laccase to reduce oxygen at the cathode); inoculated in the cathode chamber of a MFC to catalyse the cathodic reaction generated the maximum power density 320 mW/m<sup>3</sup> (Wu et al., 2012).

## 2.6 Substrate

The electron donor in a MFC serves two purposes, to provide energy for the exoelectrogenic organism to use for metabolic sustenance and also to provide an energy source for the MFC power generation. In line with common microbiological terminology, the electron donor is often referred to as the substrate and greatly influences MFC performance. There is a wide range of substrates that microorganisms can consume in MFCs including carbohydrates such as glucose, organic acids such as acetate or lactate, and more complex organic compounds found in wastewater, or even pollutants (Liu et al., 2004; Kim et al., 2007). Conversion of larger compounds, such as lignocellulosic biomass, to electric energy has also been reported (Wang et al., 2008). This wide variety of electron donor substrates triggers different metabolic responses from bacteria, which result in different electron generation pathways, power output, and coulombic efficiency of fuel cells (He et al., 2005). Studies on selection of the best substrates and their optimum concentrations in MFCs are valuable. A study on the effect of different substrates on the performance and biodiversity in MFCs revealed that performance and bacterial diversity varied with the different substrates (Ahn and Logan, 2010). A list of different substrates used in MFCs is given in Table 2.4

Table 2.4 An overview of performance of MFCs with simple substrates.

Substrate	Type of MFC	Source of inoculum	MPD (mW/m <sup>2</sup> )	Reference
D-Glucose	Double	Mixed bacterial culture	2160	(Catal et al., 2008a)
D-Galactose	Double	Mixed bacterial culture	2090	(Catal et al., 2008a)
D-Fructose	Double	Mixed bacterial culture	1810	(Catal et al., 2008a)
D-Fucose	Double	Mixed bacterial culture	1760	(Catal et al., 2008a)
L-Rhamnose	Double	Mixed bacterial culture	1320	(Catal et al., 2008a)
D-Mannose	Double	Mixed bacterial culture	1240	(Catal et al., 2008a)
D-Xylose	Double	Mixed bacterial culture	2330	(Catal et al., 2008a)
Galactitol	Single	Mixed bacterial culture	2650	(Catal et al., 2008b)
Mannitol	Single	Mixed bacterial culture	1490	(Catal et al., 2008b)
Sorbitol	Single	Mixed bacterial culture	1690	(Catal et al., 2008b)
Arabitol	Single	Mixed bacterial culture	2030	(Catal et al., 2008b)
Ribitol	Single	Mixed bacterial culture	2350	(Catal et al., 2008b)
Xylitol	Single	Mixed bacterial culture	2110	(Catal et al., 2008b)
L-Serine	Single	Domestic Waste-water	768	(Catal et al., 2008b)
L-Asparagine	Single	Domestic Waste-water	595	(Catal et al., 2008b)
L-Aspartic Acid	Single	Domestic Waste-water	601	(Yang et al., 2012)
Glucose	Single	Activated sludge	68	(Han et al., 2010)
Acetate	Single	Activated sludge	670	(Tang et al., 2015)
Acetic acid	Single	Primary wastewater	835	(Kiely et al., 2011b)
Ethanol	Single	Primary wastewater	820	(Kiely et al., 2011b)
Lactic acid	Single	Primary wastewater	739	(Kiely et al., 2011b)
Succinic acid	Single	Primary wastewater	444	(Kiely et al., 2011b)

Table 2.5 An overview of performance of MFCs with undefined wastewater substrates.

Substrate	Type of MFC	Inoculum	MPD (mW/m <sup>2</sup> )	Reference
Biodiesel wastewater	Single	Domestic waste water	2110	(Feng et al., 2011)
Brewery wastewater	Single	Anaerobic mixed culture	669	(Wen et al., 2010)
Cellulose	Single	Domestic waste water	1070	(Cheng et al., 2011)
Cheese whey	Double	Anaerobic sludge	46	(Tremouli et al., 2011)
Chocolate industry	Double	Anaerobic sludge	1500	(Patil et al., 2009)
Coal Tar wastewater	Single	Anaerobic sludge	4.5	(Park et al., 2012)
Crude glycerol	Double	Anaerobic sludge	92	(Chookaew et al., 2014)
Distillery wastewater	Double	Isolated broth culture	202	(Samsudeen et al., 2015)
Ethanol stillage	Double	Anaerobic sludge	93	(Sakdaronnarong et al., 2013)
Fermented apple juice	Double	Compost leachate	78	(Cercado et al., 2010)
Fermented corn	Single	Anaerobic sludge	1180	(Borole et al., 2012)
Food processing	Single	Anaerobic sludge	230	(Mansoorian et al., 2013)
Human urine	Single	Human urine	55	(Santoro et al., 2013)
Human feces wastewater	Double	Anaerobic sludge	71	(Fangzhou et al., 2011)
Palm oil mill effluent sludge	Double	<i>Pseudomonas aeruginosa</i> strain ZH1	451	(Nor et al., 2015)
Rice straw	Double	Mixed bacterial culture	190	(Gurung et al., 2015)
Red wine lees wastewater	Single	Denitrification tank wastewater	111	(Sciarria et al., 2015)
Sewage wastewater	Double	Anaerobic sludge	6.7	(Ghangrekar et al., 2008)
Starch processing	Single	Starch processing waste	239	(Lu et al., 2009)
Swine wastewater	Double	Swine wastewater	228	(Kim et al., 2008)
Synthetic penicillin	Single	Mixed bacterial culture	101	(Wen et al., 2011)
White wine lees wastewater	Single	Denitrification tank wastewater	262	(Sciarria et al., 2015)

## 2.7 Electrolyte

Electrolytes are the solutions found in the anode or cathode, the anolyte or catholyte, respectively, and facilitate transfer of electrons. The anolyte is usually a culture medium, typically consisting of buffer, salts, and electron donor or substrates to support growth and electricity generation by bacteria. The anolyte must be capable of stabilizing the pH, supporting nutrients, and providing high conductivity for electron transfer. The conductivity of electrolyte solution can be increased by adding salt into the solution, which leads to improvement of power output, assuming the salinity of the solution is within the tolerable range of the bacteria (Lefebvre et al., 2012). The addition of selective salts has been shown to have other impacts on the microorganisms, such as increasing bacterial metabolism which could benefit power generation, as demonstrated by the addition of  $\text{CaCl}_2$  into MFCs that led to improved biofilm formation (Fitzgerald et al., 2012).

Redox mediators or electron-shuttling compounds were added into anolyte to facilitate electron transfer before the emergence of exoelectrogens (Watanabe et al., 2009). Neutral red, thionin (Rabaey et al., 2005), and flavin (Masuda et al., 2010) were commonly applied as mediators in MFCs. Mechanisms of mediator-driven electron transfer were extensively studied on bacteria, such as *Shewanella* and *Geobacter* species (Watanabe et al., 2009). However, research revealed that mediators usually were toxic to microorganisms in anode chamber during long-term operations and after discovery of mediator-less MFCs, mediators are not studied so popularly as before.

The catholyte contains buffer solution and electron acceptor. Electron acceptors such as hexacyanoferrate or ferricyanide (Ringeisen et al., 2006) have been employed in double-chamber MFCs. In some double-chamber MFCs, oxygen is pumped into cathodic chamber and serves as electron acceptor. The function of those electron acceptors is to complete the cathodic reaction and the whole redox reaction and therefore, generate current at the circuit of MFCs. In MFCs, cathodic reactions and cathode potentials will vary with different electron acceptors while the function of them remains the same (Kim et al., 2007).

## 2.8 Hydrothermal method for nanomaterial synthesis

The Hydrothermal Technique has been the most popular one, gathering interest from scientists and technologists of different disciplines, particularly in the last fifteen years. The word “hydrothermal” has geological origin. A self-explanatory word, “hydro” meaning water and “thermal” meaning heat. British Geologist, Sir Roderick Murchison (1792–1871) was the first to use this word, to describe the action of water at elevated temperature and pressure in bringing about changes in the earth’s crust leading to the formation of various rocks and minerals (Byrappa and Yoshimura, 2001). The term hydrothermal usually refers to any heterogeneous reaction in the presence of aqueous solvents or mineralizers under high pressure and temperature conditions (Byrappa and Yoshimura, 2001).

Hydrothermal synthesis offers many advantages over conventional and non-conventional synthesis methods. Unlike many advanced methods that can prepare a large variety of forms, the respective costs for instrumentation, energy and precursors are far less for hydrothermal methods. From the environmental perspective, hydrothermal methods are more environmentally benign than many other methods (Rabenau, 1985). The low reaction temperatures also avoid other problems encountered with high temperature processes (Czochralski method, Bridgeman method) such as poor stoichiometric control due to volatilization of components (e.g., volatilization  $\text{PbO}$  in  $\text{PbWO}_4$ ) and stress-induced defects (e.g., micro-cracks) caused by phase transformations that occur as the phosphor is cooled to room temperature (Morey and Niggli, 1913). Moreover, the ability to precipitate the phosphor powders directly from solution regulates the rate and uniformity of nucleation, growth and aging, which affects size, morphology and aggregation control that is not possible with many synthesis processes. Varieties of morphologies and particle sizes are possible with hydrothermal processing. This method is beneficial to different industries which rely on powder (e.g., materials, pigments, pharmaceuticals, medical diagnostics) will benefit from having an access to powders with controlled size and morphology for a wide range of reasons (Morey and Niggli, 1913). The unique pressure-temperature interaction of the hydrothermal solution allows the preparation of different phases of  $\text{PbWO}_4$  phosphor that are difficult to prepare with other synthetic methods (Roy, 1994). Phase fields are often simpler when hydrothermal solutions are used. Materials synthesized under hydrothermal conditions often exhibit differences in point defects when compared to materials prepared by high temperature

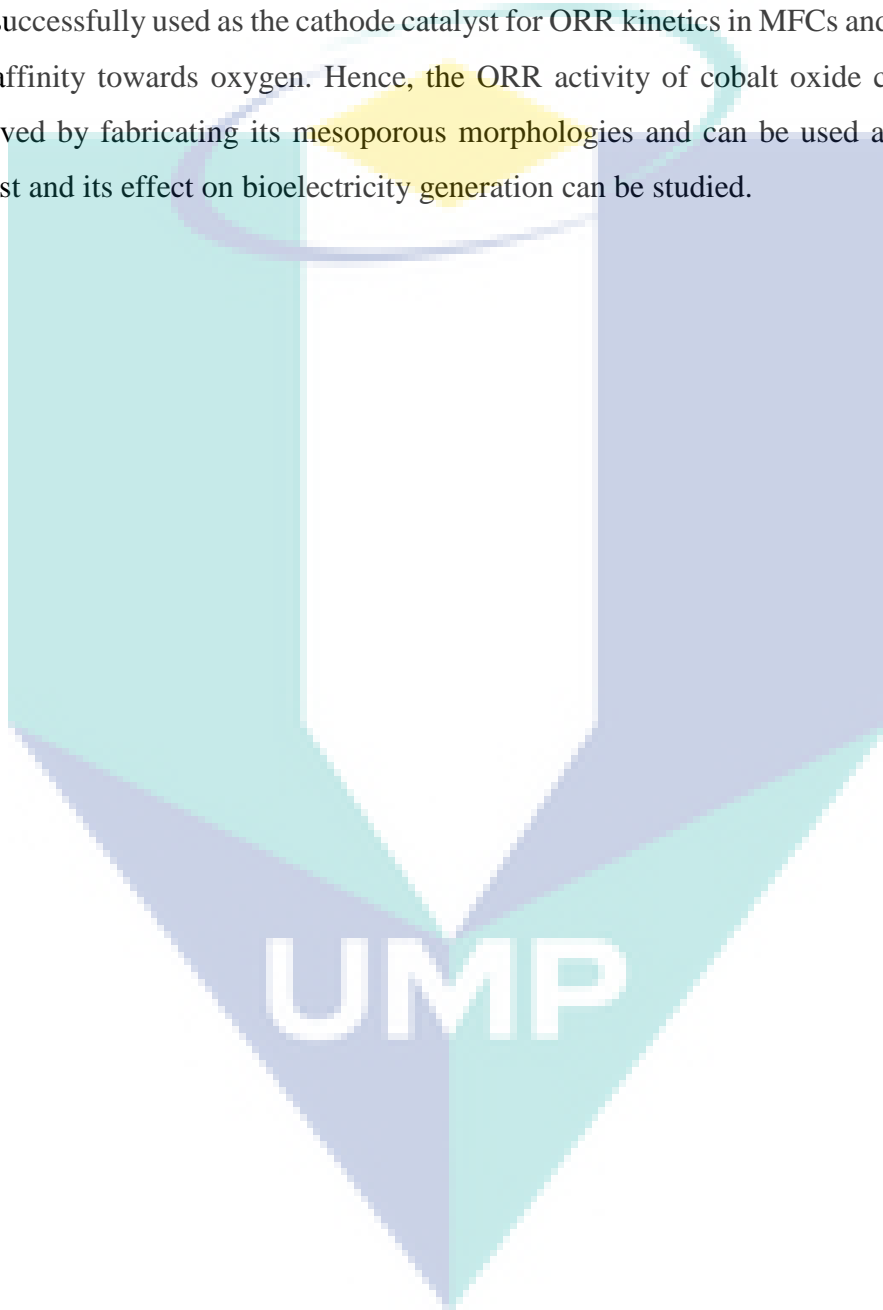
synthesis methods. e.g., Tungstates of Ca, Ba, and Sr synthesized at room temperature by a hydrothermal method do not contain Schottky defects usually present in similar materials prepared at high temperatures, which results in improved luminescent properties (Hamann, 1981).

A major advantage of hydrothermal synthesis is that this method can be hybridized with other processes like microwave, electrochemistry, ultrasound, mechano-chemistry, optical radiation and hot-pressing to gain advantages such as enhancement of reaction kinetics and increase ability to make new materials. A great amount of work has been done to enhance hydrothermal synthesis by hybridizing this method with many other processes (Cho et al., 1995). This facile method does not need any seed, catalyst, harmful and expensive surfactant or template thus it is promising for large-scale and low-cost production with high-quality crystals.

## 2.9 Summary

MFC technology has drawn a significant consideration for a decade, since it demonstrates the incredible potential to produce electrical energy from organic materials. On the anode, intensive attention has been drawn to provide large surface area and to improve the electron transfer between bacteria and the electrode surface (Minteer et al., 2012). In this regard, carbon nanotubes and graphene have been extensively used with combination of other elements. On the other hand, on the cathode, replacement of platinum is required with an efficient and cost-effective cathode catalyst improved MFC applications. Different cathode catalysts with a variety of elemental composition have been synthesized to improve the performance of the cathode in MFCs. Specifically, cobalt oxide ( $\text{Co}_3\text{O}_4$ ) and manganese oxide ( $\text{MnO}_2$ ) showed excellent oxygen reduction activity in MFCs. This is probably because  $\text{Co}_3\text{O}_4$  and  $\text{MnO}_2$  contain cations such as  $\text{Co}^{3+}$ ,  $\text{Co}^{2+}/\text{Mn}^{4+}$ ,  $\text{Mn}^{3+}$  that show high affinity towards oxygen molecules. For example,  $\text{Co}_3\text{O}_4$  nanosheets decorated on activated carbon was used as the air cathode that generated the maximum power density of ca.  $1420 \text{ mW/m}^2$  and exhibited an exchange current density 160% higher than the control (Liu et al., 2016). Besides, the Co and Mn containing cathode catalysts have shown high stability and less toxicity as compared to platinum. The literature also suggests that the ORR activity of the cathode catalysts can be significantly enhanced by developing mesoporous morphologies. Generally, the cathode catalyst with a higher BET surface area can provide higher number ORR active

sites on the cathode surface. For instance, porous ortho-hexagon nano spinel  $\text{Co}_3\text{O}_4$  showed a maximum power density of  $1500 \text{ mW/m}^2$ , which was  $\sim 96\%$  higher than the non-porous commercial  $\text{Co}_3\text{O}_4$  (Ge et al., 2015). However, no findings are reported on the morphological effect of cathode catalyst on ORR in MFCs, which can be studied by selecting a material and forming its different morphologies. Cobalt or cobalt oxide has been successfully used as the cathode catalyst for ORR kinetics in MFCs and it also shows high affinity towards oxygen. Hence, the ORR activity of cobalt oxide can be further improved by fabricating its mesoporous morphologies and can be used as the cathode catalyst and its effect on bioelectricity generation can be studied.



## CHAPTER 3

### METHODOLOGY

#### 3.1 Introduction

This chapter briefly outlines the methodology adopted to achieve the objectives of this research. Catalyst synthesis, preparation of cathodes, electrochemical characterization, and their performance in a double chamber MFC are the main steps of the methodology. All the catalysts were prepared by a hydrothermal method and the cathodes were characterized by CV, LSV, and EIS. The chapter also compiles the principle and block diagram of the instruments used and the sample preparation details for all the measurements.

#### 3.2 Research methodology

The research methodology adopted in this work is shown in *Figure 3.1*. In brief, all the catalysts were synthesized by using a facile and cost-effective hydrothermal method and further characterized by X-ray diffraction (XRD) and electron microscopic techniques. The catalyst ink of all the catalysts of varying concentration was prepared and coated on graphite electrodes, which were characterized by electrochemical techniques such as cyclic voltammetry (CV), linear sweep voltammetry (LSV), Electrochemical Impedance Spectroscopy (EIS) and ORR kinetics study by Tafel plot. Finally, polarization curves were performed to determine the maximum power density generation in the MFCs.

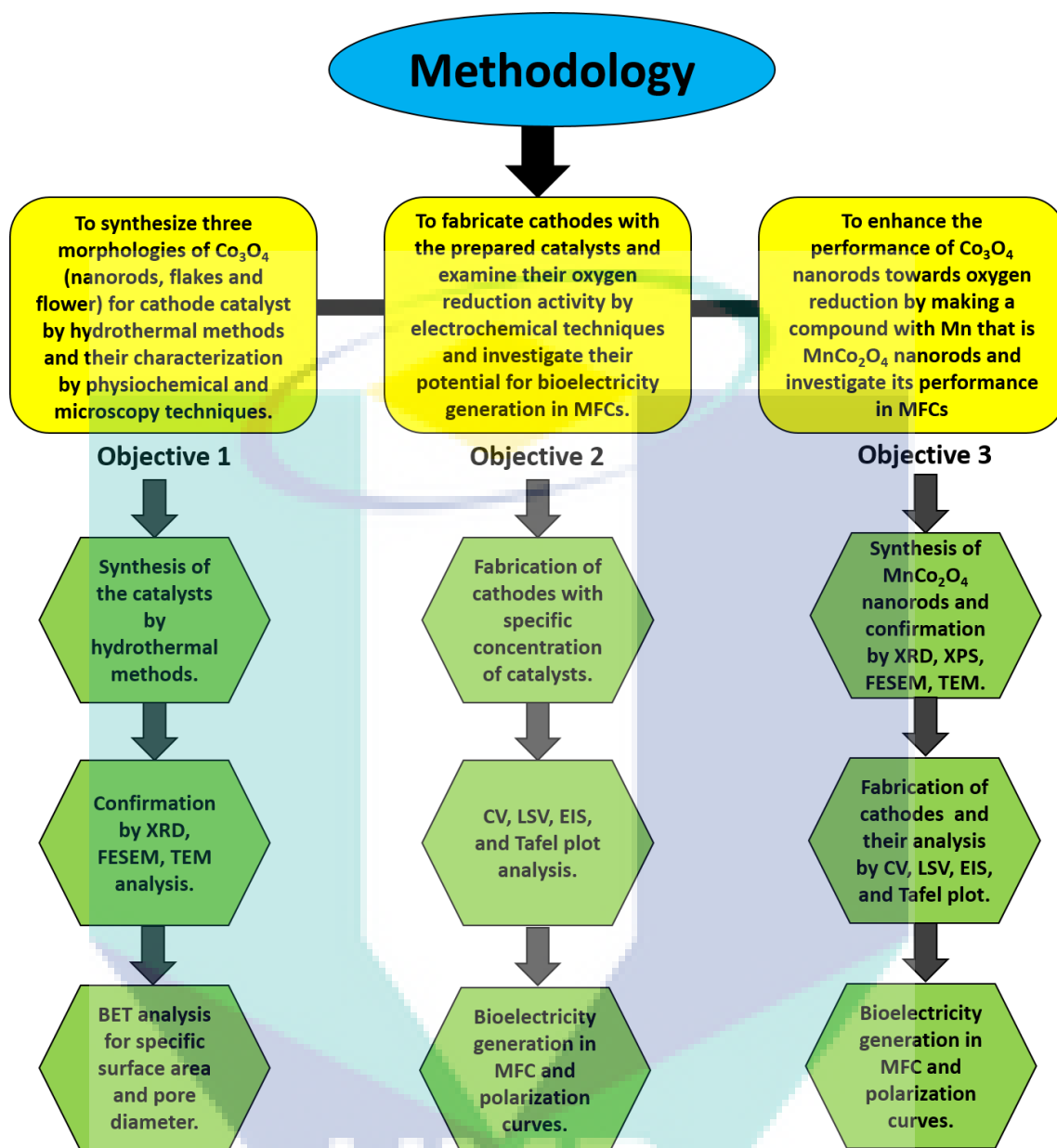


Figure 3.1 Flow chart of research methodology.

### 3.3 Synthesis of materials

#### 3.3.1 Synthesis of $\text{Co}_3\text{O}_4$ nanorods

$\text{Co}_3\text{O}_4$  nanorods were synthesized using a simple and cost-effective hydrothermal method, earlier used by Wang et al. (2009). To synthesize  $\text{Co}_3\text{O}_4$  nanorods, 3 g of cobalt chloride and 150 mg of urea were mixed in distilled water to make a homogenous solution with a final volume of 100 mL. The solution was transferred to a 100 mL Teflon-lined autoclave and kept in an oven for 6 h at 105 °C (Wang et al., 2009). The autoclave was allowed to cool at the room temperature. The resulting solution was centrifuged at 10000

rpm for 20 min to isolate the pink precipitates. The supernatant was properly discarded in a container, as per the university guidelines. The precipitates were further washed with distilled water and ethanol for several times, respectively to remove the impurities. The washed precipitates were dried in a vacuum oven overnight. The dried product was further calcined at 300 °C for 3.5 h (Wang et al., 2009). A black powder was obtained as the final product.

### **3.3.2 Synthesis of Co<sub>3</sub>O<sub>4</sub> flakes**

To synthesize Co<sub>3</sub>O<sub>4</sub> flakes, 3.4 g cobalt nitrate (Co(NO<sub>3</sub>)<sub>2</sub>·6H<sub>2</sub>O) was mixed in ethanol: water (2:1) with a final volume of 100 mL (Krishnan et al., 2016). The solution was stirred for 30 min before it was transferred to a Teflon-lined autoclave. The autoclave was kept in an oven at 200° C for 6 h (Krishnan et al., 2016). Thereafter, the autoclave was allowed to cool at room temperature. The obtained solution was centrifuged at 10000 rpm for 30 min to collect the black precipitates. The supernatant was properly discarded in a container, as per the university guidelines. Further, the precipitates were washed with 70% ethanol and distilled water several times, respectively, followed by their drying in the oven at 60 °C for an overnight. Finally, the precipitates were calcined in a furnace at 300 °C for 3 h (Krishnan et al., 2016). A black powder was obtained as the final product.

### **3.3.3 Synthesis of flower-like Co<sub>3</sub>O<sub>4</sub>**

To synthesize flower-like Co<sub>3</sub>O<sub>4</sub>, similar reactants were used as in the above method except the reaction temperature and time was varied, which were 150° C (Misnon et al., 2014) and 5.5 h, respectively, rest procedure was the same.

### **3.3.4 Synthesis of MnCo<sub>2</sub>O<sub>4</sub> nanorods**

To synthesize MnCo<sub>2</sub>O<sub>4</sub> nanorods, 3.2 g of Hexadecyl Trimethyl Ammonium Bromide (HTAB), 0.3 g of urea, 0.64 :0.62 g of CoCl<sub>2</sub>:MnCl<sub>2</sub> were mixed in water to a final volume of 100 mL (Khilari et al., 2014). The resultant solution was transferred to a 100 mL Teflon-lined autoclave and kept in an at 100 °C for 24 h. The autoclave was allowed to cool at the room temperature. The obtained solution was centrifuged at 10000 rpm for 20 min to isolate the pink precipitates. The supernatant was properly discarded in a container, as per the university guidelines. Further, the precipitates were washed with 70% ethanol and distilled water several times, respectively. The precipitates contain the

surfactant that can be removed by using an organic solvent, this was the reason alcohol was used to wash the precipitates, which is otherwise not possible with water. The washed precipitates were dried in a vacuum oven for an overnight. The dried product was further calcined at 300 °C for 3.5 h (Wang et al., 2009). A black powder was obtained as the final product. All raw materials and parameters used to synthesize the catalysts are given in Table 3.1.

Table 3.1 Precursors and parameters used to synthesize cathode catalysts.

Catalyst	Precursors	Reaction Temperature (°C)	Reaction Time (h)	Calcination Temperature (°C)	Calcination Time(h)
Co <sub>3</sub> O <sub>4</sub> nanorods	3 g CoCl <sub>2</sub> +150 mg Urea	105	6	300	3.5
Co <sub>3</sub> O <sub>4</sub> flakes	3.4 g cobalt nitrate	200	6	300	3
Flower-like Co <sub>3</sub> O <sub>4</sub>	3.4 g cobalt nitrate	150	5.5	300	3
MnCo <sub>2</sub> O <sub>4</sub> nanorods	3.2 g HTAB + 0.3 g urea + 0.64 g CoCl <sub>2</sub> + 0.62 g MnCl <sub>2</sub>	100	24	300	3.5

### 3.4 Materials characterization

The synthesized nanomaterials were characterized by the following characterization techniques: (i) X-ray diffraction (XRD), (ii) Field emission scanning electron microscopy (FESEM), (iii) Transmission electron microscopy (TEM) and (iv) Brunauer-Emmett-Teller (BET) measurement, and X-ray photoelectron spectroscopy (XPS). The experimental procedures for these measurements are briefed below.

#### 3.4.1 Powder X-ray Diffraction (XRD)

A Rigaku miniflex II X- ray spectrometer was used in the present research work for obtaining the crystal structure. The spectrometer employs CuK $\alpha$  radiation (= 1.5406 Å) with an accelerating voltage of 30 kV and a Ni Filter for producing monochromatic X- rays. An approximate sample mass of 1g is fixed for all the samples and are milled

into fine powders with the help of small mortars. These fine milled powders were carefully pressed into the sample holder by another flat glass surface. This pressing removes any surface irregularities which may result in the shifting of peak position. XRD patterns were scanned at a rate of  $2^\circ/\text{min}$  with step size of  $0.02^\circ$  within a range of  $10^\circ$  to  $80^\circ$  after placing and locking the sample holder in the diffractometer. The corresponding phases were identified by comparing the calculated  $d$  value and the line strength of the corresponding measurement with standard reference pattern (powder diffraction pattern) published by international centre for diffraction data.

#### **3.4.2 Field Emission Scanning Electron Microscopy (FESEM)**

The morphology of the samples was determined using FESEM (JEOL, 7800F, USA). Initially, the samples were coated with Au using BIO-RAD Polaron Division SEM Coating System Machine after attaching the samples to the sample holder with double sided tapes. The coating procedure lasted for 75 seconds with 0.1 mbar pressure 75 mA current. The coated material was shifted to FESEM sample holder and micrographs at different magnification of the samples were obtained after evacuating the machine with a pressure of 5 bar.

#### **3.4.3 Transmission electron microscopy (TEM)**

TEM analysis was employed to further investigate the morphology of  $\text{Co}_3\text{O}_4$  nanorods and  $\text{MnCo}_2\text{O}_4$  nanorods. Firstly, the nanomaterials were properly mixed water to prepare the samples that were placed on 400 mesh copper grids and then analyzed using ZEISS LIBRA 120 with a scale bar from 50 nm to 200 nm. The TEM studies were carried out in International Islamic University Malaysia, Kuantan, Malaysia.

#### **3.4.4 Brunauer-Emmett-Teller (BET) measurement**

The surface area of all the samples was analyzed using ASAP 2020 (Micromeritics, USA). The sample tube was filled with  $\sim 2$  mg of powder and initially degassed in the heating mantle at  $200^\circ\text{C}$  for 20 h under nitrogen flow so as get rid of impurities such as moisture and physically adsorbed volatile compounds. After the purification, the sample tube was shifted to test channel where it was immersed in to liquid nitrogen for several minutes to have nitrogen adsorption. For the pore size as well as surface area measurements, nitrogen adsorption/de-adsorption isotherms at  $77^\circ\text{K}$  and

relative pressure ( $P/P_0$ ) ranging from 0.05 - 1.0 were employed. International Union of Pure and Applied Chemistry (IUPAC) classify the adsorption isotherms based on the pore types in to four; Type I (cylindrical pores), Type II (pore blocking), Type III (plate/slit type pores), Type IV (bottle neck pore type). All these measurements are required for plotting an isotherm to calculate the distribution of average material pore size.

Usually, the range of relative pressure for gas adsorption on the micropores were  $0.01 \leq P/P_0 \leq 0.2$ . The relative pressure  $< 0.01$  is required for the gas adsorption with pore width  $< 2\text{nm}$  while  $\sim 0.01 - 0.2$  is required for wider pores and  $> 0.2$  is needed for multilayer adsorption. From the isotherm plot, using the following equations (3.1& 3.2), monolayer capacity ( $n_m$ ) and specific surface area ( $S_{BET}$ ) can be calculated.

$$\frac{1}{W((P_0/P)-1)} = \frac{1}{W_m C} + \frac{C-1}{W_m C} (P/P_0) \quad 3.1$$

$$S_{BET} = W_m L \sigma \quad 3.2$$

where  $W$  is the amount of gas adsorbed at  $P/P_0$ ,  $W_m$  is the adsorbate mass constituting a monolayer of surface coverage,  $C$  is the BET constant also known as gas solid interaction constant whose value of  $N_2$  ranges from 50 to 250,  $L$  is the Avogadro constant and is the cross-sectional area. Barrett-Joyner-Halenda (BJH) equation (3.3) is used to calculate the mean pore size and type as well as the distribution of materials by assuming that  $P/P_0$  is  $\sim 1$  and the pores are uniformly filled with liquid.

$$V_p = \left( \frac{r_{pm}}{r_{kn} + \Delta t_n / 2} \right)^2 \left( \Delta V_n - \Delta t_n \sum_{j=1}^{n-1} A c_j \right) \quad 3.3$$

where  $V_p$ ,  $r_p$ ,  $r_k$ ,  $t_n$ ,  $A c$  are pore volume, pore radius, inner capillary radius, thickness of the nitrogen absorbed layer and the area exposed by the pore from which the physically adsorbed gas is desorbed.

### 3.4.5 X-ray Photoelectron Spectroscopy (XPS)

XPS technique was used to examine the chemical composition of  $MnCo_2O_4$  nanorods and to determine the possible ORR active sites on its surface. The surface atomic structure of the samples was analyzed using X-ray photoelectron spectrometer (Thermo scientific, K-Alpha, USA) operating with an X-ray source of Al-K $\alpha$  radiation. The sample powder was uniformly spread on to a small sticky tape pasted at the centre

of a small piece of aluminium foil. The sample was hydraulically pressed for one minute after covering the sample with another aluminium foil. The cover was removed and the sample was pasted on a carbon tape placed on the sample holder for the analysis.

### 3.5 Preparation of catalyst ink and its coating on cathodes

After the confirmation of the nanomaterials by the earlier mentioned techniques, the cathodes with a catalyst ink of a concentration were prepared by the following method, as shown in *Figure 3.2*. The catalyst ink contains, for 1 mg catalyst, 1  $\mu$ l (water), 7  $\mu$ l (5 % polyvinylidene difluoride), and 2  $\mu$ l (isopropyl alcohol) were mixed and stirred for 24 h to make a homogenous solution (Logan et al., 2006). The graphite sheets were selected as the electrode material for the cathode because graphite is highly conductive and much cheaper than other electrode materials such as carbon cloth and carbon paper (Logan et al., 2007). Besides, the graphite sheets (with a projected surface area of 15 m<sup>2</sup>) were treated with a sand paper to make the electrode surface rough. This was followed by 24 h successive treatments with 1M HCl and 1M NaOH to make the electrode surface more electrophilic (Minteer et al., 2012). Finally, the prepared ink was coated uniformly on the treated electrode with a paint brush on each side of the sample electrode. Further, the electrodes were dried in an oven at 65 °C for 24 h and then stored in distilled water (Logan et al., 2006).

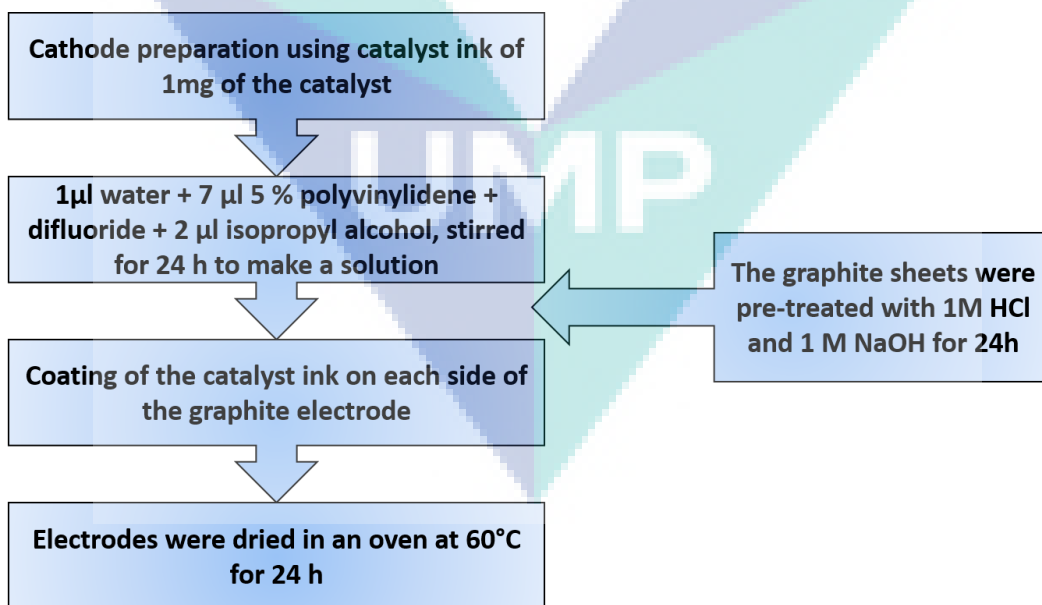


Figure 3.2 Preparation of cathodes for 1 mg catalyst.

Initially, four cathodes were prepared to optimize the catalyst concentration, one was bare cathode and other three with a catalyst ( $\text{Co}_3\text{O}_4$  nanorods) concentration of  $0.5 \text{ mg/cm}^2$ ,  $1 \text{ mg/cm}^2$ ,  $2 \text{ mg/cm}^2$  and were named as shown in Table 3.2. The higher concentrations of cathode catalysts were not used in this study because the literature suggests that the MFC performance starts decreasing with increase in the catalyst concentration (Quan et al., 2015). Later, for the other catalysts ( $\text{Co}_3\text{O}_4$  flakes, flower-like  $\text{Co}_3\text{O}_4$ ,  $\text{MnCo}_2\text{O}_4$  nanorods), only two cathodes were prepared, a bare cathode and one with the optimized concentration of the catalyst that is  $1 \text{ mg/cm}^2$  was used to investigate its performance in the MFC.

Table 3.2 Catalyst concentrations used in the study.

Catalyst	Concentration	Cathode (nomenclature)
Bare cathode	No catalyst	Bare cathode
$\text{Co}_3\text{O}_4$ nanorods	$0.5 \text{ mg/cm}^2$ -	CON-1
	$1 \text{ mg/cm}^2$ -	CON-2
	$2 \text{ mg/cm}^2$ -	CON-3
$\text{Co}_3\text{O}_4$ flakes	$1 \text{ mg/cm}^2$	COFK
Flower-like $\text{Co}_3\text{O}_4$	$1 \text{ mg/cm}^2$	COFL
$\text{MnCo}_2\text{O}_4$ nanorods	$1 \text{ mg/cm}^2$	MCON

### 3.6 Electrochemical characterization of the prepared cathodes

All the electrochemical tests were performed using a potentiostat (Gamry interface 1000, USA) using 100 mM PBS (pH=7) at room temperature  $25 \pm 2^\circ \text{C}$  in the similar MFC reactor which was further used in the experiments. A three-electrode system was used containing an Ag/AgCl electrode as the reference electrode, the platinum wire as the counter electrode and the prepared cathode as the working electrode, as shown in Figure 3.3.

#### 3.6.1 Cyclic voltammetry (CV)

In this research, CV test was performed for all the cathodes by sweeping the potential from  $-0.8\text{V}$  to  $0.8\text{V}$  at a scan rate of  $100 \text{ mV/s}$  in a three-electrode system, which contained Ag/AgCl electrode as the reference electrode, a platinum wire as the counter electrode and the prepared cathode as the working electrode. A detail of parameters used to carry out CV test is given in Appendix B.



Figure 3.3 (a) Photograph of potentiostat used in this research (b) principle of three electrode measurement.

CV is a method for investigating the electrochemical behaviour of a system. In this technique current flowing between the electrode of interest (whose potential is monitored with respect to a reference electrode) and a counter electrode is measured under the control of a potentiostat. The voltammogram determines the potentials at which different electrochemical processes occur. The working electrode is subjected to a triangular potential sweep, whereby the potential rises from a start value  $E_i$  to a final value  $E_f$  then returns back to the start potential at a constant potential sweep rate. The sweep rate applied can vary from a few millivolts per second to a hundred volts per second. A peak in the measured current is seen at a potential that is characteristic of any electrode reaction taking place. The peak width and height for a process may depend on the sweep rate, electrolyte concentration and the electrode material.

### 3.6.2 Linear sweep voltammetry (LSV)

In addition to CV, LSV was also carried out to investigate the electrochemical activity of all the cathodes. The LSV for all the cathodes was tested by sweeping the potential from -0.6 V to 0.4 V with a scan rate of 10 mV/s in the 100 mM PBS (pH=7) in the similar three-electrode system used to study CV. A detail of parameters used to carry out LSV test is given in Appendix C.

LSV is a voltammetric method where the current at a working electrode is measured while the potential between the working electrode and a reference electrode is

swept linearly in time. Oxidation or reduction of species is registered as a peak or trough in the current signal at the potential at which the species begins to be oxidized or reduced.

### 3.6.3 Electrochemical impedance spectroscopy (EIS)

The ion transport kinetics and the conductivity of the electrodes can be further evaluated using EIS studies. Therefore, EIS of all cathodes was measured over a frequency range of 1-100000 Hz at the initial open circuit potential with a sinusoidal perturbation of 10 mV amplitude. The EIS data were fitted to an equivalent electrical circuit (is shown later in the results) to calculate the activation resistance ( $R_{act}$ ) and ohmic resistance ( $R_{ohm}$ ) by using a software (Gamry Echem Analyst, USA). A detail of parameters used to carry out EIS test is given in Appendix D.

### 3.7 Oxygen reduction reaction kinetics study by Tafel plots

Tafel plots were prepared for all the cathodes to calculate the exchange current density, were recorded by sweeping the overpotential from 20 to 100 mV at 1 mV/s (Liu et al., 2014), versus Ag/AgCl as the reference electrode. The exchange current density was calculated by using the following equation:

$$\lg i = \lg i_0 - \frac{\beta n F \eta}{2.303 RT} \quad (3.1)$$

where,  $i$  is current density,  $i_0$  is exchange current density,  $R$  is gas constant ( $8.3144598(48) \text{ J} \cdot \text{mol}^{-1} \cdot \text{K}^{-1}$ ),  $T$  is temperature (Kelvin),  $F$  is Faraday constant,  $\beta$  is electron transfer coefficient,  $n$  is number of electrons, and  $\eta$  is overpotential. Besides, a linear region from Tafel plots was plotted to measure the intercept and the slope and Equation 3.1 was further solved to Equation 3.2 and used to calculate the exchange current density.

$$\log \frac{i}{i_0} = \frac{E}{b} \quad (3.2)$$

where  $i$  is current density,  $i_0$  is exchange current density,  $E$  is overpotential and  $b$  is the slope.

For example, if a linear equation,  $y=5.8101x-1.9801$  and  $E=0.07 \text{ V}$ , therefore,  $i=1.9801$ , slope= $5.8101$ , the  $i_0$  calculated was  $1.89 \text{ A/m}^2$ .

The exchange current is the current at equilibrium, i.e. the rate at which oxidized and reduced species transfer electrons with the electrode (Ge et al., 2016). In other words,

the exchange current density is the rate of reaction at the reversible potential (when the overpotential is zero by definition). At the reversible potential, the reaction is in equilibrium meaning that the forward and reverse reactions progress at the same rates. This rate is the exchange current density.

In this research work, exchange current density was taken as a key parameter to analyse the ORR activity of the cathodes because the larger the exchange current density, the faster will be the oxygen reduction, and vice versa (Ge et al., 2015), which will have a direct influence on the MFC performance. A detail of parameters used to carry out Tafel plots test is given in Appendix E.

### 3.8 Microbial fuel cell construction and operation

A double-chamber MFC was used to investigate the performance of all the prepared cathodes loaded with different concentrations of the catalyst ( $\text{Co}_3\text{O}_4$  nanorods,  $\text{Co}_3\text{O}_4$  flakes, flower-like  $\text{Co}_3\text{O}_4$ ,  $\text{MnCo}_2\text{O}_4$  nanorods). The double chamber MFC was constructed with a cylindrical Plexiglas chamber, with a total working volume of 240 mL. *Figure 3.4* shows the diagram of the MFC used in this research work. Graphite sheets were used as the anode, which were also treated similar to the cathodes. The prepared cathodes with specific concentration of the catalyst as mentioned earlier in section 3.5 were employed as the cathode.



Figure 3.4 (a) Picture of double chamber MFC used in this work (b) MFC during operation.

The distance between the anode and the cathode was 6 cm. A proton exchange membrane, Nafion 117 with a projected surface area of 10.5 cm<sup>2</sup> was placed between the two chambers. The anode and the cathode were connected with a titanium wire. 100 mM phosphate-buffered saline (PBS) (pH = 7) was used as the catholyte. The PBS contained: Na<sub>2</sub>HPO<sub>4</sub>, 9.125 g/L; NaH<sub>2</sub>PO<sub>4</sub>, 4.904 g/L; NH<sub>4</sub>Cl, 0.31g/L; KCl, 0.13 g/L. The 100 mM PBS was added with trace elements (12.5 mL/L), vitamins (12.5 mL/L) and sodium acetate (2 g/L), was used as the anolyte (Guo et al., 2015). The anode chamber was sparged with pure nitrogen gas for 30 min to ensure the anaerobic conditions in the chamber. In the cathode chamber, air was continuously sparged with an air pump to maintain a sustained concentration of oxygen during the MFC operation (Logan et al., 2007). All the MFCs were operated at the room temperature, 25±2° C. The MFC experiments were repeated three times and the average with standard deviation was taken as the final result.

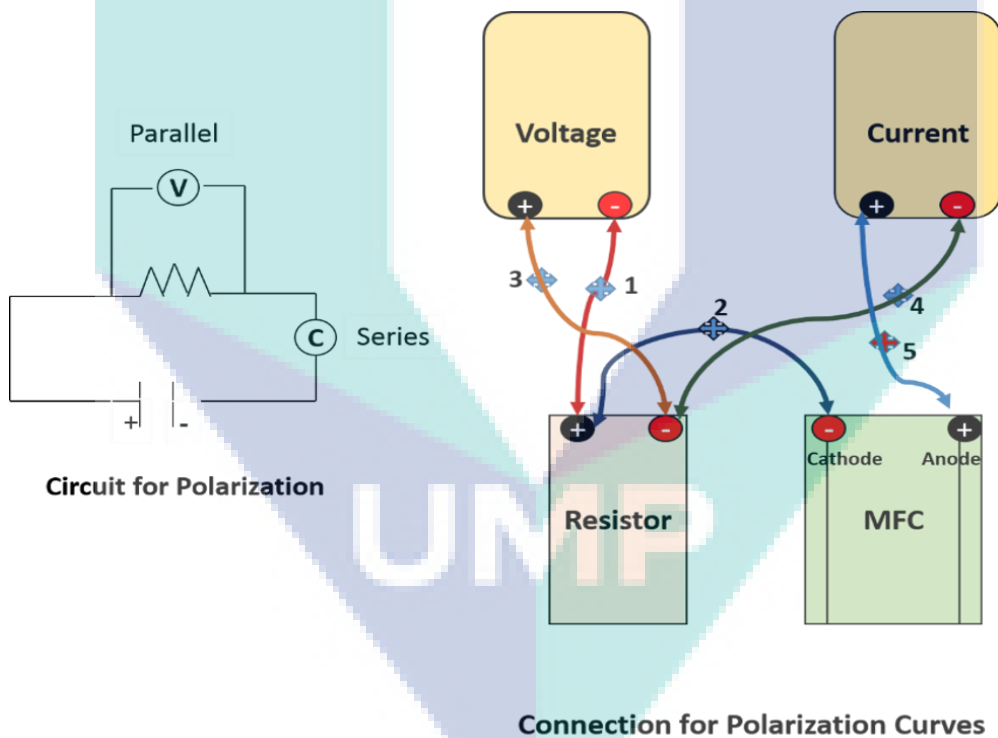


Figure 3.5 Diagram of the connection for polarization curves.

The power was calculated from the polarization curves by the formula,  $P=V \times I$ , where P is power, V is voltage and I is current (Logan et al., 2006). The current and power were normalised by projected surface area of the cathode (15 cm<sup>2</sup>) to obtain the current density and power density, respectively. Moreover, the electrode potential of anode and

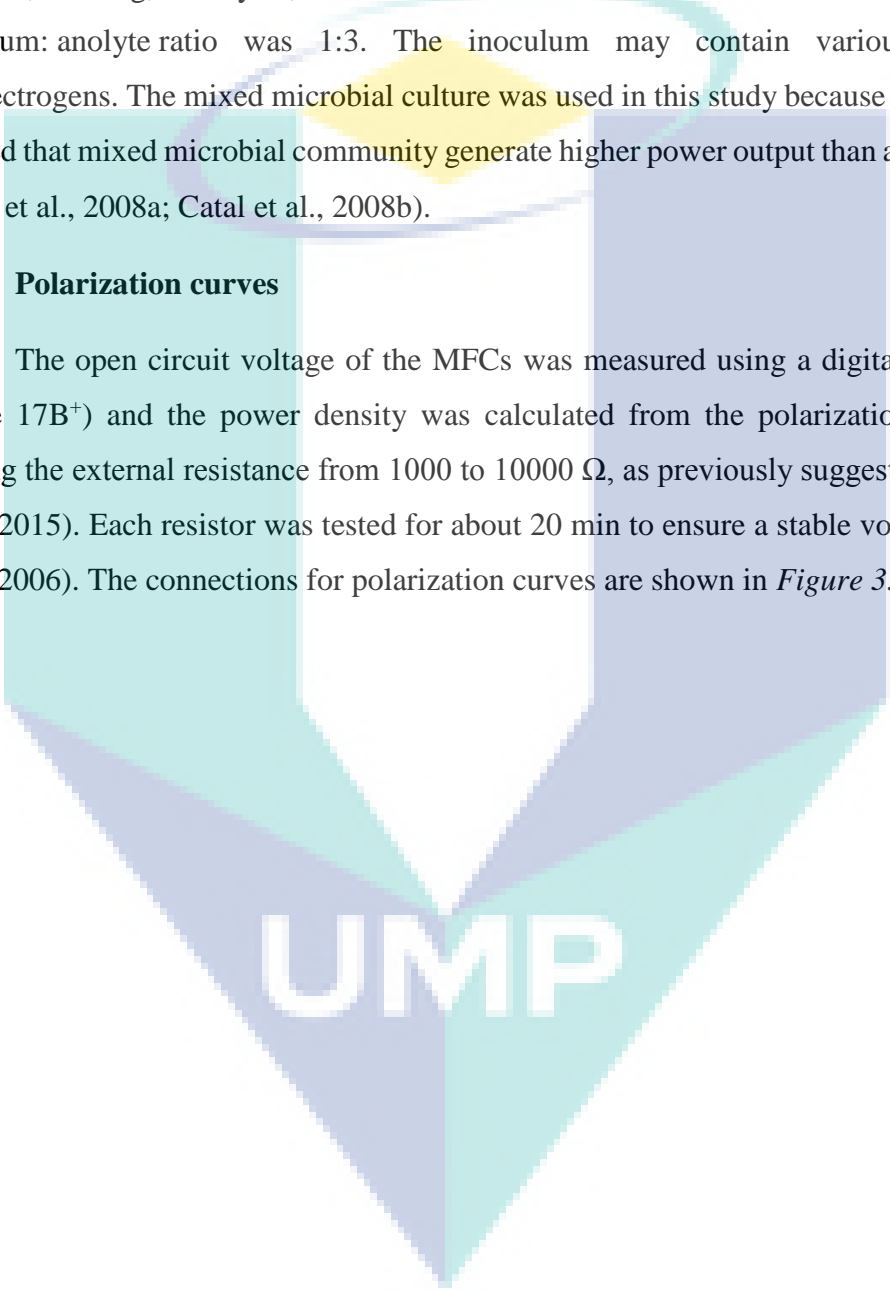
cathode was measured using Ag/AgCl as the reference electrode, by placing the reference electrode near to the working electrode (Logan et al., 2006).

### **3.9 Inoculum**

Anaerobic sludge was collected from Panching palm oil mill (FELDA) located in Kuantan, Pahang, Malaysia, was used as the inoculum for all the MFCs and the inoculum: anolyte ratio was 1:3. The inoculum may contain various types of exoelectrogens. The mixed microbial culture was used in this study because the literature showed that mixed microbial community generate higher power output than a pure culture (Catal et al., 2008a; Catal et al., 2008b).

### **3.10 Polarization curves**

The open circuit voltage of the MFCs was measured using a digital multimeter (Fluke 17B<sup>+</sup>) and the power density was calculated from the polarization curves by varying the external resistance from 1000 to 10000  $\Omega$ , as previously suggested by (Yang et al., 2015). Each resistor was tested for about 20 min to ensure a stable voltage (Logan et al., 2006). The connections for polarization curves are shown in *Figure 3.5*.



UMP

## CHAPTER 4

### RESULTS AND DISCUSSION

#### 4.1 Introduction

This chapter discusses all the results of the three objectives aimed for this research work, to study the morphological effect of cathode catalyst on ORR and power output in MFCs. Therefore, in the first objective,  $\text{Co}_3\text{O}_4$  nanorods were prepared via a hydrothermal method and studied its ORR activity and later investigated its performance for power output in a double chamber MFC. Moreover,  $\text{Co}_3\text{O}_4$  flakes and flower-like  $\text{Co}_3\text{O}_4$  were synthesized and were examined for ORR activity. Finally,  $\text{MnCo}_2\text{O}_4$  nanorods were fabricated by a hydrothermal route and its ORR activity was studied by different electrochemical techniques.

#### 4.2 To synthesize three morphologies of $\text{Co}_3\text{O}_4$ (nanorods, flakes and flower) for cathode catalyst by hydrothermal methods and their characterization by physiochemical and microscopy techniques

Cobalt oxide is recognized as a promising ORR catalyst in MFCs and its ORR catalytic activity can be further ameliorated by developing its different mesoporous morphologies. Therefore, keeping this point in mind, in the first objective of this study, three different morphologies of  $\text{Co}_3\text{O}_4$  were synthesized by using a facile and cost-effective hydrothermal method. Three morphologies fabricated were  $\text{Co}_3\text{O}_4$  nanorods,  $\text{Co}_3\text{O}_4$  flakes, and  $\text{Co}_3\text{O}_4$ -flower. These nanomaterials were further characterized by XRD and electron microscopic techniques. In addition, the surface areas and porous properties were studied by BET technique.

#### 4.2.1 XRD analysis of Co<sub>3</sub>O<sub>4</sub> nanorods, Co<sub>3</sub>O<sub>4</sub> flakes, and Co<sub>3</sub>O<sub>4</sub>-flower

The Co<sub>3</sub>O<sub>4</sub> nanorods synthesized using a simple hydrothermal method were assumed to be formed in two steps. In the first step of the hydrothermal process, an intermediate product Co<sup>II</sup>(OH)<sub>a</sub>(CO<sub>3</sub>)<sub>b</sub>Cl<sub>(2-a-2b)</sub>·nH<sub>2</sub>O could be formed. The crystalline structure of this intermediate product contains Co-OH layers and counteranions between the Co-OH layers (Hosono et al., 2005). In the subsequent calcination step, the Co-OH layers were converted into Co<sub>3</sub>O<sub>4</sub> nanoparticles through dehydration and pyrolysis of counteranions into gases (Hosono et al., 2005). The spaces between the counteranions and -OH were converted into pores, resulting porous Co<sub>3</sub>O<sub>4</sub> nanorods as the end product. On the other hand, mesoporous Co<sub>3</sub>O<sub>4</sub> flakes and Co<sub>3</sub>O<sub>4</sub>-flower were also prepared by a two-step hydrothermal method. In both the cases, in the initial step, Co(OH)<sub>2</sub> could be formed, which could be transformed into Co<sub>3</sub>O<sub>4</sub> flakes and flower-like Co<sub>3</sub>O<sub>4</sub> at 300 °C after 3 h. The crystalline structure of all the catalysts was investigated by XRD analysis. The XRD pattern of diffraction peaks for all three morphologies of Co<sub>3</sub>O<sub>4</sub> is shown in *Figure 4.1*. Different diffraction peaks were observed at different angles for Co<sub>3</sub>O<sub>4</sub> nanorods, Co<sub>3</sub>O<sub>4</sub> flakes and Co<sub>3</sub>O<sub>4</sub> flower, which are given in Table A1, Table A2, and Table A3, respectively. All the peaks can be indexed to cubic spinel structure and Fd3m: 2 space group, which were consistent with Joint committee on Power Diffraction Standards (JCPDS) Card No. 653103. Besides, no impurity peak was observed in the XRD patterns, suggesting a pure form of the final product.

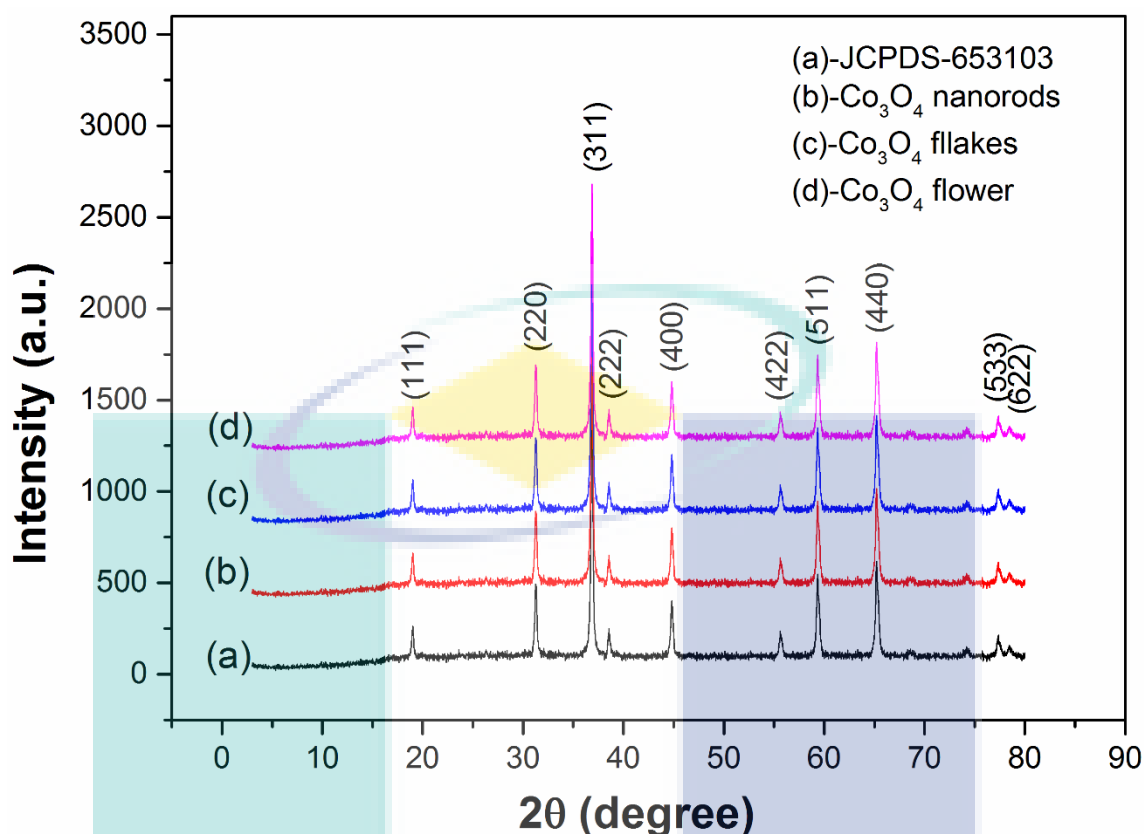


Figure 4.1 XRD pattern of Co<sub>3</sub>O<sub>4</sub> nanorods, Co<sub>3</sub>O<sub>4</sub> flakes and Co<sub>3</sub>O<sub>4</sub>-flower.

#### 4.2.2 FESEM and TEM results

Further, the morphology of all the catalysts were observed by electron microscopes. The nanorods was analyzed by FESEM and TEM technology. *Figure 4.2* shows FESEM images of Co<sub>3</sub>O<sub>4</sub> nanorods at different magnifications and *Figure 4.3* shows images of TEM. The results of FESEM and TEM confirmed that shape of the final product obtained by the hydrothermal method was rod shaped.

The morphologies of Co<sub>3</sub>O<sub>4</sub> flakes and Co<sub>3</sub>O<sub>4</sub> flower were analyzed by FESEM. *Figure 4.4* shows the FESEM images of Co<sub>3</sub>O<sub>4</sub> flakes. It can be clearly observed from the images that flakes like morphology was successfully developed in the study. Moreover, the pores can be easily seen on the surface of the flakes. *Figure 4.5* shows the FESEM images of Co<sub>3</sub>O<sub>4</sub> flower at different magnifications. A multi-layered petal forming a flower-like structure could be clearly observed in the images. Therefore, these results confirmed that the product synthesized by the hydrothermal method was flower-like Co<sub>3</sub>O<sub>4</sub>.

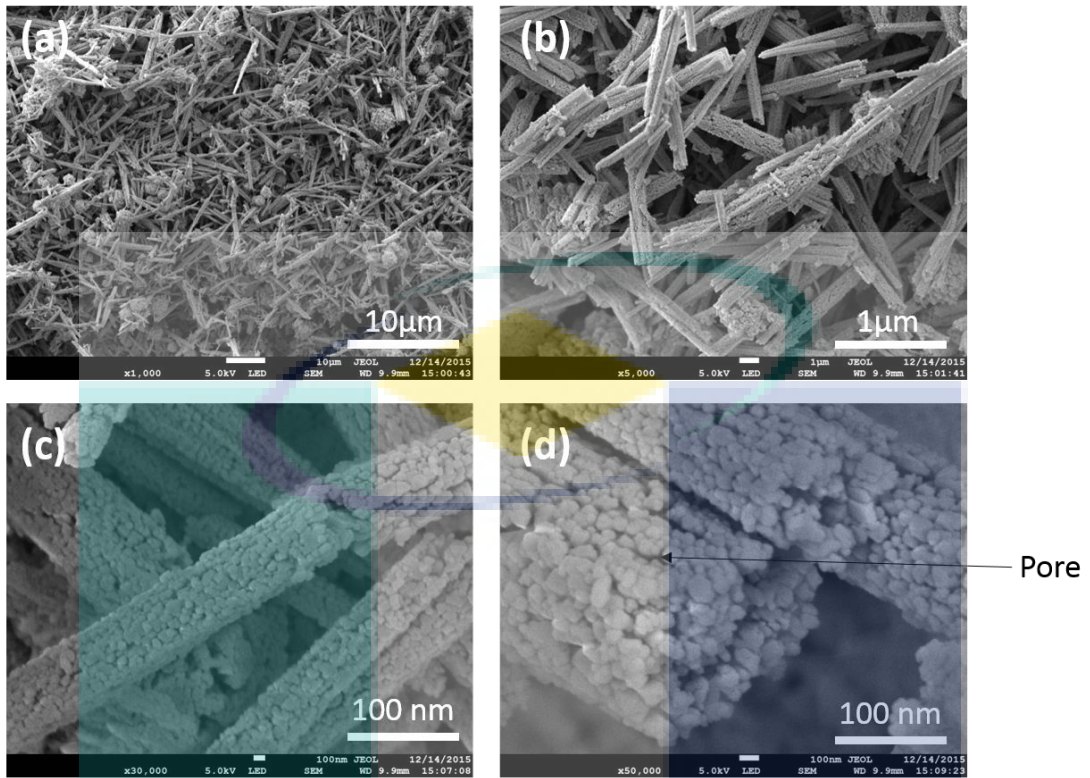


Figure 4.2 FESEM images of porous  $\text{Co}_3\text{O}_4$  nanorods at different magnifications.

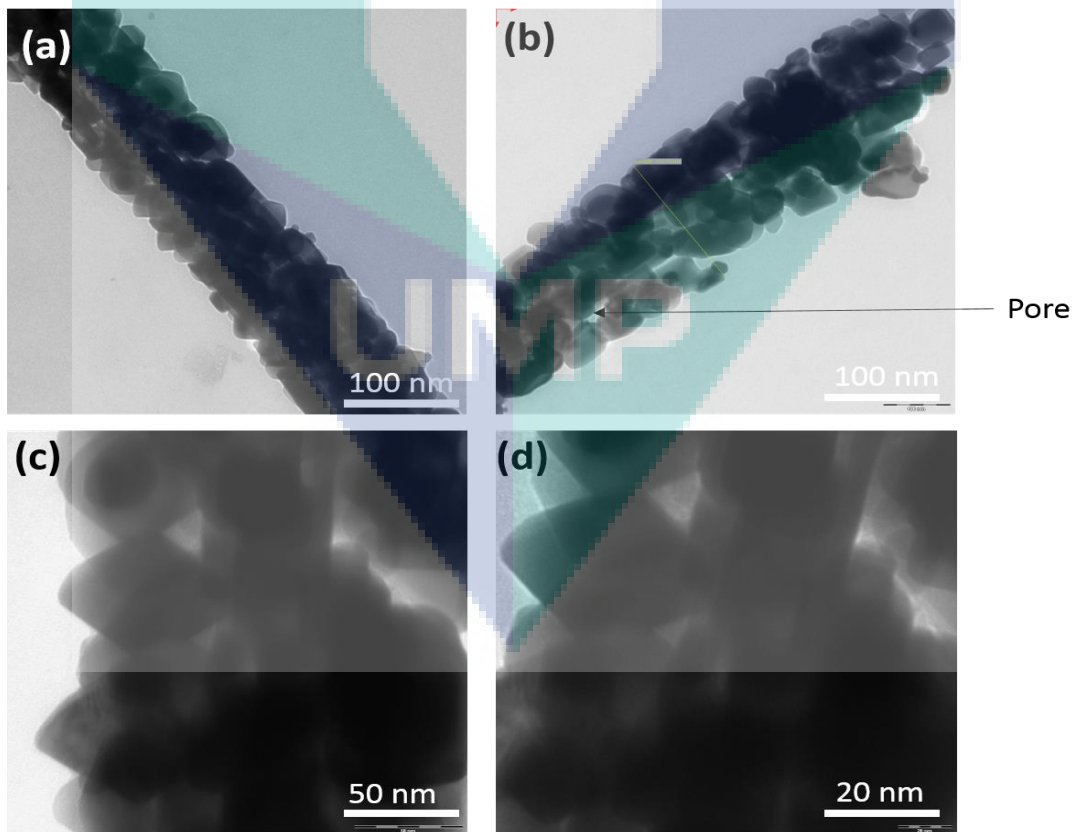


Figure 4.3 TEM images of  $\text{Co}_3\text{O}_4$  nanorods.

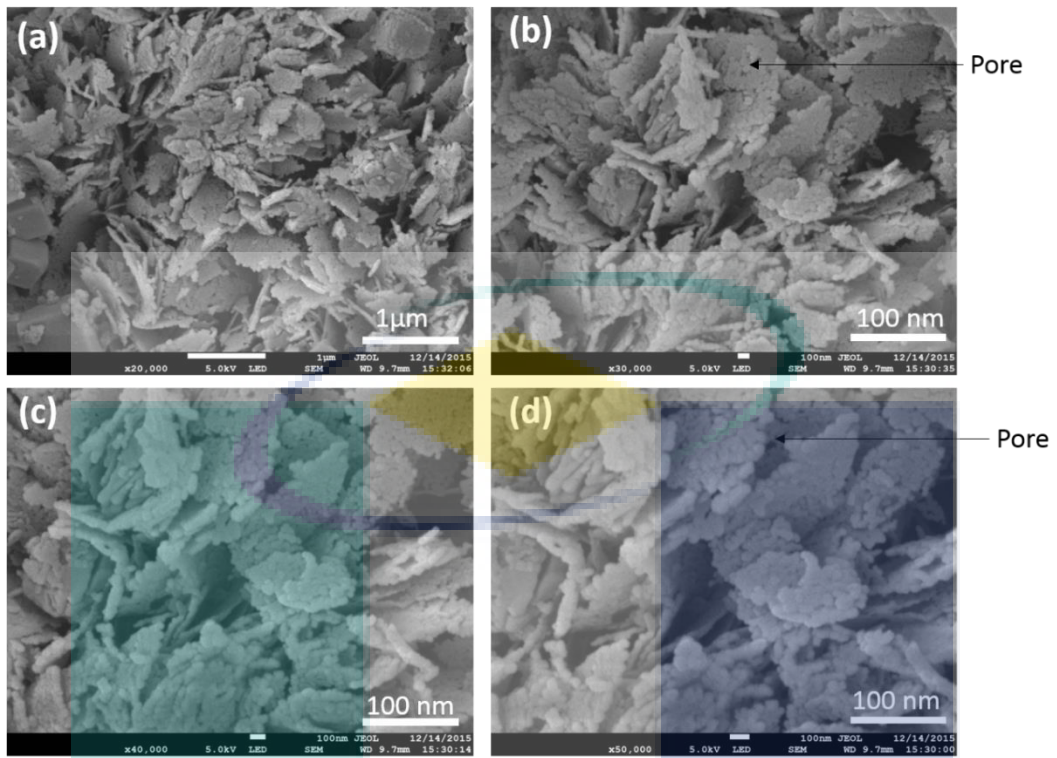


Figure 4.4 FESEM images of  $\text{Co}_3\text{O}_4$  flakes.

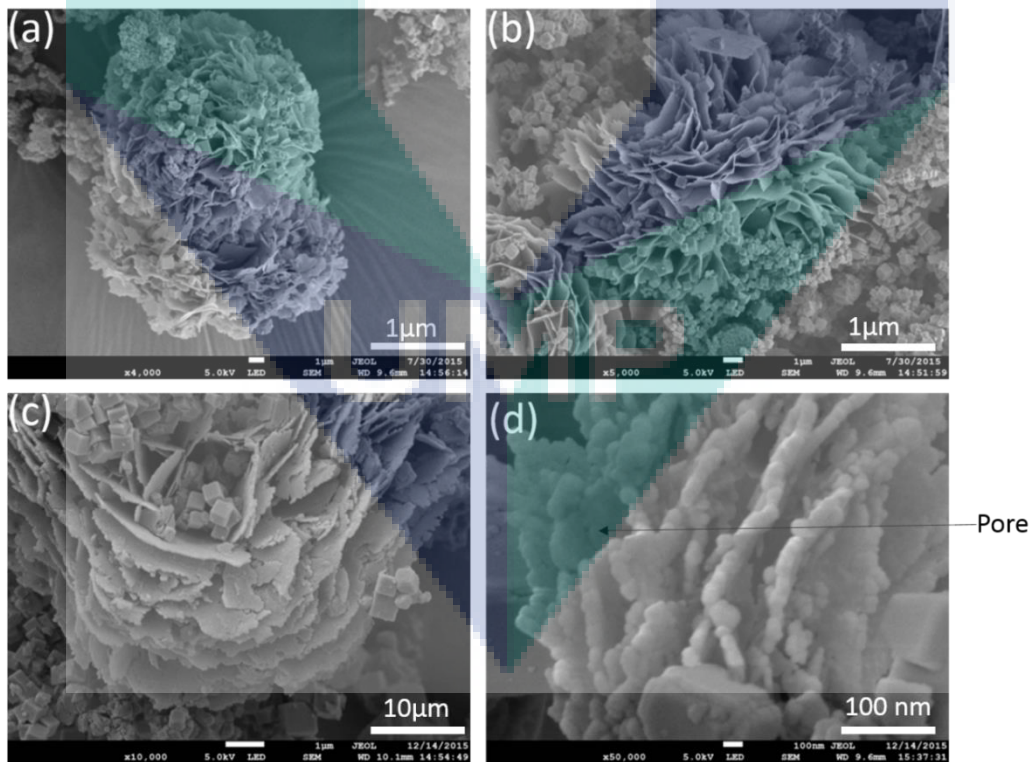


Figure 4.5 FESEM images of  $\text{Co}_3\text{O}_4$  flower at different magnifications.

### 4.2.3 BET results

Furthermore, BET analysis was carried out to investigate the surface area, pore volume and pore diameter of all the catalysts. The surface area, pore diameter and pore volume was calculated using nitrogen adsorption/de-adsorption isotherms as mentioned in the methodology chapter. The BET results for all the catalysts are presented in the following Table 4.1.

Table 4.1 BET results for different morphologies of  $\text{Co}_3\text{O}_4$ .

Catalyst	BET surface area	Average pore volume	Average pore diameter	Reference
$\text{Co}_3\text{O}_4$ nanorods	15.55 $\text{m}^2/\text{g}$	0.088 $\text{cm}^3/\text{g}$	22.70 nm	This study
$\text{Co}_3\text{O}_4$ flakes	11.05 $\text{m}^2/\text{g}$	0.013 $\text{cm}^3/\text{g}$	14.85 nm	This study
$\text{Co}_3\text{O}_4$ flower	05.03 $\text{m}^2/\text{g}$	0.082 $\text{cm}^3/\text{g}$	38.55 nm	This study
Bare-AC	1725.87 $\text{m}^2/\text{g}$	-	-	(Ge et al., 2015)
Spinel $\text{Co}_3\text{O}_4$ -AC	1536.51 $\text{m}^2/\text{g}$	-	-	(Ge et al., 2015)
$\text{Co}(\text{OH})_2$ -AC	1753 $\text{m}^2/\text{g}$	0.25 $\text{cm}^3/\text{g}$	-	(Liu et al., 2016)
$\text{Co}_3\text{O}_4$ nanosheets-AC	1873.95 $\text{m}^2/\text{g}$	0.26 $\text{cm}^3/\text{g}$	-	(Liu et al., 2016)
$\text{NiCo}_2\text{O}_4$ -AC	104.4 $\text{m}^2/\text{g}$	-	46.8	(Ge et al., 2016)

The BET surface area of  $\text{Co}_3\text{O}_4$  nanorods was  $\sim 15.55 \text{ m}^2/\text{g}$ . The average width of a pore in the nanorods was 22.70 nm, which was taken mean of the adsorption and the desorption pore width. Moreover, the pore volume in  $\text{Co}_3\text{O}_4$  nanorods was  $0.088 \text{ cm}^3/\text{g}$ , which was higher than the catalysts  $\text{Co}_3\text{O}_4/\text{AC}$  and  $\text{Co}(\text{OH})_2/\text{AC}$  used in the recent study (Liu et al., 2016). The adsorption isotherm curve for  $\text{Co}_3\text{O}_4$  nanorods is shown in *Figure 4.6*, which is type III isotherm, proving the mesoporous structure of the nanomaterial. Thus it can be suggested that  $\text{Co}_3\text{O}_4$  nanorods was mesoporous. The higher pore volume of  $\text{Co}_3\text{O}_4$  nanorods could provide the higher number of pores on the catalyst surface and consequently, more active sites for oxygen molecules. It has been suggested that the porous architecture of the nanomaterials could provide more accessible surface area for oxygen adsorption and passage of electrolyte and other ions through the pores could enhance the electrocatalytic activity (Liu et al., 2016). The mesoporous property has successfully enhanced the ORR activity of the nanomaterials in MFC applications (He et al., 2016; Song et al., 2015; Liang et al., 2012). Evidently, mesoporous microvillus-like carbon nanotubes showed much higher ORR activity than the bare electrode and the results were also comparable to many other conventional catalysts (He et al., 2016). This is particularly because the pores on the catalyst surface provided extra active sites to reduce oxygen molecules and improved the ORR kinetics significantly and ultimately,

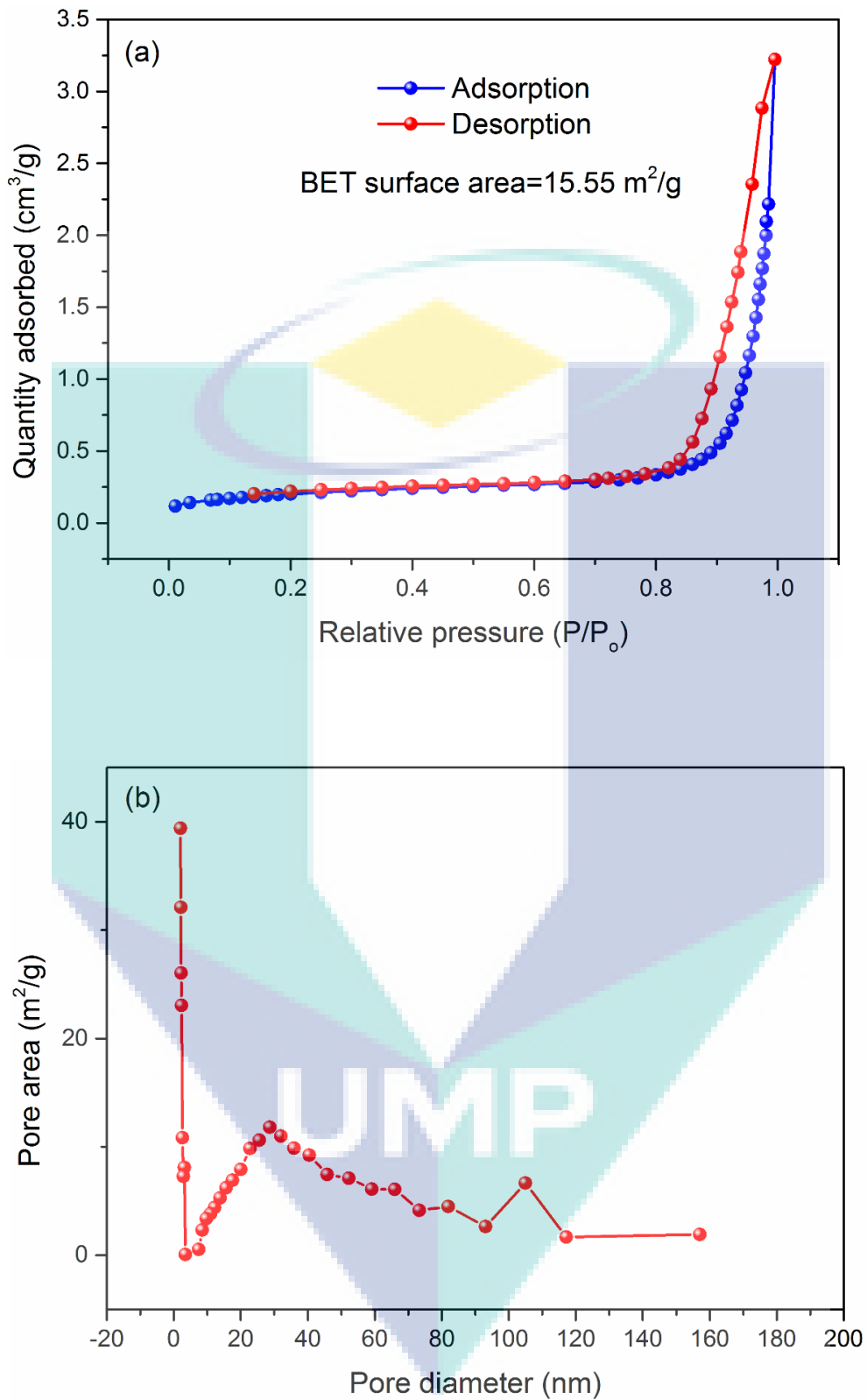


Figure 4.6 (a) Nitrogen adsorption-desorption isotherms of  $\text{Co}_3\text{O}_4$  nanorods, (b) variations in pore diameter of  $\text{Co}_3\text{O}_4$  nanorods.

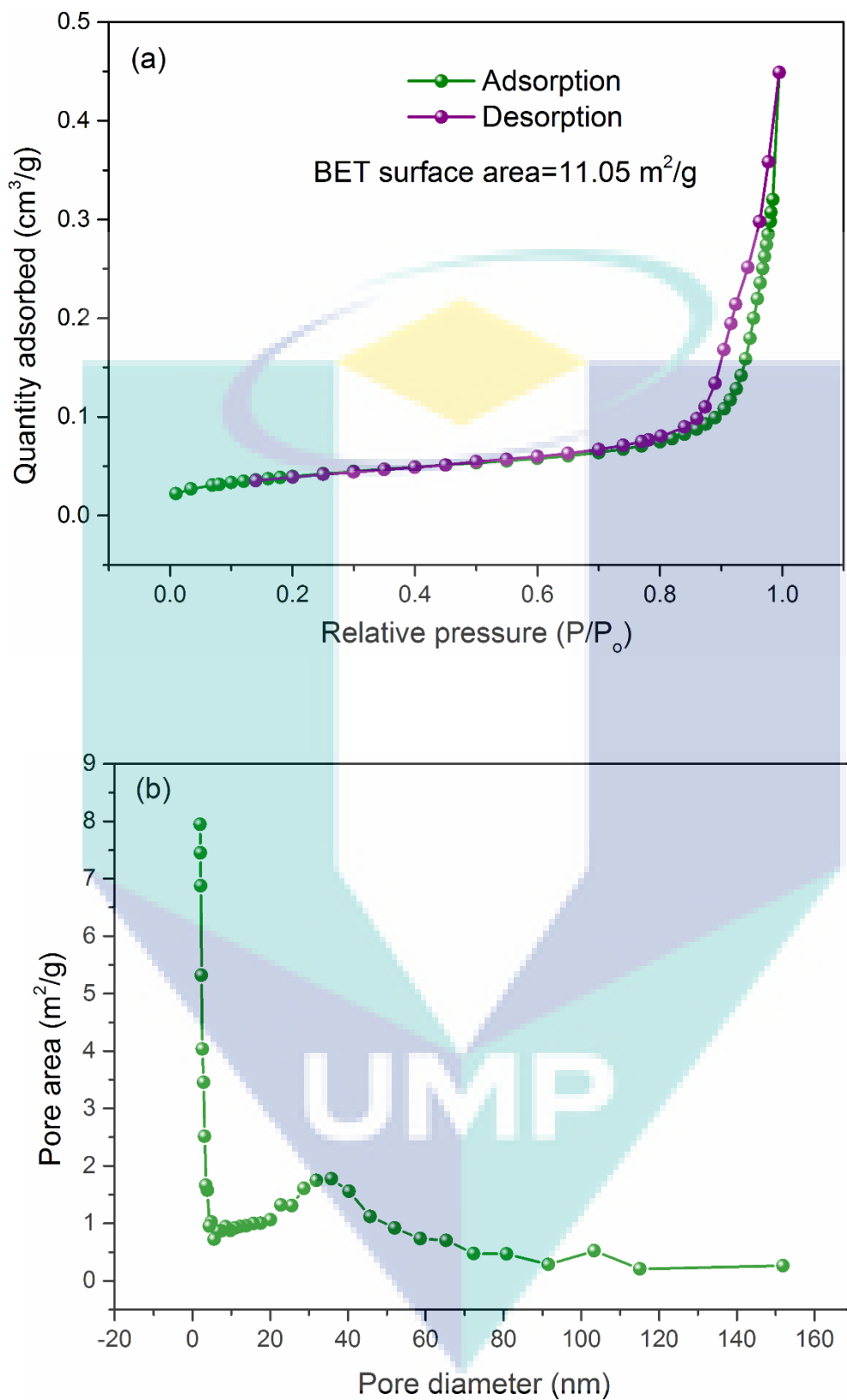


Figure 4.7 (a) Nitrogen adsorption-desorption isotherms of  $\text{Co}_3\text{O}_4$  flakes, (b) variations in pore diameter of  $\text{Co}_3\text{O}_4$  flakes.

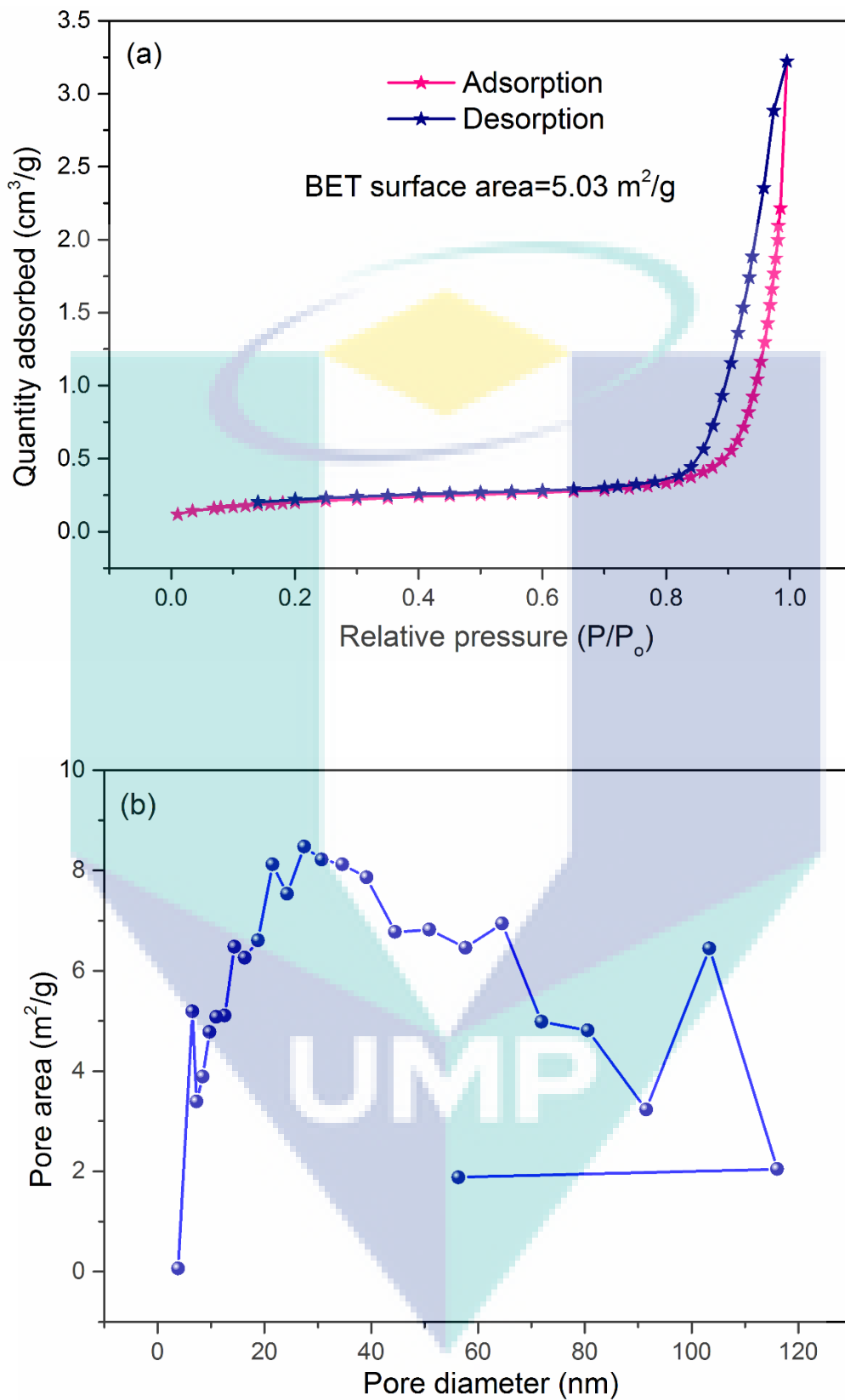


Figure 4.8 (a) Nitrogen adsorption-desorption isotherms of  $\text{Co}_3\text{O}_4$  flower, (b) variations in pore diameter of  $\text{Co}_3\text{O}_4$  flower.

enhanced the power output in MFCs. Moreover, cobalt oxide has high affinity towards oxygen molecules, which makes it more favorable for chemisorptions of oxygen molecules onto the catalyst surface and hence, enhances the ORR activity (Winfield et al., 2016).

The BET surface areas shown by  $\text{Co}_3\text{O}_4$  flakes and  $\text{Co}_3\text{O}_4$  flower were lesser as compared to  $\text{Co}_3\text{O}_4$  nanorods. The results demonstrated that  $\text{Co}_3\text{O}_4$  flakes and  $\text{Co}_3\text{O}_4$  flower exhibited the BET surface area of  $11.05 \text{ m}^2/\text{g}$  and  $5.03 \text{ m}^2/\text{g}$ , respectively. Therefore, it can be suggested that BET surface area of  $\text{Co}_3\text{O}_4$  flakes was approximately 40% lower than the nanorods and ~119% higher than  $\text{Co}_3\text{O}_4$  flower. On the other hand, Besides, the pore volume in  $\text{Co}_3\text{O}_4$  flakes and  $\text{Co}_3\text{O}_4$  flower was  $0.013 \text{ cm}^3/\text{g}$  and  $0.082 \text{ cm}^3/\text{g}$ , respectively. The average pore diameter in  $\text{Co}_3\text{O}_4$  flakes was  $14.85 \text{ nm}$  while average pore diameter in  $\text{Co}_3\text{O}_4$  flower was  $38.55 \text{ nm}$ . The adsorption isotherm curves for  $\text{Co}_3\text{O}_4$  flakes and  $\text{Co}_3\text{O}_4$  flower are shown in *Figure 4.7* and *Figure 4.8*, respectively. It can be clearly observed that the isotherm curves shown by  $\text{Co}_3\text{O}_4$  flakes and  $\text{Co}_3\text{O}_4$  flower are type III isotherm, which prove the mesoporous structure of both the nanomaterials. The variation in the BET surface is primarily dependant on the morphology of the nanomaterial. The different morphologies bring out the different arrangement of atoms inside the crystal structure, which ultimately changes the sites for the gas adsorption. The different morphologies could exhibit dissimilar surface area and porous properties that ultimately play an important role in its electrocatalytic activity. For example, in this study, a similar material that is  $\text{Co}_3\text{O}_4$  showed a large variation in the BET surface in its three morphologies and the quantity of pores in the nanostructure was also diverse. The higher BET surface area and larger pore volume can provide higher ORR active sites and can improve the ORR activity of the cathodes and consequently, the power output in MFCs.

### 4.3 To fabricate cathodes with the prepared catalysts and examine their oxygen reduction activity by electrochemical techniques and investigate their potential for bioelectricity generation in MFCs

In the previous objective, three different morphologies of  $\text{Co}_3\text{O}_4$  were successfully synthesized and identified by physiochemical and microscopic techniques. These three forms of  $\text{Co}_3\text{O}_4$  were used the cathode catalyst for oxygen reduction in MFCs. Therefore, a catalyst ink of all the catalysts was prepared as mentioned in the methodology section and coated on the graphite electrodes. The concentrations of the catalysts used in this study are given in Table 4.2. The concentration of catalyst was limited to  $2 \text{ mg/cm}^2$  initially because the literature showed that the higher concentration of the cathode catalyst resulted in lesser power density in MFCs (Awan et al., 2014; Burkitt et al., 2014; Chang et al., 2014; Cheng et al., 2006). This could be because the higher catalyst concentration forms multiple layers on the cathode surface and the oxygen molecules couldn't access the active sites present in the inner layers of the catalyst. In other words, a higher concentration of a cathode catalyst does not provide more accessible sites for oxygen reduction (Cheng et al., 2006). On the other hand, an optimum concentration of the cathode catalyst can provide higher ORR active sites and would be suitable for a higher ORR activity and subsequently, for improved MFC performance.

Table 4.2 Cathodes prepared with specific concentration of the catalyst.

Cathode	Catalyst	Concentration
Bare cathode	No catalyst	-
CON-1	$\text{Co}_3\text{O}_4$ nanorods	$0.5 \text{ mg/cm}^2$
CON-2	$\text{Co}_3\text{O}_4$ nanorods	$1 \text{ mg/cm}^2$
CON-3	$\text{Co}_3\text{O}_4$ nanorods	$2 \text{ mg/cm}^2$
COFK	$\text{Co}_3\text{O}_4$ flakes	$1 \text{ mg/cm}^2$
COFL	$\text{Co}_3\text{O}_4$ flower	$1 \text{ mg/cm}^2$

Initially, three concentrations of the cathode catalyst ( $\text{Co}_3\text{O}_4$  nanorods) was experimented in this study to find out the optimum concentration for the later catalysts. The results showed that the cathode with  $1 \text{ mg/cm}^2$  of  $\text{Co}_3\text{O}_4$  nanorods achieved 4.6 times higher power density than the bare cathode in the MFC while the subsequent increase in the concentration that is  $2 \text{ mg/cm}^2$  of  $\text{Co}_3\text{O}_4$  nanorods could increase the power output only by  $\sim 10\%$ . Therefore,  $1 \text{ mg/cm}^2$  was found more advantageous for MFC performance and was further used for the other catalysts as well.

### 4.3.1 Cyclic voltammetry of all the cathodes

All the cathodes coated with varying concentration of  $\text{Co}_3\text{O}_4$  nanorods,  $\text{Co}_3\text{O}_4$  flakes, and  $\text{Co}_3\text{O}_4$  flower were characterized by CV to evaluate the ORR performance in 100 mM PBS saturated with oxygen. The bare cathode was taken as a control cathode. The CV of all the cathodes were recorded by sweeping the potential from -0.8V to 0.8V (V vs. Ag/AgCl) at the scan rate of 100 mV/s. The cyclic voltammograms of all the cathodes with  $\text{Co}_3\text{O}_4$  nanorods (CON-1, CON-2, and CON-3) are shown in *Figure 4.9* while *Figure 4.10a* and *Figure 4.10b* show the cyclic voltammograms of the cathodes with  $\text{Co}_3\text{O}_4$  flakes (COFK) and  $\text{Co}_3\text{O}_4$  flower (COFL), respectively.

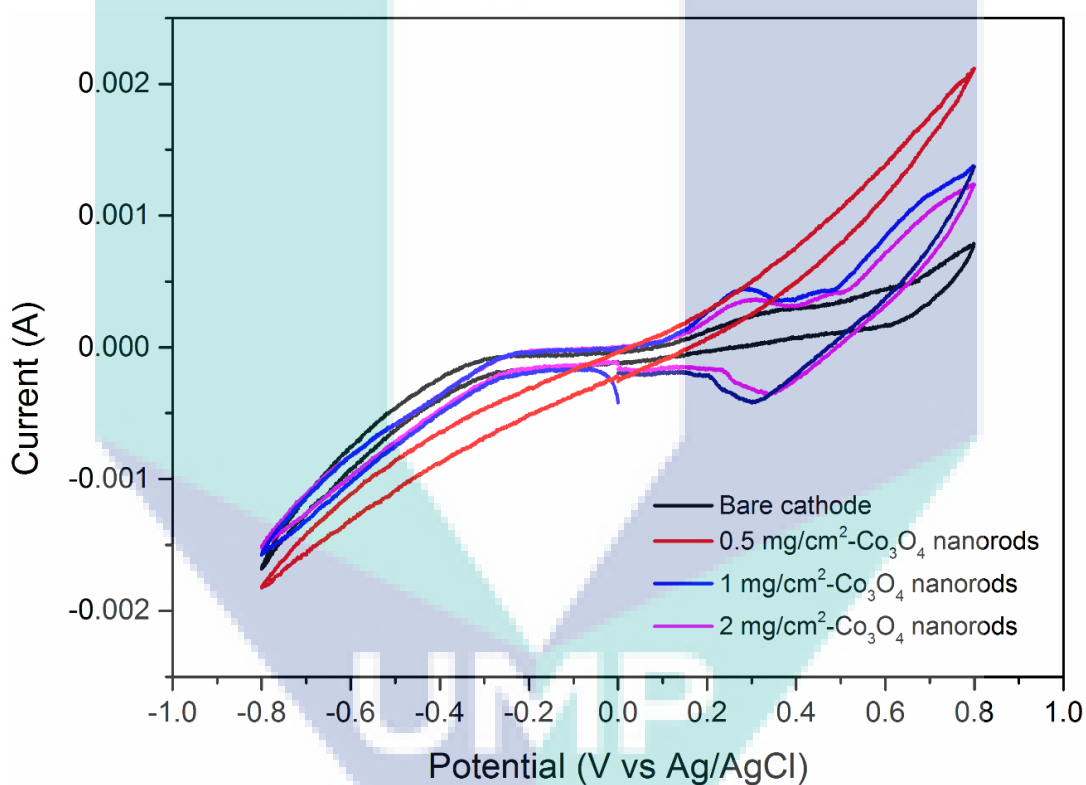


Figure 4.9 Cyclic voltammograms of all the cathodes with  $\text{Co}_3\text{O}_4$  nanorods.

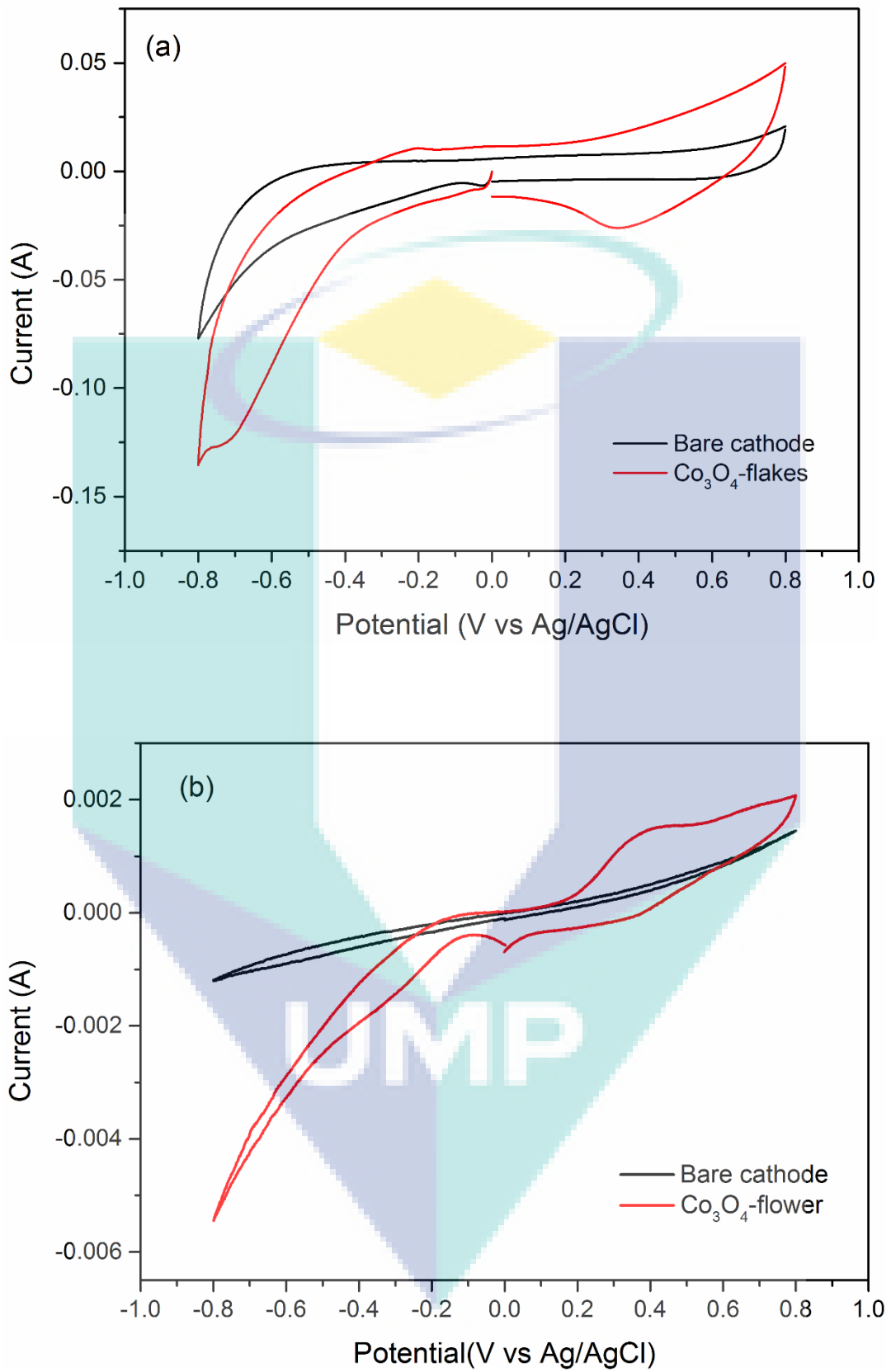


Figure 4.10 (a) Cyclic voltammogram of the cathode with  $\text{Co}_3\text{O}_4$  flakes and (b) the cathode with  $\text{Co}_3\text{O}_4$  flower.

The results demonstrated that the cathode with  $2 \text{ mg/cm}^2$   $\text{Co}_3\text{O}_4$  nanorods (CON-3) showed a sharp cathodic peak at the potential  $0.39 \text{ V}$  vs.  $\text{Ag/AgCl}$ , which was most positive than the other cathodes i.e.  $1 \text{ mg/cm}^2$   $\text{Co}_3\text{O}_4$  (CON-2),  $0.5 \text{ mg/cm}^2$   $\text{Co}_3\text{O}_4$  (CON-1), and bare cathode. The improved ORR activity can be attributed to the availability of abundant pores on the electrode surface that provided more active sites for oxygen molecules. Therefore, the electrode with the maximum concentration of  $\text{Co}_3\text{O}_4$  nanorods obviously have the higher number of active sites for the electron acceptor (oxygen) and thus showed the best catalytic activity for ORR among the other cathodes. Moreover, the CV results of  $\text{Co}_3\text{O}_4$  flakes suggested that addition of  $\text{Co}_3\text{O}_4$  flakes ameliorated the oxygen reduction activity of the cathode. Evidently, bare cathode did not show any reduction peak in the cyclic voltammogram, However, COFK exhibited a clear reduction peak at a potential of  $0.36 \text{ V}$ , which determined its higher ORR activity as compared to other cathodes. Moreover, the higher activity of COFK could be also gleaned from the higher peak current. The higher ORR activity of COF-2 could be attributed to mesoporous  $\text{Co}_3\text{O}_4$  flakes that provided increased number of effective active sites on the cathode surface, which enhanced the oxygen reduction. Besides, the pores on  $\text{Co}_3\text{O}_4$  flakes surface might have represented extra accessible ORR active sites that improved the electrocatalytic activity of COF-2. However, the onset potential achieved by COFK was slightly lower than the CON-2. It suggests that  $\text{Co}_3\text{O}_4$  nanorods showed higher ORR activity than  $\text{Co}_3\text{O}_4$  flakes, which can be attributed to the higher BET surface area of  $\text{Co}_3\text{O}_4$  nanorods, moreover,  $\text{Co}_3\text{O}_4$  nanorods exhibited higher pore volume that provided additional ORR active sites and reduced more oxygen molecules.

On the other hand, similar to  $\text{Co}_3\text{O}_4$  nanorods and  $\text{Co}_3\text{O}_4$  flakes,  $\text{Co}_3\text{O}_4$  flower also enhanced the electrocatalytic activity of the cathode and showed an oxygen reduction peak on a more positive potential than the bare cathode. The cyclic voltammogram shows that COFL showed an oxygen reduction peak at a potential of  $0.27 \text{ V}$ . The positive onset potential than the bare cathode could be ascribed to the excellent ORR activity catalysed by mesoporous flower-like  $\text{Co}_3\text{O}_4$  on the cathode surface, on the other hand, the bare cathode could not reduce the oxygen molecules effectively and hence, no clear reduction peak was observed. However, the onset potential achieved by CON-2 and COFK was higher than the COFL, which can be attributed to the higher BET surface area of  $\text{Co}_3\text{O}_4$  nanorods and  $\text{Co}_3\text{O}_4$  flakes that provided additional ORR active sites and reduced more oxygen molecules comparatively.

### 4.3.2 Linear sweep voltammetry of all the cathodes

LSV was carried out for all the cathodes to evaluate their electrocatalytic activity by sweeping the potential from -0.6 V to 0.4 V with a scan rate of 10 mV/s in 100 mM PBS (pH = 7) in a three electrode system. *Figure 4.11* shows the results of LSV for the bare cathode and cathodes with different concentrations of  $\text{Co}_3\text{O}_4$  nanorods. The results demonstrate that the cathodes with increasing concentration of  $\text{Co}_3\text{O}_4$  nanorods showed the current density accordingly. In other words, the cathode with CON-3 exhibited the highest current density and the bare cathode showed the least. CON-3 achieved a maximum current density of  $1.13 \text{ A/m}^2$  at a potential of -0.6 V, which was manifolds higher than the bare cathode at the similar potential. The current density achieved by CON-2 and CON-1 was  $0.79 \text{ A/m}^2$  and  $0.45 \text{ A/m}^2$ , respectively, which were ~203% and 70% higher than the bare cathode ( $0.26 \text{ A/m}^2$ ).

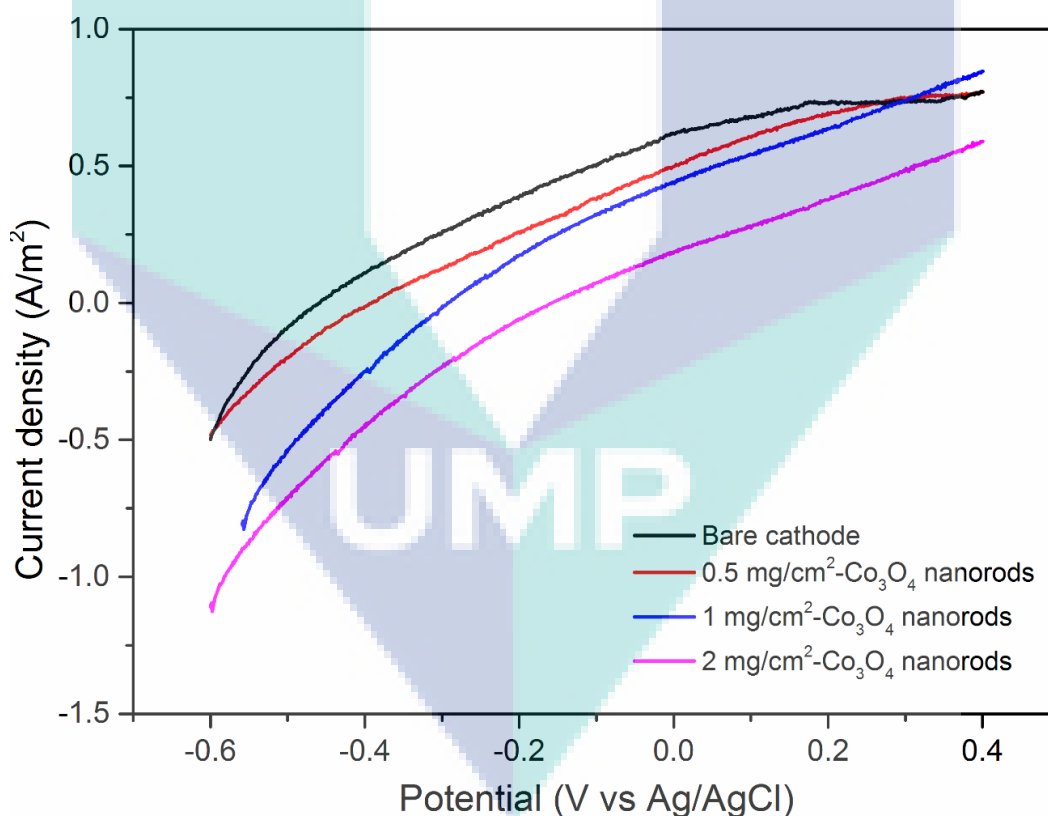


Figure 4.11 LSVs of cathodes with different concentrations of  $\text{Co}_3\text{O}_4$  nanorods at a scan rate of 10 mV/s.

Generally, cobalt oxide exhibits a higher affinity for oxygen molecules and contains  $\text{Co}^{2+}$  and  $\text{Co}^{3+}$  on its surface that might act as accessible active sites for ORR (Xu et al., 2012). Moreover, the pores on the surface of  $\text{Co}_3\text{O}_4$  nanorods provided some extra ORR active sites that substantially increased the ORR activity and generated higher current density as compared to the bare electrode. Therefore, the higher current density achieved by CON-3 and CON-2 can be ascribed to higher concentration of the catalyst that obviously provided additional active sites for oxygen reduction as compared to the bare cathode and CON-1 and increased the ORR activity. This enhanced ORR activity of the cathodes can improve the electric output of the MFC significantly.

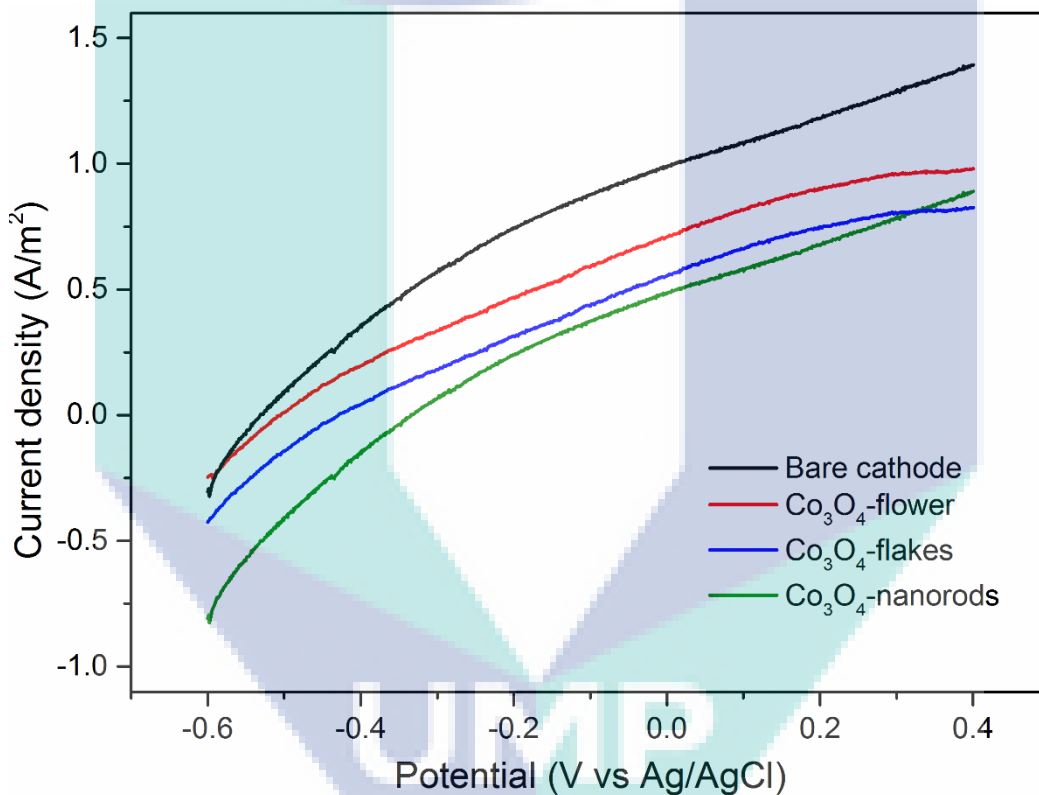


Figure 4.12 LSVs of cathodes with  $\text{Co}_3\text{O}_4$  nanorods,  $\text{Co}_3\text{O}_4$  flakes and  $\text{Co}_3\text{O}_4$  flower at a scan rate of 10 mV/s.

LSV was also carried out for the cathodes coated with  $\text{Co}_3\text{O}_4$  flakes (COFK) and  $\text{Co}_3\text{O}_4$  flower (COFL) and the results were compared to  $\text{Co}_3\text{O}_4$  nanorods (CON-2). *Figure 4.12* shows the LSV results for all these cathodes. It can be clearly observed from the LSV curves that CON-2 achieved highest current density as compared to COFK and COFL. Evidently, CON-2 obtained a current density of  $0.80 \text{ A/m}^2$  at a potential of  $-0.6 \text{ V}$

while the current density achieved by COFK and COFL was 0.42 A/m<sup>2</sup> and 0.30 A/m<sup>2</sup>, respectively. The current density showed by CON-2 was 90% higher than COFK and 166% more than COFL. This enhanced current density can be credited to the excellent ORR activity by the nanorods. As earlier mentioned, Co<sub>3</sub>O<sub>4</sub> contains Co<sup>2+</sup> and Co<sup>3+</sup> that act as the possible ORR active sites (Xu et al., 2012). A possible oxygen reduction mechanism by Co ions is presented in following *Figure 4.13*. The oxygen reduction mechanism Co ions can take place by the following reactions: -



Co<sub>3</sub>O<sub>4</sub> nanorods exhibited a higher BET surface area and pore volume as compared to the flakes and the flower, which means the nanorods can expose more Co<sup>2+</sup> and Co<sup>3+</sup> on its surface and subsequently more oxygen molecules could be adsorbed on the surface of the cathode coated with Co<sub>3</sub>O<sub>4</sub> nanorods that improved the ORR kinetics considerably. Moreover, the mesoporous architecture of the catalyst allows more oxygen molecules and ions to pass through the catalyst layers that also helps to ameliorate the ORR activity of the cathode.

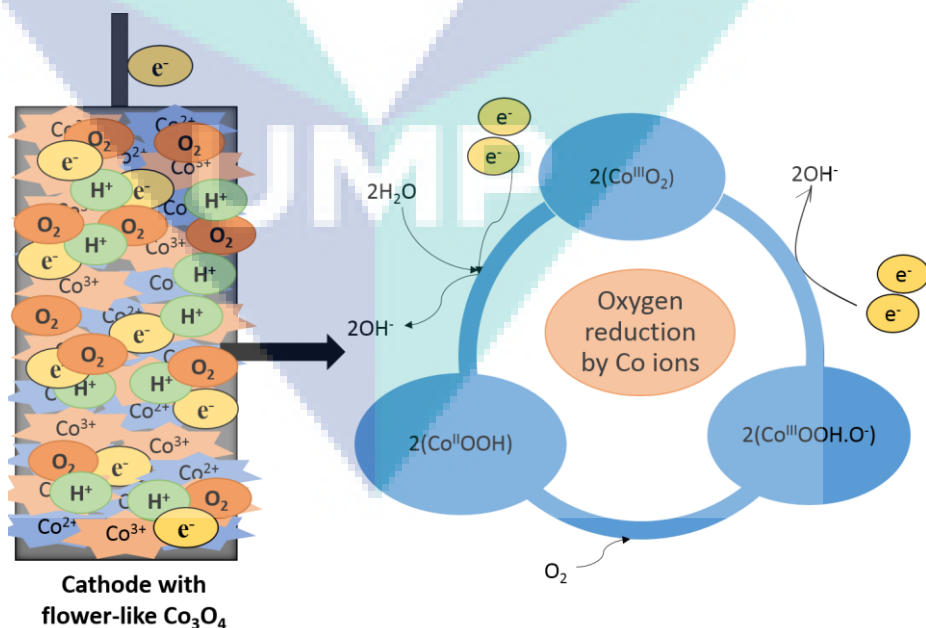


Figure 4.13 A possible oxygen reduction mechanism by Co ions on the surface of the cathodes.

### 4.3.3 Nyquist plots to estimate the resistance

The EIS technique was used to determine the resistance of cathodic reaction for all the cathode samples using three electrode system containing an Ag/AgCl electrode as the reference electrode, the platinum wire as the counter electrode and the prepared cathode as working electrode. Furthermore, an equivalent circuit model was prepared by using a software (Gamry Echem Analyst, USA). The equivalent circuit model is given in Figure 4.14 as below.

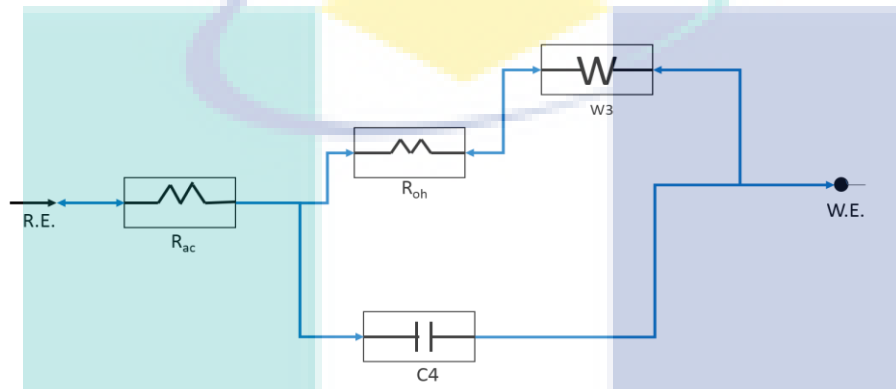


Figure 4.14 Equivalent circuit for Nyquist plots.

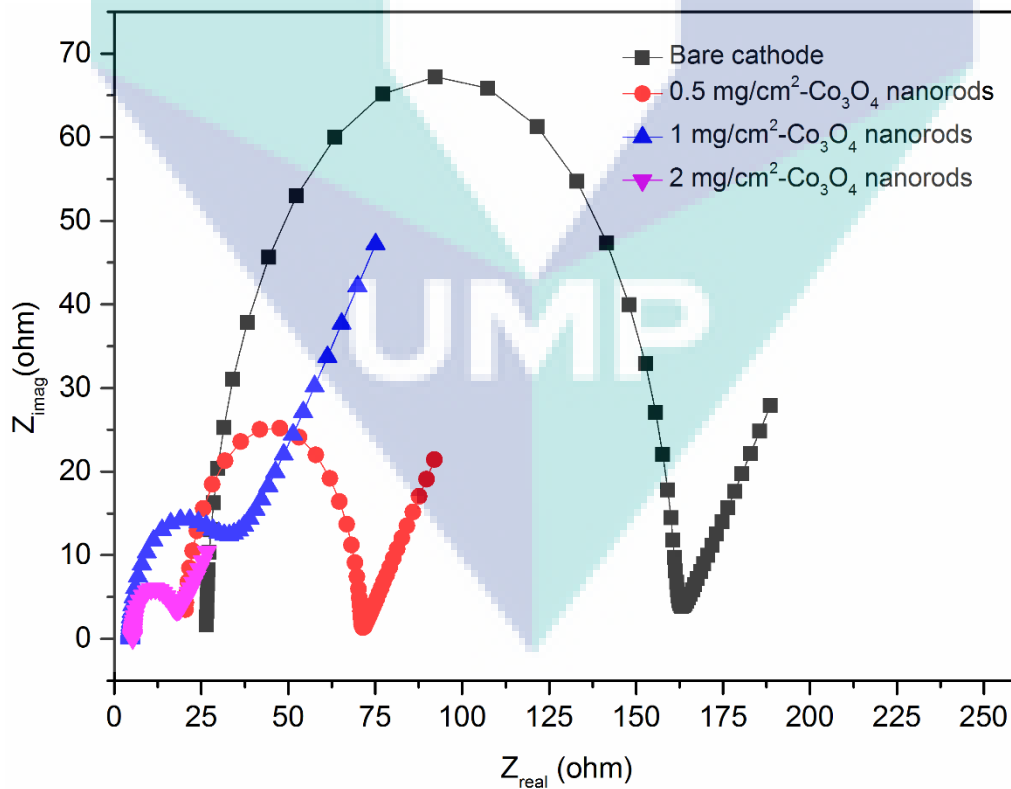


Figure 4.15 Nyquist plots of cathodes coated with  $\text{Co}_3\text{O}_4$  nanorods.

The Nyquist plots obtained for the different cathodes were fitted in the equivalent circuit model to determine the value of each parameter, are shown in *Figure 4.15*. The ohmic resistance that includes the ionic resistance of the electrolyte, the intrinsic resistance of active materials, and the contact resistance is valued as  $R_{ohm}$  and the activation resistance that shows charge transfer resistance is valued as  $R_{act}$  in the equivalent circuit model. The Warburg resistance and capacitance are denoted as  $W$  and  $C$ , respectively. The results indicated that there was a substantial decrease in the resistance in the MFC system after the addition of porous  $Co_3O_4$  nanorods as the cathode catalyst. The bare cathode showed higher values for both  $R_{ohm}$  and  $R_{act}$  as compared to CON-1, CON-2, and CON-3. The values of  $R_{ohm}$  and  $R_{act}$  for bare cathode were  $134.2 \Omega$  and  $26.51 \Omega$ , respectively. The  $R_{ohm}$  and  $R_{act}$  for all the cathodes exhibited a similar trend as: CON-3 < CON-2 < CON-1 < bare electrode. The  $R_{ohm}$  achieved for CON-3 was  $11.27 \Omega$ , which was  $\sim 1090\%$  less than the bare electrode, and  $347\%$  and  $120\%$  lower than CON-1 and CON-2, respectively. The decrease in ohmic resistance indicates that addition of  $Co_3O_4$  nanorods increased the conductivity of the electrode surface and enhanced the charge transfer processes. Besides, there was a substantial reduction in  $R_{act}$  for  $Co_3O_4$  nanorods coated cathodes. The CON-3 exhibited  $R_{act}$  of  $4.55 \Omega$ , which was  $582\%$  less than as compared to the bare electrode. The  $R_{act}$  achieved by CON-3 in this demonstration can be compared with other cathode catalysts. For example, in a recent study,  $R_{act}$  obtained by platinum was  $\sim 5 \Omega$ , which is  $\sim 10\%$  higher than CON-3 (Hou et al., 2016). Moreover, CON-3 exhibited lesser  $R_{act}$  as compared to CoNi/CNT catalyst (Hou et al., 2016). The CON-2 and CON-1 also showed lower values for  $R_{act}$ , which were approximately  $408\%$  and  $31\%$  lesser than the bare cathode, respectively. This substantial reduction in the resistance could be also attributed to the porous  $Co_3O_4$  nanorods on the cathode surface, which are assumed to provide extra active sites for oxygen molecules that consequently, lead to the better electrocatalytic activity of the cathode for ORR in MFCs. As a result, the reduction in overall resistance of the MFC system will increase the power density by manifolds.

Nyquist plots were carried out for the cathodes with  $\text{Co}_3\text{O}_4$  flakes (COFK) and  $\text{Co}_3\text{O}_4$  flower (COFL) and the results were compared to  $\text{Co}_3\text{O}_4$  nanorods (CON-2). The Nyquist plots are given in *Figure 4.16* and the values calculated for  $R_{\text{ohm}}$  and  $R_{\text{act}}$  for all the cathodes are compared in the following Table 4.3.

Table 4.3 Resistance values for all the cathodes calculated from the Nyquist plots.

Cathode	$R_{\text{ohm}}$ ( $\Omega$ )	$R_{\text{act}}$ ( $\Omega$ )
Bare cathode	134.2	26.51
CON-1	50.48	20.21
CON-2	24.80	5.21
CON-3	11.27	4.55
COFK	26.32	7.81
COFL	32.51	16.24

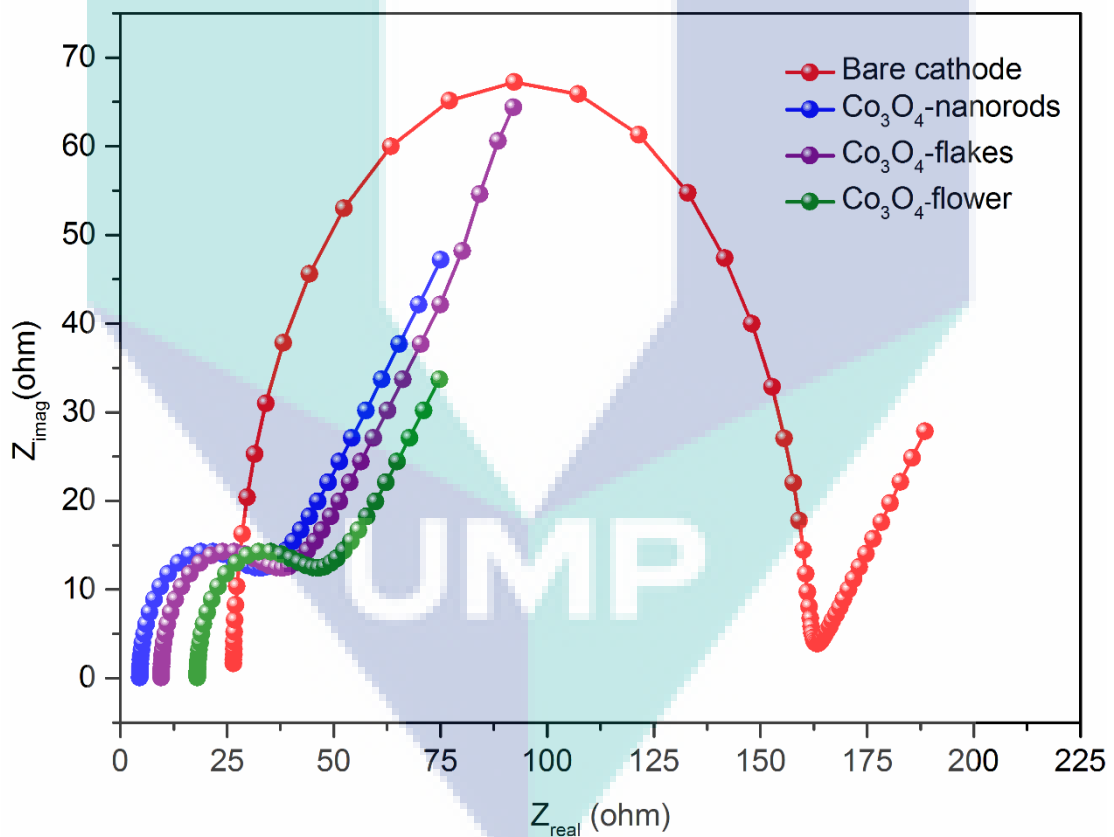


Figure 4.16 Nyquist plots of cathodes coated with  $\text{Co}_3\text{O}_4$  nanorods,  $\text{Co}_3\text{O}_4$  flakes and  $\text{Co}_3\text{O}_4$  flower.

The EIS results demonstrated that Co<sub>3</sub>O<sub>4</sub> nanorods (CON-2) showed lesser values for R<sub>ohm</sub> and R<sub>act</sub> as compared to Co<sub>3</sub>O<sub>4</sub> flakes (COFK) and Co<sub>3</sub>O<sub>4</sub> flower (COFL), which suggested that CON-2 exhibited faster electron transfer on the cathode interfaces. Evidently, CON-2 showed R<sub>ohm</sub> of 24.80 Ω and R<sub>act</sub> of 5.21 Ω, which were the lowest among COFK and COFL. The resistance values of R<sub>ohm</sub> and R<sub>act</sub> calculated for COFL were 32.51 Ω and 16.24 Ω, which were 31% and 211% higher than CON-2, respectively. Besides, COFK showed lower resistance values for R<sub>ohm</sub> and R<sub>act</sub> in comparison to COFL that is 26.32 Ω and 7.81 Ω, which were 23% and 107% lower than COFL. The resistance values obtained for COFK were found competitive to CON-2. Therefore, it can be concluded that the addition of Co<sub>3</sub>O<sub>4</sub> nanorods and Co<sub>3</sub>O<sub>4</sub> flakes greatly reduced the resistance of the system as compared to Co<sub>3</sub>O<sub>4</sub> flower. The higher resistance shown by Co<sub>3</sub>O<sub>4</sub> flower could be due to its comparative slower ORR activity on the cathode surface. The comparatively lower surface area of the flower could expose lesser cobalt ions for the oxygen reduction. Moreover, the multilayer structure of the flower can also make the inner layers inaccessible to the oxygen and can block the passage of the electrolyte through it, thereby, increasing the electrolytic resistance and the charge resistance.

#### 4.3.4 Analysis of ORR kinetics by Tafel plot study

The ORR catalytic activity of all the cathode samples was further analyzed by plotting the Tafel plots. The exchange current density (*i*<sub>o</sub>) for ORR can be easily calculated from the Tafel plots, which provides a potential parameter to evaluate the electron transfer rate of a catalyst. Generally, the magnitude of the *i*<sub>o</sub> is directly proportional to the electron transfer rate of ORR and thus for the electrocatalytic activity of a catalyst for ORR. The *i*<sub>o</sub> calculated from the Tafel plots is given in the following Table 4.4.

Table 4.4 Exchange current density of all the cathodes.

Cathode	Linear fitting equation (R <sup>2</sup> )	<i>i</i> <sub>o</sub> (A/m <sup>2</sup> )
Bare cathode	y = -1.9823 + 5.8101x (0.995)	1.89
CON-1	y = -2.7167 + 5.4690x (0.996)	2.62
CON-2	y = -5.4873 + 5.7858x (0.994)	5.34
CON-3	y = -5.8204 + 5.8264x (0.997)	5.67
COFK	y = -3.6497 + 5.4719x (0.996)	3.54
COFL	y = -2.5450 + 5.3426x (0.995)	2.46

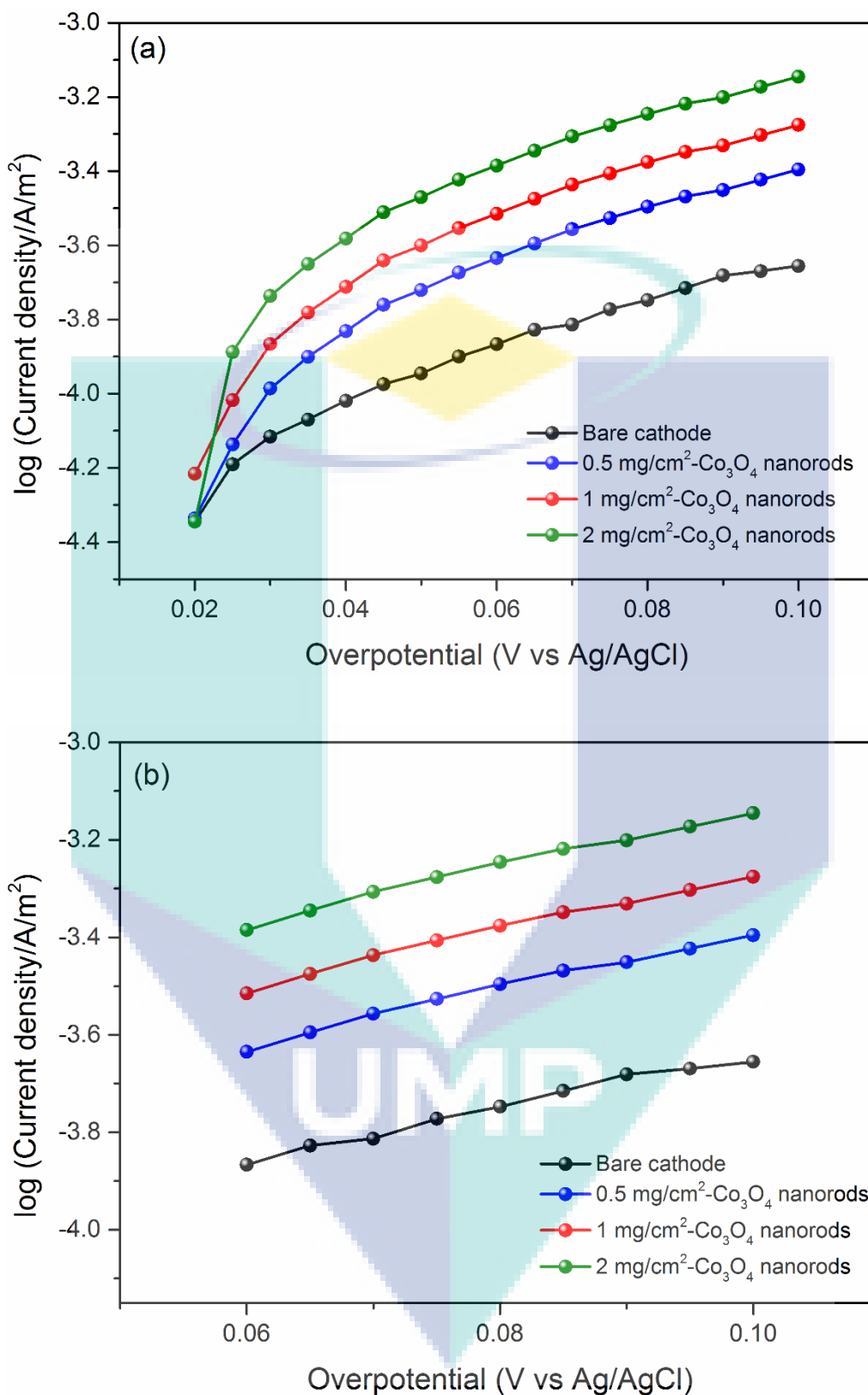
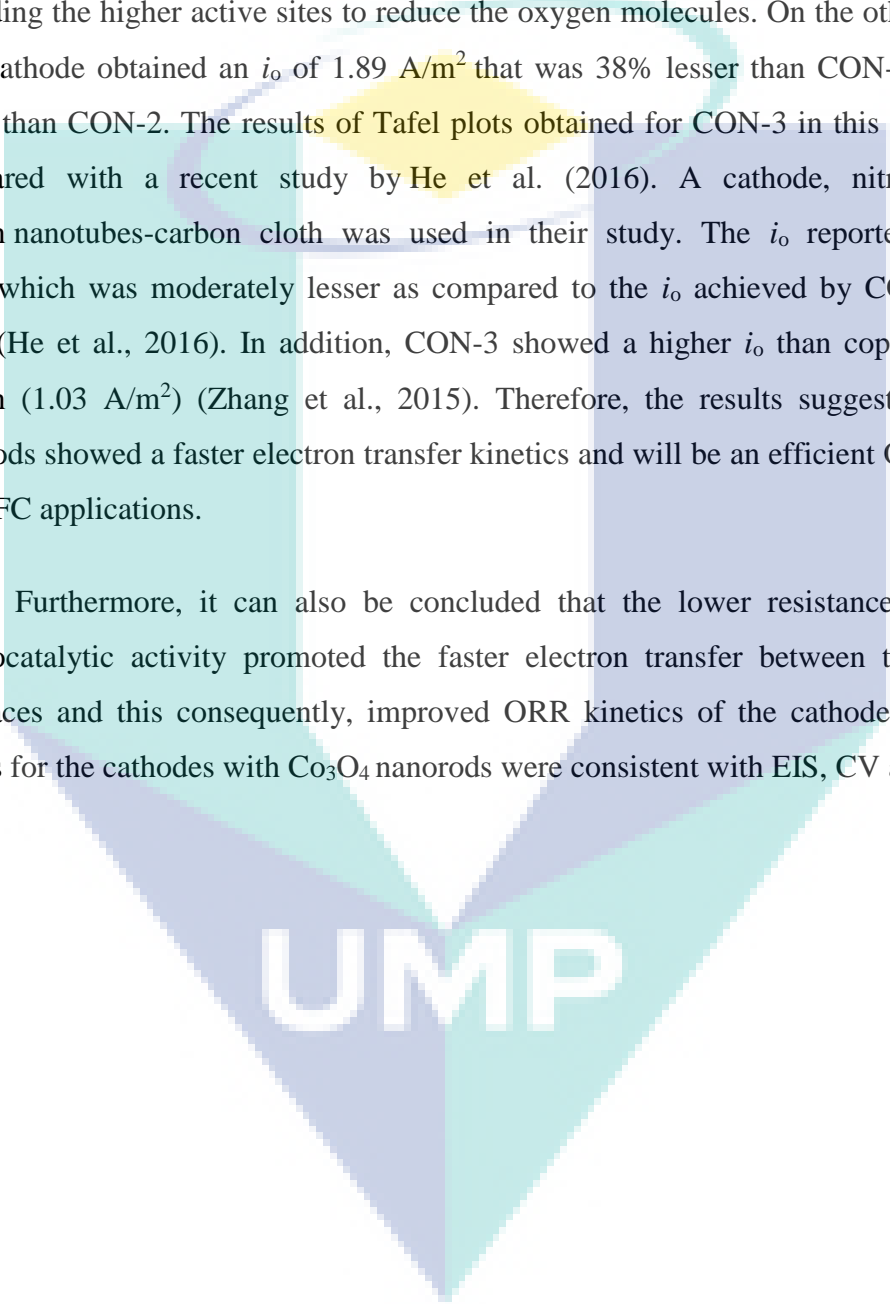


Figure 4.17 (a) Tafel plots of different cathodes with varying concentration of Co<sub>3</sub>O<sub>4</sub> nanorods by sweeping the overpotential from 20 mV to 100 mV at 1 mVs<sup>-1</sup> and (b) linear fit for the Tafel plots of overpotential from 60 to 80 mV.

Figure 4.17 shows the Tafel results for the cathodes coated with  $\text{Co}_3\text{O}_4$  nanorods. The results demonstrated that CON-3 achieved the highest  $i_0$  that is  $5.67 \text{ A/m}^2$ , which was 200% higher than the bare cathode. The  $i_0$  obtained by CON-2 and CON-1 was  $5.34 \text{ A/m}^2$  and  $2.62 \text{ A/m}^2$ , respectively. The enhanced  $i_0$  obtained by CON-2 and CON-3 could be ascribed to the existence of higher concentrations of  $\text{Co}_3\text{O}_4$  nanorods on the cathode, providing the higher active sites to reduce the oxygen molecules. On the other hand, the bare cathode obtained an  $i_0$  of  $1.89 \text{ A/m}^2$  that was 38% lesser than CON-1 and 182% lesser than CON-2. The results of Tafel plots obtained for CON-3 in this study can be compared with a recent study by He et al. (2016). A cathode, nitrogen doped-carbon nanotubes-carbon cloth was used in their study. The  $i_0$  reported was  $5.13 \text{ A/m}^2$ , which was moderately lesser as compared to the  $i_0$  achieved by CON-3 in this study (He et al., 2016). In addition, CON-3 showed a higher  $i_0$  than copper/activated carbon ( $1.03 \text{ A/m}^2$ ) (Zhang et al., 2015). Therefore, the results suggest that  $\text{Co}_3\text{O}_4$  nanorods showed a faster electron transfer kinetics and will be an efficient ORR catalyst for MFC applications.

Furthermore, it can also be concluded that the lower resistance and higher electrocatalytic activity promoted the faster electron transfer between the electrode interfaces and this consequently, improved ORR kinetics of the cathodes. The Tafel results for the cathodes with  $\text{Co}_3\text{O}_4$  nanorods were consistent with EIS, CV and LSV.

The logo for UIMP (Universiti Malaysia Perlis) is a large, stylized letter 'V' shape. The left side of the 'V' is light blue, the right side is light green, and the bottom point is a darker blue. The letters 'UIMP' are written in white, bold, sans-serif font across the center of the 'V'.

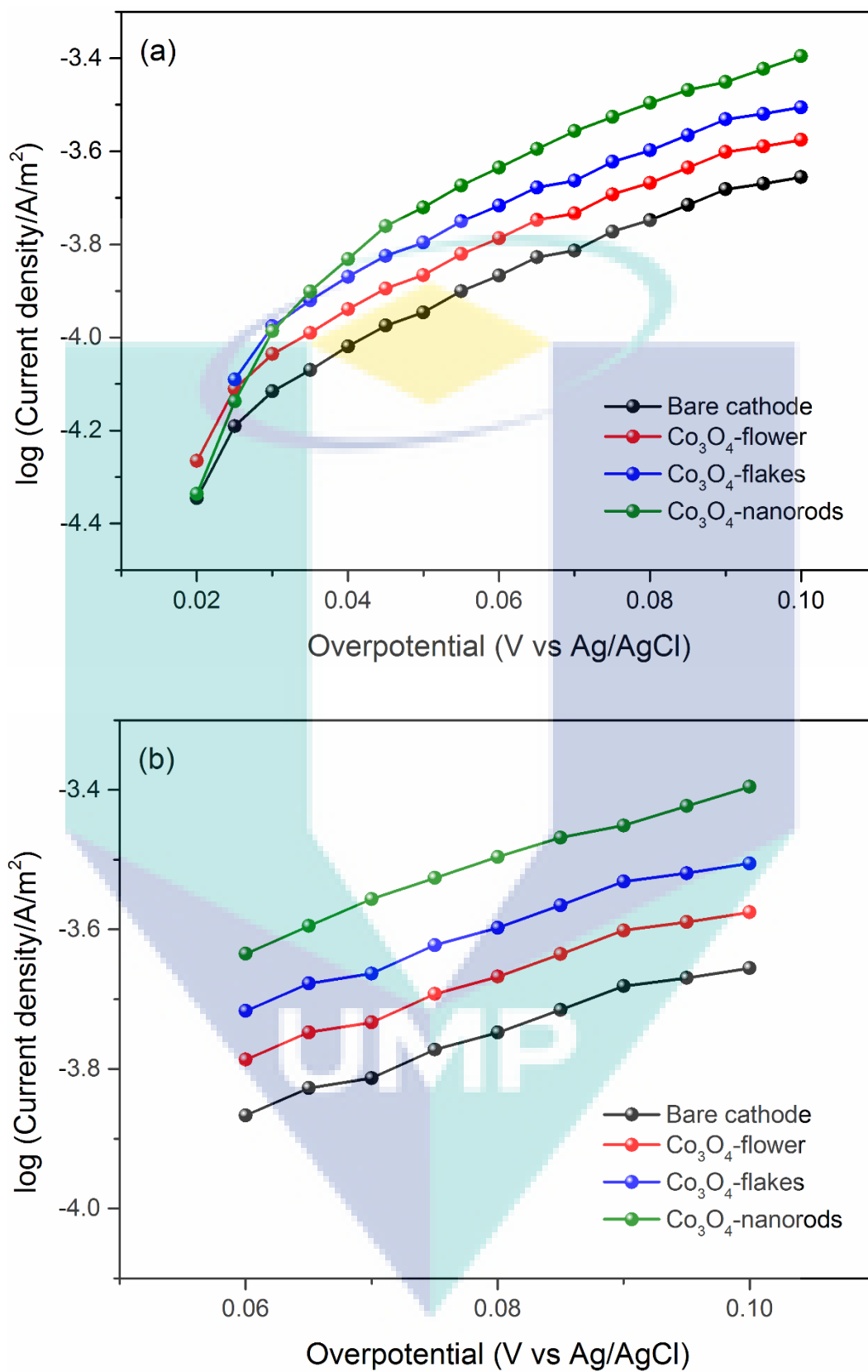


Figure 4.18 (a) Tafel plots of different cathodes with  $\text{Co}_3\text{O}_4$  nanorods, flakes and the flower by sweeping the overpotential from 20 mV to 100 mV at  $1 \text{ mVs}^{-1}$  and (b) linear fit for the Tafel plots of overpotential from 60 to 80 mV.

*Figure 4.18* shows the Tafel results for the cathodes with  $\text{Co}_3\text{O}_4$  flakes (COFK) and  $\text{Co}_3\text{O}_4$  flower (COFL), which were compared with  $\text{Co}_3\text{O}_4$  nanorods (CON-2). The results suggested that the cathodes exhibited an  $i_0$  in a trend: CON-2 > COFK > COFL > bare cathode. COFK achieved an  $i_0$  of  $3.54 \text{ A/m}^2$ , which was 50% lower than CON-2 and 44% higher than COFL. On the other hand, COFL showed an  $i_0$  of  $2.46 \text{ A/m}^2$ , which was 30% higher than the bare cathode. CON-2, as expected showed better oxygen reduction rate as compared to COFK and COFL that can be ascribed to the presence of more number of active sites on the surface of the cathode due to its higher surface area and pore volume. The possible mechanism for oxygen reduction has been given in *Figure 4.13*. Additionally, it has been reported that  $\text{Co}_3\text{O}_4$  obeys nearly four-electron pathway for ORR (Ge et al., 2015; Cao et al., 2016). For example, Ge et al. used ortho-hexagon nano spinel  $\text{Co}_3\text{O}_4$  as a cathode catalyst in air-cathode MFC and the number of electrons transferred in the ORR was 3.99 in their study (Ge et al., 2015). In an alternative study, mesoporous  $\text{Co}_3\text{O}_4$  was used as the cathode catalyst and the electron transfer number for the ORR was 3.80 in the study (Cao et al., 2016). Therefore, it can be suggested that all the catalysts might also followed a nearly between three and four-electron pathway for ORR.

#### **4.3.5 Performance of the cathodes for bioelectricity generation in MFCs**

All the prepared cathodes were deployed in double chamber MFCs. Power density was taken as the key parameter to compare performances of all the MFCs for electricity generation. Therefore, polarization curves were measured after five days of operation to determine the maximum power density achieved by each MFC. Table 4.5 compares the results of polarization curves of all the cathodes. *Figure 4.19a* shows the results of polarization curves for the cathodes containing different concentrations of  $\text{Co}_3\text{O}_4$  nanorods. The results demonstrated that the addition in  $\text{Co}_3\text{O}_4$  nanorods improved the power generation significantly. Moreover, it was also found that the power density increased with increase in  $\text{Co}_3\text{O}_4$  concentration. Expectedly, the MFC with CON-3 generated a maximum power density of  $503 \text{ mW/m}^2$ , which was 413% higher than the bare cathode ( $98 \text{ mW/m}^2$ ). The enhanced power generation was mainly due to the faster ORR kinetics on the cathode, as confirmed by the varying cathode potentials. The anode potentials were almost similar in all the MFCs (*Figure 4.19b*). Moreover, the results were consistent with LSV and Tafel plots. Besides, the lesser internal resistance in the MFC also contributed in enhanced power generation. The maximum power density achieved in

this study was higher than the previously reported value i.e. 135 mW/m<sup>2</sup> (nitrogen doped-carbon nanotubes-carbon cloth as a cathode) and also from carbon nanotubes/Pt composites that produced a power density of 139 mW/m<sup>2</sup> (He et al., 2016).

Table 4.5 Maximum power density achieved by the cathodes in a double-chamber air-cathode MFC.

Cathode	Maximum power density (mW/m <sup>2</sup> )
Bare cathode	98
CON-1	318
CON-2	454
CON-3	503
COFK	305
COFL	171

Furthermore, CON-3 generated more power density than platinum, which was ca. 321% higher than platinum (120 mW/m<sup>2</sup>) and approximately equally higher than copper-phthalocyanine (118 mW/m<sup>2</sup>) (Ghasemi et al., 2013). In addition to this, Co-naphthalocyanine was used as the cathode catalyst in a demonstration but could produce a maximum power density of 64.7 mW/m<sup>2</sup> (Kim et al., 2011), which is manifolds lesser than the power density achieved by CON-3 in this study. It further strengthens the fact that porous nanomaterials act as more efficient cathode catalyst as compared to other catalysts. Another noticeable point was that the MFC with a catalyst concentration of 0.5 mg/cm<sup>2</sup> (CON-1) and 1 mg/cm<sup>2</sup> (CON-2) produced 220% and 363% more power density than the bare electrode, respectively. But a further increase in the catalyst concentration i.e. 2 mg/cm<sup>2</sup> (CON-3) merely improved the power generation by 10.7%. This possibly suggests that the oxygen molecules could only access the active sites that were present on upper layers of the catalyst or might be the multiple layers of Co<sub>3</sub>O<sub>4</sub> nanorods decreased the availability of pores/active sites in the inner layers of the catalyst present on the cathode surface, indicating that an optimum catalyst concentration is preferred for substantial electricity generation.

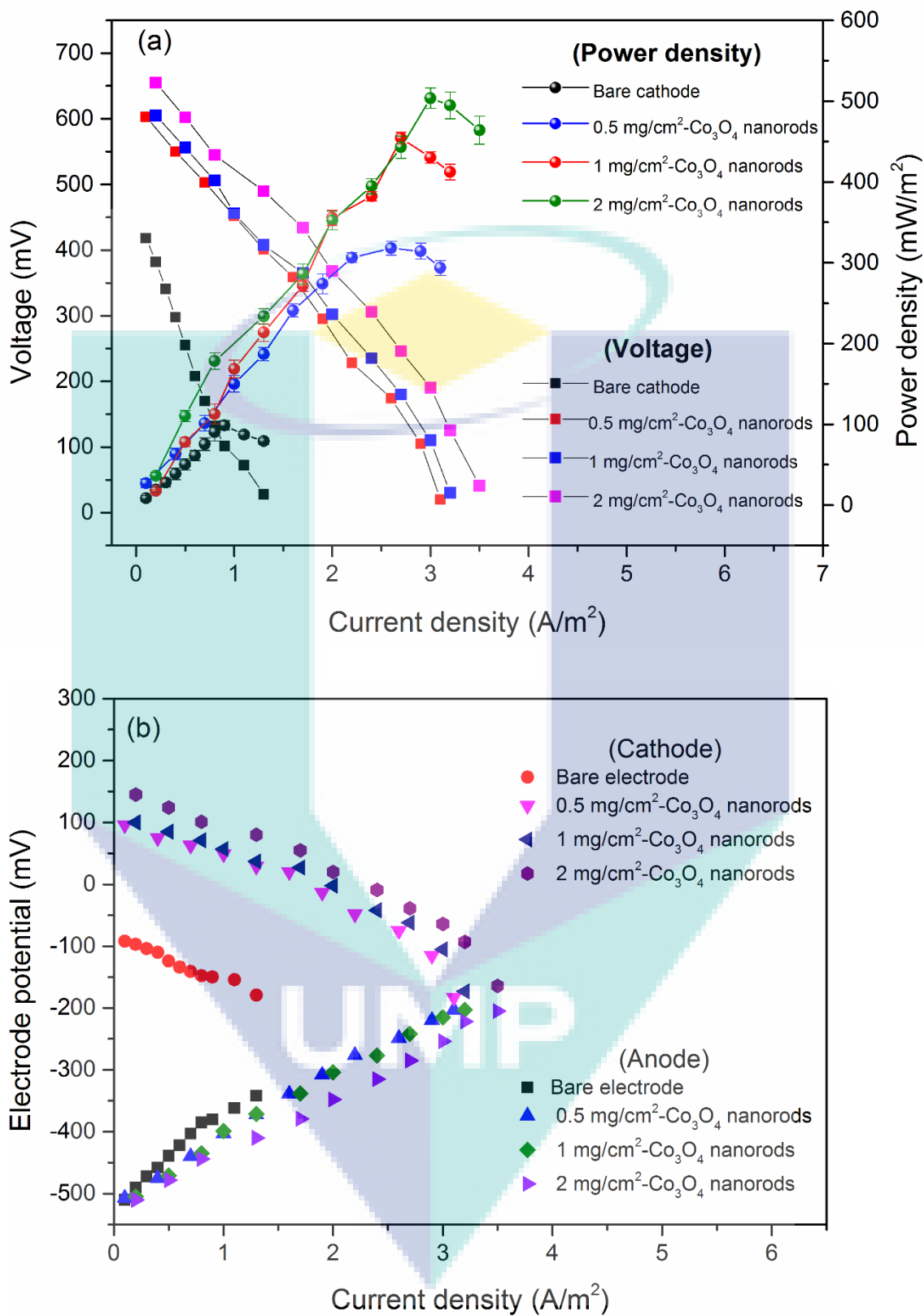


Figure 4.19 (a) Polarization and power density curves of MFCs and (b) electrode potentials using different concentration of  $\text{Co}_3\text{O}_4$  nanorods.

A little credit for higher power generation in all the MFCs can also be given to the microbial activities shown by the mixed bacterial community at the anode. The possible proteins involved in electron transfer mechanisms are shown below in *Figure 4.20*.

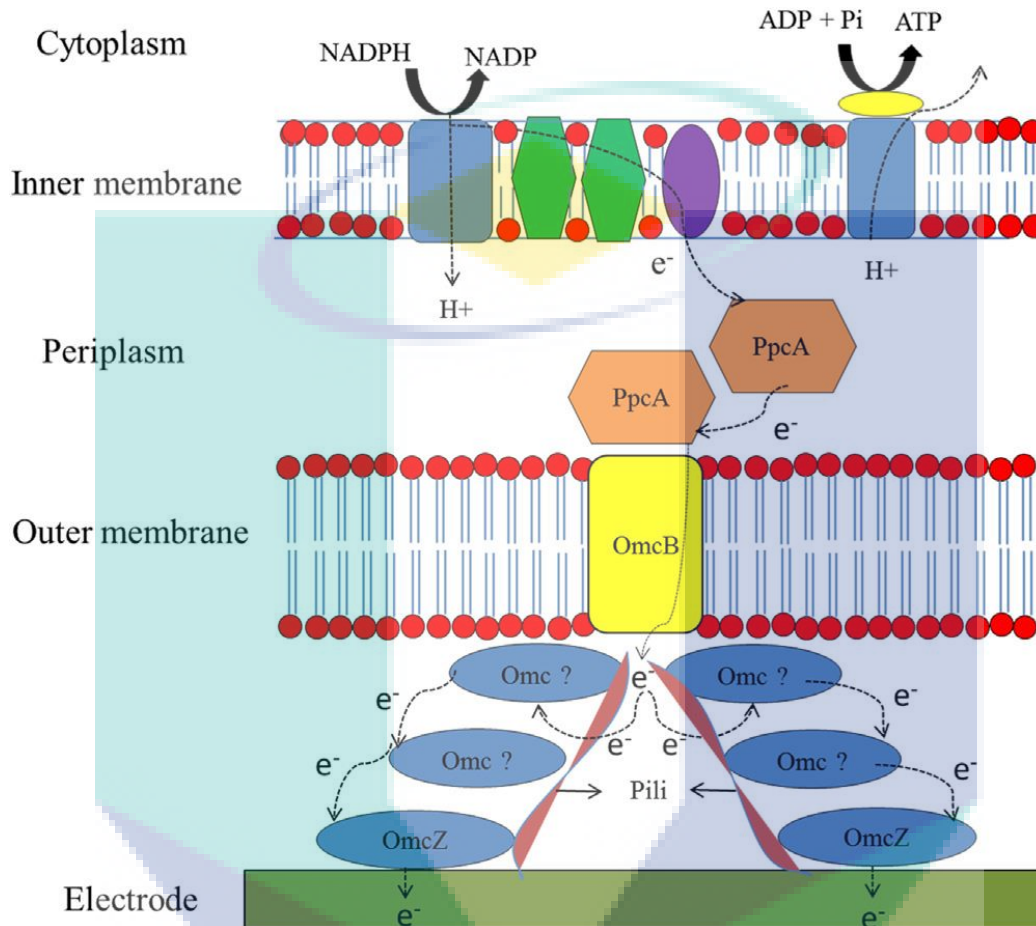


Figure 4.20 Proteins involved in electron transfer mechanisms.

All the applications of MFC technology are particularly interesting because of the molecular machinery of the bacteria that helps in transferring the electrons to an electrode surface and vice-versa. The molecular machinery means the biomolecules, proteins or the genes that help to donate or accept the electrons between bacterial and electrode interface, which chiefly lies between the inner and the outer membrane of the bacteria. So far, only two bacteria namely, *Geobacter spp.* and *Shewanella spp.* have been extensively investigated to explore the extracellular electron transfer (EET) mechanisms. Two types of EET mechanisms have been confirmed in both the bacteria (Nevin et al., 2008). The first is direct electron transfer (DET) mechanism and the second is mediated electron transfer (MET) mechanism. It has been found that *G. sulfurreducens* in its initial stages

of biofilm formation relies on MET for electron transport. The exoelectrogen secretes flavin molecules such as riboflavin in the single layer biofilms. The riboflavin combines with outer membrane c-type cytochromes (OM c-Cyts) to make a complex that furthers the electron transfer to the electrode surface (Rabaey et al., 2005). As the biofilm grows *G. sulfurreducens* adapts to DET for extracellular electron transport. In a multi-layered biofilm, *G. sulfurreducens* active adjacent to electrode surface utilizes OM c-Cyts (essentially OmcZ) for extracellular electron transfer while the bacteria respiring distant from the electrode produce conductive nanowires (type IV pili) that assist in transporting the electrons inside the biofilm and finally onto the electrode surface (Nevin et al., 2008). The other exoelectrogen studied extensively for MFC applications is *Shewanella oneidensis*. The bacterium is the most versatile exoelectrogen in the MFCs because it exhibits the potential to reduce a variety of electron acceptors (Ringeisen et al., 2006). Earlier *S. oneidensis* MR-1 was thought to produce conductive nanowires like type IV pili of *G. sulfurreducens*. But it is now confirmed that *S. oneidensis* does not contain nanowires and these nanowires like structures are the extensions of periplasmic and outer membrane multiheme cytochromes associated with outer membrane vesicles (Torres et al., 2010). This exoelectrogen secretes mainly two types of flavin molecules. The first is riboflavin (RF) and the second is flavin mononucleotide (FMN). These flavin molecules act as cofactors for the cytochromes such as OmcA and MtrC. It has been found that RF acts as a cofactor for OmcA while FMN contains the binding sites for MtrC (Watanabe et al., 2009). These complexes, RF-OmcA and FMN-MtrC further promote the electron transfer to the electrode surfaces (Watanabe et al., 2009). In this study, the anode that contained primarily *Pseudomonas* spp. might transferred the electrons by mediated electron transfer proteins (Masuda et al., 2010). The other microorganisms present in the anode are also believed to transfer the electrons through direct or mediated electron transfer intermediators (Reguera et al., 2006; Qu et al., 2012; Fitzgerald et al., 2012).

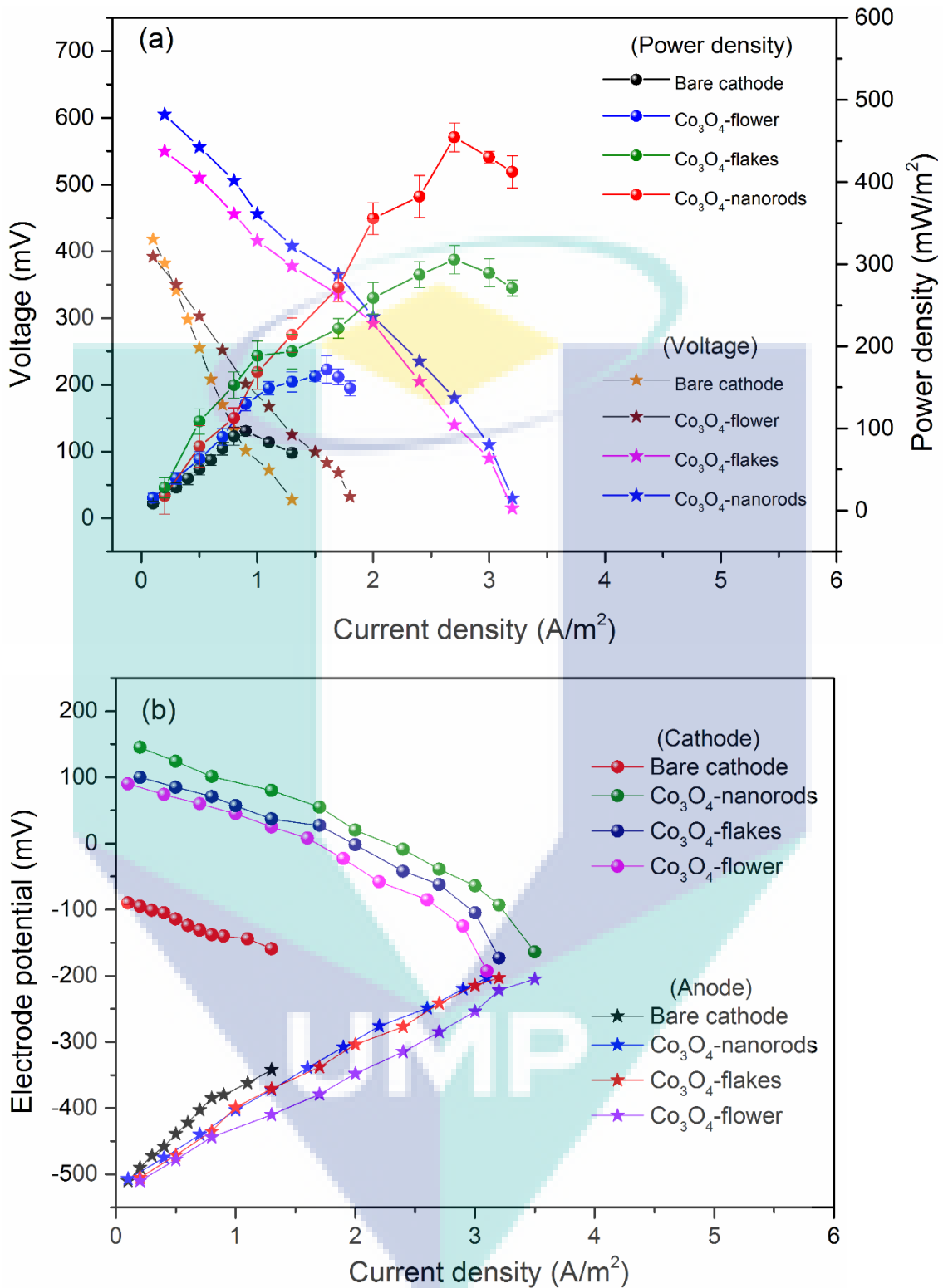


Figure 4.21 (a) Polarization and power density curves of MFCs and (b) electrode potentials using cathodes with Co<sub>3</sub>O<sub>4</sub> nanorods, Co<sub>3</sub>O<sub>4</sub> flakes, and Co<sub>3</sub>O<sub>4</sub> flower.

Figure 4.21 shows the results of polarization curves for COFK, COFL and CON-2. It can be clearly observed from the results that CON-2 achieved higher power density as compared to COFK and COFL. Evidently, CON-2 generated a maximum power density of 454 mW/m<sup>2</sup> that was 32% higher than COFK (305 mW/m<sup>2</sup>) and 62% higher than COFL (171 mW/m<sup>2</sup>). The higher power density shown by CON-2 can be attributed to excellent ORR activity of Co<sub>3</sub>O<sub>4</sub> nanorods, as demonstrated by CV and LSV results. Besides, the nanorods also showed less activation resistance and charge resistance as compared to the flakes and the flower, which means the nanorods promoted the electron transfer through the electrolyte and the electrode surface. Moreover, the Tafel results suggested that CON-2 showed higher oxygen reduction rate as compared to COFL and COFK. To conclude, the faster ORR kinetics at CON-2 and lesser resistance in the MFC system allowed to generate the higher power output in the MFC. The performance of other cathode catalysts is compared in Table 4.6.

Table 4.6 Performance of different oxygen reduction catalysts in MFCs.

Catalyst	Cathode material	Inoculum	Power Density (mW/m <sup>2</sup> )	Reference
CoNPc	CP	AS	64.7	(Kim et al., 2011)
Co <sub>3</sub> O <sub>4</sub> nanoparticles	CC	AS	654	(Ahmed et al., 2012)
Nickel-cobalt	CC	IW	136	(O-Martinez et al., 2016)
Co <sub>3</sub> O <sub>4</sub> -NGO	CC	AS	321	(Song et al., 2015)
Co <sub>3</sub> O <sub>4</sub> -NCNT	CC	AS	469	(Li et al., 2014)
Binuclear-Co-PC	CC	IW	369	(Li et al., 2015)
Pyrolyzed-Co-PC	CC	IW	604	(Roche et al., 2009)
MnO <sub>2</sub>	CC	AS	161	(Liew et al., 2015)
MnO <sub>2</sub> -CNT	CC	AS	520	(Liew et al., 2015)
Nanostructured-MnO <sub>2</sub>	CP	Leachate	119	(Haoran et al., 2014)
Co <sub>3</sub> O <sub>4</sub> nanorods	Graphite	AS	503	This study
Co <sub>3</sub> O <sub>4</sub> flakes	Graphite	AS	305	This study
Co <sub>3</sub> O <sub>4</sub> flower	Graphite	AS	171	This study

Note: CP=carbon paper; CC=carbon cloth; AS=anaerobic sludge; IW=industrial wastewater

#### **4.4 To enhance the performance of $\text{Co}_3\text{O}_4$ nanorods towards oxygen reduction by making a compound with Mn that is $\text{MnCo}_2\text{O}_4$ nanorods and investigate its ORR activity and electricity generation potential in MFCs**

In the previous objectives,  $\text{Co}_3\text{O}_4$  nanorods showed higher ORR activity as compared to  $\text{Co}_3\text{O}_4$  flakes and  $\text{Co}_3\text{O}_4$  flower. The performance of  $\text{Co}_3\text{O}_4$  nanorods was further enhanced with the addition of manganese (Mn) and synthesized  $\text{MnCo}_2\text{O}_4$  nanorods. Mn or  $\text{MnO}_2$  has also shown a promising ORR activity in MFCs ((Li et al., 201; Liew et al., 2015; Haoran et al., 2014; Touach et al., 2016), therefore, the idea to form a compound with Mn was to further improve the ORR activity of the nanorods that could provide different cations (Mn and Co ions) for active sites to reduce oxygen with a faster rate at a low overpotential.  $\text{MnCo}_2\text{O}_4$  nanorods were synthesized by a simple hydrothermal method, which were further characterized by XRD, FESEM and TEM. Further,  $\text{MnCo}_2\text{O}_4$  nanorods ( $1 \text{ mg/cm}^2$ ) were uniformly coated on a graphite sheet to prepare a cathode. This cathode was investigated by CV and LSV to examine their electrocatalytic activity and their ORR kinetics was studied by Tafel plots. Finally, polarization curves were performed to determine the maximum power density generation in the MFCs.

##### **4.4.1 XRD and electron microscopy results**

The synthesis of nanomaterials via hydrothermal method is an easy and very cost-effective as compared to the other methods such as electrospinning and chemical precipitation. Therefore, in this research work  $\text{MnCo}_2\text{O}_4$  nanorods (MCON) were developed by a simple hydrothermal method using  $\text{MnCl}_2$  and  $\text{CoCl}_2$  as the metal precursors and HTAB was applied as the complexing and surface-functionalizing agent that plays a critical role in the control of shape and size of the nanomaterial. The MCON are assumed to be formed in two steps. A complex of Mn-Co precursors could be formed in the first step, which could be transformed into a nanorod like structure resulting in  $\text{MnCo}_2\text{O}_4$  nanorods after the calcination step. This end product of hydrothermal process was identified by XRD analysis. *Figure 4.22* show the XRD results of  $\text{MnCo}_2\text{O}_4$  nanorods. A detail of XRD data is given in Table A4.

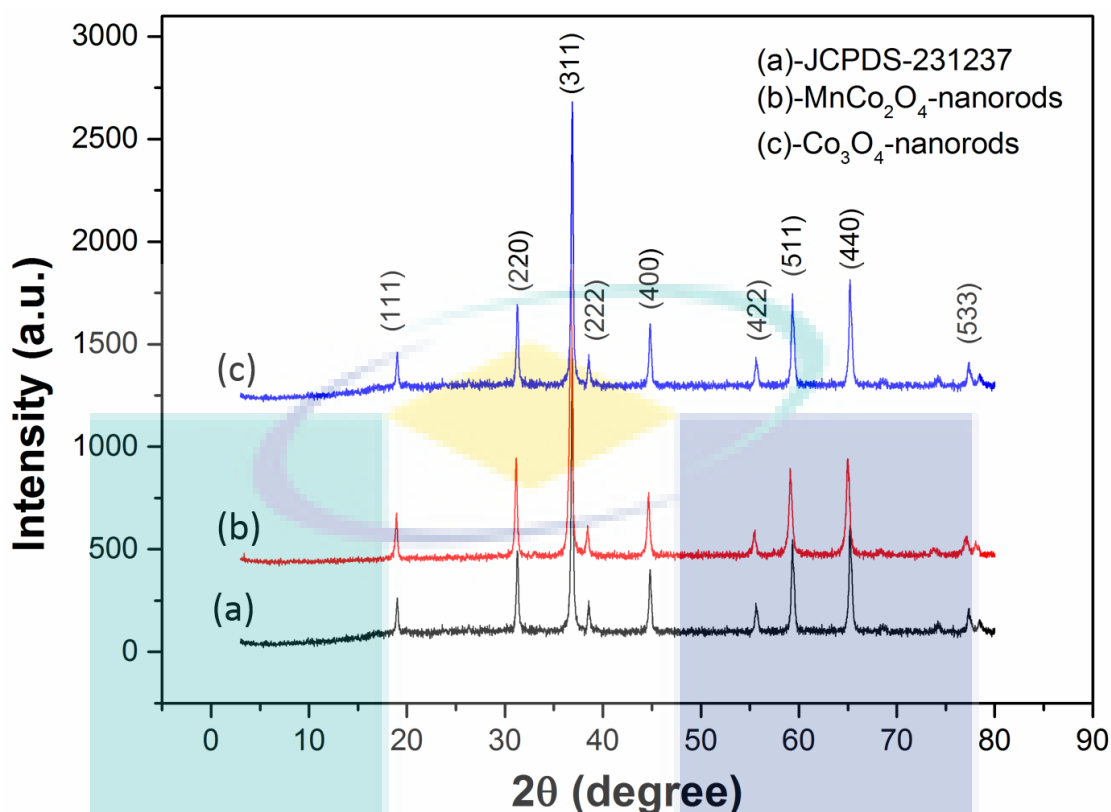


Figure 4.22 XRD pattern of  $\text{MnCo}_2\text{O}_4$  nanorods.

Different diffraction peaks were observed at different angles that is  $19.01^\circ$ ,  $31.09^\circ$ ,  $36.56^\circ$ ,  $38.41^\circ$ ,  $44.71^\circ$ ,  $55.47^\circ$ ,  $59.11^\circ$ ,  $64.91^\circ$ , and  $76.98^\circ$ , which indexed to (111), (220), (311), (222), (400), (422), (511), (440), and (533) of  $\text{MnCo}_2\text{O}_4$ , respectively. These results were consistent with the standard values of JCPDS Card No. 231237. Moreover, the diffraction peaks correspond to the space group 225: Fm-3m. Besides, no impurity peaks were found, suggesting a pure form of  $\text{MnCo}_2\text{O}_4$ .

Further, the structure and morphology of the nanomaterial was analysed by FESEM and TEM. *Figure 4.23* and *Figure 4.24* show the FESEM images of  $\text{MnCo}_2\text{O}_4$  and  $\text{Co}_3\text{O}_4$  nanorods, respectively. *Figure 4.25* shows TEM images of  $\text{MnCo}_2\text{O}_4$  nanorods. It can be clearly observed from the images that the final product obtained from the hydrothermal method was nanorod-shaped. Hence the results of XRD and electron microscopy confirmed that MCON were successfully formed in the process.

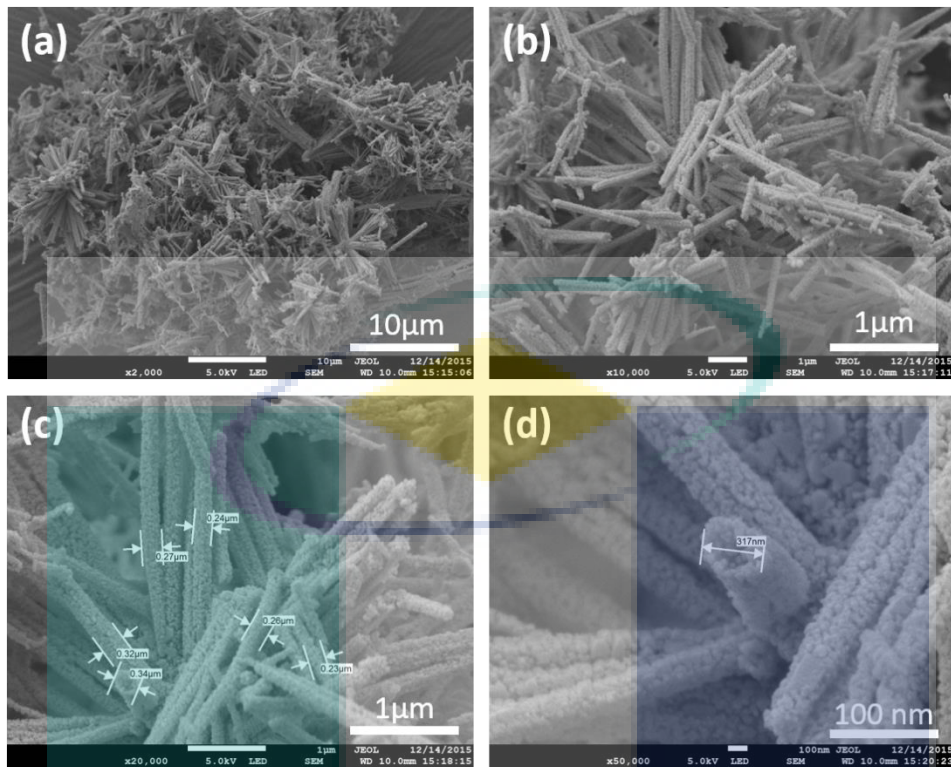


Figure 4.23 FESEM images of  $\text{MnCo}_2\text{O}_4$  nanorods at different magnifications.

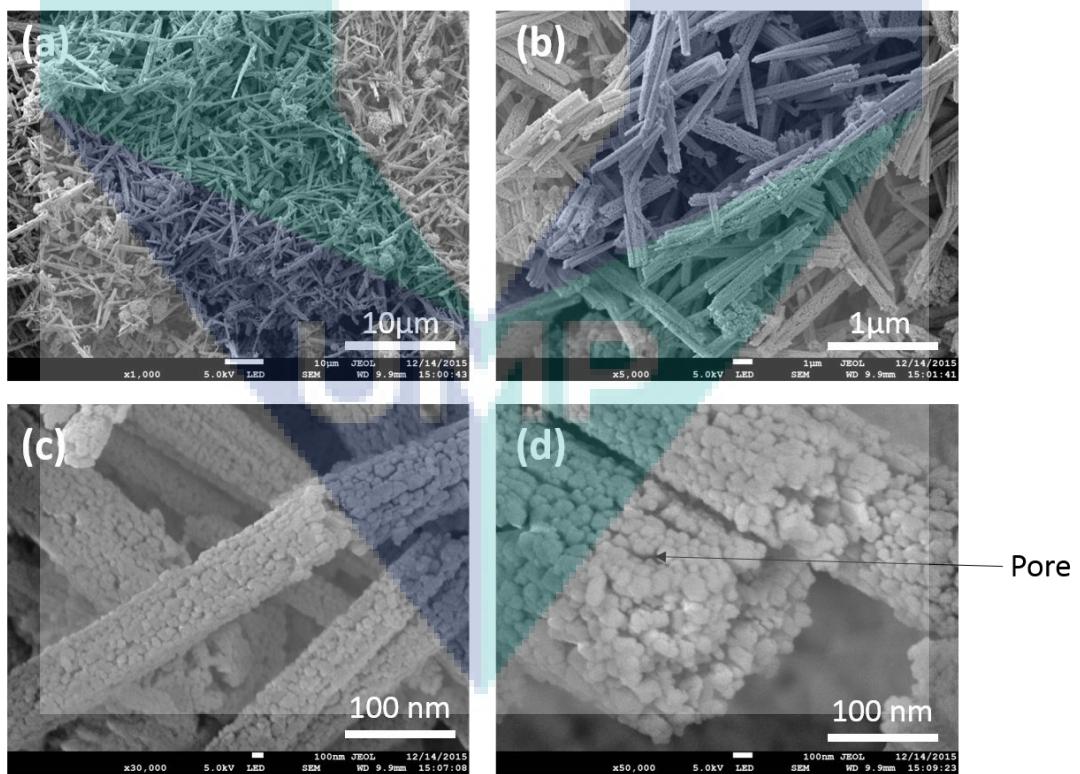


Figure 4.24 FESEM images of  $\text{Co}_3\text{O}_4$  nanorods at different magnifications.

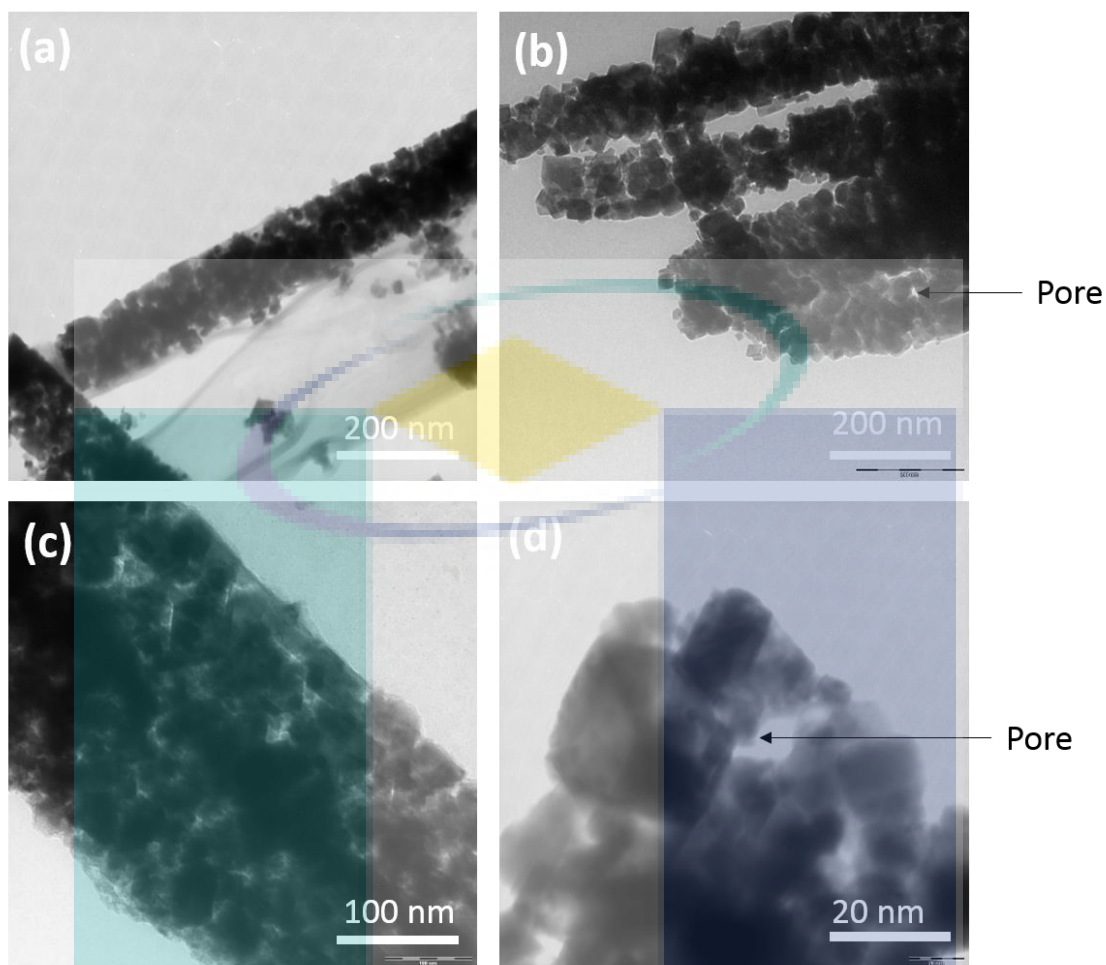


Figure 4.25 TEM images of  $\text{MnCo}_2\text{O}_4$  nanorods at different scales.

#### 4.4.2 BET analysis of $\text{MnCo}_2\text{O}_4$ nanorods

Furthermore, the BET surface area, pore volume and pore diameter of MCON was examined, are given in Table 4.7.

Table 4.7 BET results of  $\text{MnCo}_2\text{O}_4$  nanorods and  $\text{Co}_3\text{O}_4$  nanorods.

Catalyst	BET surface area	Average pore volume	Average pore diameter
$\text{MnCo}_2\text{O}_4$ nanorods	23.49 $\text{m}^2/\text{g}$	0.160 $\text{cm}^3/\text{g}$	41.65 nm
$\text{Co}_3\text{O}_4$ nanorods	15.55 $\text{m}^2/\text{g}$	0.088 $\text{cm}^3/\text{g}$	22.70 nm

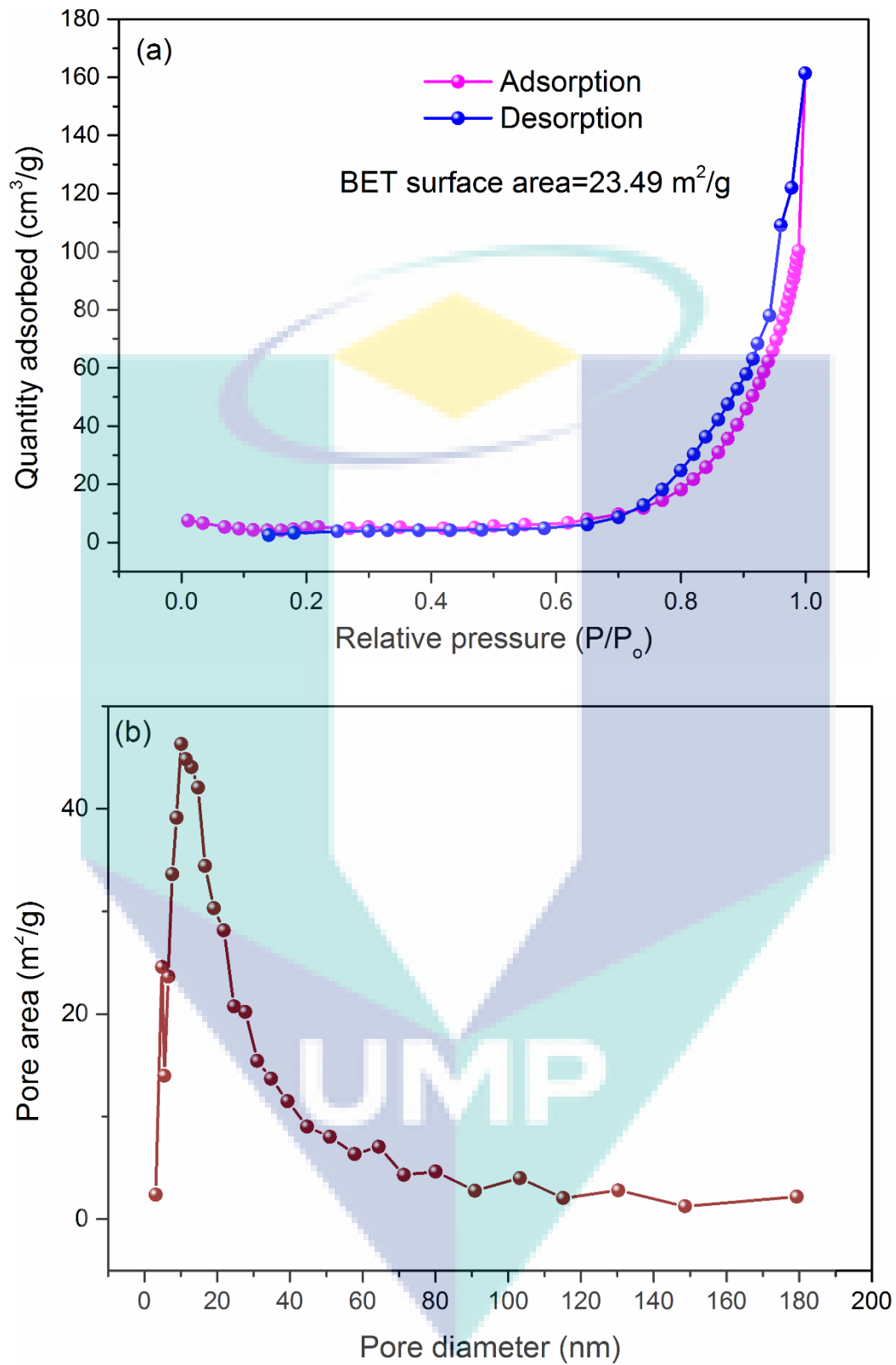
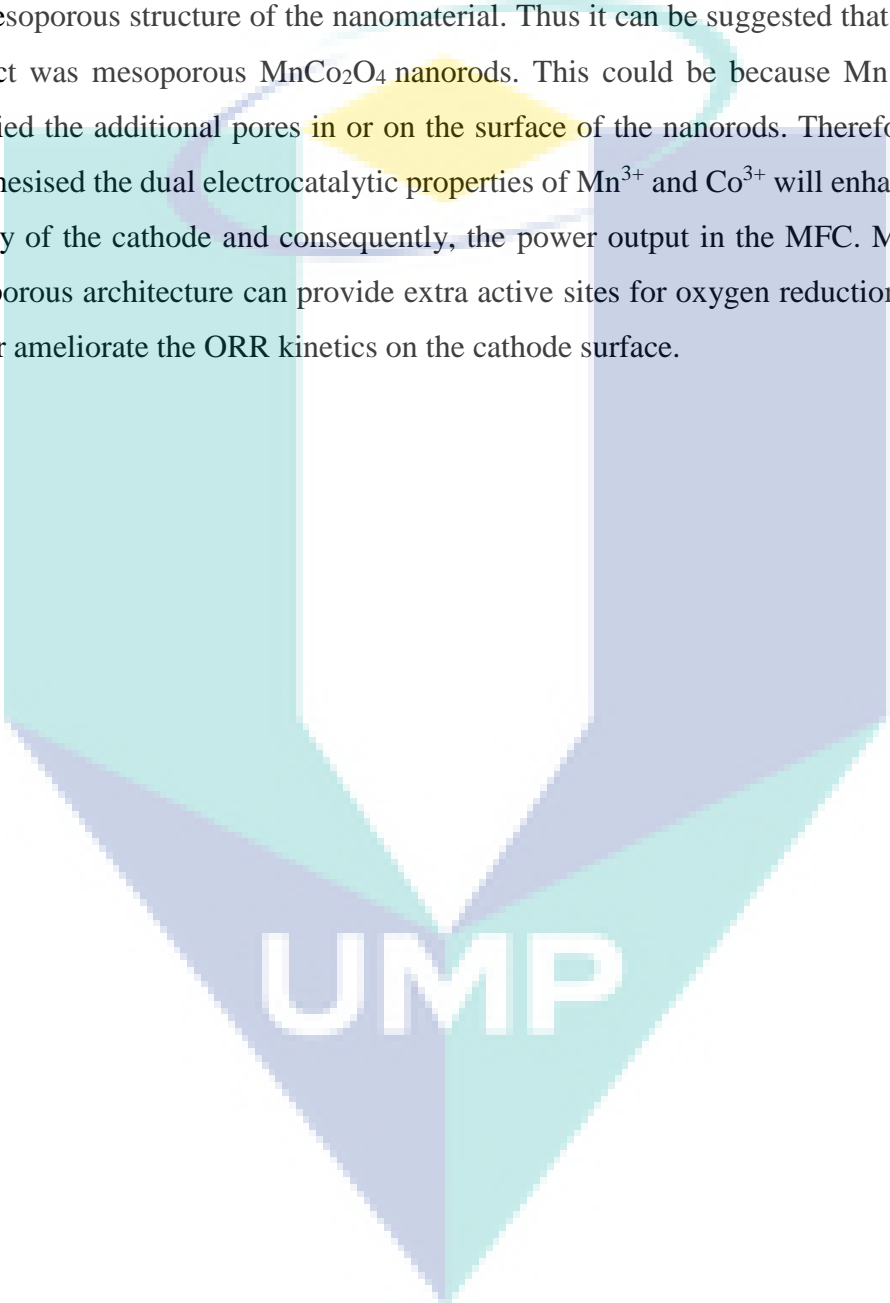


Figure 4.26 (a) Nitrogen adsorption-desorption isotherms of MnCo<sub>2</sub>O<sub>4</sub> nanorods, (b) variations in pore diameter of MnCo<sub>2</sub>O<sub>4</sub> nanorods.

The results showed that MCON exhibited the BET surface area of 23.49 m<sup>2</sup>/g, which was ~51% higher than Co<sub>3</sub>O<sub>4</sub> nanorods while the pore volume in MnCo<sub>2</sub>O<sub>4</sub> nanorods measured was 0.160 cm<sup>3</sup>/g that was also higher than Co<sub>3</sub>O<sub>4</sub> nanorods. The average diameter of a pore in MnCo<sub>2</sub>O<sub>4</sub> nanorods was 41.65 nm. The adsorption isotherm curve for MnCo<sub>2</sub>O<sub>4</sub> nanorods is shown in *Figure 4.26*, which is type III isotherm proving the mesoporous structure of the nanomaterial. Thus it can be suggested that the obtained product was mesoporous MnCo<sub>2</sub>O<sub>4</sub> nanorods. This could be because Mn ions (Mn<sup>3+</sup>) occupied the additional pores in or on the surface of the nanorods. Therefore, it can be hypothesised the dual electrocatalytic properties of Mn<sup>3+</sup> and Co<sup>3+</sup> will enhance the ORR activity of the cathode and consequently, the power output in the MFC. Moreover, the mesoporous architecture can provide extra active sites for oxygen reduction, which will further ameliorate the ORR kinetics on the cathode surface.

The logo for UMP (Universiti Malaysia Perlis) is a large, downward-pointing arrow shape. It is composed of several overlapping, semi-transparent geometric shapes in shades of teal, light blue, and purple. The letters 'UMIP' are printed in a bold, white, sans-serif font across the center of the arrow's shaft.

UMIP

#### 4.4.3 X-ray Photoelectron Spectroscopy (XPS) results of MnCo<sub>2</sub>O<sub>4</sub> nanorods

XPS analysis was performed to further investigate the surface chemical composition of porous MnCo<sub>2</sub>O<sub>4</sub> nanorods. *Figure 4.27* shows the XPS results of MnCo<sub>2</sub>O<sub>4</sub> nanorods.

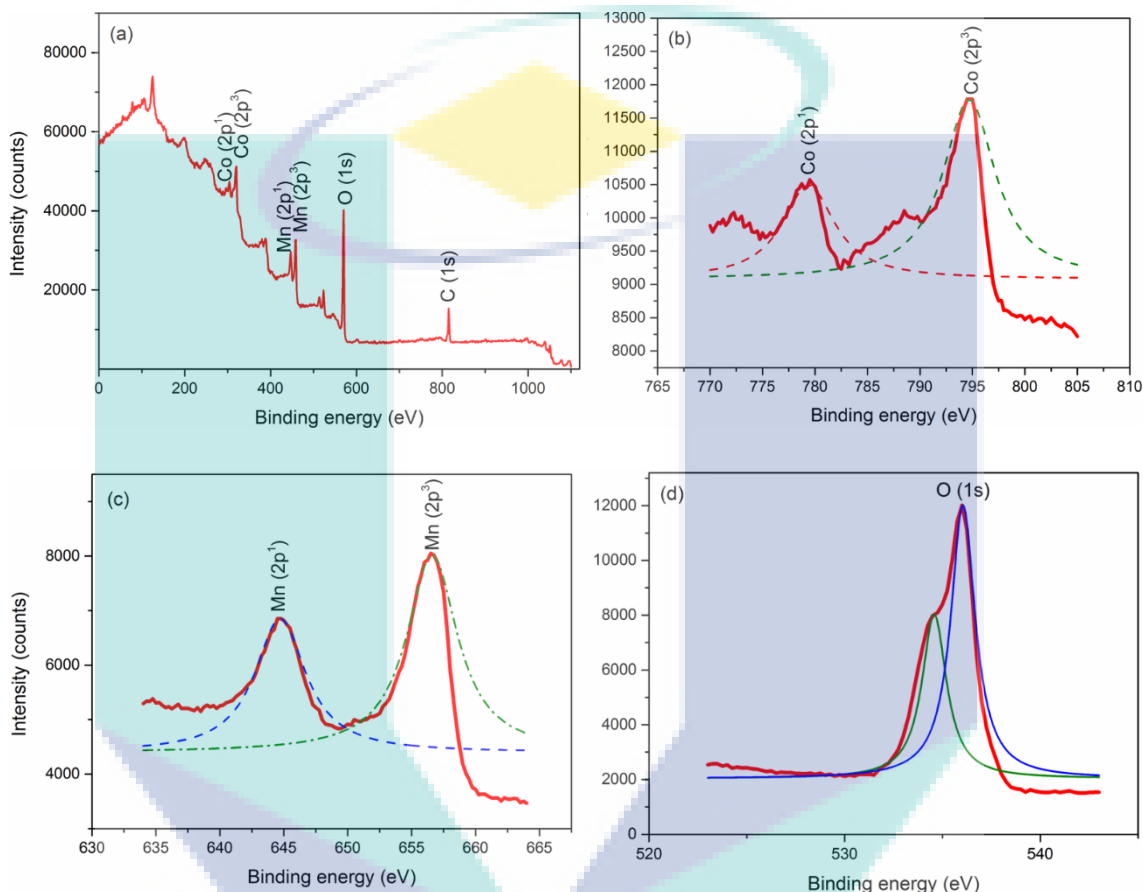


Figure 4.27 XPS Survey spectra of (a) MnCo<sub>2</sub>O<sub>4</sub> nanorods, Individual XPS spectrum of (b) Co 2p, (c) Mn 2p and (d) O 1s.

The survey spectrum (*Figure 4.26a*) of MnCo<sub>2</sub>O<sub>4</sub> nanorods shows the presence of Mn, Co, O and C in the material. In the Co 2p spectrum (*Fig. 4(b)*), two major peaks were observed at binding energies of 780.08 eV (Co2p<sub>3/2</sub>) and 795.23 eV (Co 2p<sub>1/2</sub>), with two weak shakeup satellite peaks. The Co 2p spectrum (*Figure 4.26b*) was fitted with the Gaussian fitting method considering the two spin-orbit doublet characteristic of Co<sup>2+</sup> and Co<sup>3+</sup> ions. The binding-energy separation between the two main peaks was about 15.2 eV, in line with previous reports (Kim et al., 2015; Ge et al., 2014). Similarly, in the Mn 2p spectrum (*Figure 4.26c*), the Mn 2p<sub>3/2</sub> and Mn 2p<sub>1/2</sub> peaks were observed at binding energies of 642.00 eV and 653.51 eV, respectively, which can be resolved into four peak

components. The two peaks at binding energies of 641.8 eV and 653.3 eV are attributed to  $\text{Mn}^{3+}$  ions, whereas the other two peaks at binding energies of 644.2 and 654.7 eV are assigned to  $\text{Mn}^{4+}$  ions (Kim et al., 2015; Ge et al., 2014). *Figure 4.26d* shows the resolved peak of O 1s of  $\text{MnCo}_2\text{O}_4$  nanorods. The oxygen peak indicates the presence of oxygen in metal ions as well as O-H and H-O-H in  $\text{MnCo}_2\text{O}_4$  nanorods (Naveen et al., 2016).

#### 4.4.4 Electrochemical characterization of cathodes

The mesoporous MCON ( $1 \text{ mg/cm}^2$ ) were uniformly coated on the graphite sheet and the cathode was prepared as earlier mentioned in methodology. This prepared cathode and the bare cathode was further characterized by electrochemical techniques prior to use in the MFC. These cathodes were tested by CV, LSV and EIS. All the electrochemical analysis was carried out in a three-electrode system in 100 mM PBS (pH=7) using a potentiostat (Gamry Interface 1000). Firstly, CV curves for both the cathodes were recorded by sweeping the potential from -0.8 V to 0.8 V (V vs. Ag/AgCl) at a scan rate of 100 mV/s.

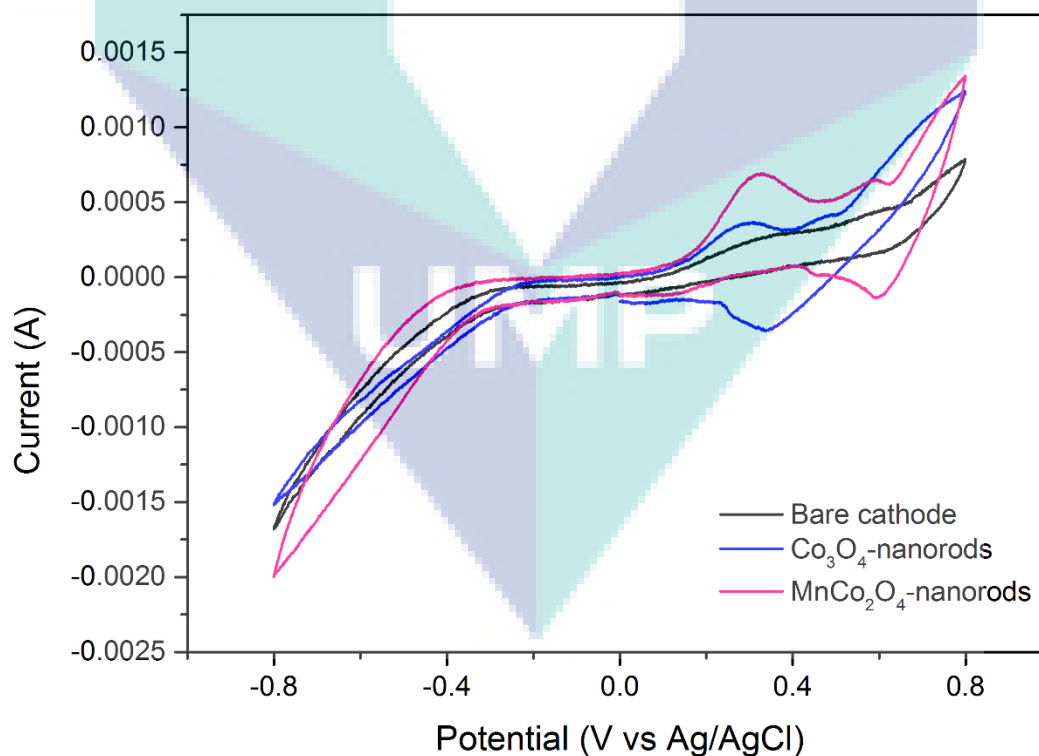


Figure 4.28 CV of  $\text{MnCo}_2\text{O}_4$  nanorods.

All the electrochemical results for MCON were compared with CON-2 (cathode with 1 mg/cm<sup>2</sup> of Co<sub>3</sub>O<sub>4</sub> nanorods). *Figure 4.28* shows the results of CV analysis, which suggested that addition of mesoporous MCON significantly enhanced the oxygen reduction activity of the cathode. It can be clearly observed from the CV curves that no clear reduction peak was obtained by the bare cathode, however, in contrast, a sharp oxygen reduction peak can be clearly seen at a potential of 0.593 V, which was more positive as compared to CON-2 (0.39 V). Therefore, it can be suggested that MCON was more electrochemical active than CON-2, which can be attributed to higher BET surface area and pore volume of MnCo<sub>2</sub>O<sub>4</sub> nanorods. Moreover, this enhanced activity of MCON could be attributed to the excellent electrocatalytic activity shown by Mn<sup>3+</sup>/ Mn<sup>4+</sup> and Co<sup>2+</sup>/Co<sup>3+</sup> on the surface of MnCo<sub>2</sub>O<sub>4</sub> nanorods, as confirmed by the XPS results. The possible mechanism of oxygen reduction on the surface of MCON is given in *Figure 4.29*. Moreover, the pores on the nanorods provided comparatively more reduction sites for oxygen and enhanced the ORR activity of the cathode significantly. The oxygen reduction mechanism by Mn and Co ions can take place by the following reactions: -



Moreover, LSV was performed to further investigate the electrochemical behaviour of the cathodes. LSV curves were recorded by sweeping the potential from -0.6 V to 0.4 V with a scan rate of 10 mV/s in 100 mM PBS (pH=7) in a three-electrode system. The LSV curves for the cathodes are shown in *Figure 4.30*. The results demonstrated that MCON achieved the highest limiting current density as compared to the bare cathode and CON-2. Expectedly, MCON showed a current density of 1.55 A/m<sup>2</sup> (at a potential of -0.6 V), which was ~67% higher than the bare cathode and 29% higher than CON-2 at the similar potential. This enhanced current density shown by MCON can

be attributed to faster electron transfer at the cathode surface, which could be probably due the higher ORR activity by  $\text{MnCo}_2\text{O}_4$  nanorods.

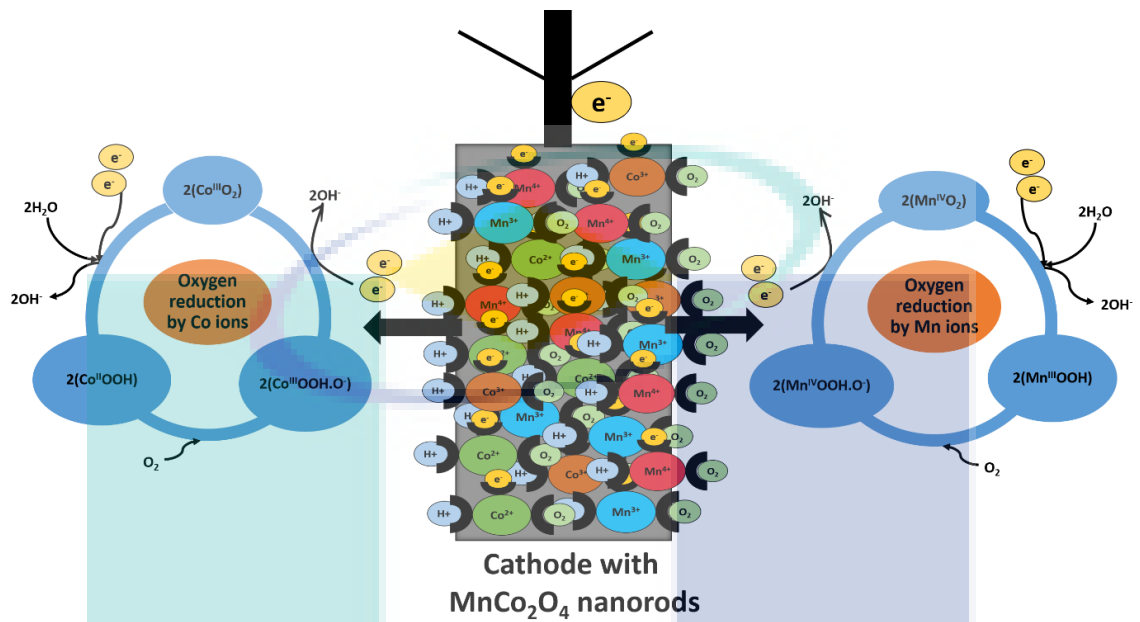


Figure 4.29 Possible mechanism of oxygen reduction by  $\text{MnCo}_2\text{O}_4$  nanorods.

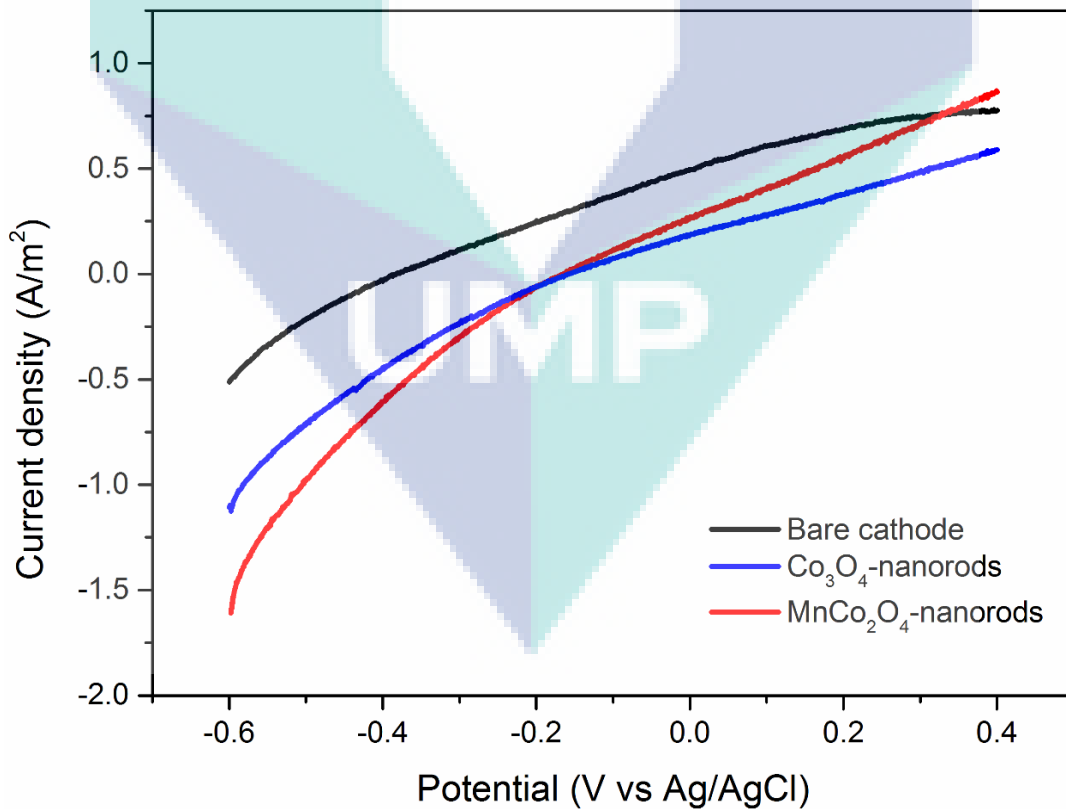


Figure 4.30 LSVs of  $\text{MnCo}_2\text{O}_4$  nanorods at a scan rate of 10 mV/s.

A previous study demonstrated the application of Mn-Co oxides for oxygen reduction in alkaline medium, which suggested that oxygen reduction occurred through the oxidation of Mn (III), cyclically produced by reduction of Mn (IV) (Lima et al., 2009). On the other hand, Xu et al. used cobalt oxide nanorods as the electrocatalyst for oxygen reduction in anion-exchange membrane fuel cells, which demonstrated that the ORR is usually carried out at the active sites which are associated with  $\text{Co}^{3+}$  ions on the surface of  $\text{Co}_2\text{O}_4$  nanorods (Xu et al., 2012). Besides, in this work, the XPS results also determined the presence of  $\text{Mn}^{3+}/\text{Mn}^{4+}$  and  $\text{Co}^{2+}/\text{Co}^{3+}$  on the surface of  $\text{MnCo}_2\text{O}_4$  nanorods that acted as the oxygen reduction sites and improved the ORR activity significantly.

Furthermore, Nyquist plots were recorded for both the cathodes in a three-electrode system over a frequency range of 1 Hz–100,000 Hz at the initial open circuit potential with a sinusoidal perturbation of 10 mV amplitude. Further, the results of Nyquist plots were fitted into this equivalent circuit (*Figure 4.14*) to determine the value of  $R_{\text{ohm}}$  and  $R_{\text{act}}$ , similarly to the previous objectives.  $R_{\text{ohm}}$  represents a combination of different resistances that is ionic resistance of the electrolyte, intrinsic resistance of active materials, and contact resistance while  $R_{\text{act}}$  shows charge transfer resistance. The results of Nyquist plots are shown in *Figure 4.31*.

Table 4.8 Resistance values for the cathodes calculated from the fitting results of Nyquist plots.

Cathode	$R_{\text{ohm}}$ ( $\Omega$ )	$R_{\text{act}}$ ( $\Omega$ )
Bare cathode	134.2	26.51
CON-2	24.80	5.21
MCON	6.23	2.85

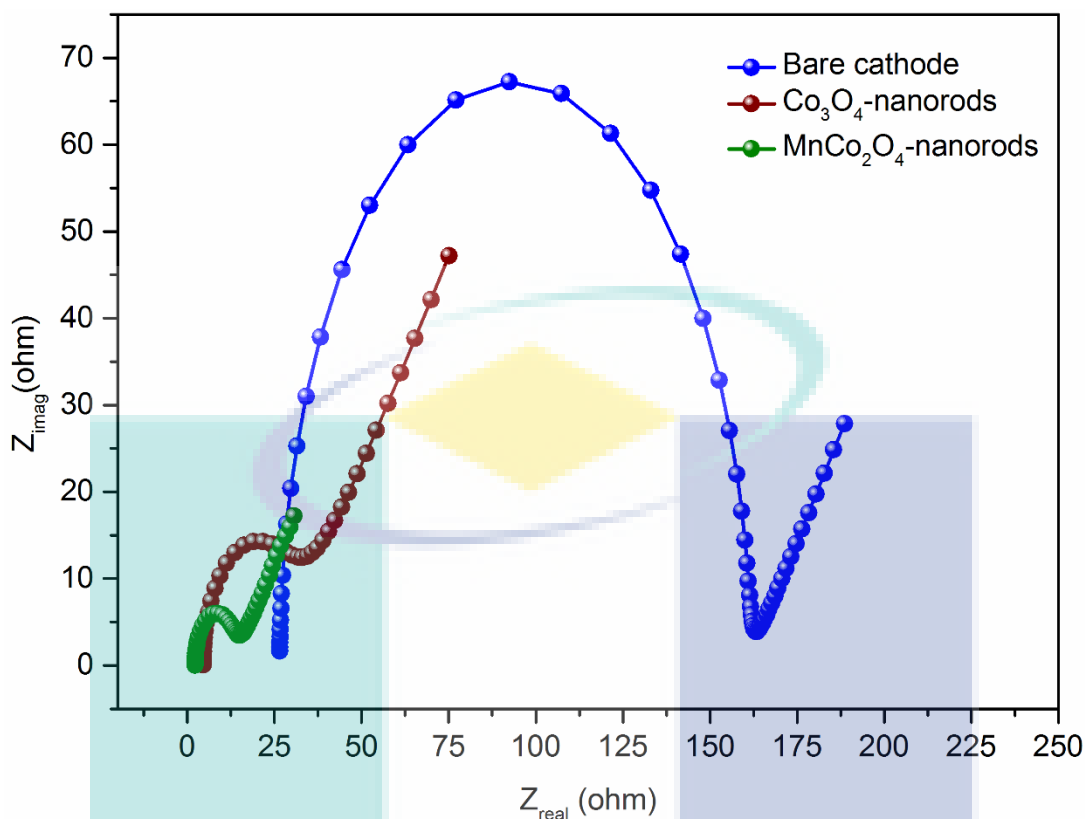


Figure 4.31 Nyquist plot of the cathodes measured over a frequency range of 1 Hz-100000 Hz at the initial open circuit potential with a sinusoidal perturbation of 10 mV amplitude.

The resistance values calculated from the Nyquist plots are given in Table 4.8. The results demonstrated that the addition of MCON onto the cathode greatly reduced the overall resistance of the system. Evidently, MCON showed lesser resistance values for  $R_{ohm}$  and  $R_{act}$  as compared to the bare cathode and CON-2.  $R_{ohm}$  measured for MCON was  $6.23 \Omega$ , which was manifolds lower than the bare cathode and 298% lower than CON-2. In addition, a significant reduction was also determined in  $R_{act}$  for MCON and the cathode showed a resistance value of  $2.85 \Omega$ , which was extremely lower than the bare cathode ( $26.51 \Omega$ ). This substantial reduction in the resistance can be attributed to the excellent electrocatalytic activity shown by MCON that allowed the transfer of electrons faster through the electrolyte, electrode surfaces, and external circuit. The resistance values for  $R_{ohm}$  and  $R_{act}$  obtained for MCON was the lowest from other catalysts ( $Co_3O_4$  flakes, and flower-like  $Co_3O_4$ ) of similar concentration ( $1 \text{ mg/cm}^2$ ) used in the previous objectives. This could be because MCON provided higher number of accessible reduction

sites for oxygen, therefore, improved the ORR activity considerably and reduced the resistance of the system significantly.

#### 4.4.5 ORR kinetics by Tafel plots

The ORR kinetics of both the cathodes were studied by Tafel plots. The exchange current density ( $i_0$ ) was calculated from the Tafel plots.  $i_0$  is a promising parameter to analyse the rate of oxygen reduction on the cathode surface. Tafel plots were measured by sweeping the overpotential from 20 mV to 100 mV at a scan rate of 1 mVs<sup>-1</sup> against Ag/AgCl. Besides, a linear region was extracted by taking the values from overpotential of 60 mV to 100 mV with  $R^2 > 0.99$ . The results of Tafel plots are shown in *Figure 4.32* and the  $i_0$  calculated from the Tafel plots are given in Table 4.9.

Table 4.9 Exchange current densities for the cathodes.

Cathode	Linear fitting equation ( $R^2$ )	$i_0$ (A/m <sup>2</sup> )
Bare cathode	$y = -1.9823 + 5.8101x$ (0.995)	1.89
CON-2	$y = -5.4873 + 5.7858x$ (0.994)	5.34
MCON	$y = -6.2551 + 5.8029x$ (0.997)	6.10

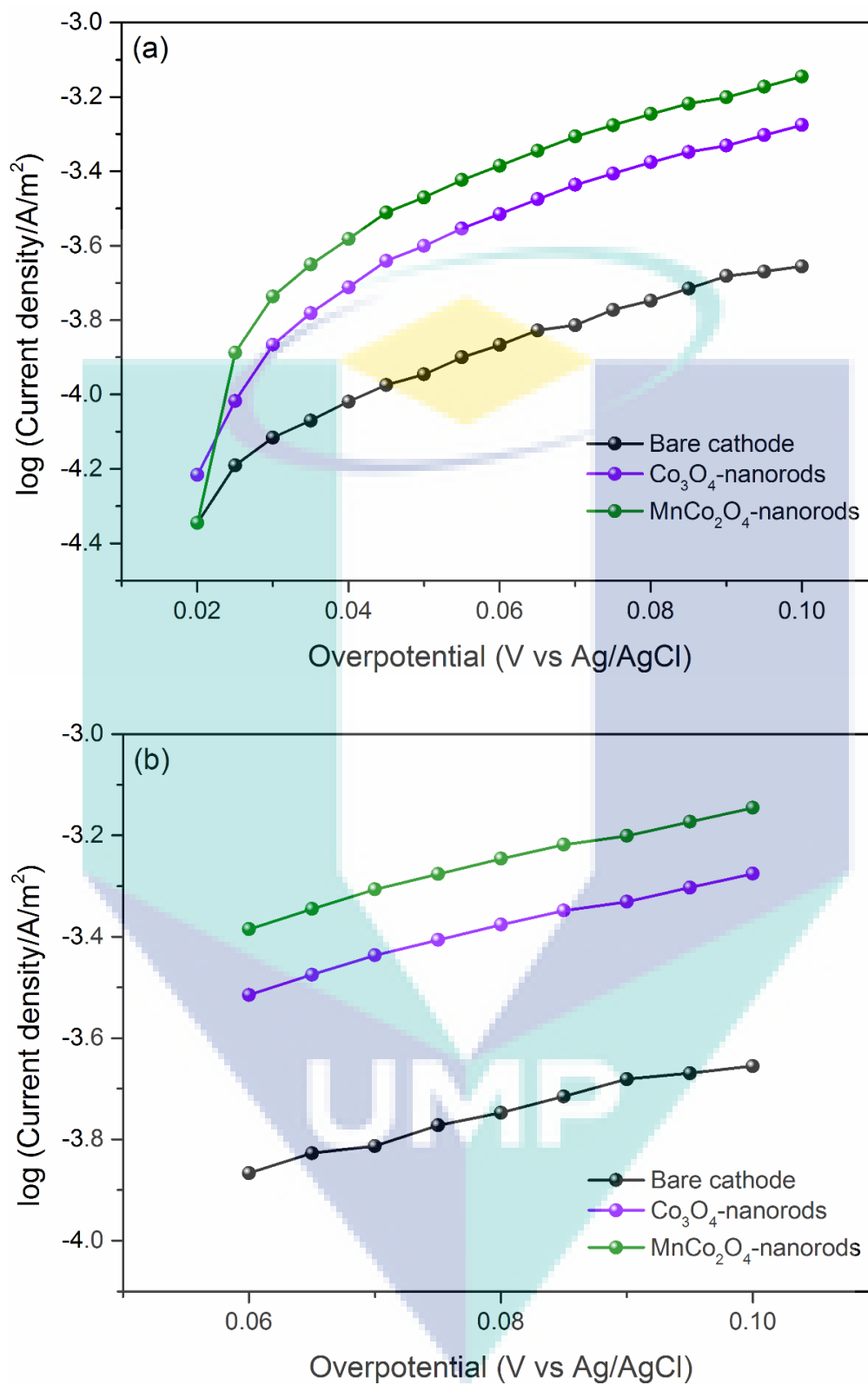


Figure 4.32 (a) Tafel plots of the cathodes by sweeping the overpotential from 20 mV to 100 mV at  $1 \text{ mVs}^{-1}$  and (b) the linear fit for the Tafel plots of overpotential from 60 to 80 mV.

The results demonstrated the cathode with mesoporous MCON reduced oxygen molecules with a faster reduction rate and the cathode achieved an  $i_o$  of 6.10 A/m<sup>2</sup>. On the other hand, the bare cathode obtained an  $i_o$  of 1.89 A/m<sup>2</sup>, which was 222% lower than MnCo<sub>2</sub>O<sub>4</sub> nanorods. Besides, the  $i_o$  achieved by MCON was higher than CON-2 (5.34 A/m<sup>2</sup>), COFK (3.54 A/m<sup>2</sup>), and COFL (2.46 A/m<sup>2</sup>) experimented previously. Tafel results were consistent with CV, LSV, and EIS. Moreover, the results were also comparable to the other ORR catalysts. For example, Zhang et al. applied Cu/activated carbon as the cathode catalyst and achieved an  $i_o$  of 1.03 A/m<sup>2</sup>, which was manifolds lower than MCON showed in this work (Zhang et al., 2015). In addition, He et al. demonstrated the application of nitrogen doped-carbon nanotubes as the cathode catalyst that obtained of an  $i_o$  5.13 A/m<sup>2</sup>, which was approximately 19% lower than MCON (He et al., 2016). This enhanced ORR activity can be ascribed to the excellent electrocatalytic activity of MCON. The improved ORR activity can also be credited to the mesoporous architecture of the nanorods that presented more active site for oxygen adsorption. Besides, the lower resistance in the system also allowed faster electron transfer across the cathode interface, as suggested by the EIS results.

Besides, Hu et al. studied the ORR kinetics of carbon-supported spinel nanoparticle MnCo<sub>2</sub>O<sub>4</sub> in MFCs, which demonstrated that MnCo<sub>2</sub>O<sub>4</sub> followed a direct 4-electron reaction pathway in alkaline solution (Hu et al., 2015). In addition, Mahmoud et al. also utilized spinel manganese-cobalt oxide as a cathode catalyst in air-cathode MFC that also followed a nearly 4-electron reaction pathway in ORR (Mahmoud et al., 2011). Therefore, it can be suggested that mesoporous MCON might also followed a nearly between three and four-electron pathway for ORR.

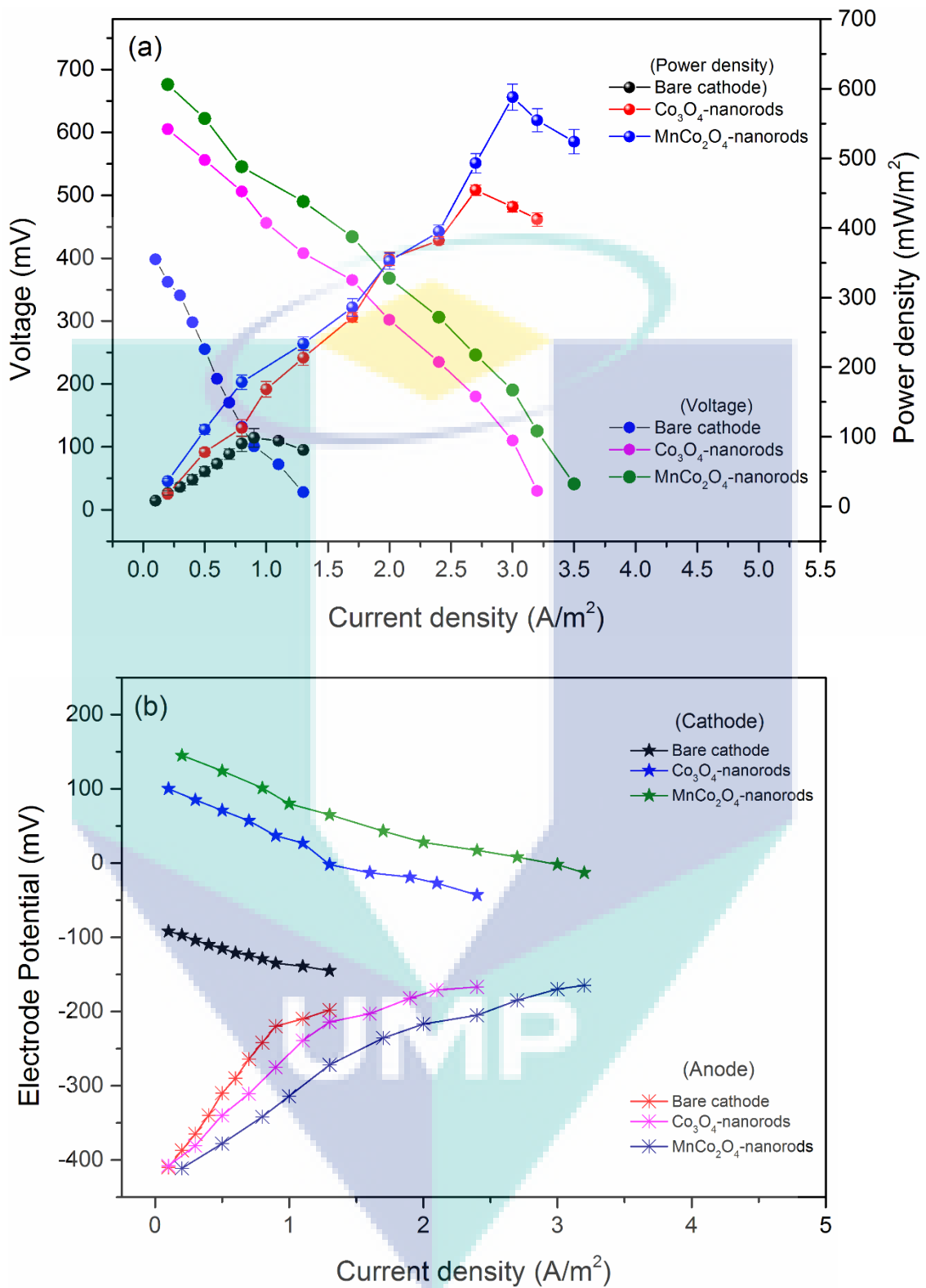


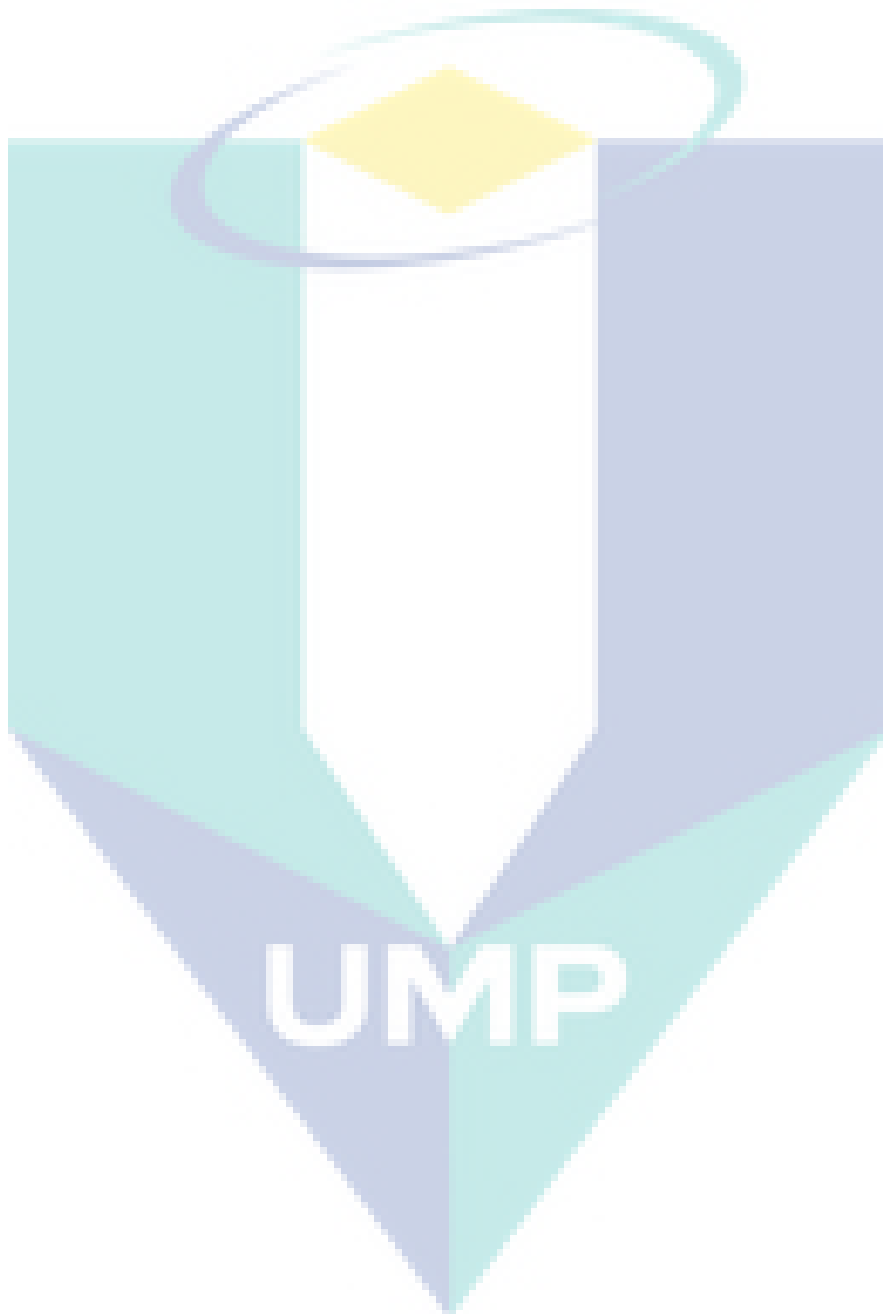
Figure 4.33 (a) Polarization and power density curves of MFCs and (b) electrode potentials of bare cathode, MnCo<sub>2</sub>O<sub>4</sub> nanorods, and Co<sub>3</sub>O<sub>4</sub> nanorods.

#### 4.4.6 Performance of the cathodes for bioelectricity generation in MFCs

After the investigation of electrochemical characterization, the cathodes were used in a double chamber MFC and their potential for electricity generation was examined by performing the polarization curves. The MFCs were operated in a batch mode and the polarization curves were recorded after three days of operation to measure the maximum power density. The results of polarization curves are shown in *Figure 4.33a*, which suggested that MCON improved the power output of the MFC considerably. Expectedly, the MFC with MCON achieved a maximum power density of  $587 \text{ mW/m}^2$ , which was ca. 498% higher than the bare cathode. Moreover, the power density shown by MCON was ~18% higher than CON-2 ( $454 \text{ mW/m}^2$ ), which indicates that the addition of Mn was a good idea to improve power output in the MFC. The excellent performance of MCON in the MFC was mainly due to their significant ORR activity because there was a much variation in the cathode potentials as compared to the anode potentials, as shown in *Figure 4.33b*.

The results obtained in this study were also comparable to other catalysts as well. For example, in a study,  $\text{MnO}_2\text{-CNT}$  was used as the cathode catalyst that produced a power density of  $210 \text{ mW/m}^2$ , which was ~179% lower than the power density obtained by MCON in this work (Zhang et al., 2011). In addition, Li et al. applied binuclear-cobalt-phthalocyanine as a cathode catalyst and reported a maximum power density of  $368 \text{ mW/m}^2$ , which was 59.5% lower than MCON (Li et al., 2014). Further, MCON also produced higher power density as compared to the Mn-Co composites used in the previous studies. For instance, Mahmoud et al. demonstrated the application of spinel manganese–cobalt (Mn–Co) oxide in an air-cathode MFC that generated a highest power density of  $113 \text{ mW/m}^2$ , which was manifolds lower than MCON (Mahmoud et al., 2011). In an alternative study,  $\text{MnCo}_2\text{O}_4$  spinel nanoparticles were investigated in MFCs that achieved a power density of  $545 \text{ mW/m}^2$ , which was also less as compared to MCON used in this work (Hu et al., 2014). This boost in power output can be attributed to the excellent electrocatalytic activity and the improved ORR activity shown by MCON and also to the mesoporous architecture of the nanorods that presented more active sites for oxygen adsorption. Moreover, the lower resistance in the system also ameliorated electron transfer across the cathode interface and boosted the power density. Therefore, it can be

concluded from the results that mesoporous morphologies of the catalysts could be advantageous to improve their performance for MFC applications.



## CHAPTER 5

### CONCLUSIONS

#### 5.1 Conclusions

In first objective, three morphologies of  $\text{Co}_3\text{O}_4$  that is  $\text{Co}_3\text{O}_4$  nanorods,  $\text{Co}_3\text{O}_4$  flakes, and  $\text{Co}_3\text{O}_4$  flower were successfully prepared by the hydrothermal methods. XRD and electron microscopy results confirmed the pure form and the morphology of all the catalysts. The BET results suggested that  $\text{Co}_3\text{O}_4$  nanorods showed highest BET surface area among the other catalyst that is  $15.55 \text{ m}^2/\text{g}$ , which was  $\sim 40\%$  higher than  $\text{Co}_3\text{O}_4$  flakes and  $\sim 209\%$  higher than  $\text{Co}_3\text{O}_4$  flower.

In second objective, the cathodes with optimized concentration of  $\text{Co}_3\text{O}_4$  flakes (COFK) and  $\text{Co}_3\text{O}_4$  flower (COFL) were prepared as their performance was compared with  $\text{Co}_3\text{O}_4$  nanorods (CON-2). The electrochemical studies demonstrated that CON-2 showed higher electrocatalytic activity as compared to COFK and COFL, as suggested by more positive onset potential for oxygen reduction in CV and higher limiting current density in LSV. Besides, CON-2 showed comparatively lesser resistance values for  $R_{\text{ohm}}$  and  $R_{\text{act}}$ , are summarized in Table 5.1. Finally, the polarization results showed that the MFC with CON-2 generated a maximum power density of  $454 \text{ mW}/\text{m}^2$  that was  $\sim 48\%$  higher than COFK ( $305 \text{ mW}/\text{m}^2$ ) and  $\sim 165\%$  higher than COFL ( $171 \text{ mW}/\text{m}^2$ ). The higher power density shown by CON-2 can be ascribed to excellent ORR activity of  $\text{Co}_3\text{O}_4$  nanorods, as demonstrated by CV and LSV results. Besides, the nanorods also showed less activation resistance and charge resistance as compared to the flakes and the flower, which means the nanorods promoted the electron transfer through the electrolyte and the electrode surface.

Table 5.1 Performance of all catalysts used in this study and comparison with previous studies.

Catalyst	BET surface area (m <sup>2</sup> /g)	Resistance ( $\Omega$ )		$i_o$ (A/m <sup>2</sup> )	PD (mW/m <sup>2</sup> )	Reference
		$R_{ohm}$	$R_{act}$			
Bare cathode	-	134.2	26.51	1.89	98	This study
Co <sub>3</sub> O <sub>4</sub> nanorods	15.55	24.80	5.21	5.34	454	This study
Co <sub>3</sub> O <sub>4</sub> flakes	11.05	11.27	7.81	3.54	305	This study
Co <sub>3</sub> O <sub>4</sub> flower	05.03	32.51	16.24	2.46	171	This study
MnCo <sub>2</sub> O <sub>4</sub> nanorods	23.49	6.23	2.85	6.01	587	This study
Bare-AC	1725.87 m <sup>2</sup> /g	13.84	1.74	5.56	760	(Ge et al., 2015)
Spinel Co <sub>3</sub> O <sub>4</sub> -AC	1536.51 m <sup>2</sup> /g	9.33	0.45	13.9	1390	(Ge et al., 2015)
Co(OH) <sub>2</sub> -AC	1753 m <sup>2</sup> /g	11.70	4.65	9.9	1234	(Liu et al., 2016)
Co <sub>3</sub> O <sub>4</sub> nanosheets-AC	1873.95 m <sup>2</sup> /g	11.44	4.38	15.7	1420	(Liu et al., 2016)
NiCo <sub>2</sub> O <sub>4</sub> -AC	104.4 m <sup>2</sup> /g	9.58	1.23	17.0	1574	(Ge et al., 2016)

Note: AC=activated carbon

In third objective, MnCo<sub>2</sub>O<sub>4</sub> nanorods were synthesized and the results were compared to Co<sub>3</sub>O<sub>4</sub> nanorods (CON-2). The electrochemical studies demonstrated that MCON showed higher ORR activity and lesser resistance as compared to CON-2. Besides, Tafel results demonstrated that MCON reduced oxygen molecules with a faster reduction rate and achieved an exchange current density of 6.01A/m<sup>2</sup>, which was ~ 14% higher than CON-2. Finally, the performance of MCON for electricity generation was evaluated and maximum power density was calculated from the polarization curves, which demonstrated that the MFC with MCON achieved a maximum power density of 587 mW/m<sup>2</sup>, which was ~ 29% higher than CON-2 and ~ 498% higher than the bare cathode. Overall, high performance of MCON over CON-2 can be ascribed to its higher surface area and pore volume, and excellent ORR activity shown by Co<sup>2+</sup>/Co<sup>3+</sup> and Mn<sup>3+</sup>/Mn<sup>4+</sup> ions on the cathode surface.

## 5.2 Recommendations for Future Work

This research work was only limited to investigate the morphological effect of the cathode catalyst, therefore, there is a possibility to further enhance the performance of these catalysts.

1. All the cathode catalysts used in this work showed very low BET surface area as compared to other conventional cathode catalysts, hence these catalysts can be combined with other catalysts of high BET surface area such as activated carbon and graphene and their ORR activity can be improved significantly, which would be the promising alternative for Pt to scale-up the technology.
2. In this research work, the morphological effect of the cathode catalyst was studied, similarly, the effect of pores can also be studied in the future. For example,  $\text{Co}_3\text{O}_4$  nanorods with different pore sizes (micropore, mesopore, macropore) can be synthesized and their ORR activity can be experimented in MFCs.
3. In this study, the morphological effect of the cathode catalyst was limited for electricity generation only, therefore, its impact on other MFC applications such as wastewater treatment will be interesting to examine in the near future.
4. Moreover, an inoculum of selected exoelectrogens such as *Geobacter* sp. and *Shewanella* sp. can be used in anode chamber, further, its effect on bioelectricity generation and wastewater treatment can be studied.

## REFERENCES

- Aelterman, P., Rabaey, K., Pham, H. T., Boon, N., & Verstraete, W. (2006). Continuous electricity generation at high voltages and currents using stacked microbial fuel cells. *Environmental science & technology*, 40(10), 3388-3394.
- Adler, S. B. (1998). Mechanism and kinetics of oxygen reduction on porous  $\text{La}_{1-x}\text{Sr}_x\text{CoO}_{3-\delta}$  electrodes. *Solid State Ionics*, 111(1), 125-134.
- Ahmed, J., Kim, H. J., & Kim, S. (2014). Embedded cobalt oxide nano particles on carbon could potentially improve oxygen reduction activity of cobalt phthalocyanine and its application in microbial fuel cells. *RSC Advances*, 4(83), 44065-44072.
- Ahmed, J., Yuan, Y., Zhou, L., & Kim, S. (2012). Carbon supported cobalt oxide nanoparticles-iron phthalocyanine as alternative cathode catalyst for oxygen reduction in microbial fuel cells. *Journal of Power Sources*, 208, 170-175.
- Ahn, Y., & Logan, B. E. (2010). Effectiveness of domestic wastewater treatment using microbial fuel cells at ambient and mesophilic temperatures. *Bioresource technology*, 101(2), 469-475.
- Awan, Z., Nahm, K. S., & Xavier, J. S. (2014). Nanotubular  $\text{MnO}_2$ /graphene oxide composites for the application of open air-breathing cathode microbial fuel cells. *Biosensors and Bioelectronics*, 53, 528-534.
- Baranitharan, E., Khan, M.R., Yousuf, A., Teo, W.F.A., Tan, G.Y.A., and Cheng, C. K. (2015). Enhanced power generation using controlled inoculum from palm oil mill effluent fed microbial fuel cell. *Fuel*, 143, 72-79.
- Bergel, A., Féron, D., & Mollica, A. (2005). Catalysis of oxygen reduction in PEM fuel cell by seawater biofilm. *Electrochemistry Communications*, 7(9), 900-904.
- Borole, A. P., Hamilton, C. Y., & Schell, D. J. (2012). Conversion of residual organics in corn stover-derived biorefinery stream to bioenergy via a microbial fuel cell. *Environmental science & technology*, 47(1), 642-648.
- BP Statistical Review of World Energy; 2011.
- BP Energy Outlook 2030; 2012.
- Burkitt, R., Whiffen, T. R., & Yu, E. H. (2016). Iron phthalocyanine and  $\text{MnO}_x$  composite catalysts for microbial fuel cell applications. *Applied Catalysis B: Environmental*, 181, 279-288.
- Byrappa, K., & Yoshimura, M. (2001). Handbook of Hydrothermal Technology A technology for Crystal Growth and Materials Processing. *Toronto, Will%o AndrewPublishing*, 531-535.

- Carbajosa, S., Malki, M., Caillard, R., Lopez, M. F., Palomares, F. J., Martín-Gago, J. A., ... & De Lacey, A. L. (2010). Electrochemical growth of *Acidithiobacillus ferrooxidans* on a graphite electrode for obtaining a biocathode for direct electrocatalytic reduction of oxygen. *Biosensors and Bioelectronics*, 26(2), 877-880.
- Cao, C., Wei, L., Su, M., Wang, G., & Shen, J. (2016). Enhanced power generation using nano cobalt oxide anchored nitrogen-decorated reduced graphene oxide as a high-performance air-cathode electrocatalyst in biofuel cells. *RSC Advances*, 6(58), 52556-52563.
- Catal, T., Li, K., Bermek, H., & Liu, H. (2008a). Electricity production from twelve monosaccharides using microbial fuel cells. *Journal of Power Sources*, 175(1), 196-200.
- Catal, T., Xu, S., Li, K., Bermek, H., & Liu, H. (2008b). Electricity generation from polyalcohols in single-chamber microbial fuel cells. *Biosensors and Bioelectronics*, 24(4), 849-854.
- Cercado Q. B., Delia, M. L., & Bergel, A. (2010). Testing various food-industry wastes for electricity production in microbial fuel cell. *Bioresource technology*, 101(8), 2748-2754.
- Chang, Y. Y., Zhao, H. Z., Zhong, C., & Xue, A. (2014). Effects of different Pt-M (M= Fe, Co, Ni) alloy as cathodic catalyst on the performance of two-chambered microbial fuel cells. *Russian Journal of Electrochemistry*, 50(9), 885-890.
- Chaudhuri, S. K., & Lovley, D. R. (2003). Electricity generation by direct oxidation of glucose in mediatorless microbial fuel cells. *Nature biotechnology*, 21(10), 1229-1232.
- Cheng, S., Kiely, P., & Logan, B. E. (2011). Pre-acclimation of a wastewater inoculum to cellulose in an aqueous-cathode MEC improves power generation in air-cathode MFCs. *Bioresource technology*, 102(1), 367-371.
- Cheng, S., & Logan, B. E. (2007). Ammonia treatment of carbon cloth anodes to enhance power generation of microbial fuel cells. *Electrochemistry Communications*, 9(3), 492-496.
- Cheng, S., Liu, H., & Logan, B. E. (2006). Power densities using different cathode catalysts (Pt and CoTMPP) and polymer binders (Nafion and PTFE) in single chamber microbial fuel cells. *Environmental science & technology*, 40(1), 364-369.
- Chen, G., Wei, B., Logan, B. E., & Hickner, M. A. (2012). Cationic fluorinated polymer binders for microbial fuel cell cathodes. *RSC advances*, 2(13), 5856-5862.

- Chen, S., Liu, G., Zhang, R., Qin, B., & Luo, Y. (2012). Development of the microbial electrolysis desalination and chemical-production cell for desalination as well as acid and alkali productions. *Environmental science & technology*, 46(4), 2467-2472.
- Chen, S., Chen, Y., He, G., He, S., Schröder, U., & Hou, H. (2012). Stainless steel mesh supported nitrogen-doped carbon nanofibers for binder-free cathode in microbial fuel cells. *Biosensors and Bioelectronics*, 34(1), 282-285.
- Chen, Y., Lv, Z., Xu, J., Peng, D., Liu, Y., Chen, J., ... & Wei, C. (2012). Stainless steel mesh coated with MnO<sub>2</sub>/carbon nanotube and polymethylphenyl siloxane as low-cost and high-performance microbial fuel cell cathode materials. *Journal of Power Sources*, 201, 136-141.
- Chen, Z., Li, K., & Pu, L. (2014). The performance of phosphorus (P)-doped activated carbon as a catalyst in air-cathode microbial fuel cells. *Bioresource technology*, 170, 379-384.
- Chen, Z., Li, K., Zhang, P., Pu, L., Zhang, X., & Fu, Z. (2015). The performance of activated carbon treated with H<sub>3</sub>PO<sub>4</sub> at 80° C in the air-cathode microbial fuel cell. *Chemical Engineering Journal*, 259, 820-826.
- Chookaew, T., Prasertsan, P., & Ren, Z. J. (2014). Two-stage conversion of crude glycerol to energy using dark fermentation linked with microbial fuel cell or microbial electrolysis cell. *New biotechnology*, 31(2), 179-184.
- Cho WS, Yashima M, Kakihana M, Kudo A, Sakata T, Yoshimura M. Room-temperature preparation of the highly crystallized luminescent CaWO<sub>4</sub> film by an electrochemical method. *Applied physics letters*. 1995 Feb 27;66(9):1027-9.
- Chung, D. D. L. (2002). Review graphite. *Journal of materials science*, 37(8), 1475-1489.
- Cui, Y., Rashid, N., Hu, N., Rehman, M. S. U., & Han, J. I. (2014). Electricity generation and microalgae cultivation in microbial fuel cell using microalgae-enriched anode and bio-cathode. *Energy Conversion and Management*, 79, 674-680.
- Cusick, R. D., Kim, Y., & Logan, B. E. (2012). Energy capture from thermolytic solutions in microbial reverse-electrodialysis cells. *Science*, 335(6075), 1474-1477.
- Dai, L., Xue, Y., Qu, L., Choi, H. J., & Baek, J. B. (2015). Metal-free catalysts for oxygen reduction reaction. *Chemical reviews*, 115(11), 4823-4892.
- del Campo, A. G., Cañizares, P., Rodrigo, M. A., Fernández, F. J., & Lobato, J. (2013). Microbial fuel cell with an algae-assisted cathode: a preliminary assessment. *Journal of Power Sources*, 242, 638-645
- Deng, L., Zhou, M., Liu, C., Liu, L., Liu, C., & Dong, S. (2010). Development of high performance of Co/Fe/N/CNT nanocatalyst for oxygen reduction in microbial fuel cells. *Talanta*, 81(1), 444-448.

- Dong, H., Yu, H., Wang, X., Zhou, Q., & Sun, J. (2013). Carbon-supported perovskite oxides as oxygen reduction reaction catalyst in single chambered microbial fuel cells. *Journal of Chemical Technology and Biotechnology*, 88(5), 774-778.
- Donnet, J. B. (Ed.). (1993). *Carbon black: science and technology*. CRC Press.
- Dumas, C., Mollica, A., Féron, D., Basséguy, R., Etcheverry, L., & Bergel, A. (2007). Marine microbial fuel cell: use of stainless steel electrodes as anode and cathode materials. *Electrochimica Acta*, 53(2), 468-473.
- Duteanu, N., Erable, B., Kumar, S. S., Ghangrekar, M. M., & Scott, K. (2010). Effect of chemically modified Vulcan XC-72R on the performance of air-breathing cathode in a single-chamber microbial fuel cell. *Bioresource technology*, 101(14), 5250-5255.
- El-Naggar, M. Y., Wanger, G., Leung, K. M., Yuzvinsky, T. D., Southam, G., Yang, J., ... & Gorby, Y. A. (2010). Electrical transport along bacterial nanowires from *Shewanella oneidensis* MR-1. *Proceedings of the National Academy of Sciences*, 107(42), 18127-18131.
- Erable, B., Duteanu, N., Kumar, S. S., Feng, Y., Ghangrekar, M. M., & Scott, K. (2009). Nitric acid activation of graphite granules to increase the performance of the non-catalyzed oxygen reduction reaction (ORR) for MFC applications. *Electrochemistry Communications*, 11(7), 1547-1549.
- Fang, Z., Assaoudi, H., Guthrie, R. I., Kozinski, J. A., & Butler, I. S. (2007). Continuous Synthesis of Tin and Indium Oxide Nanoparticles in Sub- and Supercritical Water. *Journal of the American Ceramic Society*, 90(8), 2367-2371.
- Fangzhou, D., Zhenglong, L., Shaoqiang, Y., Beizhen, X., & Hong, L. (2011). Electricity generation directly using human feces wastewater for life support system. *Acta Astronautica*, 68(9), 1537-1547.
- Feng, L., Chen, Y., & Chen, L. (2011). Easy-to-operate and low-temperature synthesis of gram-scale nitrogen-doped graphene and its application as cathode catalyst in microbial fuel cells. *ACS nano*, 5(12), 9611-9618.
- Feng, L., Yan, Y., Chen, Y., & Wang, L. (2011). Nitrogen-doped carbon nanotubes as efficient and durable metal-free cathodic catalysts for oxygen reduction in microbial fuel cells. *Energy & Environmental Science*, 4(5), 1892-1899.
- Feng, Y., Yang, Q., Wang, X., & Logan, B. E. (2010). Treatment of carbon fiber brush anodes for improving power generation in air-cathode microbial fuel cells. *Journal of Power Sources*, 195(7), 1841-1844.
- Feng, Y., Yang, Q., Wang, X., Liu, Y., Lee, H., & Ren, N. (2011). Treatment of biodiesel production wastes with simultaneous electricity generation using a single-chamber microbial fuel cell. *Bioresource technology*, 102(1), 411-415.

- Fitzgerald, L. A., Petersen, E. R., Gross, B. J., Soto, C. M., Ringeisen, B. R., El-Naggar, M. Y., & Biffinger, J. C. (2012). Aggrandizing power output from *Shewanella oneidensis* MR-1 microbial fuel cells using calcium chloride. *Biosensors and Bioelectronics*, 31(1), 492-498.
- Freguia, S., Rabaey, K., Yuan, Z., & Keller, J. (2007). Non-catalyzed cathodic oxygen reduction at graphite granules in microbial fuel cells. *Electrochimica Acta*, 53(2), 598-603.
- Freguia, S., Tsujimura, S., & Kano, K. (2010). Electron transfer pathways in microbial oxygen biocathodes. *Electrochimica Acta*, 55(3), 813-818.
- Ge, B., Li, K., Fu, Z., Pu, L., & Zhang, X. (2015). The addition of ortho-hexagon nano spinel  $\text{Co}_3\text{O}_4$  to improve the performance of activated carbon air cathode microbial fuel cell. *Bioresource technology*, 195, 180-187.
- Ge, B., Li, K., Fu, Z., Pu, L., Zhang, X., Liu, Z., and Huang, K. (2016). The performance of nano urchin-like  $\text{NiCo}_2\text{O}_4$  modified activated carbon as air cathode for microbial fuel cell. *Journal of Power Sources*, 303, 325-332.
- Ge, X., Liu, Y., Goh, F. T., Hor, T. A., Zong, Y., Xiao, P., ... & Liu, Z. (2014). Dual-phase spinel  $\text{MnCo}_2\text{O}_4$  and spinel  $\text{MnCo}_2\text{O}_4$ /nanocarbon hybrids for electrocatalytic oxygen reduction and evolution. *ACS applied materials & interfaces*, 6(15), 12684-12691.
- Ghangrekar, M. M., & Shinde, V. B. (2008). Simultaneous sewage treatment and electricity generation in membrane-less microbial fuel cell. *Water Science and Technology*, 58(1), 37-43.
- Ghasemi, M., Daud, W.R.W., Rahimnejad, M., Rezayi, M., Fatemi, A., Jafari, Y., Somalu, M.R., and Manzour, A. (2013). Copper-phthalocyanine and nickel nanoparticles as novel cathode catalysts in microbial fuel cells. *International Journal of Hydrogen Energy*, 38, 9533-9540.
- Ghasemi, M., Daud, W. R. W., Hassan, S. H., Jafary, T., Rahimnejad, M., Ahmad, A., and Yazdi, M. H. (2016). Carbon nanotube/polypyrrole nanocomposite as a novel cathode catalyst and proper alternative for Pt in microbial fuel cell. *International Journal of Hydrogen Energy*, 41(8), 4872-4878.
- Ghasemi, M., Shahgaldi, S., Ismail, M., Kim, B. H., Yaakob, Z., & Daud, W. R. W. (2011). Activated carbon nanofibers as an alternative cathode catalyst to platinum in a two-chamber microbial fuel cell. *International Journal of Hydrogen Energy*, 36(21), 13746-13752.
- Gong, X.B., You, S.J., Wang, X.H., Zhang, J.N., Gan, Y., and Ren, N.Q. (2014). A novel stainless steel mesh/cobalt oxide hybrid electrode for efficient catalysis of oxygen reduction in a microbial fuel cell. *Biosensors Bioelectronics*, 55, 237-41.
- Gong, K., Du, F., Xia, Z., Durstock, M., & Dai, L. (2009). Nitrogen-doped carbon nanotube arrays with high electrocatalytic activity for oxygen reduction. *Science*, 323(5915), 760-764.

- Gurung, A., & Oh, S. E. (2015). Rice straw as a potential biomass for generation of bioelectrical energy using Microbial Fuel Cells (MFCs). *Energy Sources, Part A: Recovery, Utilization, and Environmental Effects*, 37(24), 2625-2631.
- Guo, K., Soeriyadi, A.H., Feng, H., PrévotEAU, A., Patil, S.A., Gooding, J.J. and Rabaey, and K., (2015). Heat-treated stainless steel felt as scalable anode material for bioelectrochemical systems. *Bioresource Technology*, 195, 46-50.
- Haoran, Y., Lifang, D., Tao, L., & Yong, C. (2014). Hydrothermal synthesis of nanostructured manganese oxide as cathodic catalyst in a microbial fuel cell fed with leachate. *The Scientific World Journal*, 2014.
- Hamann, S. D. (1981). Properties of electrolyte solutions at high pressures and temperatures. *Physics and Chemistry of the Earth*, 13, 89-111.
- Han, J. L., Wang, C. T., Hu, Y. C., Liu, Y., Chen, W. M., Chang, C. T., ... & Chen, B. Y. (2010). Exploring power generation of single-chamber microbial fuel cell using mixed and pure cultures. *Journal of the Taiwan Institute of Chemical Engineers*, 41(5), 606-611.
- Hassan, S. H., Kim, Y. S., & Oh, S. E. (2012). Power generation from cellulose using mixed and pure cultures of cellulose-degrading bacteria in a microbial fuel cell. *Enzyme and microbial technology*, 51(5), 269-273.
- He, Y.-R., Du, F., Huang, Y.-X., Dai, L.-M., Li, W.-W., and Yu, H.-Q. (2016). Preparation of microvillus-like nitrogen-doped carbon nanotubes as the cathode of a microbial fuel cell. *Journal of Materials Chemistry A*, 4, 1632-1636.
- He, Z., Minteer, S. D., & Angenent, L. T. (2005). Electricity generation from artificial wastewater using an upflow microbial fuel cell. *Environmental science & technology*, 39(14), 5262-5267.
- He, Z., Huang, Y., Manohar, A. K., & Mansfeld, F. (2008). Effect of electrolyte pH on the rate of the anodic and cathodic reactions in an air-cathode microbial fuel cell. *Bioelectrochemistry*, 74(1), 78-82.
- Holze, R., & Vielstich, W. (1984). The Kinetics of Oxygen Reduction at Porous Teflon-Bonded Fuel Cell Electrodes. *Journal of The Electrochemical Society*, 131(10), 2298-2303.
- Hosono, E., Fujihara, S., Honma, I., Zhou, H., 2005. Fabrication of morphology and crystal structure controlled nanorod and nanosheet cobalt hydroxide based on the difference of oxygen-solubility between water and methanol, and conversion into Co<sub>3</sub>O<sub>4</sub>. *Journal of Material Chemistry*, 15, 1938-1945.
- Hou, Y., Yuan, H., Wen, Z., Cui, S., Guo, X., He, Z., and Chen, J. (2016). Nitrogen-doped graphene/CoNi alloy encased within bamboo-like carbon nanotube hybrids as cathode catalysts in microbial fuel cells. *Journal of Power Sources*, 307, 561-568.
- Hu, D., Zhang, G., Wang, J., & Zhong, Q. (2015). Carbon-Supported Spinel Nanoparticle MnCo<sub>2</sub>O<sub>4</sub> as a Cathode Catalyst towards Oxygen Reduction Reaction in Dual-Chamber Microbial Fuel Cell. *Australian Journal of Chemistry*, 68(6), 987-994.

- Huang, J., Zhu, N., Yang, T., Zhang, T., Wu, P., Dang, Z. (2015a). Nickel oxide and carbon nanotube composite (NiO/CNT) as a novel cathode non-precious metal catalyst in microbial fuel cells. *Biosensors Bioelectronics*, 72, 332-339.
- Huang, J., Liu, Y., & You, T. (2010). Carbon nanofiber based electrochemical biosensors: A review. *Analytical Methods*, 2(3), 202-211.
- Huang, L., Liu, Y., Yu, L., Quan, X., Chen, G. (2015b). A new clean approach for production of cobalt dihydroxide from aqueous Co(II) using oxygen-reducing biocathode microbial fuel cells. *Journal of Cleaner Production*, 86, 441-446.
- Huang, J., & Kaner, R. B. (2004). A general chemical route to polyaniline nanofibers. *Journal of the American Chemical Society*, 126(3), 851-855.
- Hubenova, Y., & Mitov, M. (2010). Potential application of *Candida melibiosica* in biofuel cells. *Bioelectrochemistry*, 78(1), 57-61.
- Huggins, T.M., Pietron, J.J., Wang, H., Ren, Z.J. and Biffinger, J.C., (2015). Graphitic biochar as a cathode electrocatalyst support for microbial fuel cells, *Bioresource Technology*, 195, 147-153.
- Inglesby, A. E., Beatty, D. A., & Fisher, A. C. (2012). *Rhodospseudomonas palustris* purple bacteria fed *Arthrospira maxima* cyanobacteria: demonstration of application in microbial fuel cells. *RSC Advances*, 2(11), 4829-4838.
- IPCC Fourth Assessment Report: Climate Change 2007.
- Jiang, Y., Xu, Y., Yang, Q., Chen, Y., Zhu, S., & Shen, S. (2014). Power generation using polyaniline/multi-walled carbon nanotubes as an alternative cathode catalyst in microbial fuel cells. *International Journal of Energy Research*, 38(11), 1416-1423.
- Kang, C. S., Eaktasang, N., Kwon, D. Y., & Kim, H. S. (2014). Enhanced current production by *Desulfovibrio desulfuricans* biofilm in a mediator-less microbial fuel cell. *Bioresource technology*, 165, 27-30.
- Katuri, K. P., Enright, A. M., O'Flaherty, V., & Leech, D. (2012). Microbial analysis of anodic biofilm in a microbial fuel cell using slaughterhouse wastewater. *Bioelectrochemistry*, 87, 164-171.
- Khilari, S., Pandit, S., Ghangrekar, M. M., Das, D., & Pradhan, D. (2013). Graphene supported  $\alpha$ -MnO<sub>2</sub> nanotubes as a cathode catalyst for improved power generation and wastewater treatment in single-chambered microbial fuel cells. *Rsc Advances*, 3(21), 7902-7911.
- Khilari, S., Pandit, S., Das, D., & Pradhan, D. (2014). Manganese cobaltite/polypyrrole nanocomposite-based air-cathode for sustainable power generation in the single-chambered microbial fuel cells. *Biosensors and Bioelectronics*, 54, 534-540.
- Kiely, P. D., Cusick, R., Call, D. F., Selembo, P. A., Regan, J. M., & Logan, B. E. (2011a). Anode microbial communities produced by changing from microbial fuel cell to

- microbial electrolysis cell operation using two different wastewaters. *Bioresource technology*, 102(1), 388-394.
- Kiely, P. D., Rader, G., Regan, J. M., & Logan, B. E. (2011b). Long-term cathode performance and the microbial communities that develop in microbial fuel cells fed different fermentation endproducts. *Bioresource technology*, 102(1), 361-366.
- Kim, B. H., Chang, I. S., & Gadd, G. M. (2007). Challenges in microbial fuel cell development and operation. *Applied microbiology and biotechnology*, 76(3), 485-494.
- Kim, J.R., Kim, J.Y., Han, S.B., Park, K.W., Saratale, G.D., and Oh, S.E. (2011). Application of Co naphthalocyanine (CoNpc) as alternative cathode catalyst and support structure for microbial fuel cells. *Bioresource Technology*, 102, 342–347.
- Kim, J. R., Jung, S. H., Regan, J. M., & Logan, B. E. (2007). Electricity generation and microbial community analysis of alcohol powered microbial fuel cells. *Bioresource technology*, 98(13), 2568-2577.
- Kim, J. R., Dec, J., Bruns, M. A., & Logan, B. E. (2008). Removal of odors from swine wastewater by using microbial fuel cells. *Applied and environmental microbiology*, 74(8), 2540-2543.
- Kim, J. G., Kim, Y., Noh, Y., & Kim, W. B. (2015). MnCo<sub>2</sub>O<sub>4</sub> nanowires anchored on reduced graphene oxide sheets as effective bifunctional catalysts for Li–O<sub>2</sub> battery cathodes. *ChemSusChem*, 8(10), 1752-1760.
- Kim, Y., & Logan, B. E. (2011a). Series assembly of microbial desalination cells containing stacked electro dialysis cells for partial or complete seawater desalination. *Environmental science & technology*, 45(13), 5840-5845.
- Kim, Y., & Logan, B. E. (2011b). Microbial reverse electro dialysis cells for synergistically enhanced power production. *Environmental science & technology*, 45(13), 5834-5839.
- Kimura, Z. I., Chung, K. M., Itoh, H., Hiraishi, A., & Okabe, S. (2014). *Raoultella electrica* sp. nov., isolated from anodic biofilms of a glucose-fed microbial fuel cell. *International journal of systematic and evolutionary microbiology*, 64(4), 1384-1388.
- Kracke, F., Vassilev, I., & Krömer, J.O. (2015). Microbial electron transport and energy conservation –the foundation for optimizing bioelectrochemical systems. *Frontiers in Microbiology* 6:575.
- Krishnan, S. G., Ab Rahim, M. H., & Jose, R. (2016). Synthesis and characterization of MnCo<sub>2</sub>O<sub>4</sub> cuboidal microcrystals as a high performance pseudocapacitor electrode. *Journal of Alloys and Compounds*, 656, 707-713.
- Lai, L., Potts, J. R., Zhan, D., Wang, L., Poh, C. K., Tang, C., ... & Ruoff, R. S. (2012). Exploration of the active center structure of nitrogen-doped graphene-based catalysts for oxygen reduction reaction. *Energy & Environmental Science*, 5(7), 7936-7942.

- Lefebvre, O., Tan, Z., Kharkwal, S., & Ng, H. Y. (2012a). Effect of increasing anodic NaCl concentration on microbial fuel cell performance. *Bioresource Technology*, 112, 336-340.
- Lefebvre, O., Tang, Z., Fung, M. P., Chua, D. H., Chang, I. S., & Ng, H. Y. (2012b). Electrical performance of low cost cathodes prepared by plasma sputtering deposition in microbial fuel cells. *Biosensors and Bioelectronics*, 31(1), 164-169.
- Li, B., Zhou, X., Wang, X., Liu, B., & Li, B. (2014). Hybrid binuclear-cobalt-phthalocyanine as oxygen reduction reaction catalyst in single chamber microbial fuel cells. *Journal of Power Sources*, 272, 320-327.
- Li, D., Qu, Y., Liu, J., He, W., Wang, H., & Feng, Y. (2014). Using ammonium bicarbonate as pore former in activated carbon catalyst layer to enhance performance of air cathode microbial fuel cell. *Journal of Power Sources*, 272, 909-914.
- Li, R., Dai, Y., Chen, B., Zou, J., Jiang, B., and Fu, H. (2016). Nitrogen-doped Co/Co<sub>9</sub>S<sub>8</sub>/partly-graphitized carbon as durable catalysts for oxygen reduction in microbial fuel cells. *Journal of Power Sources*, 307, 1-10.
- Li, B., Zhou, X., Wang, X., Liu, B., & Li, B. (2014). Hybrid binuclear-cobalt-phthalocyanine as oxygen reduction reaction catalyst in single chamber microbial fuel cells. *Journal of Power Sources*, 272, 320-327.
- Li, B., Wang, M., Zhou, X., Wang, X., Liu, B., & Li, B. (2015). Pyrolyzed binuclear-cobalt-phthalocyanine as electrocatalyst for oxygen reduction reaction in microbial fuel cells. *Bioresource technology*, 193, 545-548.
- Li, R., Dai, Y., Chen, B., Zou, J., Jiang, B., & Fu, H. (2016). Nitrogen-doped Co/Co<sub>9</sub>S<sub>8</sub>/partly-graphitized carbon as durable catalysts for oxygen reduction in microbial fuel cells. *Journal of Power Sources*, 307, 1-10.
- Li, X., Hu, B., Suib, S., Lei, Y., & Li, B. (2011). Electricity generation in continuous flow microbial fuel cells (MFCs) with manganese dioxide (MnO<sub>2</sub>) cathodes. *Biochemical Engineering Journal*, 54(1), 10-15.
- Li, X., Zhong, G. Z., Qiao, Y., Huang, J., Hu, W. H., Wang, X. G., & Li, C. M. (2014). A high performance xylose microbial fuel cell enabled by *Ochrobactrum* sp. 575 cells. *RSC Advances*, 4(75), 39839-39843.
- Liang, P., Wang, H., Xia, X., Huang, X., Mo, Y., Cao, X., & Fan, M. (2011). Carbon nanotube powders as electrode modifier to enhance the activity of anodic biofilm in microbial fuel cells. *Biosensors and Bioelectronics*, 26(6), 3000-3004.
- Liang, Y., Wang, H., Diao, P., Chang, W., Hong, G., Li, Y., & Regier, T. Z. (2012). Oxygen reduction electrocatalyst based on strongly coupled cobalt oxide nanocrystals and carbon nanotubes. *Journal of the American Chemical Society*, 134(38), 15849-15857.

- Liang, J., Jiao, Y., Jaroniec, M., & Qiao, S. Z. (2012). Sulfur and nitrogen dual-doped mesoporous graphene electrocatalyst for oxygen reduction with synergistically enhanced performance. *Angewandte Chemie International Edition*, 51(46), 11496-11500.
- Liu, B., Brückner, C., Lei, Y., Cheng, Y., Santoro, C., and Li, B. (2014). Cobalt porphyrin-based material as methanol tolerant cathode in single chamber microbial fuel cells (SCMFCs). *Journal of Power Sources*, 257, 246-253.
- Liu, H., Ramnarayanan, R., & Logan, B. E. (2004). Production of electricity during wastewater treatment using a single chamber microbial fuel cell. *Environmental science & technology*, 38(7), 2281-2285.
- Liu, H., & Logan, B. E. (2004). Electricity generation using an air-cathode single chamber microbial fuel cell in the presence and absence of a proton exchange membrane. *Environmental science & technology*, 38(14), 4040-4046.
- Liu, S., Wu, J., Zhou, J., Fang, G., & Liang, S. (2015). Mesoporous NiCo<sub>2</sub>O<sub>4</sub> nanoneedles grown on three dimensional graphene networks as binder-free electrode for high-performance lithium-ion batteries and supercapacitors. *Electrochimica Acta*, 176, 1-9.
- Liu, X. W., Sun, X. F., Huang, Y. X., Sheng, G. P., Zhou, K., Zeng, R. J., ... & Yu, H. Q. (2010). Nano-structured manganese oxide as a cathodic catalyst for enhanced oxygen reduction in a microbial fuel cell fed with a synthetic wastewater. *Water research*, 44(18), 5298-5305.
- Liu, Z., Ge, B., Li, K., Zhang, X., and Huang, K. (2016). The excellent performance and mechanism of activated carbon air cathode doped with different type of cobalt for microbial fuel cells. *Fuel*, 176, 173-180.
- Liu, Z., Ge, B., Li, K., Zhang, X., & Huang, K. (2016). The excellent performance and mechanism of activated carbon air cathode doped with different type of cobalt for microbial fuel cells. *Fuel*, 176, 173-180.
- Liew, K. B., Daud, W. R. W., Ghasemi, M., Loh, K. S., Ismail, M., Lim, S. S., & Leong, J. X. (2015). Manganese oxide/functionalised carbon nanotubes nanocomposite as catalyst for oxygen reduction reaction in microbial fuel cell. *International Journal of Hydrogen Energy*, 40(35), 11625-11632.
- Lima, F. H., Calegari, M. L., & Ticianelli, E. A. (2006). Investigations of the catalytic properties of manganese oxides for the oxygen reduction reaction in alkaline media. *Journal of Electroanalytical Chemistry*, 590(2), 152-160.
- Lu, A.-H., Salabas, E. L. and Schüth, F. (2007). Magnetic nanoparticles: Synthesis, protection, functionalization, and application. *Angewandte Chemie International Edition*, 46(8), 1222-1244.
- Logan, B. E., Hamelers, B., Rozendal, R., Schröder, U., Keller, J., Freguia, S., ... & Rabaey, K. (2006). Microbial fuel cells: methodology and technology. *Environmental science & technology*, 40(17), 5181-5192.

- Logan, B., Cheng, S., Watson, V., & Estadt, G. (2007). Graphite fiber brush anodes for increased power production in air-cathode microbial fuel cells. *Environmental science & technology*, 41(9), 3341-3346.
- Lu, M., Kharkwal, S., Ng, H. Y., & Li, S. F. Y. (2011). Carbon nanotube supported MnO<sub>2</sub> catalysts for oxygen reduction reaction and their applications in microbial fuel cells. *Biosensors and Bioelectronics*, 26(12), 4728-4732.
- Lu, M., Guo, L., Kharkwal, S., Ng, H. Y., & Li, S. F. Y. (2013). Manganese–polypyrrole–carbon nanotube, a new oxygen reduction catalyst for air-cathode microbial fuel cells. *Journal of Power Sources*, 221, 381-386.
- Lu, N., Zhou, S. G., Zhuang, L., Zhang, J. T., & Ni, J. R. (2009). Electricity generation from starch processing wastewater using microbial fuel cell technology. *Biochemical engineering journal*, 43(3), 246-251.
- Luo, J., Jang, H. D., Sun, T., Xiao, L., He, Z., Katsoulidis, A. P., ... & Huang, J. (2011). Compression and aggregation-resistant particles of crumpled soft sheets. *Acs Nano*, 5(11), 8943-8949.
- Mahmoud, M., Gad-Allah, T. A., El-Khatib, K. M., & El-Gohary, F. (2011). Power generation using spinel manganese–cobalt oxide as a cathode catalyst for microbial fuel cell applications. *Bioresource technology*, 102(22), 10459-10464.
- Mansoorian, H. J., Mahvi, A. H., Jafari, A. J., Amin, M. M., Rajabizadeh, A., & Khanjani, N. (2013). Bioelectricity generation using two chamber microbial fuel cell treating wastewater from food processing. *Enzyme and microbial technology*, 52(6), 352-357.
- Marsh, H., & Reinoso, F. R. (2006). *Activated carbon*. Elsevier.
- Masuda, M., Freguia, S., Wang, Y. F., Tsujimura, S., & Kano, K. (2010). Flavins contained in yeast extract are exploited for anodic electron transfer by *Lactococcus lactis*. *Bioelectrochemistry*, 78(2), 173-175.
- Mehanna, M., Saito, T., Yan, J., Hickner, M., Cao, X., Huang, X., & Logan, B. E. (2010). Using microbial desalination cells to reduce water salinity prior to reverse osmosis. *Energy & Environmental Science*, 3(8), 1114-1120.
- Min, B., Cheng, S., & Logan, B. E. (2005a). Electricity generation using membrane and salt bridge microbial fuel cells. *Water research*, 39(9), 1675-1686.
- Min, B., Kim, J., Oh, S., Regan, J. M., & Logan, B. E. (2005b). Electricity generation from swine wastewater using microbial fuel cells. *Water research*, 39(20), 4961-4968.
- Mink, J. E., Rojas, J. P., Logan, B. E., & Hussain, M. M. (2012). Vertically grown multiwalled carbon nanotube anode and nickel silicide integrated high performance micro-sized (1.25  $\mu$ L) microbial fuel cell. *Nano letters*, 12(2), 791-795.

- Misonon, I. I., Aziz, R. A., Zain, N. K. M., Vidhyadharan, B., Krishnan, S. G., & Jose, R. (2014). High performance MnO<sub>2</sub> nanoflower electrode and the relationship between solvated ion size and specific capacitance in highly conductive electrolytes. *Materials Research Bulletin*, 57, 221-230.
- Minteer, S. D., Atanassov, P., Luckarift, H. R., & Johnson, G. R. (2012). New materials for biological fuel cells. *Materials Today*, 15(4), 166-173.
- More, T. T., & Ghangrekar, M. M. (2010). Improving performance of microbial fuel cell with ultrasonication pre-treatment of mixed anaerobic inoculum sludge. *Bioresource technology*, 101(2), 562-567.
- Nandy, A., Kumar, V., & Kundu, P. P. (2013). Utilization of proteinaceous materials for power generation in a mediatorless microbial fuel cell by a new electrogenic bacteria *Lysinibacillus sphaericus* VA5. *Enzyme and microbial technology*, 53(5), 339-344.
- Natarajan, D., & Van Nguyen, T. (2003). Three-dimensional effects of liquid water flooding in the cathode of a PEM fuel cell. *Journal of Power Sources*, 115(1), 66-80.
- Naveen, A. N., & Selladurai, S. (2016). Novel synthesis of highly porous three-dimensional nickel cobaltite for supercapacitor application. *Ionics*, 22(8), 1471-1483.
- Nevin, K. P., Richter, H., Covalla, S. F., Johnson, J. P., Woodard, T. L., Orloff, A. L., ... & Lovley, D. R. (2008). Power output and coulombic efficiencies from biofilms of *Geobacter sulfurreducens* comparable to mixed community microbial fuel cells. *Environmental microbiology*, 10(10), 2505-2514.
- Nor, M. H. M., Mubarak, M. F. M., Elmi, H. S. A., Ibrahim, N., Wahab, M. F. A., & Ibrahim, Z. (2015). Bioelectricity generation in microbial fuel cell using natural microflora and isolated pure culture bacteria from anaerobic palm oil mill effluent sludge. *Bioresource technology*, 190, 458-465.
- Nørskov, J. K., Rossmeisl, J., Logadottir, A., Lindqvist, L. R. K. J., Kitchin, J. R., Bligaard, T., & Jonsson, H. (2004). Origin of the overpotential for oxygen reduction at a fuel-cell cathode. *The Journal of Physical Chemistry B*, 108(46), 17886-17892.
- Novoselov, K. S., Geim, A. K., Morozov, S. V., Jiang, D., Zhang, Y., Dubonos, S. V., ... & Firsov, A. A. (2004). Electric field effect in atomically thin carbon films. *Science*, 306(5696), 666-669.
- Ortiz-Martínez, V. M., Salar-García, M. J., Touati, K., Hernández-Fernández, F. J., de los Ríos, A. P., Belhoucine, F., & Berrabbah, A. A. (2016). Assessment of spinel-type mixed valence Cu/Co and Ni/Co-based oxides for power production in single-chamber microbial fuel cells. *Energy*, 113, 1241-1249.

- Pandit, S., Khilari, S., Roy, S., Pradhan, D., & Das, D. (2014). Improvement of power generation using *Shewanella putrefaciens* mediated bioanode in a single chambered microbial fuel cell: Effect of different anodic operating conditions. *Bioresource technology*, 166, 451-457.
- Pant, D., Van Bogaert, G., De Smet, M., Diels, L., & Vanbroekhoven, K. (2010). Use of novel permeable membrane and air cathodes in acetate microbial fuel cells. *Electrochimica Acta*, 55(26), 7710-7716.
- Park, H. I., Wu, C., & Lin, L. S. (2012). Coal tar wastewater treatment and electricity production using a membrane-less tubular microbial fuel cell. *Biotechnology and Bioprocess Engineering*, 17(3), 654-660.
- Parot, S., Nercessian, O., Delia, M. L., Achouak, W., & Bergel, A. (2009). Electrochemical checking of aerobic isolates from electrochemically active biofilms formed in compost. *Journal of applied microbiology*, 106(4), 1350-1359.
- Patil, S.A., Surakasi, V.P., Koul, S., Ijmulwar, S., Vivek, A., Shouche, Y.S. and Kapadnis, B.P. (2009). Electricity generation using chocolate industry wastewater and its treatment in activated sludge based microbial fuel cell and analysis of developed microbial community in the anode chamber. *Bioresource Technology*, 100, 5132-5139.
- Patil, S. A., Harnisch, F., Koch, C., Hübschmann, T., Fetzer, I., Carmona-Martínez, A. A., ... & Schröder, U. (2011). Electroactive mixed culture derived biofilms in microbial bioelectrochemical systems: the role of pH on biofilm formation, performance and composition. *Bioresource technology*, 102(20), 9683-9690.
- Peng, L., You, S. J., & Wang, J. Y. (2010). Carbon nanotubes as electrode modifier promoting direct electron transfer from *Shewanella oneidensis*. *Biosensors and Bioelectronics*, 25(5), 1248-1251.
- Potter, M. C. (1911). Electrical effects accompanying the decomposition of organic compounds. *Proceedings of the Royal Society of London. Series B, Containing Papers of a Biological Character*, 84(571), 260-276.
- Prasad, D., Arun, S., Murugesan, M., Padmanaban, S., Satyanarayanan, R. S., Berchmans, S., & Yegnaraman, V. (2007). Direct electron transfer with yeast cells and construction of a mediatorless microbial fuel cell. *Biosensors and Bioelectronics*, 22(11), 2604-2610.
- Qiao, Y., Bao, S. J., Li, C. M., Cui, X. Q., Lu, Z. S., & Guo, J. (2007). Nanostructured polyaniline/titanium dioxide composite anode for microbial fuel cells. *Acs Nano*, 2(1), 113-119.
- Qiao, Y., Li, C. M., Bao, S. J., Lu, Z., & Hong, Y. (2008). Direct electrochemistry and electrocatalytic mechanism of evolved *Escherichia coli* cells in microbial fuel cells. *Chemical communications*, 11, 1290-1292.
- Qu, Y., Feng, Y., Wang, X., & Logan, B. E. (2012). Use of a coculture to enable current production by *Geobacter sulfurreducens*. *Applied and environmental microbiology*, 78(9), 3484-3487.

- Quan, X., Mei, Y., Xu, H., Sun, B., & Zhang, X. (2015). Optimization of Pt-Pd alloy catalyst and supporting materials for oxygen reduction in air-cathode Microbial Fuel Cells. *Electrochimica Acta*, *165*, 72-77.
- Rabaey, K., Clauwaert, P., Aelterman, P., & Verstraete, W. (2004). Tubular microbial fuel cells for efficient electricity generation. *Environmental science & technology*, *39*(20), 8077-8082.
- Rabaey, K., & Verstraete, W. (2005). Microbial fuel cells: novel biotechnology for energy generation. *Trends in Biotechnology*, *23*(6), 291-298.
- Rabenau, A. (1985). The role of hydrothermal synthesis in preparative chemistry. *Angewandte Chemie International Edition in English*, *24*(12), 1026-1040.
- Reguera, G., Nevin, K. P., Nicoll, J. S., Covalla, S. F., Woodard, T. L., & Lovley, D. R. (2006). Biofilm and nanowire production leads to increased current in *Geobacter sulfurreducens* fuel cells. *Applied and environmental microbiology*, *72*(11), 7345-7348.
- Raghavulu, S. V., Goud, R. K., Sarma, P. N., & Mohan, S. V. (2011). *Saccharomyces cerevisiae* as anodic biocatalyst for power generation in biofuel cell: influence of redox condition and substrate load. *Bioresource technology*, *102*(3), 2751-2757.
- Ringeisen, B. R., Henderson, E., Wu, P. K., Pietron, J., Ray, R., Little, B., ... & Jones-Meehan, J. M. (2006). High power density from a miniature microbial fuel cell using *Shewanella oneidensis* DSP10. *Environmental science & technology*, *40*(8), 2629-2634.
- Roche, I., Katuri, K., & Scott, K. (2010). A microbial fuel cell using manganese oxide oxygen reduction catalysts. *Journal of applied electrochemistry*, *40*(1), 13-21.
- Roy, R. (1994). Accelerating the kinetics of low-temperature inorganic syntheses. *Journal of Solid State Chemistry*, *111*(1), 11-17.
- Saito, T., Merrill, M. D., Watson, V. J., Logan, B. E., & Hickner, M. A. (2010). Investigation of ionic polymer cathode binders for microbial fuel cells. *Electrochimica Acta*, *55*(9), 3398-3403.
- Saito, T., Mehanna, M., Wang, X., Cusick, R. D., Feng, Y., Hickner, M. A., & Logan, B. E. (2011a). Effect of nitrogen addition on the performance of microbial fuel cell anodes. *Bioresource technology*, *102*(1), 395-398.
- Saito, T., Roberts, T. H., Long, T. E., Logan, B. E., & Hickner, M. A. (2011b). Neutral hydrophilic cathode catalyst binders for microbial fuel cells. *Energy & Environmental Science*, *4*(3), 928-934.
- Sakdaronnarong, C. K., Thanosawan, S., Chaithong, S., Sinbuathong, N., & Jeraputra, C. (2013). Electricity production from ethanol stillage in two-compartment MFC. *Fuel*, *107*, 382-386.
- Samsudeen, N., Radhakrishnan, T. K., & Matheswaran, M. (2015). Bioelectricity production from microbial fuel cell using mixed bacterial culture isolated from distillery wastewater. *Bioresource technology*, *195*, 242-247.

- Sanchez, D. V., Huynh, P., Kozlov, M. E., Baughman, R. H., Vidic, R. D., & Yun, M. (2010). Carbon nanotube/platinum (Pt) sheet as an improved cathode for microbial fuel cells. *Energy & Fuels*, 24(11), 5897-5902.
- Santoro, C., Stadlhofer, A., Hacker, V., Squadrito, G., Schröder, U., & Li, B. (2013a). Activated carbon nanofibers (ACNF) as cathode for single chamber microbial fuel cells (SCMFCs). *Journal of Power Sources*, 243, 499-507.
- Santoro, C., Ieropoulos, I., Greenman, J., Cristiani, P., Vadas, T., Mackay, A., & Li, B. (2013b). Power generation and contaminant removal in single chamber microbial fuel cells (SCMFCs) treating human urine. *International Journal of Hydrogen Energy*, 38(26), 11543-11551.
- Schaefer, A. L., Greenberg, E. P., Oliver, C. M., Oda, Y., Huang, J. J., Bittan-Banin, G., ... & Harwood, C. S. (2008). A new class of homoserine lactone quorum-sensing signals. *Nature*, 454(7204), 595-599.
- Schneider, S. H. (1989). The greenhouse effect: science and policy. *Science*, 243, (4892), 771-781.
- Schaetzle, O., Barrière, F., & Baronian, K. (2008). Bacteria and yeasts as catalysts in microbial fuel cells: electron transfer from micro-organisms to electrodes for green electricity. *Energy & Environmental Science*, 1(6), 607-620.
- Sciarria, T. P., Merlino, G., Scaglia, B., D'Epifanio, A., Mecheri, B., Borin, S., ... & Adani, F. (2015). Electricity generation using white and red wine lees in air cathode microbial fuel cells. *Journal of Power Sources*, 274, 393-399.
- Shao, Y., Liu, J., Wang, Y., & Lin, Y. (2008). Novel catalyst support materials for PEM fuel cells: current status and future prospects. *Journal of Materials Chemistry*, 19(1), 46-59.
- Shi, X., Feng, Y., Wang, X., Lee, H., Liu, J., Qu, Y., ... & Ren, N. (2012). Application of nitrogen-doped carbon powders as low-cost and durable cathodic catalyst to air-cathode microbial fuel cells. *Bioresource technology*, 108, 89-93.
- Song, T.-S., Wang, D.-B., Wang, H., Li, X., Liang, Y., and Xie, J. (2015). Cobalt oxide/nanocarbon hybrid materials as alternative cathode catalyst for oxygen reduction in microbial fuel cell. *International Journal of Hydrogen Energy*, 40, 3868-3874.
- Strik, D. P., Snel, J. F., & Buisman, C. J. (2008). Green electricity production with living plants and bacteria in a fuel cell. *International Journal of Energy Research*, 32(9), 870-876.
- Sun, D., Call, D., Wang, A., Cheng, S., & Logan, B. E. (2014a). *Geobacter* sp. SD-1 with enhanced electrochemical activity in high-salt concentration solutions. *Environmental microbiology reports*, 6(6), 723-729.

- Sun, D., Wang, A., Cheng, S., Yates, M., & Logan, B. E. (2014b). *Geobacter anodireducens* sp. nov., an exoelectrogenic microbe in bioelectrochemical systems. *International journal of systematic and evolutionary microbiology*, 64(10), 3485-3491.
- Sun, J. J., Zhao, H. Z., Yang, Q. Z., Song, J., & Xue, A. (2010). A novel layer-by-layer self-assembled carbon nanotube-based anode: Preparation, characterization, and application in microbial fuel cell. *Electrochimica Acta*, 55(9), 3041-3047.
- Tang, J., Chen, S., Yuan, Y., Cai, X., & Zhou, S. (2015). In situ formation of graphene layers on graphite surfaces for efficient anodes of microbial fuel cells. *Biosensors and Bioelectronics*, 71, 387-395.
- Thrash, J. C., Van Trump, J. I., Weber, K. A., Miller, E., Achenbach, L. A., & Coates, J. D. (2007). Electrochemical stimulation of microbial perchlorate reduction. *Environmental science & technology*, 41(5), 1740-1746.
- Torres, C. I., Marcus, A. K., Lee, H. S., Parameswaran, P., Krajmalnik-Brown, R., & Rittmann, B. E. (2010). A kinetic perspective on extracellular electron transfer by anode-respiring bacteria. *FEMS Microbiology Reviews*, 34(1), 3-17.
- Touach, N., Ortiz-Martínez, V. M., Salar-García, M. J., Benzaouak, A., Hernández-Fernández, F., de los Ríos, A. P., ... & Lotfi, E. M. (2016). Influence of the preparation method of MnO<sub>2</sub>-based cathodes on the performance of single-chamber MFCs using wastewater. *Separation and Purification Technology*, 171, 174-181.
- Tremouli, A., Antonopoulou, G., Bebelis, S., & Lyberatos, G. (2013). Operation and characterization of a microbial fuel cell fed with pretreated cheese whey at different organic loads. *Bioresource technology*, 131, 380-389.
- Tsai, H. Y., Wu, C. C., Lee, C. Y., & Shih, E. P. (2009). Microbial fuel cell performance of multiwall carbon nanotubes on carbon cloth as electrodes. *Journal of Power Sources*, 194(1), 199-205.
- Van Dommele, S., Romero-Izquierdo, A., Brydson, R., De Jong, K. P., & Bitter, J. H. (2008). Tuning nitrogen functionalities in catalytically grown nitrogen-containing carbon nanotubes. *Carbon*, 46(1), 138-148.
- Wan, Y. and Zhao. (2007). On the controllable soft-templating approach to mesoporous silicates. *Chemical Reviews*, 107(7), 2821-2860.
- Wang, X., Feng, Y. J., & Lee, H. (2008). Electricity production from beer brewery wastewater using single chamber microbial fuel cell. *Water Science and Technology*, 57(7), 1117-1121.
- Wang, Y.X., Cui, X.Z., Chen, L.S., Wei, C.Y., Cui, F.M., Yao, H.L., Shi, J.L., Li, Y.S. (2014). One-step replication and enhanced catalytic activity for cathodic oxygen reduction of the mesostructured Co<sub>3</sub>O<sub>4</sub> /carbon composites. *Royal Society of Chemistry*, 43, 4163–4168.
- Wang, G., Shen, X., Horvat, J., Wang, B., Liu, H., Wexler, D., and Yao, J., (2009). Hydrothermal Synthesis and Optical, Magnetic, and Supercapacitance Properties of Nanoporous Cobalt Oxide Nanorods. *Journal of Physical Chemistry C*, 113, 4357–4361.

- Wang, H., Maiyalagan, T., & Wang, X. (2012). Review on recent progress in nitrogen-doped graphene: synthesis, characterization, and its potential applications. *Acs Catalysis*, 2(5), 781-794.
- Wang, H., Wu, Z., Plaseied, A., Jenkins, P., Simpson, L., Engtrakul, C., & Ren, Z. (2011). Carbon nanotube modified air-cathodes for electricity production in microbial fuel cells. *Journal of Power Sources*, 196(18), 7465-7469.
- Wang, Q., Zhang, X., Lv, R., Chen, X., Xue, B., Liang, P., & Huang, X. (2016). Binder-free nitrogen-doped graphene catalyst air-cathodes for microbial fuel cells. *Journal of Materials Chemistry A*, 4(32), 12387-12391.
- Wang, X., Feng, Y., Liu, J., Shi, X., Lee, H., Li, N., & Ren, N. (2010). Power generation using adjustable Nafion/PTFE mixed binders in air-cathode microbial fuel cells. *Biosensors and Bioelectronics*, 26(2), 946-948.
- Wang, X., Gao, N., Zhou, Q., Dong, H., Yu, H., & Feng, Y. (2013). Acidic and alkaline pretreatments of activated carbon and their effects on the performance of air-cathodes in microbial fuel cells. *Bioresource technology*, 144, 632-636.
- Watanabe, K., Manefield, M., Lee, M., & Kouzuma, A. (2009). Electron shuttles in biotechnology. *Current opinion in biotechnology*, 20(6), 633-641.
- Watson, V. J., Delgado, C. N., & Logan, B. E. (2013). Improvement of activated carbons as oxygen reduction catalysts in neutral solutions by ammonia gas treatment and their performance in microbial fuel cells. *Journal of Power Sources*, 242, 756-761.
- Wen, Q., Wang, S., Yan, J., Cong, L., Pan, Z., Ren, Y., & Fan, Z. (2012). MnO<sub>2</sub>-graphene hybrid as an alternative cathodic catalyst to platinum in microbial fuel cells. *Journal of power sources*, 216, 187-191.
- Wen, Q., Wang, S., Yan, J., Cong, L., Chen, Y., & Xi, H. (2014). Porous nitrogen-doped carbon nanosheet on graphene as metal-free catalyst for oxygen reduction reaction in air-cathode microbial fuel cells. *Bioelectrochemistry*, 95, 23-28.
- Wen, Q., Kong, F., Zheng, H., Cao, D., Ren, Y., & Yin, J. (2011). Electricity generation from synthetic penicillin wastewater in an air-cathode single chamber microbial fuel cell. *Chemical engineering journal*, 168(2), 572-576.
- Winfield, J., Gajda, I., Greenman, J. and Ieropoulos, I. (2016). A review into the use of ceramics in microbial fuel cells. *Bioresource Technology*, 215, 296-303.
- Wrighton, K. C., Thrash, J. C., Melnyk, R. A., Bigi, J. P., Byrne-Bailey, K. G., Remis, J. P., ... & Coates, J. D. (2011). Evidence for direct electron transfer by a Gram-positive bacterium isolated from a microbial fuel cell. *Applied and environmental microbiology*, 77(21), 7633-7639.
- Wu, C., Liu, X. W., Li, W. W., Sheng, G. P., Zang, G. L., Cheng, Y. Y., ... & Yu, H. Q. (2012). A white-rot fungus is used as a biocathode to improve electricity production of a microbial fuel cell. *Applied energy*, 98, 594-596.
- Xafenias, N., Zhang, Y., & Banks, C. J. (2013). Enhanced performance of hexavalent chromium reducing cathodes in the presence of *Shewanella oneidensis* MR-1 and lactate. *Environmental science & technology*, 47(9), 4512-4520.

- Xiao, L., Damien, J., Luo, J., Jang, H. D., Huang, J., & He, Z. (2012). Crumpled graphene particles for microbial fuel cell electrodes. *Journal of Power Sources*, 208, 187-192.
- Xie, X., Hu, L., Pasta, M., Wells, G. F., Kong, D., Criddle, C. S., & Cui, Y. (2010). Three-dimensional carbon nanotube– textile anode for high-performance microbial fuel cells. *Nano letters*, 11(1), 291-296.
- Xie, X., Ye, M., Hu, L., Liu, N., McDonough, J. R., Chen, W., ... & Cui, Y. (2012). Carbon nanotube-coated macroporous sponge for microbial fuel cell electrodes. *Energy & Environmental Science*, 5(1), 5265-5270.
- Xie, X., Yu, G., Liu, N., Bao, Z., Criddle, C. S., & Cui, Y. (2012). Graphene–sponges as high-performance low-cost anodes for microbial fuel cells. *Energy & Environmental Science*, 5(5), 6862-6866.
- Xie, X., Pasta, M., Hu, L., Yang, Y., McDonough, J., Cha, J., ... & Cui, Y. (2011). Nano-structured textiles as high-performance aqueous cathodes for microbial fuel cells. *Energy & Environmental Science*, 4(4), 1293-1297.
- Xing, D., Zuo, Y., Cheng, S., Regan, J. M., & Logan, B. E. (2008). Electricity generation by *Rhodospseudomonas palustris* DX-1. *Environmental science & technology*, 42(11), 4146-4151.
- Xu, J., Gao, P., and Zhao, T.S. (2012). Non-precious  $\text{Co}_3\text{O}_4$  nano-rod electrocatalyst for oxygen reduction reaction in anion-exchange membrane fuel cells. *Energy Environmental Science*, 5, 5333–5339.
- Xu, S., & Liu, H. (2011). New exoelectrogen *Citrobacter* sp. SX-1 isolated from a microbial fuel cell. *Journal of applied microbiology*, 111(5), 1108-1115.
- Yan, H., Saito, T., & Regan, J. M. (2012). Nitrogen removal in a single-chamber microbial fuel cell with nitrifying biofilm enriched at the air cathode. *Water research*, 46(7), 2215-2224.
- Yan, Z., Wang, M., Lu, Y., Liu, R., & Zhao, J. (2014). Ethylene glycol stabilized  $\text{NaBH}_4$  reduction for preparation carbon-supported Pt–Co alloy nanoparticles used as oxygen reduction electrocatalysts for microbial fuel cells. *Journal of Solid State Electrochemistry*, 18(4), 1087-1097.
- Yang, G., Sun, Y., Yuan, Z., Lü, P., Kong, X., Li, L., ... & Lu, T. (2014). Application of surface-modified carbon powder in microbial fuel cells. *Chinese Journal of Catalysis*, 35(5), 770-775.
- Yang, Q., Wang, X., Feng, Y., Lee, H., Liu, J., Shi, X., ... & Ren, N. (2012). Electricity generation using eight amino acids by air–cathode microbial fuel cells. *Fuel*, 102, 478-482.
- Yang, T., Li, K., Pu, L., Liu, Z., Ge, B., Pan, Y. and Liu, Y. (2016). Hollow-spherical Co/NC nanoparticle as an efficient electrocatalyst used in air cathode microbial fuel cell, *Biosensors Bioelectronics*, 86, 129-134.
- Yang, W., Kim, K.Y. and Logan, B.E. (2015). Development of carbon free diffusion layer for activated carbon air cathode of microbial fuel cells. *Bioresource Technology*, 197, 318-322.

- Yang, X., Zou, W., Su, Y., Zhu, Y., Jiang, H., Shen, J., & Li, C. (2014). Activated nitrogen-doped carbon nanofibers with hierarchical pore as efficient oxygen reduction reaction catalyst for microbial fuel cells. *Journal of Power Sources*, 266, 36-42.
- Yang, X., Lu, J., Zhu, Y., Shen, J., Zhang, Z., Zhang, J., ... & Li, C. (2011). Microbial fuel cell cathode with dendrimer encapsulated Pt nanoparticles as catalyst. *Journal of Power Sources*, 196(24), 10611-10615.
- Yazdi, A.A., D'Angelo, L., Omer, N., Windiasti, G., Lu, X. and Xu, J. (2016). Carbon nanotube modification of microbial fuel cell electrodes. *Biosensors Bioelectronics*, 85, 536-552.
- You, S., Gong, X., Wang, W., Qi, D., Wang, X., Chen, X., & Ren, N. (2016). Enhanced Cathodic Oxygen Reduction and Power Production of Microbial Fuel Cell Based on Noble-Metal-Free Electrocatalyst Derived from Metal-Organic Frameworks. *Advanced Energy Materials*, 6(1).
- Yu, E. H., Burkitt, R., Wang, X., & Scott, K. (2012). Application of anion exchange ionomer for oxygen reduction catalysts in microbial fuel cells. *Electrochemistry Communications*, 21, 30-35.
- Yuan, H., Hou, Y., Wen, Z., Guo, X., Chen, J., & He, Z. (2015). Porous carbon nanosheets codoped with nitrogen and sulfur for oxygen reduction reaction in microbial fuel cells. *ACS applied materials & interfaces*, 7(33), 18672-18678.
- Yuan, Y., Chen, Q., Zhou, S., Zhuang, L., & Hu, P. (2011). Bioelectricity generation and microcystins removal in a blue-green algae powered microbial fuel cell. *Journal of hazardous materials*, 187(1), 591-595.
- Zhang, B., Wen, Z., Ci, S., Mao, S., Chen, J., & He, Z. (2014). Synthesizing nitrogen-doped activated carbon and probing its active sites for oxygen reduction reaction in microbial fuel cells. *ACS applied materials & interfaces*, 6(10), 7464-7470.
- Zhang, F., Brastad, K. S., & He, Z. (2011). Integrating forward osmosis into microbial fuel cells for wastewater treatment, water extraction and bioelectricity generation. *Environmental science & technology*, 45(15), 6690-6696.
- Zhang, J. N., You, S. J., Yuan, Y. X., Zhao, Q. L., & Zhang, G. D. (2011). Efficient electrocatalysis of cathodic oxygen reduction with Pt-Fe alloy catalyst in microbial fuel cell. *Electrochemistry Communications*, 13(9), 903-905.
- Zhang, J., Yang, G., Zhou, S., Wang, Y., Yuan, Y., & Zhuang, L. (2013). *Fontibacter ferrireducens* sp. nov., an Fe (III)-reducing bacterium isolated from a microbial fuel cell. *International journal of systematic and evolutionary microbiology*, 63(3), 925-929.
- Zhang, L., Liu, C., Zhuang, L., Li, W., Zhou, S., & Zhang, J. (2009). Manganese dioxide as an alternative cathodic catalyst to platinum in microbial fuel cells. *Biosensors and Bioelectronics*, 24(9), 2825-2829.
- Zhang, L., Lu, Z., Li, D., Ma, J., Song, P., Huang, G., ... & Cai, L. (2016). Chemically activated graphite enhanced oxygen reduction and power output in catalyst-free microbial fuel cells. *Journal of Cleaner Production*, 115, 332-336.

- Zhang, P., Li, K., & Liu, X. (2014). Carnation-like MnO<sub>2</sub> modified activated carbon air cathode improve power generation in microbial fuel cells. *Journal of Power Sources*, 264, 248-253.
- Zhang, T., Cui, C., Chen, S., Ai, X., Yang, H., Shen, P., & Peng, Z. (2006). A novel mediatorless microbial fuel cell based on direct biocatalysis of *Escherichia coli*. *Chemical communications*, 21, 2257-2259.
- Zhang, X., Li, K., Yan, P., Liu, Z., and Pu, L. (2015). N-type Cu<sub>2</sub>O doped activated carbon as catalyst for improving power generation of air cathode microbial fuel cells. *Bioresource Technology*, 187, 299–304.
- Zhang, X., Cheng, S., Wang, X., Huang, X., & Logan, B. E. (2009). Separator characteristics for increasing performance of microbial fuel cells. *Environmental Science & Technology*, 43(21), 8456-8461.
- Zhang, X., Pant, D., Zhang, F., Liu, J., He, W., & Logan, B. E. (2014). Long-term performance of chemically and physically modified activated carbons in air cathodes of microbial fuel cells. *ChemElectroChem*, 1(11), 1859-1866.
- Zhang, Y., Hu, Y., Li, S., Sun, J., & Hou, B. (2011). Manganese dioxide-coated carbon nanotubes as an improved cathodic catalyst for oxygen reduction in a microbial fuel cell. *Journal of Power Sources*, 196(22), 9284-9289.
- Zhao, F., Harnisch, F., Schröder, U., Scholz, F., Bogdanoff, P., & Herrmann, I. (2006). Challenges and constraints of using oxygen cathodes in microbial fuel cells. *Environmental science & technology*, 40(17), 5193-5199.
- Zhou, L., Fu, P., Cai, X., Zhou, S., & Yuan, Y. (2016). Naturally derived carbon nanofibers as sustainable electrocatalysts for microbial energy harvesting: A new application of spider silk. *Applied Catalysis B: Environmental*, 188, 31-38.
- Zhou, M., He, H., Jin, T., & Wang, H. (2012). Power generation enhancement in novel microbial carbon capture cells with immobilized *Chlorella vulgaris*. *Journal of Power Sources*, 214, 216-219.
- Zhuang, L., Zhou, S., Wang, Y., Liu, C., & Geng, S. (2009). Membrane-less cloth cathode assembly (CCA) for scalable microbial fuel cells. *Biosensors and Bioelectronics*, 24(12), 3652-3656.
- Zou, Y., Xiang, C., Yang, L., Sun, L. X., Xu, F., & Cao, Z. (2008). A mediatorless microbial fuel cell using polypyrrole coated carbon nanotubes composite as anode material. *International Journal of Hydrogen Energy*, 33(18), 4856-4862.
- Zuo, Y., & Logan, B. E. (2011). Power generation in MFCs with architectures based on tubular cathodes or fully tubular reactors. *Water Science and Technology*, 64(11), 2253-2258.
- Zuo, Y., Cheng, S., Call, D., & Logan, B. E. (2007). Tubular membrane cathodes for scalable power generation in microbial fuel cells. *Environmental science & technology*, 41(9), 3347-3353.

## APPENDIX A

Table A1 XRD data of Co<sub>3</sub>O<sub>4</sub> nanorods.

Number	2-theta	d (nm)	Lattice plane		
			h	k	l
1	19.01	0.46	1	1	1
2	31.27	0.28	2	2	0
3	36.85	0.24	3	1	1
4	38.56	0.23	2	2	2
5	44.81	0.20	4	0	0
6	55.66	0.16	4	2	2
7	59.33	0.15	5	1	1
8	65.23	0.14	4	4	0
9	77.36	0.12	5	3	3
10	78.42	0.12	6	2	2

Table A2 XRD data of Co<sub>3</sub>O<sub>4</sub> flakes.

Number	2-theta	d (nm)	Lattice plane		
			h	k	l
1	19.00	0.46	1	1	1
2	31.28	0.28	2	2	0
3	36.84	0.24	3	1	1
4	38.54	0.23	2	2	2
5	44.80	0.20	4	0	0
6	55.64	0.16	4	2	2
7	59.34	0.15	5	1	1
8	65.20	0.14	4	4	0
9	77.30	0.12	5	3	3
10	78.41	0.12	6	2	2

Table A3 XRD data of Co<sub>3</sub>O<sub>4</sub> flower.

Number	2-theta	d (nm)	Lattice plane		
			h	k	l
1	18.93	0.46	1	1	1
2	31.11	0.28	2	2	0
3	36.66	0.24	3	1	1
4	38.36	0.23	2	2	2
5	44.62	0.20	4	0	0
6	55.50	0.16	4	2	2
7	59.09	0.15	5	1	1
8	64.94	0.14	4	4	0
9	76.98	0.12	5	3	3
10	78.35	0.12	6	2	2

Table A4 XRD data of MnCo<sub>2</sub>O<sub>4</sub> nanorods.

Number	2-theta	d (nm)	Lattice plane		
			h	k	l
1	19.01	0.46	1	1	1
2	31.09	0.28	2	2	0
3	36.56	0.24	3	1	1
4	38.41	0.23	2	2	2
5	44.71	0.20	4	0	0
6	55.47	0.16	4	2	2
7	59.11	0.15	5	1	1
8	64.91	0.14	4	4	0
9	76.98	0.12	5	3	3

UMP

## APPENDIX B

### PARAMETERS USED TO RECORD CV CURVES IN POTENTIOSTAT

Cyclic Voltammetry

Default Save Restore OK Cancel

Pstat  IFC1000-07225

Test Identifier

Output File

Electrode Area

Notes...

Initial E (V)   vs Eref  vs Eoc

Scan Limit 1 (V)   vs Eref  vs Eoc

Scan Limit 2 (V)   vs Eref  vs Eoc

Final E (V)   vs Eref  vs Eoc

Scan Rate (mV/s)

Step Size (mV)

Cycles (#)

I/E Range Mode  Auto  Fixed

Max Current (mA)

IRComp  None  PF  CI

PF Corr. (ohm)

Equil. Time (s)

Init. Delay  Off Time(s)  Stab. (mV/s)

Conditioning  Off Time(s)  E (V)

Sampling Mode  Fast  Noise Reject  Surface

Advanced Pstat Setup  Off

Electrode Setup  On

## APPENDIX C

### PARAMETERS USED TO RECORD LSV CURVES IN POTENTIOSTAT

Linear Sweep Voltammetry

Default Save Restore OK Cancel

Pstat  IFC1000-07225

Test Identifier Linear Sweep Voltammetry

Output File MFC 3, LSV 3.DTA

Electrode Area 15

Notes...

Initial E (V) -0.6  vs Eref  vs Eoc

Final E (V) 0.4  vs Eref  vs Eoc

Scan Rate (mV/s) 10

Step Size (mV) 1

I/E Range Mode  Auto  Fixed

Max Current (mA) 450

IRComp  None  PF  CI

PF Corr. (ohm) 50

Equil. Time (s) 100

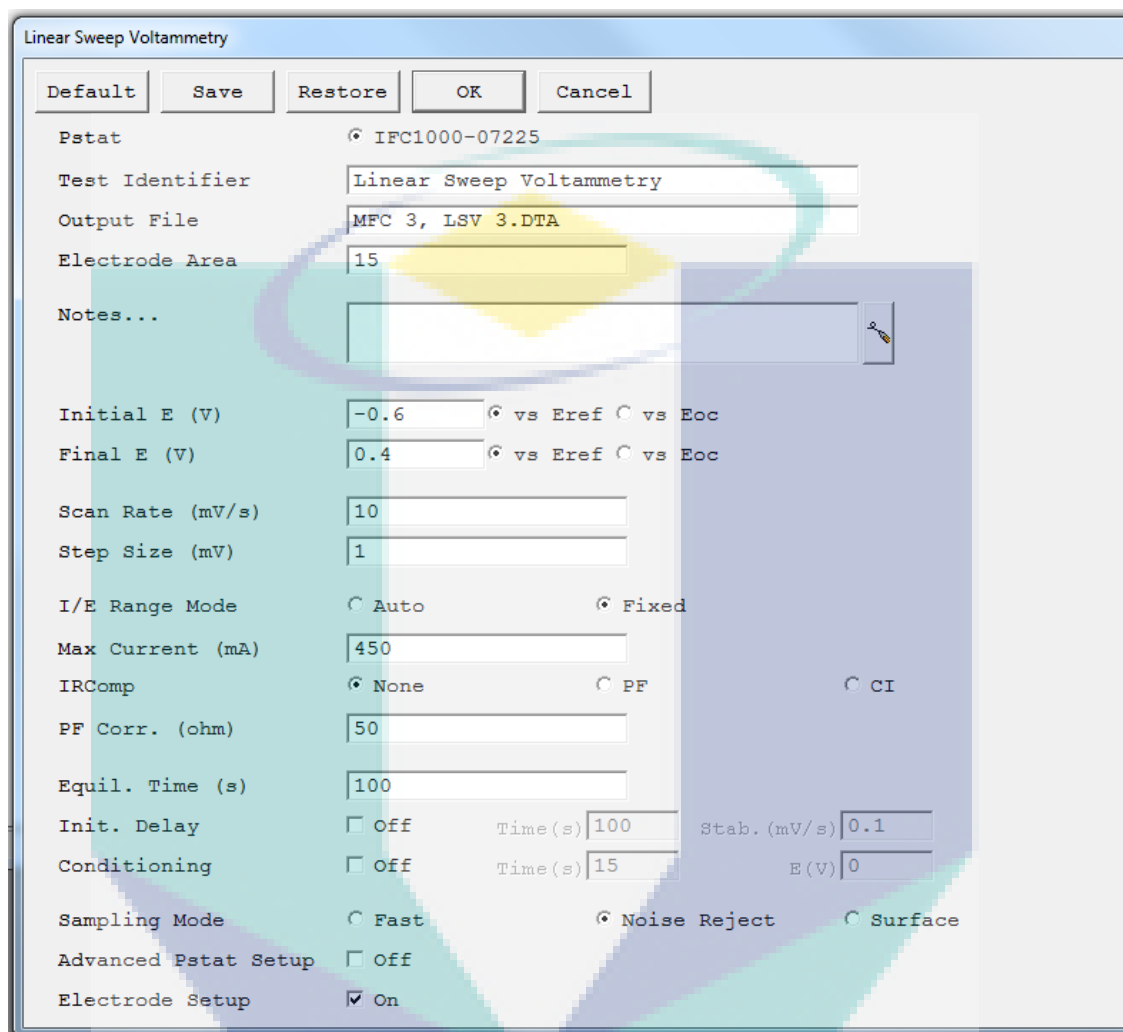
Init. Delay  Off Time(s) 100 Stab. (mV/s) 0.1

Conditioning  Off Time(s) 15 E(V) 0

Sampling Mode  Fast  Noise Reject  Surface

Advanced Pstat Setup  Off

Electrode Setup  On



## APPENDIX D

### PARAMETERS USED TO RECORD NYQUIST PLOTS IN POTENTIOSTAT

Galvanostatic EIS

Default Save Restore OK Cancel

Estat  IFC1000-07225

Test Identifier Galvanostatic EIS

Output File MFC 3, EIS 3.DTA

Notes...

Initial Freq. (Hz) 100000

Final Freq. (Hz) 1

Points/decade 10

AC Current (A rms) 0.0001

DC Current (A) 0

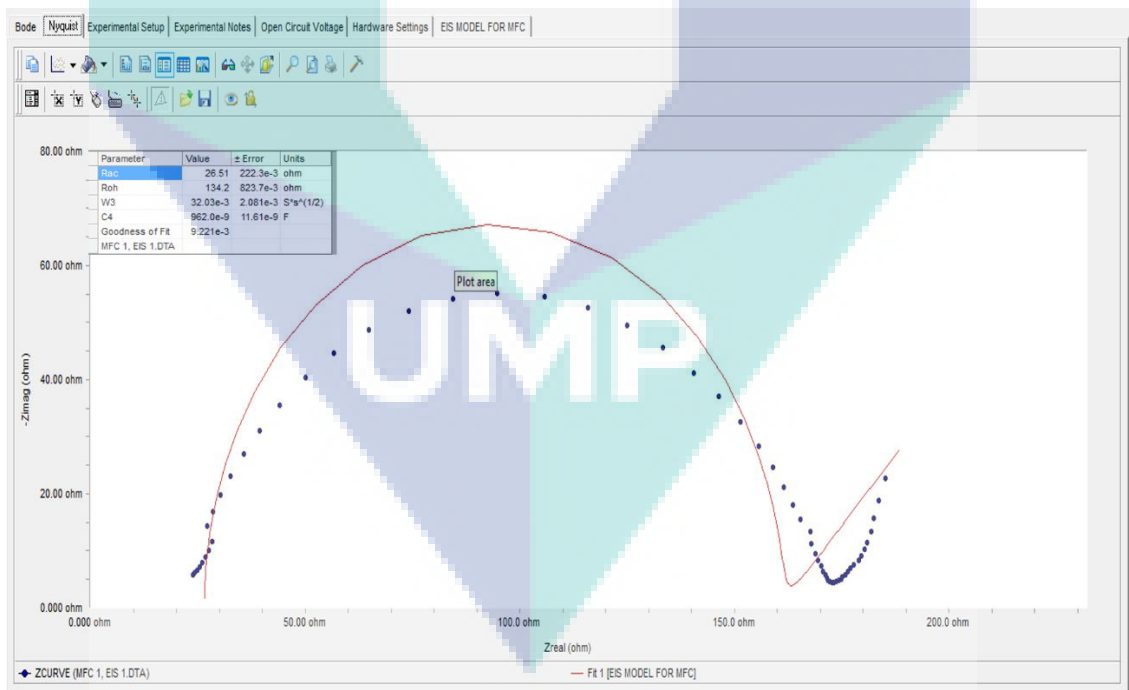
Area (cm<sup>2</sup>) 15

Conditioning  Off Time (s) 15 E (V) 0

Init. Delay  On Time (s) 100 Stab. (mV/s) 2

Estimated Z (ohms) 100

Optimize for:  Fast  Normal  Low Noise



## APPENDIX E

### PARAMETERS USED TO RECORD TAFEL CURVES IN POTENTIOSTAT

Tafel

Default Save Restore OK Cancel

Pstat IFC1000-07225

Test Identifier Tafel Scan

Output File MFC 3, TAFEL 3.DTA

Notes...

Initial E (V) 0.02 vs Eref vs Eoc

Final E (V) 0.1 vs Eref vs Eoc

Scan Rate (mV/s) 1

Sample Period (s) 5

Sample Area (cm<sup>2</sup>) 15

Density (g/cm<sup>3</sup>) 2.26

Equiv. Wt 0.081

Conditioning  Off Time(s) 15 E (V) 0

Init. Delay  On Time(s) 100 Stab. (mV/s) 0.1

IR Comp  Off

Equil. Time (s) 100

## APPENDIX F

### PUBLICATIONS

#### 1. Journals

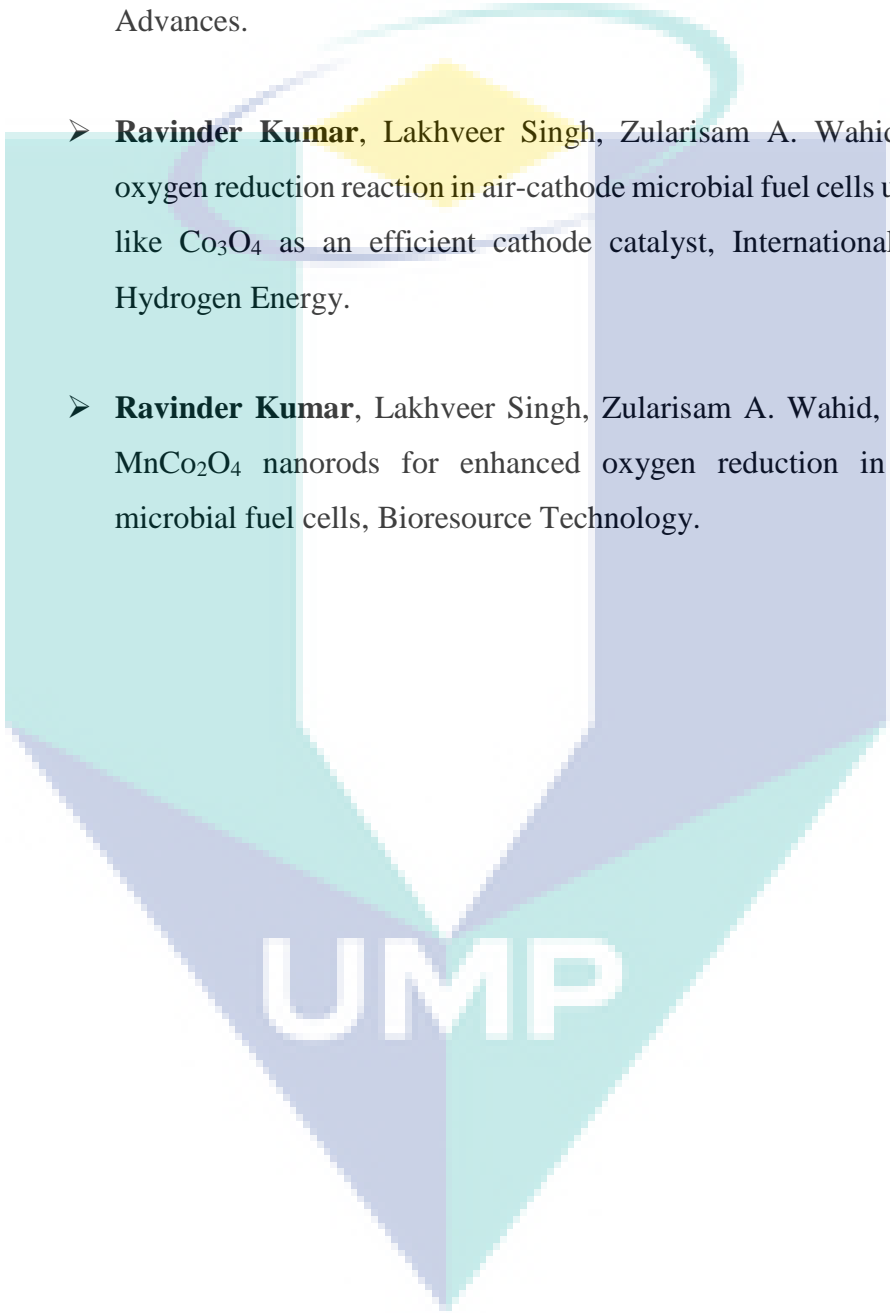
- **Ravinder Kumar**, Lakhveer Singh, Zularisam A. Wahid, Exoelectrogens: Recent advances in molecular drivers involved in extracellular electron transfer and strategies used to improve it for microbial fuel cell applications, *Renewable & Sustainable Energy Reviews* 56: 1322–1336, 2016.
- **Ravinder Kumar**, Lakhveer Singh, Zularisam A. Wahid, Potential of porous  $\text{Co}_3\text{O}_4$  nanorods as cathode catalyst for oxygen reduction reaction in microbial fuel cells, *Bioresource Technology* 220: 537-542, 2016.
- **Ravinder Kumar**, Lakhveer Singh, Zularisam A. Wahid, Mohd Fadhil Md. Din, Exoelectrogens in microbial fuel cells towards bioelectricity generation: a review, *International Journal of Energy Research* 39: 1048-1067, 2015.

#### 2. Book Chapters & Conferences

- **Ravinder Kumar**, Lakhveer Singh, Zularisam A. Wahid, Role of microorganisms in microbial fuel cells towards bioelectricity generation. A Book Chapter in the book “Microbial Factories”, 135-154, published by Springer.
- **Ravinder Kumar**, Lakhveer Singh, Zularisam A. Wahid, Microbial Fuel Cells: types and applications. A Book Chapter submitted in Springer for publication, Accepted.
- **Ravinder Kumar**, Lakhveer Singh, Zularisam A. Wahid, Development of a metal oxide cathode catalyst for air-cathode microbial fuel cells, in National Conference for Postgraduate Research 2016 at Universiti Malaysia Pahang.

### 3. Research Articles Under Review

- **Ravinder Kumar**, Lakhveer Singh, Zularisam A. Wahid, Mesoporous  $\text{Co}_3\text{O}_4$  nanoflakes as an efficient and non-precious cathode catalyst for oxygen reduction reaction in air-cathode microbial fuel cells, RSC Advances.
- **Ravinder Kumar**, Lakhveer Singh, Zularisam A. Wahid, Enhanced oxygen reduction reaction in air-cathode microbial fuel cells using flower-like  $\text{Co}_3\text{O}_4$  as an efficient cathode catalyst, International Journal of Hydrogen Energy.
- **Ravinder Kumar**, Lakhveer Singh, Zularisam A. Wahid, Mesoporous  $\text{MnCo}_2\text{O}_4$  nanorods for enhanced oxygen reduction in air-cathode microbial fuel cells, Bioresource Technology.



UMP